

University of Windsor

## Scholarship at UWindor

---

Electronic Theses and Dissertations

Theses, Dissertations, and Major Papers

---

2013

### Design of battery pack and internal combustion engine thermal models for hybrid electric vehicles

Gabriele Catacchio  
*University of Windsor*

Follow this and additional works at: <https://scholar.uwindsor.ca/etd>

---

#### Recommended Citation

Catacchio, Gabriele, "Design of battery pack and internal combustion engine thermal models for hybrid electric vehicles" (2013). *Electronic Theses and Dissertations*. 4964.  
<https://scholar.uwindsor.ca/etd/4964>

This online database contains the full-text of PhD dissertations and Masters' theses of University of Windsor students from 1954 forward. These documents are made available for personal study and research purposes only, in accordance with the Canadian Copyright Act and the Creative Commons license—CC BY-NC-ND (Attribution, Non-Commercial, No Derivative Works). Under this license, works must always be attributed to the copyright holder (original author), cannot be used for any commercial purposes, and may not be altered. Any other use would require the permission of the copyright holder. Students may inquire about withdrawing their dissertation and/or thesis from this database. For additional inquiries, please contact the repository administrator via email ([scholarship@uwindsor.ca](mailto:scholarship@uwindsor.ca)) or by telephone at 519-253-3000ext. 3208.

# **Design of battery pack and internal combustion engine thermal models for hybrid electric vehicles**

By

**Gabriele Catacchio**

A Thesis  
Submitted to the Faculty of Graduate Studies  
through the Department of Mechanical, Automotive and Materials Engineering  
in Partial Fulfillment of the Requirements for  
the Degree of Master of Applied Science  
at the University of Windsor

Windsor, Ontario, Canada

2013

© 2013 Gabriele Catacchio

# **Design of battery pack and internal combustion engine thermal models for hybrid electric vehicles**

By

**Gabriele Catacchio**

Approved by:

---

Dr. Peter Frise, Co-Advisor  
Department of Mechanical, Automotive and Materials Engineering

---

Dr. Narayan Kar, Co-Advisor  
Department of Electrical and Computer Engineering

---

Dr. Jennifer Johrendt, Program Reader  
Department of Mechanical, Automotive and Materials Engineering

---

Dr. Chris Lee, Outside Program Reader  
Department of Civil and Environmental Engineering

August 12<sup>th</sup>, 2013

## **DECLARATION OF ORIGINALITY**

I hereby certify that I am the sole author of this thesis and that no part of this thesis has been published or submitted for publication.

I certify that, to the best of my knowledge, my thesis does not infringe upon anyone's copyright nor violate any proprietary rights and that any ideas, techniques, quotations, or any other material from the work of other people included in my thesis, published or otherwise, are fully acknowledged in accordance with the standard referencing practices. Furthermore, to the extent that I have included copyrighted material that surpasses the bounds of fair dealing within the meaning of the Canada Copyright Act, I certify that I have obtained a written permission from the copyright owner(s) to include such material(s) in my thesis and have included copies of such copyright clearances to my appendix.

I declare that this is a true copy of my thesis, including any final revisions, as approved by my thesis committee and the Graduate Studies office, and that this thesis has not been submitted for a higher degree to any other University or Institution.

## **ABSTRACT**

This thesis focuses on the design of computational models, capable of simulating the thermal behaviour of a battery pack and internal combustion engine equipping a hybrid electric vehicle tested over a given driving cycle. Both the models manage a lot of input variables and take into account all the thermophysical aspects regulating the heat exchange phenomena between the battery and engine devices and the cooling medium used to maintain their thermal control.

The main objective of the research is to design the two models and integrate them in the simulation tool used by Chrysler to predict the performance of hybrid vehicles in the early design stages. After that, using the battery cooling system model, a sensitivity study is performed to understand which are the most important factor affecting the thermal behaviour of the battery cells. Finally, a validation phase is conducted for both the software to guarantee the validity of their results.

## DEDICATION

*To my grandma,  
who always believed in me.*

## ACKNOWLEDGEMENTS

This work is the result of the cooperation of two universities, the Politecnico di Torino and the University of Windsor, and two companies, FIAT and Chrysler, and it is thanks to the precious guidance of many people from all these institutions that this thesis has been developed.

Firstly, I would like to express my deepest gratitude to my FIAT tutor Dr. Vittorio Ravello, who always gave me professional and moral support during the whole project. I am also profoundly grateful to Prof. Andrea Tonoli and Prof. Alberto Tenconi, from the Politecnico di Torino, for all their help and suggestions.

Then, I would like to thank my advisors Dr. Peter Frise and Dr. Narayan Kar from the University of Windsor, for their important assistance both during the academic year and during the writing of the thesis. Moreover, I am particularly grateful to Jan Stewart and Mike Houston, for their patience and their continuous support.

Furthermore, I would like to express my deepest gratitude to all the people who assisted me in Chrysler, starting from my tutors Oliver Gross and Mengyang Zhang, who always helped me during the internship period and allowed me to live a fantastic professional experience in Auburn Hills. Special thanks go also to my Chrysler supervisor Mohammed Malik and to all the colleagues I worked with, for their guidance and suggestions: Craig, Sachin, Joydip, Carrie, Tony, Witt, Joel, Rene, Julie and Lucille.

Last but not least, I am profoundly grateful to Prof. Giovanni Belingardi from Politecnico di Torino and Dr. Edoardo Rabino from FIAT, for their precious advices.

The most important thanks are reserved to my fantastic parents and brother, to my adorable girlfriend Martina and to my friends Andrea, Maurizio, Gianmarco, Carlo and Yupeng, who made this experience wonderful and unforgettable.

# LIST OF CONTENTS

DECLARATION OF ORIGINALITY .....	iii
ABSTRACT.....	iv
DEDICATION .....	v
ACKNOWLEDGEMENTS .....	vi
LIST OF TABLES .....	xv
LIST OF FIGURES .....	xvii
NOMENCLATURE .....	xxiii
ABBREVIATIONS .....	xxix
<b>1 INTRODUCTION.....</b>	<b>1</b>
1.1 Objectives.....	2
1.2 Thesis organization .....	3
<b>2 LITERATURE REVIEW .....</b>	<b>5</b>
2.1 Latest developments in the worldwide automotive scenario.....	5
2.1.1 Environmental effects of fossil fuels .....	5
2.1.2 Sustainable transportation solutions .....	7
2.2 Innovative features introduced by vehicle hybridization .....	9
2.2.1 Fuel consumption and emission levels reductions .....	10
2.2.2 Environmental impact of hybrid car batteries .....	10
2.3 Hybrid drivetrains .....	11
2.3.1 General concepts about hybrid vehicle drivetrains.....	11
2.3.2 Parallel configuration.....	12
2.3.2.1 Parallel hybrid strengths .....	14
2.3.2.2 Description of the integrated starter generator.....	14



2.3.3 Series configuration.....	16
2.3.3.1 Series hybrid strengths.....	18
2.3.4 Series-parallel configuration.....	19
2.3.4.1 The Toyota Hybrid Synergy Drive system .....	20
2.3.4.2 Series-parallel hybrid strengths.....	21
2.4 Degrees of hybridization .....	21
2.4.1 Micro hybrids .....	22
2.4.2 Mild hybrids .....	23
2.4.3 Full hybrids.....	24
2.4.4 Plug-in hybrids .....	24
2.4.5 Battery electric vehicles.....	25
2.5 The battery.....	25
2.5.1 BEV and HEV battery design requirements.....	27
2.5.2 Battery basics.....	28
2.5.3 Battery types .....	30
2.5.3.1 Lead-acid battery.....	31
2.5.3.2 Nickel-cadmium battery.....	32
2.5.3.3 Nickel-metal hydride battery .....	32
2.5.3.4 Lithium-ion battery .....	33
2.5.3.5 Lithium-polymer battery .....	34
2.5.4 Battery key parameters .....	34
2.5.4.1 Ampere-hour capacity.....	34
2.5.4.2 C-rate.....	35
2.5.4.3 Specific energy.....	35
2.5.4.4 Specific power .....	35

2.5.4.5 Energy and power densities .....	35
2.5.4.6 Internal resistance .....	36
2.5.4.7 State of charge (SOC) .....	36
2.5.4.8 Depth of discharge (DOD).....	36
2.5.4.9 State of health (SOH).....	36
2.5.4.10 Cycle life.....	37
2.5.4.11 Calendar life.....	37
2.5.4.12 Efficiency.....	37
2.5.5 Battery state of the art.....	37
2.5.6 Battery integration and control systems .....	39
2.5.6.1 Battery thermal control .....	40
2.5.6.2 Desired attributes of a thermal management system .....	40
2.5.6.3 Battery cooling concepts.....	41
2.5.6.3.1 Air cooling and liquid cooling systems.....	41
2.5.6.3.2 Active and passive cooling systems .....	43
2.5.6.3.3 Cooling only and cooling/heating systems.....	45
2.5.6.3.4 Series and parallel cooling systems.....	46
2.5.6.4 Usefulness analysis of battery thermal management systems .....	46
2.6 Existing thermal models for HEV's engine and battery .....	47
<b>3 DESIGN AND METHODOLOGY .....</b>	<b>49</b>
3.1 Chrysler HEV prediction model.....	49
3.1.1 Brief description of the driving cycles.....	50
3.1.1.1 New European Driving Cycle .....	52
3.1.1.1.1 Cycle main characteristics.....	53
3.1.1.1.2 Criticism .....	54

3.1.1.2 EPA Federal Test Procedure .....	55
3.1.1.2.1 FTP-72.....	56
3.1.2 Chrysler HEV prediction model features .....	57
3.1.3 Chrysler HEV prediction model strengths.....	60
3.1.4 Chrysler HEV prediction model weaknesses .....	61
3.1.4.1 Internal combustion engine coolant temperature .....	62
3.1.4.2 High voltage battery temperature.....	63
3.1.4.3 Necessity for an update of the Chrysler HEV prediction model.....	66
3.2 Brief description of the Matlab® and Simulink® virtual platforms .....	67
3.2.1 Basic structure of the Matlab® and Simulink® files of the new thermal models .....	69
3.3 Internal combustion engine cooling system model design.....	71
3.3.1 Basic concepts about internal combustion engine operations .....	72
3.3.2 Driving cycle input data and creation of the Matlab® base file .....	74
3.3.3 Internal combustion engine cooling system model theoretical and virtual design .....	75
3.3.3.1 Combustion heat rate .....	77
3.3.3.2 Exhaust heat rate .....	80
3.3.3.3 Mechanical power.....	82
3.3.3.4 Cabin heater heat rate.....	84
3.3.3.5 Surroundings heat rate .....	87
3.3.3.6 Radiator heat rate .....	92
3.3.3.7 Coolant heat rate .....	97
3.3.4 Internal combustion engine cooling system model simulation running .....	101
3.3.5 New features introduced by the internal combustion engine cooling system model .....	103

3.4 Battery cooling system model design.....	107
3.4.1 Battery pack geometric characteristics and cooling solutions.....	108
3.4.2 Battery cooling system model implementation and background theory, system configuration.....	113
3.4.3 Battery cooling system model implementation and background theory, thermodynamic and flow studies.....	115
3.4.3.1 Types of fluid flow regime.....	117
3.4.3.2 Nusselt number and convective heat transfer coefficient.....	119
3.4.3.2.1 Nusselt number determination, laminar flow.....	123
3.4.3.2.2 Nusselt number determination, turbulent flow.....	123
3.4.3.2.3 Convective heat transfer coefficient determination.....	125
3.4.3.3 Overall heat transfer coefficient determination.....	125
3.4.4 Battery cooling system model implementation and background theory, software creation.....	133
3.4.4.1 Reynolds and Prandtl numbers computation.....	135
3.4.4.2 Nusselt number computation.....	137
3.4.4.3 Convective heat transfer coefficient computation.....	139
3.4.4.4 Overall heat transfer coefficients computation.....	140
3.4.4.5 Coolant outlet and battery temperatures computation.....	143
3.4.4.5.1 Coolant outlet temperature.....	145
3.4.4.5.2 Battery temperature.....	149
3.4.5 Battery cooling system model simulation running.....	153
3.4.6 New features introduced by the battery cooling system model.....	158
<b>4 ANALYSIS OF RESULTS.....</b>	<b>172</b>
4.1 Introduction to the analysis of the results.....	172

4.2 Internal combustion engine cooling system model simulation and validation phase .....	173
4.2.1 Engine and driving cycle characteristics and input data.....	174
4.2.1.1 Thermostat working principles .....	178
4.2.1.2 Thermostat modeling .....	179
4.2.2 Internal combustion engine cooling system model simulation phase .....	182
4.2.2.1 Excitation driving profile .....	183
4.2.2.2 Analysis of the combustion heat rate .....	185
4.2.2.3 Analysis of the exhaust heat rate.....	188
4.2.2.4 Analysis of the mechanical power .....	190
4.2.2.5 Analysis of the cabin heater heat rate .....	192
4.2.2.6 Analysis of the surroundings heat rate.....	193
4.2.2.7 Analysis of the radiator heat rate .....	195
4.2.2.8 Analysis of the coolant heat rate .....	198
4.2.2.9 Analysis of the coolant temperature time trend .....	201
4.2.3 Internal combustion engine cooling system model validation phase .....	206
4.3 Battery cooling system model simulation and validation phase .....	211
4.3.1 Battery pack and driving cycle characteristics and input data.....	212
4.3.1.1 Definition of the main simulation cases of study.....	215
4.3.1.2 List of the main simulation cases of study .....	216
4.3.1.2.1 Case of study A .....	217
4.3.1.2.2 Case of study B .....	217
4.3.1.2.3 Case of study C .....	217
4.3.1.2.4 Case of study D .....	218
4.3.1.2.5 Case of study E.....	218

4.3.1.2.6 Case of study F .....	219
4.3.2 Battery cooling system model simulation phase .....	219
4.3.2.1 Introduction to the simulations .....	220
4.3.2.2 Simulation - 1 .....	221
4.3.2.3 Simulation - 2.....	223
4.3.2.4 Simulation - 3.....	224
4.3.2.5 Simulation - 4.....	226
4.3.2.6 Simulation - 5.....	228
4.3.2.7 Simulation - 6.....	230
4.3.2.8 Simulation - 7.....	231
4.3.2.9 Simulation - 8.....	233
4.3.2.10 Simulation - 9.....	234
4.3.2.11 Simulation - 10.....	236
4.3.2.12 Simulation - 11.....	237
4.3.2.13 Simulation - 12.....	239
4.3.2.14 Simulation - 13.....	240
4.3.2.15 Simulation - 14.....	241
4.3.2.16 Simulation - 15.....	243
4.3.2.17 Simulation - 16.....	244
4.3.2.18 Simulation - 17.....	246
4.3.3 Overall analysis of the simulation results and basic sensitivity study .....	249
4.3.4 Battery cooling system model validation phase .....	254
<b>5 CONCLUSIONS AND RECOMMENDATIONS.....</b>	<b>260</b>
5.1 Conclusions .....	261
5.2 Recommendations .....	262

REFERENCES .....	265
VITA AUCTORIS .....	273

## LIST OF TABLES

Table 2.1 - Costs and fuel efficiency gains introduced by the new vehicles' electric system [15].....	22
Table 2.2 - Nominal energy density of different sources [19].....	26
Table 2.3 - Typical values of the battery key parameters for HEV, BEV and PHEV applications [27].....	39
Table 3.1 - NEDC driving cycle main characteristics .....	55
Table 3.2 - FTP-72 driving cycle main characteristics .....	57
Table 3.3 - Nusselt number constant values for laminar flow regimes.....	124
Table 3.4 - Thicknesses and thermal conductivities of the different layers constituting the battery module structure.....	129
Table 3.5 - Boundary conditions and main characteristics of the simulation (FTP-72 driving cycle) .....	155
Table 4.1 - HWFET driving cycle main characteristics.....	176
Table 4.2 - Engine angular speed and radiator coolant volume flow rate .....	179
Table 4.3 - Main input values considered for the A-type simulations .....	217
Table 4.4 - Main input values considered for the B-type simulations .....	217
Table 4.5 - Main input values considered for the C-type simulations .....	218
Table 4.6 - Main input values considered for the D-type simulations.....	218
Table 4.7 - Main input values considered for the E-type simulations .....	219
Table 4.8 - Main input values considered for the F-type simulations .....	219
Table 4.9 - Input variables background of simulation number 1 .....	221
Table 4.10 - Input variables background of simulation number 2 .....	223
Table 4.11 - Input variables background of simulation number 3 .....	224
Table 4.12 - Input variables background of simulation number 4 .....	226



Table 4.13 - Input variables background of simulation number 5 .....	228
Table 4.14 - Input variables background of simulation number 6 .....	230
Table 4.15 - Input variables background of simulation number 7 .....	231
Table 4.16 - Input variables background of simulation number 8 .....	233
Table 4.17 - Input variables background of simulation number 9 .....	235
Table 4.18 - Input variables background of simulation number 10 .....	236
Table 4.19 - Input variables background of simulation number 11 .....	237
Table 4.20 - Input variables background of simulation number 12 .....	239
Table 4.21 - Input variables background of simulation number 13 .....	240
Table 4.22 - Input variables background of simulation number 14 .....	242
Table 4.23 - Input variables background of simulation number 15 .....	243
Table 4.24 - Input variables background of simulation number 15 (anode collector thickness values) .....	243
Table 4.25 - Input variables background of simulation number 16 .....	245
Table 4.26 - Input variables background of simulation number 17 .....	246

## LIST OF FIGURES

Figure 2.1 - Annual carbon emissions by region [2].....	6
Figure 2.2 - Oil pricing time evolution (the price is intended in US dollars per barrel) [5] .....	7
Figure 2.3 - Vehicle market shares trend [7] .....	8
Figure 2.4 - Traditional HEV architectures [4].....	12
Figure 2.5 - Parallel hybrid configuration scheme [10].....	12
Figure 2.6 - Parallel hybrid detailed configuration scheme [4] .....	13
Figure 2.7 - Belt drive and direct couple drive ISG configurations [12] .....	15
Figure 2.8 - Series hybrid configuration scheme [10] .....	17
Figure 2.9 - Series hybrid detailed configuration scheme [4].....	18
Figure 2.10 - Series hybrid configuration scheme [10] .....	19
Figure 2.11 - Toyota Hybrid Synergy Drive system [13].....	20
Figure 2.12 - Typical battery basic scheme [22].....	29
Figure 2.13 - Specific power and energy of different battery types [7].....	31
Figure 2.14 - Specific energy and energy density of different battery types [31] .....	38
Figure 2.15 - Transient and steady state comparison of the oil and air cooling solutions [34].....	42
Figure 2.16 - Passive cooling, outside air ventilation [34] .....	43
Figure 2.17 - Passive cooling/heating, cabin air ventilation [34] .....	43
Figure 2.18 - Passive cooling, liquid circulation [34].....	44
Figure 2.19 - Active moderate cooling/heating, liquid circulation [34] .....	44
Figure 2.20 - Active moderate cooling/heating, liquid circulation [34] .....	45

Figure 2.21 - Maximum discharge power dependence on temperature of a Panasonic prismatic 6.5 Ah NiMH module [33].....	45
Figure 3.1 - Vehicle speed profile of the ECE driving cycle .....	52
Figure 3.2 - Vehicle speed profile of the EUDC driving cycle .....	53
Figure 3.3 - Vehicle speed profile of the NEDC driving cycle.....	54
Figure 3.4 - Vehicle speed profile of the FTP-72 driving cycle .....	56
Figure 3.5 - Main control Simulink® interface of the Chrysler HEV prediction model ...	58
Figure 3.6 - Multi-points map interpolation system computing of the HVB open circuit voltage and internal resistance .....	64
Figure 3.7 - Start simulation button of the main Simulink® interface .....	69
Figure 3.8 - Typical “if/else” sub-block taken from the Simulink® library.....	70
Figure 3.9 - Example of internal combustion engine [45] .....	73
Figure 3.10 - Overall Simulink® structure of the internal combustion engine cooling system model .....	77
Figure 3.11 - Combustion heat rate computational block.....	79
Figure 3.12 - Combustion heat rate time trend .....	79
Figure 3.13 - Exhaust heat rate computational block .....	81
Figure 3.14 - Exhaust heat rate time trend.....	81
Figure 3.15 - Mechanical power computational block .....	83
Figure 3.16 - Mechanical power time trend.....	83
Figure 3.17 - Cabin heating system layout [48].....	84
Figure 3.18 - Cabin heater heat rate computational block .....	85
Figure 3.19 - Cabin heater heat rate time trend .....	86
Figure 3.20 - Engine wall, cooling medium and surrounding ambient simplified view....	88
Figure 3.21 - Surroundings heat rate computational block.....	91
Figure 3.22 - Surroundings heat rate time trend .....	91

Figure 3.23 - U-pattern radiator constructive scheme [56].....	93
Figure 3.24 - Radiator heat rate computational block.....	95
Figure 3.25 - Radiator heat rate time trend .....	96
Figure 3.26 - ECU signal to the thermostat time trend .....	97
Figure 3.27 - Coolant heat rate time trend .....	99
Figure 3.28 - Coolant temperature computational block .....	100
Figure 3.29 - Coolant temperature computational block (detail).....	100
Figure 3.30 - Engine coolant temperature time trend .....	102
Figure 3.31 - Internal combustion engine sub-block enclosed in the Chrysler HEV prediction model .....	104
Figure 3.32 - Toyota Prius 2nd generation NiMH battery pack [14].....	109
Figure 3.33 - Toyota Prius 1 <sup>st</sup> and 2 <sup>nd</sup> generation battery pack location [57].....	110
Figure 3.34 - FIAT 500e battery pack [58].....	111
Figure 3.35 - HVB cooling solutions .....	112
Figure 3.36 - Battery pack modules constructive configuration considered for the design of the battery thermal model .....	113
Figure 3.37 - Battery pack module and heat transfer directions .....	114
Figure 3.38 - Constructive and geometric characteristics of the battery cooling ducts ...	121
Figure 3.39 - Different layers constituting the internal layered structure of a cell .....	128
Figure 3.40 - Overall Simulink® structure of the battery cooling system model.....	134
Figure 3.41 - Reynolds and Prandtl numbers computational block (external view) .....	136
Figure 3.42 - Reynolds number computational block (internal view) .....	137
Figure 3.43 - Prandtl number computational block (internal view).....	137
Figure 3.44 - Logical block responsible for the determination of the flow regime type and for the computation of the Nusselt number.....	138

Figure 3.45 - Internal view of the logical block implementing the Petukhov and Popov correlation .....	138
Figure 3.46 - Convective heat transfer coefficient computational block .....	139
Figure 3.47 - Longitudinal overall and transverse heat transfer coefficients computational block (external view) .....	141
Figure 3.48 - Longitudinal overall and transverse heat transfer coefficients computational block (internal view) .....	141
Figure 3.49 - Overall structure of the coolant outlet temperature computational block (internal view) .....	147
Figure 3.50 - Overall structure of the coolant outlet temperature computational block (external view) .....	148
Figure 3.51 - Overall structure of the battery temperature computational block (internal view) .....	151
Figure 3.52 - Overall structure of the battery temperature computational block (external view) .....	152
Figure 3.53 - Battery and coolant temperature time trends (FTP-72 driving cycle).....	155
Figure 3.54 - Battery current profile (FTP-72 driving cycle, charge depleting mode)....	156
Figure 3.55 - Dissipated power time trend (FTP-72 driving cycle).....	157
Figure 3.56 - HVB “OCV” channel of the original Chrysler HEV prediction model .....	160
Figure 3.57 - HVB “OCV” channel of the updated Chrysler HEV prediction model.....	162
Figure 3.58 - HVB “Voltage Drop” block of the updated Chrysler HEV prediction model and internal view of the new thermal battery sub-model.....	164
Figure 3.59 - FEM thermal analysis of a typical battery prismatic module.....	167
Figure 4.1 - Chrysler 3.6-L Pentastar engine [61] .....	174
Figure 4.2 - Vehicle speed profile of the HWFET cycle .....	175
Figure 4.3 - Characteristic curves of the radiator coolant volume flow rate and engine angular speed .....	180

Figure 4.4 - Coolant mass flow rate flowing in the engine cooling circuit.....	182
Figure 4.5 - Vehicle speed profile of the “modified” FTP-75 driving cycle .....	184
Figure 4.6 - Combustion heat rate time trend .....	186
Figure 4.7 - Fuel mass flow rate injected in the engine cylinders .....	187
Figure 4.8 - Exhaust temperature at the outlet manifold.....	189
Figure 4.9 - Exhaust heat rate time trend.....	190
Figure 4.10 - Mechanical power time trend.....	191
Figure 4.11 - Cabin heater heat rate time trend .....	193
Figure 4.12 - Surroundings heat rate time trend .....	194
Figure 4.13 - ECU signal to the thermostat time trend .....	196
Figure 4.14 - Radiator heat rate time trend .....	197
Figure 4.15 - Coolant heat rate time trend .....	199
Figure 4.16 - Engine coolant temperature time trend .....	202
Figure 4.17 - Engine coolant temperature detail (seconds 1300/1900) .....	203
Figure 4.18 - Engine coolant temperature detail (seconds 2300/3200) .....	205
Figure 4.19 - Engine cooling model validation picture .....	207
Figure 4.20 - Engine cooling model validation picture detail (seconds 0/700) .....	209
Figure 4.21 - Engine cooling model validation picture with two highlighted sections ...	210
Figure 4.22 - Battery current profile (FTP-72 driving cycle, charge depleting and sustaining modes).....	213
Figure 4.23 - Upload procedure Matlab® code .....	216
Figure 4.24 - Output graph generated by the simulation number 1 .....	222
Figure 4.25 - Output graph generated by the simulation number 2 .....	224
Figure 4.26 - Output graph generated by the simulation number 3 .....	225
Figure 4.27 - Output graph generated by the simulation number 4 .....	227

Figure 4.28 - Output graph generated by the simulation number 5 .....	229
Figure 4.29 - Output graph generated by the simulation number 6 .....	230
Figure 4.30 - Output graph generated by the simulation number 7 .....	232
Figure 4.31 - Output graph generated by the simulation number 8 .....	233
Figure 4.32 - Output graph generated by the simulation number 9 .....	235
Figure 4.33 - Output graph generated by the simulation number 10 .....	237
Figure 4.34 - Output graph generated by the simulation number 11 .....	238
Figure 4.35 - Output graph generated by the simulation number 12 .....	239
Figure 4.36 - Output graph generated by the simulation number 13 .....	241
Figure 4.37 - Output graph generated by the simulation number 14 .....	242
Figure 4.38 - Output graph generated by the simulation number 15 .....	244
Figure 4.39 - Output graph generated by the simulation number 16 .....	245
Figure 4.40 - Output graph generated by the simulation number 17 .....	247
Figure 4.41 - Battery heat rate time trend computed during simulation number 17 .....	248
Figure 4.42 - Internal resistance and coolant volume flow rate contribution .....	252
Figure 4.43 - Cells dimensions and number contribution .....	253
Figure 4.44 - Dow Kokam SLPB 100216216H pouch cell geometry [65] .....	257
Figure 4.45 - Excitation current profile [65] .....	257
Figure 4.46 - Battery thermal model validation picture .....	258

## NOMENCLATURE

$A$	Battery external surface
$A_c$	Cross sectional area of the battery cooling system channels
$A_{CH}$	Cross sectional area of the cabin heater
$A_{eng}$	Engine external surface
$A_{L1}$	Minor cell surface facing the inlet side of the pack
$A_{L2}$	Minor cell surface facing the outlet side of the pack
$A_{T1}$	Major cell surface extended along the length of the module
$A_{T2}$	Major cell surface extended along the length of the module
$A_w$	Generic external surface
$C$	Coefficient used to convert a volume flow rate from gpm to l/s
$c_p$	Generic specific heat of a coolant
$c_{p\_c}$	Cell specific heat
$c_{p\_cool}$	Engine coolant specific heat
$c_{p\_coolB}$	Battery coolant specific heat
$c_{p\_ex}$	Exhaust specific heat
$d$	Distance existing between two adjacent cells of the pack
$D_h$	Hydraulic diameter of the battery cooling system channels
$h$	Height of the cells
$h_a$	Air convective heat transfer coefficient
$h_c$	Engine coolant convective heat transfer coefficient



$h_{cool}$	Battery coolant convective heat transfer coefficient
$h_f$	Convective heat transfer coefficient of the fluid
$I$	Electric current
$k$	Thermal conductivity of the fluid
$k_{an}$	Anode current collector thermal conductivity
$k_B$	Battery thermal conductivity
$k_{cat}$	Cathode current collector thermal conductivity
$k_i$	Thermal conductivity of a battery layer
$k_L$	Battery longitudinal thermal conductivity
$k_{sep}$	Polymeric separator thermal conductivity
$k_T$	Battery transverse thermal conductivity
$k_w$	Engine wall thermal conductivity
$l$	Length of the cells
$L$	Typical length of the investigated system
$L_{an}$	Anode current collector thickness
$L_{cat}$	Cathode current collector thickness
$L_i$	Thickness of a battery layer
$L_{sep}$	Polymeric separator thickness
$LHV$	Fuel lower heating value
$\dot{m}$	Generic coolant mass flow rate
$\dot{m}_{air}$	Air mass flow rate entering the cylinders
$\dot{m}_{air\_CH}$	Air mass flow rate passing through the cabin heater

$m_b$	Blue line angular coefficient (Figure 4.3)
$m_c$	Cell mass
$\dot{m}_{cool}$	Engine coolant mass flow rate
$\dot{m}_{coolB}$	Battery coolant mass flow rate flowing around a single cell
$\dot{m}_{coolB\_TOT}$	Battery overall coolant mass flow rate
$\dot{m}_{coolR}$	Engine coolant mass flow rate entering the radiator
$\dot{m}_{exhaust}$	Exhaust mass flow rate
$\dot{m}_{fuel}$	Fuel mass flow rate entering the cylinders
$m_r$	Red line angular coefficient (Figure 4.3)
$n$	Engine angular speed [rpm]
$N_c$	Number of cells contained in the pack
$n_l$	Number of layers constituting a battery module
$Nu$	Nusselt number
$P$	Mechanical power
$P_{diss}$	Power dissipated as heat for Joule effect
$Pr$	Prandtl number
$P_w$	Wetted perimeter of the engine cooling system channels
$\dot{q}$	Generic heat flux
$\dot{Q}$	Generic heat rate
$\dot{Q}_{combustion}$	Combustion heat rate
$\dot{q}_{cond}$	Conductive heat flux
$\dot{q}_{conv}$	Convective heat flux

$\dot{Q}_{coolant}$	Coolant heat rate
$Q_{ev}$	Fuel heat of vaporization
$\dot{Q}_{heater}$	Cabin heater heat rate
$\dot{Q}_L$	Longitudinal heat rate battery/coolant
$\dot{Q}_{L1}$	Longitudinal heat rate battery/coolant at the pack inlet side
$\dot{Q}_{L2}$	Longitudinal heat rate battery/coolant at the pack outlet side
$\dot{Q}_{radiator}$	Radiator heat rate
$\dot{Q}_{surrounding}$	Surroundings heat rate
$\dot{Q}_T$	Transverse heat rate battery/coolant
$\dot{Q}_{T1}$	First transverse heat rate battery/coolant
$\dot{Q}_{T2}$	Second transverse heat rate battery/coolant
$R$	Electrical resistance
$Re$	Reynolds number
$T$	Torque generated at the engine crankshaft
$T_1$	Generic coolant initial temperature
$T_2$	Generic coolant final temperature
$T_a$	Ambient temperature
$T_{amb}$	Ambient temperature
$t_B$	Battery thickness considered from the medium point of the cell
$T_B$	Battery temperature considered at the medium point of the cell
$T_{B\_actual}$	Battery temperature (actual iteration)
$T_{B\_prev}$	Battery temperature (previous iteration)

$t_{BL}$	Battery longitudinal thickness
$t_{BT}$	Battery transverse thickness
$T_c$	Engine coolant temperature
$T_{cool}$	Battery coolant temperature
$T_{cool\_actual}$	Engine coolant temperature considered at the actual iteration
$T_{cool\_IN}$	Battery coolant inlet temperature
$T_{cool\_M}$	Battery coolant temperature at the midpoint of the cell length
$T_{cool\_OUT}$	Battery coolant outlet temperature
$T_{cool\_prev}$	Engine coolant temperature considered at the previous iteration
$T_{cOUT\_actual}$	Battery coolant outlet temperature (actual iteration)
$T_{cOUT\_prev}$	Battery coolant outlet temperature (previous iteration)
$T_{exhaust}$	Exhaust temperature
$T_{fresh}$	Fresh charge temperature
$T_{rad\_IN}$	Coolant temperature at the inlet section of the radiator
$T_{rad\_OUT}$	Coolant temperature at the outlet section of the radiator
$T_s$	Battery temperature considered at the surface of the cell
$t_w$	Engine wall thickness
$T_{wa}$	Engine ambient-side surface temperature
$T_{wc}$	Engine coolant-side surface temperature
$u$	Velocity of the fluid
$U$	Overall heat transfer coefficient battery/coolant
$u_{coolB}$	Battery coolant speed

$U_L$	Overall longitudinal heat transfer coefficient battery/coolant
$U_{surrounding}$	Overall heat transfer coefficient engine/surroundings
$U_T$	Overall transverse heat transfer coefficient battery/coolant
$v$	Vehicle linear speed
$\dot{V}_{coolR}$	Engine coolant volume flow rate entering the radiator
$w$	Width of the cells
$w_m$	Factor linking the engine speed and the radiator coolant rate
$\alpha$	Thermal diffusivity of the fluid
$\alpha_{stoich}$	Stoichiometric air-to-fuel ratio
$\eta_{combustion}$	Combustion efficiency
$\lambda$	Lambda sensor signal
$\mu$	Dynamic viscosity of the fluid
$\nu$	Kinematic viscosity of the fluid
$\rho$	Density of the fluid
$\rho_{air}$	Air density
$\rho_{cool}$	Engine coolant density
$\rho_{coolB}$	Battery coolant density
$\omega$	Engine angular speed [rad/s]

## ABBREVIATIONS

ABS	Antilock brake system
AC	Alternating current
BEV	Battery electric vehicle
BSG	Belt starter generator
CAD	Computer-aided design
CO <sub>2</sub>	Carbon dioxide
DC	Direct current
DOD	Depth of discharge
ECE	Economic Commission for Europe
ECU	Electronic control unit
EPA	US Environmental Protection Agency
EUDC	Extra-Urban Driving Cycle
EV	Electric vehicle
FEM	Finite element method
FTP	Federal Test Procedure
H <sub>2</sub> SO <sub>4</sub>	Sulfuric acid
HC	Unburned hydrocarbons
HEV	Hybrid electric vehicle
HHV	Higher heating value
HVB	High voltage battery

HWFET	Highway Fuel Economy Driving Schedule
ICE	Internal combustion engine
IGBT	Insulated-gate bipolar transistor
ISG	Integrated starter generator
LHV	Lower heating value
Li-Ion	Lithium-ion
Li-P	Lithium-polymer
MG1	Toyota Prius secondary starter/generator motor
MG2	Toyota Prius primary drive/regeneration motor
MOSFET	Metal-oxide-semiconductor field-effect transistor
NEDC	New European Driving Cycle
Ni-Cd	Nickel-cadmium
NiMH	Nickel-metal hydride
NO <sub>x</sub>	Nitrogen oxides
NREL	US National Renewable Energy Laboratory
NVH	Noise, vibration and harshness
OCV	Open circuit voltage
Pb-acid	Lead-acid
PbO <sub>2</sub>	Lead dioxide
PHEV	Plug-in hybrid electric vehicle
RBS	Regenerative braking system
SOC	State of charge

SOH	State of health
UDC	Urban Driving Cycle
UDDS	Urban Dynamometer Driving Schedule
US	United States of America
VRLA	Valve regulated lead-acid



# CHAPTER 1

## INTRODUCTION

The continuous worldwide diffusion of vehicles, intended as means of personal transportation, has led to the development of several studies aimed at analyzing the effects of the actual automotive technologies on the health of the environment. These studies have underlined that the current personal transportation system is not sustainable in the long run, not only because it relies heavily on non-renewable energy sources, but also because it dramatically affects the natural equilibrium of the earth's climate. The most widespread automotive propulsion technology, in fact, is based on the use of internal combustion engines that burn mixtures of air and fossil fuels that, ignited and oxidized, produce noxious gases, like nitrogen oxides and unburned hydrocarbons, and notable amounts of carbon dioxide. The noxious emissions are the major cause of air pollution, which ultimately affects human health, while the CO<sub>2</sub> is considered the cause of the so-called greenhouse effect, responsible for global temperature increases and dangerous climate instability in many parts of the world. Moreover, conventional engine-powered vehicles are characterized by a poor overall efficiency that leads to the waste of most of the energy created through the burning process and by considerably high levels of fuel consumption. All these issues make it clear that the automotive companies must satisfy the increasing demand of personal transportation in a sustainable way, investigating alternative environmentally friendly energy sources and designing new vehicle solutions that have high performance and are more efficient. In this regard, car makers have started to develop and produce battery and hybrid electric vehicles, trying to substitute the fossil fuel/engine system with a battery/electric motor propulsion technology, capable of reducing the fuel consumption and emissions levels. However, there are a lot of technical and economical difficulties that are slowing down the transition process from a fossil fuel-based to an electricity-based transportation system; hence, advanced research and studies on the pure electric and hybrid vehicle technologies are conducted.

In this context, the present thesis project has been realized in the Electrified Powertrain department at Chrysler that is currently working on the development of advanced hybrid electric vehicle (HEV) models, economically attractive for the customer and characterized by a reduced fuel consumption and emission level. The design activity is realized by the research and development teams of the department using predictive tools that simulate the performance and fuel economy of the new hybrid models during the early project stages. These tools must be characterized by optimized computational and logical architectures and, finally, they have to represent every operating aspect of the investigated hybrid model.

## **1.1 Objectives**

The availability of predictive software capable of simulating the overall behaviour of new vehicle models, has a relevant role in the design process of automotive products. Dealing with hybrid vehicles, in particular, huge amounts of money are invested in the creation of innovative electrified drivetrain solutions and, hence, accurate analyses are necessary to determine if the projects are going to meet the targets defined in terms of fuel consumption and performance levels. In particular, understanding if the design activity is evolving in the correct direction is very important; in fact, it gives to the research and development teams the opportunity to implement eventually necessary modifications to the project in its early stages, when updates and revisions are less expensive to realize.

At this point, it can be underlined that the main objective of the thesis is to create two prediction tools capable of simulating the thermal behaviour of the internal combustion engine (ICE) and high voltage battery (HVB) devices, respectively, that equip the HEV model being investigated, virtually tested while running a certain driving cycle. The Electrified Powertrain department at Chrysler, in fact, conducts in the early design stage virtual analysis on the new hybrid models, using a powerful prediction software that simulates the vehicle behaviour given an input speed profile of excitation. In order to obtain accurate predictions, the software has to represent every operating aspect of the whole vehicle system, considering the mechanical, electrical and thermal phenomena. In this regard, it must be stated that the Chrysler HEV simulation tool is not

provided with computational structures that simulate the thermal behaviour of the engine and the battery, whose temperature time trends are not determined during the driving cycle. The temperature levels of the ICE and HVB, however, strongly affect the performance and fuel economy of the vehicle and hence a thorough representation of their cooling systems is necessary to obtain accurate and precise simulation results. The implementation of two new thermal models to be added to the whole HEV prediction tool, assumes in this way a decisive role for a complete and comprehensive description of the vehicle operating features.

The second main objective of the thesis is finally related to the use of the battery thermal software as an autonomous tool, activated to perform a sensitivity study and individuate the most important factor affecting the thermal behaviour of the modules constituting the battery pack. Running a sequence of simulations changing the magnitude of the input variables, several scenarios are depicted to understand the influence of the geometry and electrochemistry of the cells and of the type of cooling system on the heat exchange phenomena taking place inside the pack.

To sum up, the architecture of the project is organized on the basis of the following pillars, built step by step during the internship at Chrysler:

1. design the engine and battery cooling system models using the Matlab® and Simulink® virtual platforms;
2. validation of the new software managed through a comparison of simulated and experimental temperature time trends;
3. integration of the tools in the overall Chrysler prediction software;
4. simulation phase completed through the battery thermal model to realize a thorough sensitivity study.

## **1.2 Thesis organization**

The thesis is organized in five chapters, which are briefly described in the following paragraphs.

Chapter 1 introduces the overall project, underlining the role of the hybrid technology in the actual worldwide automotive market and presenting the objectives and organization of the thesis.

Chapter 2 contains a detailed literature survey related to HEV world and, in particular, to battery technology. First of all, the current scenario of personal transportation is depicted, highlighting the negative effects caused by the use of fossil fuels. Then, in this regard, the ameliorations involved by vehicle hybridization are described, together with the typical features and drivetrain configurations offered by HEV technology. Finally, different types of battery chemistry are investigated and a detailed study of the most important battery pack cooling solutions is realized.

Chapter 3 analyzes the complete design and modeling activity of the thesis research. It is divided in two main sections: the first one related to the creation of the engine cooling system model and the second one to the creation of the battery thermal software. Both the models are described in detail, focusing the attention on the background theory and thermophysical equations used to build their basic structure. Then, a deep analysis of the logical and computational Simulink® architectures is performed, highlighting the main features offered by the tools. Finally, the integration procedure is described with the objective to compare the predictions' accuracy level offered by the original and updated versions of the overall Chrysler simulation software.

Chapter 4 provides the results of the project and their thorough analysis. Firstly, the outputs variables generated by the newly designed ICE cooling model, activated to investigate the behaviour of a Chrysler 3.6-L Pentastar engine, are presented and studied. Then, the battery thermal software is used to simulate the temperature time trend of a typical nickel-metal hydride battery pack with specific electric, geometrical and thermal characteristics and to perform an advanced sensitivity study. Finally, the validation steps completed for both the models are described, underlining which are the innovations introduced by the two thermal software.

Chapter 5 presents, in the end, the conclusions and the recommendations. The ICE and HVB thermal model designs are summarized and the main results are reported once again. Future activities and studies are proposed to further develop the research on the basis of the target already reached.

# **CHAPTER 2**

## **LITERATURE REVIEW**

### **2.1 Latest developments in the worldwide automotive scenario**

To understand why, in the 21<sup>st</sup> century, the electric and hybrid electric vehicle technologies have generated such a high level of interest in the worldwide automotive companies and, at the same time, amongst customers, it is necessary to analyze the evolution that personal transportation has experienced in the last years. Nowadays, world globalization has led people to travel more, and to cover larger distances, than in the past and this phenomenon has been supported by technological progress in the transportation fields and infrastructure. Moreover, the increasing welfare state that has been established after War World II, has made possible that in the developed nations almost all the population can afford to buy means of personal transportation. As a consequence, there has been a continuous growth in the number of automobiles produced and sold worldwide; while the average number of vehicles sold during the 1990's was 39.2 millions of units, in 2012, 62.4 million cars have been sold all over the world and the forecasted value for 2013 is 4.2% higher [1].

However, a significant problem affects the current personal transportation system since it relies on oil to produce the energy and power necessary to obtain the motion of the vehicle. In this regard, it has to be underlined that petroleum resources are limited and are going to finish in the near future (probably next century) and that, moreover, the oil burning products lead to negative climate changes, corrupting the air quality and the overall health of the environment.

#### **2.1.1 Environmental effects of fossil fuels**

Hence, the dependence of the transportation system on oil introduces a great challenge relative to environmental problems and global climate changes. The emissions from burning fossil fuels increase the carbon dioxide (CO<sub>2</sub>) concentration in the atmosphere, leading to the so-called greenhouse effect that determines an excessive heat

absorption of the earth surface and to a consequent global temperature increase and dangerous climate instability. Figure 2.1 depicts the trend of carbon dioxide emissions from fossil fuels in the last two centuries in the different regions of the world: it can be seen that the most dramatic increase has happened starting around 1950, when petroleum became the most important energy source used for human activities.

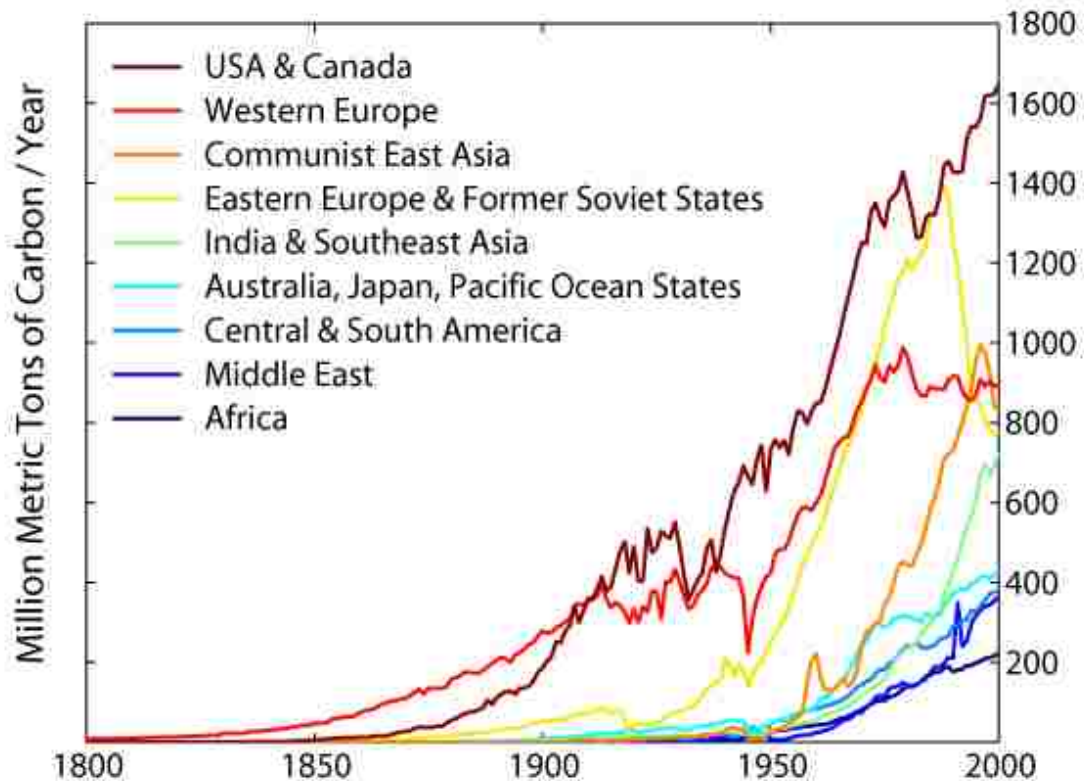


Figure 2.1 - Annual carbon emissions by region [2]

In 2008, 30.19 billion tons of CO<sub>2</sub> were released in the atmosphere, 37% which was due to oil burnt all over the world for personal and industrial applications [3]. The carbon dioxide atmospheric concentration, in particular, is continuously increasing year after year, leading to a thicker and denser atmosphere that, finally, represents the primary cause for global warming, the rise in the average temperature of earth's atmosphere and oceans that took place since the late 19<sup>th</sup> century. This phenomenon is related to the greenhouse effect, defined as the process by which thermal radiation from the earth's surface is absorbed by the greenhouse gases and is radiated again in all directions; since part of this

radiation is back towards to the ground, it results in an abnormal elevation of the average surface temperature.

Moreover, it has to be remembered that not only the CO<sub>2</sub> is generated by the combustion process that takes place inside the engines: also noxious gases such as nitrogen oxides (NO<sub>x</sub>) and unburned hydrocarbons (HC) are emitted during engine operations and they are cause of many human health problems, in particular related to the respiratory system [4]. In total, vehicles are responsible for the 32% and 27% of all hydrocarbons and nitrogen oxides, respectively, released into the atmosphere annually.

### 2.1.2 Sustainable transportation solutions

At this point, it can be stated that the current personal transportation system is not sustainable in the long run, because of the environmental problems associated with the use of fossil fuels that, moreover, are showing a considerable decrease in their overall quantity still available to be extracted and refined. Figure 2.2 represents the price trend shown by petroleum in the last 20 years that, because of its shortage and increasing demand, has experienced a steep rise, in particular starting from the new century.

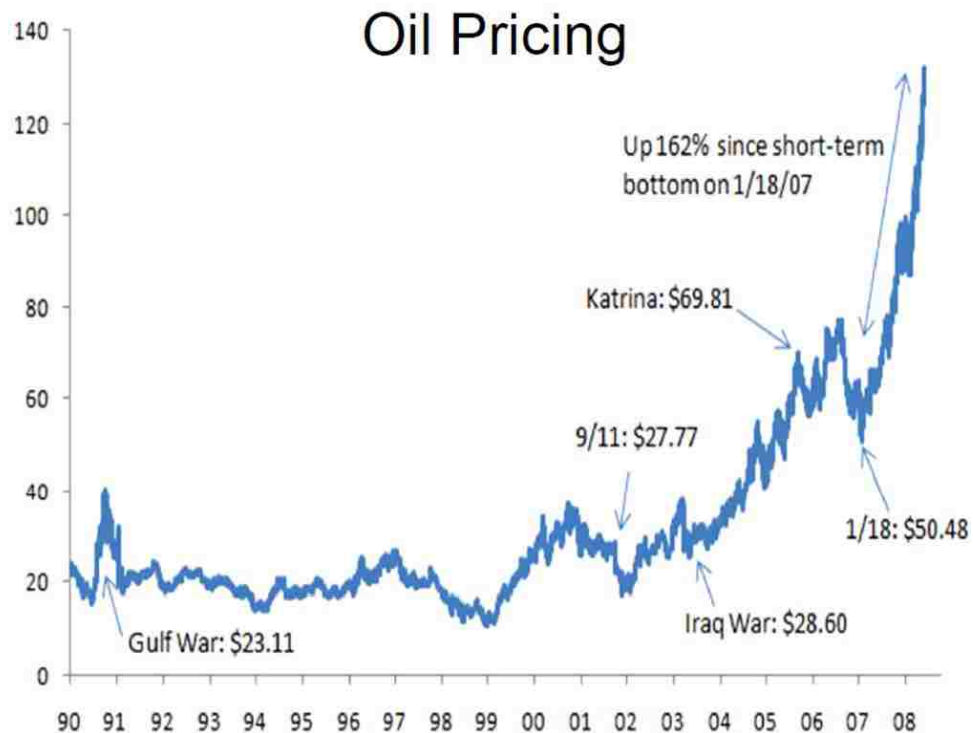


Figure 2.2 - Oil pricing time evolution (the price is intended in US dollars per barrel) [5]

Hence, alternative energy sources must be found to allow the development of an advanced transportation fleet, capable of reducing the level of emissions typical of vehicles equipped with internal combustion engines that work burning considerable quantities of fossil fuels. A viable pathway to sustainable transportation is a global transition to vehicles driven only by electricity generated from clean and renewable energies, produced from hydroelectric, wind, solar and biomass sources. However, today’s battery electric vehicles (BEV) have several technological limits, such as reduced driving range and long charging time, as well as high battery cost; this makes decisive the development of an intermediate step towards the full electrification of the transportation sector, represented by the hybrid electric vehicles (HEV), which use both an internal combustion engine (ICE) and an electric motor to produce the power required to drive the vehicle [6]. Still based on the use of the ICE, HEVs have the capability of significantly reducing fuel consumption and pollutant emissions thanks to the advanced features offered by the “electric side” of the car. A further solution is represented by plug-in hybrid electric vehicles (PHEVs), which are equipped with a larger battery pack that can be charged from the grid and allows the car to be driven for a limited distance (30-60 km) using electricity only and, hence, without consuming fuel and emitting noxious and greenhouse gases in the atmosphere.

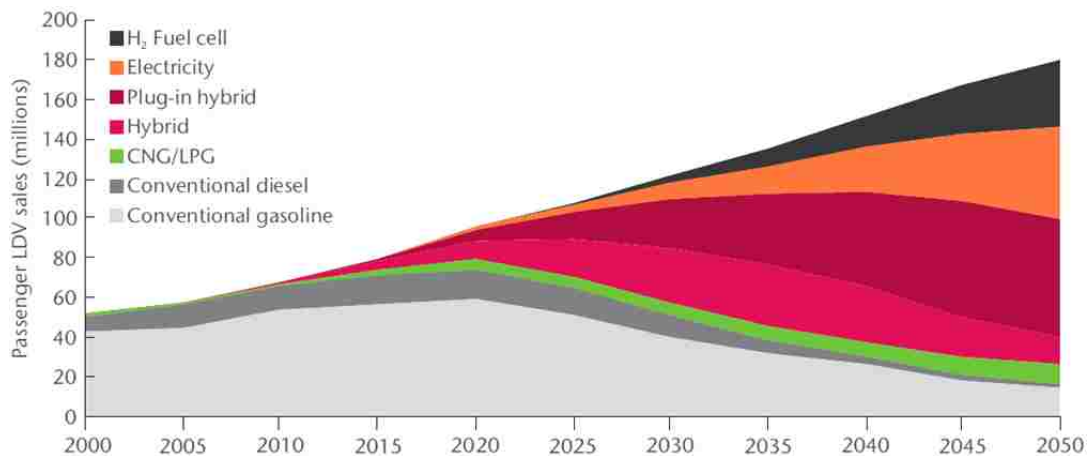


Figure 2.3 - Vehicle market shares trend [7]

Considering the new electric and hybrid vehicles described in the previous paragraph, the conventional gasoline and diesel cars, the compressed natural gas and



liquefied petroleum solutions and, finally, the advanced fuel cell automotive models, Figure 2.3 can be depicted to analyze the past, actual and forecasted future market shares covered by the different propulsion systems; in particular it can be seen that, starting from 2025, the HEV and BEV technologies will experience a very aggressive rate of market penetration [7]. Hence, in general, the next generation of personal transportation vehicles will rely on hybridization to realize gains in fuel efficiency and reduced emissions; hybrid electric power trains are becoming, in fact, well-accepted near-term solutions to the global concerns over CO<sub>2</sub>. This means that a paradigm shift is now in progress within the global automotive industry [4].

## **2.2 Innovative features introduced by vehicle hybridization**

It is important to focus the attention on the innovative features provided by hybridization, that allow to obtain an improved fuel economy and a general lowered emissions level. The main powertrain features introduced by the hybrid electric vehicles are presented and described as follows.

- **Start and stop function:** it conserves fuel by not burning it for non-propulsion events. Fuel conservation is obtained by shutting off the engine fuel supply during decelerations and by completely switching off the engine during stop events, followed by an ICE restart managed by the electric motor.
- **Torque augmentation:** since one or more electric motors are present in the power train, it is possible to obtain a torque boost from their shaft when requested by the driver, for example during passing maneuvers. The torque response of the electric motor, moreover, is generally faster than that of the ICE and results in a rapid increment of the torque sent instantaneously to the wheels. The torque augmentation offered by the electric motor, furthermore, makes possible to equip the HEV with a downsized engine, characterized by lower levels of fuel consumption and emissions.
- **Regenerative braking:** this feature allows recovery of the kinetic energy of the vehicle during braking actions, avoiding losses to the external environment as heat through the braking pads. The kinetic energy is converted by the system into electric, thanks to the electric motor that switches to generator mode and sends the

energy to the HEV's battery pack. The regenerative braking system (RBS) must be managed by the antilock brake system (ABS) simultaneously with the conventional mechanical brake, in order to provide the exact braking torque requested by the driver and to avoid delivering too much energy to the battery, exceeding its electric operational limits.

### **2.2.1 Fuel consumption and emission levels reductions**

Thanks mainly to the three features described in the previous section, the hybrid electric vehicles typically achieve an improved fuel economy and lower emission levels than conventional internal combustion engine vehicles. In fact, the possibility to use a smaller engine, characterized by less internal losses and lower weight, to recover the kinetic energy normally lost at the brake pads and, finally, to shut down the engine during traffic stops and idle periods, makes the HEV technology achieve a considerably high reduction in the fuel consumption and in the consequent generation of greenhouse and noxious gases.

In particular, hybrid vehicle emissions today are getting close to or even lower than the recommended level set by the US Environmental Protection Agency (EPA), which was created in 1970 for the purpose of protecting human health and the environment by writing and enforcing regulations based on laws passed by Congress [8]. The maximum betterment involved by HEVs settles, in fact, at 90% of NO<sub>x</sub> and HC reduction and to halved carbon dioxide emissions [9].

### **2.2.2 Environmental impact of hybrid car batteries**

Though hybrid cars are more environmentally friendly than conventional cars, there is an important issue to be considered regarding the environmental damage of the hybrid car battery. The most widespread battery solution today is represented by the nickel-metal hydride (NiMH) or lithium-ion (Li-Ion) technology, more effective and less toxic than the lead-acid one which is used for the typical starter batteries of conventional vehicles. In general, the toxicity level of the battery modules must be carefully taken into account to organize the disposal of the battery packs at the end of their life and, in this regard, it

has to be taken into account that batteries such as the nickel-cadmium can cause teratogenic effects.

## **2.3 Hybrid drivetrains**

Taking advantage of the high energy density of petroleum fuels, conventional internal combustion engine vehicles provide good performance and long operating range. However, they also have the disadvantages of poor fuel economy and environmental pollution caused by notable mismatched engine fuel efficiency characteristics with the vehicle operation requirements, significant amount of energy dissipation in braking especially while operating in urban areas, and low efficiency hydraulic transmissions stop and go driving patterns [4]. Battery-powered electric vehicles, on the other hand, shows some advantages over conventional ICE vehicles, like high energy efficiency and zero environmental pollution. But the overall performance, especially the operating range per battery charge, are far less than that of conventional vehicles, due to the lower specific energy content of the batteries with respect to the specific energy content typical of gasoline. Hybrid electric vehicles, which use both the thermal and electric power sources, are characterized by the main advantages of both the conventional and electric vehicles and can overcome their disadvantages.

### **2.3.1 General concepts about hybrid vehicle drivetrains**

A hybrid vehicle drivetrain consists of two power sources: at present, internal combustion engines represent the first selection for the primary power source (perhaps they will be substituted by the fuel cells in the future) while the secondary power source is constituted by the electric motor and related components. The architecture of a hybrid vehicle is defined on the basis of the connection between the main components that define the energy flow routes inside the system. Traditionally, HEVs are classified into three basic types, functionally shown in Figure 2.4: series, parallel and series-parallel or combination.

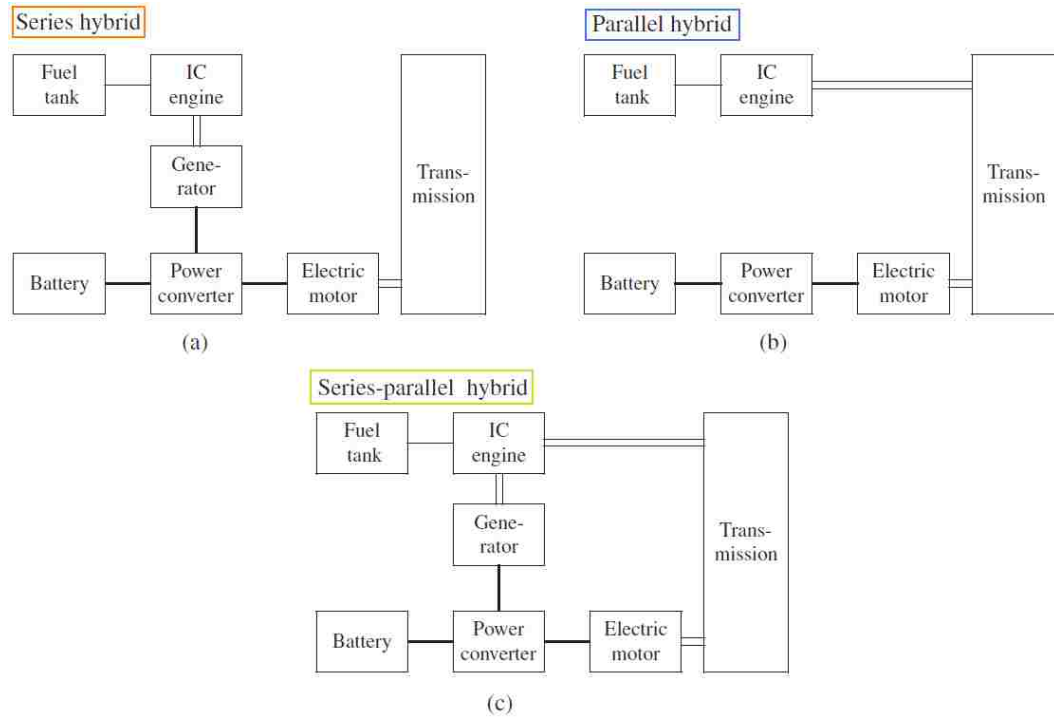


Figure 2.4 - Traditional HEV architectures [4]

### 2.3.2 Parallel configuration

Parallel hybrid systems, which are most commonly produced at present, have both the internal combustion engine and the electric motor directly coupled with the transmission shaft; the typical parallel configuration of the HEV components is depicted in Figure 2.5.

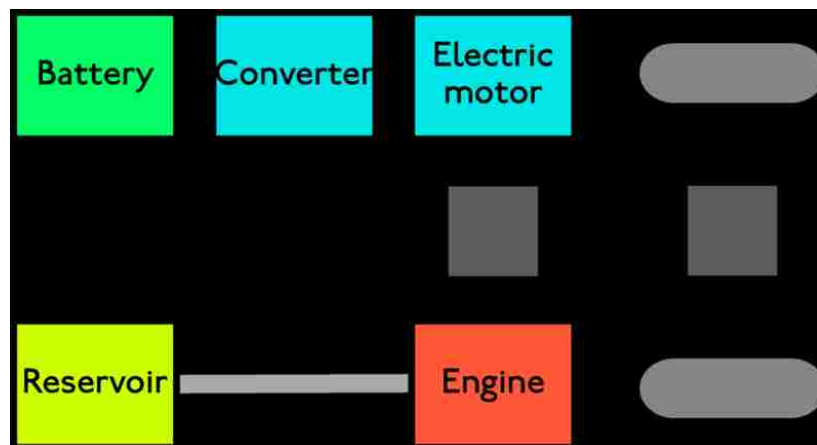
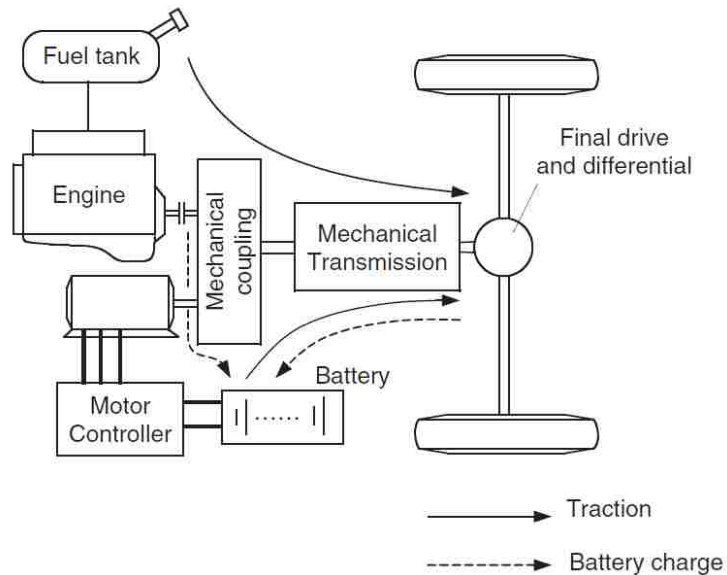


Figure 2.5 - Parallel hybrid configuration scheme [10]

The rotational speeds of the two energy sources are equal and their torques are combined, with the electric motor adding or subtracting its contribution to the system as necessary [10]. Dealing with parallel hybrids, the concept of electric fraction, a metric used to characterize what proportion of the total peak driveline power is supplied via the electric machine, must be investigated. It is defined as the ratio of the electric motor peak power to the sum of both the peak power contributions. For example, a parallel hybrid having a 60 kW ICE and a 40 kW electric motor has an electric fraction equal to the 40% [4]. Hence, while a series hybrid drivetrain couples primary and secondary power sources together electrically (as it will be discussed later), a parallel hybrid drivetrain couples them together mechanically: the ICE supplies its power to the wheels as in a conventional vehicle but now it is assisted by an electric motor that, like the engine, is connected to the transmission by means of a mechanical coupling, as shown in Figure 2.6.



**Figure 2.6 - Parallel hybrid detailed configuration scheme [4]**

Parallel hybrids can be further categorized depending on how balanced the thermal and electric portions are at providing motive power. In some cases, the combustion engine is dominant and the electric motor provides only a boost action; in other cases, the vehicle can run with the only electric system operating for a limited distance.

Usually, in parallel hybrids, the electric motor can operate also as a generator and is located between the ICE and the transmission, substituting both the starter and the

alternator. This technology takes the name of integrated starter generator (ISG) and it can be characterized by two different configurations, that are going to be described in the following sections; the features of this system rely in the possibility to provide a start-stop function, to realize regenerative braking actions and to assist the ICE when requested.

### **2.3.2.1 Parallel hybrid strengths**

The advantages offered by this system are represented by the possibility to run the vehicle using the electric motor at low gears (the ones that determine the highest fuel consumption of the engine) and to eliminate the fuel burning when the vehicle is stopped, thanks to a complete engine switch off. Moreover, since the thermal motor can be supported by the electric one, it can be downsized with cost and weight benefits; generally speaking, engine downsizing becomes possible when the electric fraction exceeds approximately the 20%, involving considerable fuel economy gains. This hybrid configuration is so preferred for city vehicles and not for long distance applications. Moreover, the parallel hybrid architecture is widely used because the vehicle propulsion architecture is not very different from the one of a conventional vehicle: the addition of the “electric side” seems like a pure overlay but, unfortunately, integrating an electric machine into the vehicle’s transmission requires considerable redesign cost and time that must be taken into account.

### **2.3.2.2 Description of the integrated starter generator**

When a single electric machine is used to carry out both functions of the starter and the alternator, it is generally called an integrated starter generator. The ISG is a typical mild parallel hybrid technology that aroused increasing interest in the last decade for its characteristics of fuel economy improvement, low weight and low cost. With this system, the functions of engine start-up and on-board generation of electric energy are fulfilled by an electric machine alone, instead of the separated conventional starter and alternator.

The reciprocal operating principle of the electric machines, which can be used both in motoring and generating mode, is complicated by the difficulties related to the control of the whole system; this complication has been solved, in recent times, with the developments in the field of AC electric machines and power electronics that have made

the ISG system feasible for implementation in vehicle powertrains. The ISG device, together with its associated electronics and battery pack, has the ability to perform many functions, including engine start-stop, regenerative braking actions, electric torque boost, early fuel cut-off and higher efficiency electric energy generation [11].

The ISG system configuration depends on the location of the electric machine in the powertrain and on its connection to the engine crankshaft; there are mainly two packaging options, characterized by two different drive solutions: the direct coupled drive and the belt drive, represented in Figure 2.7.

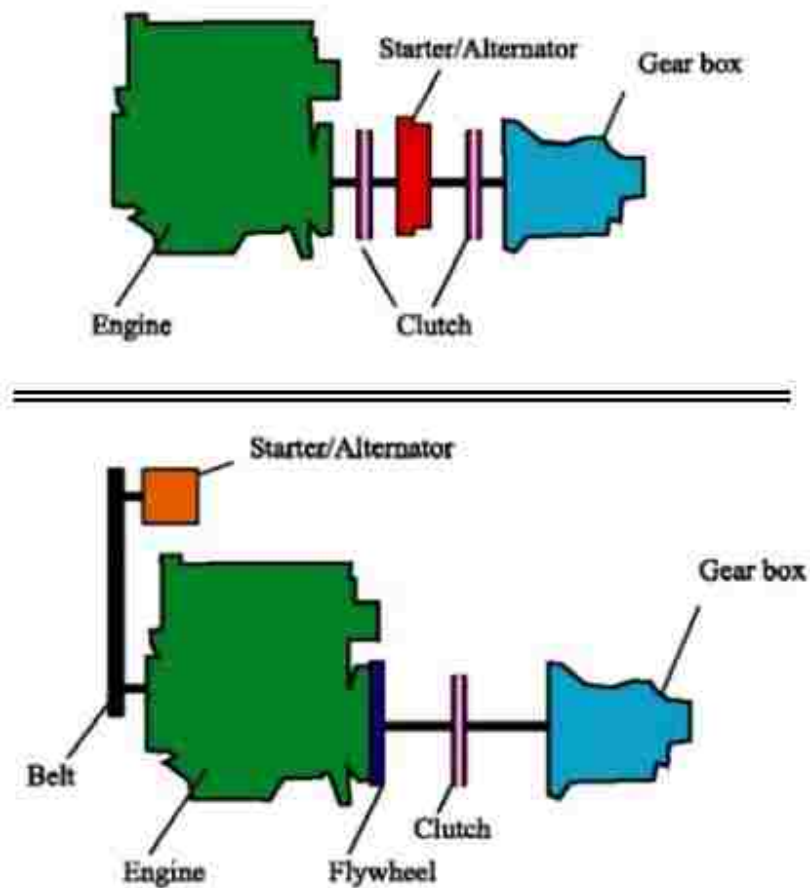


Figure 2.7 - Direct couple drive and belt drive ISG configurations [12]

In the first solution, the electric machine is placed directly on the crankshaft, either between the transmission and the engine, in the location of the flywheel, or on the accessory side. Including the electric motor on the crankshaft eliminates the need of other mechanical engagement mechanisms and their associated losses, thus reducing the

number of system components and increasing the whole reliability. Depending on the design, the direct coupling may also enable the replacement of the flywheel by the machine rotor, further reducing component requirements. However, when powertrain packaging is an important issue, such as in vehicles with transverse engine arrangement, the direct coupling is critical in both the configurations because the powertrain length has to be increased to accommodate the electric machine.

The second solution, usually called belt starter generator (BSG), is probably the most convenient in terms of packaging, since the connection between electric motor and crankshaft is realized on the accessory side either including the electric machine in the existing accessory drive or using a separate dedicated belt drive [11]. The former requires an increase in the belt and pulley widths, in order to accommodate the increased load capacity; the latter instead requires extending the crankshaft in order to install the dedicated belt that, moreover, involves extra costs. In general, the BSG is characterized by low cost, minimal modifications in the existing powertrain design, more freedom in packaging, no lubrication required and very low noise generation.

### **2.3.3 Series configuration**

Series hybrids are characterized by the direct connection of the electric motor to the transmission, as can be seen from Figure 2.8, with the internal combustion engine not coupled with the transmission but with the “electric side” of the vehicle, in order to manage the generation of the electric energy necessary to recharge the battery and to activate the electric machine. A series hybrid drivetrain, in particular, is characterized by the presence of two power sources feeding the electric motor that directly propels the vehicle. The typical primary power source is ICE, coupled to an electric generator turned by the engine shaft to produce a three phase electric energy; the output of the generator is routed through an electric power bus to an electronic converter (rectifier), that performs an AC/DC conversion sending the energy to the battery pack. Battery represents the secondary power source of the system, connected to the bus by means of a power electronics DC/DC converter, directly linked to the electric traction motor that, finally, can be controlled either as a motor or a generator, either in forward or reverse motion.



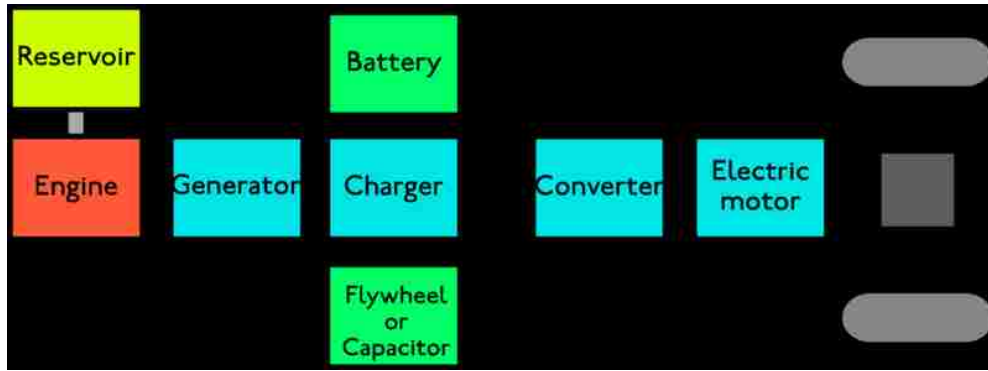


Figure 2.8 - Series hybrid configuration scheme [10]

Carefully analyzing Figure 2.9, it is possible to list the different operating modes potentially offered by the series hybrid electric drivetrains [4].

- Pure electric mode: the engine is turned off and the vehicle is propelled only from the batteries.
- Pure engine mode: the vehicle electric traction power comes only from the generator activated by the ICE, while the batteries do not supply any power to the drivetrain; the electric machine, in other words, serves as an electric transmission from the engine to the wheels.
- Hybrid mode: the traction power is drawn from both the ICE-activated generator and the battery pack.
- Engine traction and battery charging mode: the generator, powered by the engine, supplies energy to charge the batteries and to propel the vehicle.
- Regenerative braking mode: the electric motor switches to the generator mode and recovers the kinetic energy from the wheels through its conversion to electrical energy (then stored in the battery), a process which in turn is able to slow down the vehicle preventing waste of its kinetic energy as heat within the friction brakes.
- Battery charging mode: the electric motor receives no power from the ICE-activated generator that, on the contrary, is charging the batteries.
- Hybrid battery charging mode: both the ICE-activated generator and the electric motor (working as generator) charge the batteries during braking events.

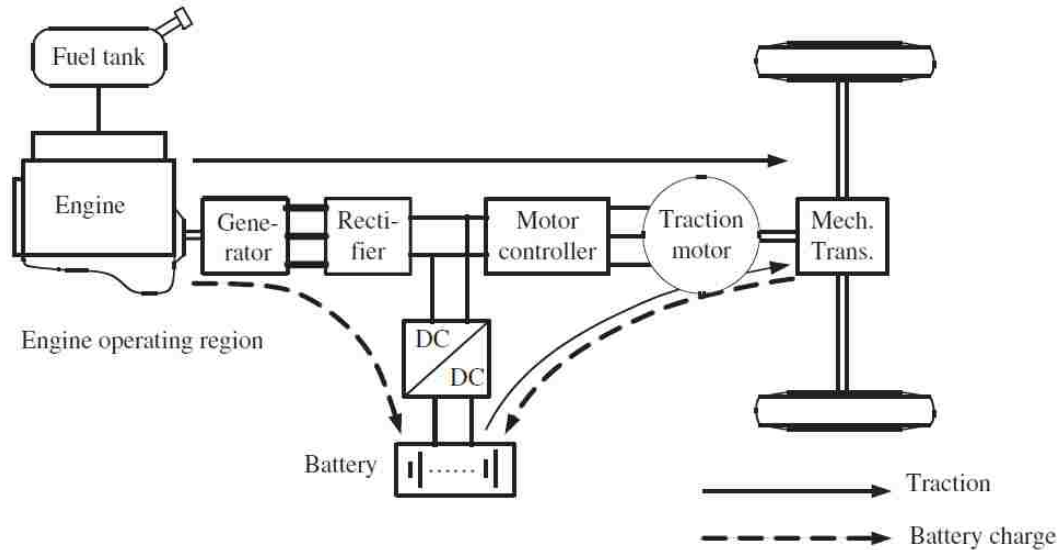


Figure 2.9 - Series hybrid detailed configuration scheme [4]

### 2.3.3.1 Series hybrid strengths

Because a series hybrid omits a mechanical link between the combustion engine and the wheels, the thermal engine can be run at a constant rate even as the vehicle changes speed, fixing the ICE operations at the most efficient operating points. In this way, the engine can potentially be operated solely within its maximum efficiency region and, in particular, its fuel economy and emissions characteristics can be further improved by optimal design and control in this narrow zone, which is much easier and allows greater improvements than an optimization across the entire operating range. The engine can thus maintain an efficiency closer to the theoretical limit of 37%, rather than the current average of 20%, finally reaching an overall efficiency increase of about 50% [10]. The use of an electric motor directly linked to the transmission allows elimination of the conventional gearbox and differential, therefore the construction is greatly simplified and the cost is reduced.

In case of electric motors used directly integrated into the wheels, a disadvantage is that the unsprung masses increase causing a decrease in the suspension responsiveness, which impacts ride performance and potentially safety. Moreover, series hybrid electric drivetrains suffer some other disadvantages: the energy from the engine is converted twice (mechanical to electrical in the generator and electrical to mechanical in the traction motor) and so energy losses may be significant; the generator adds additional weight and

cost; finally, the traction electric motor must be sized for maximum requirements since it is the only powerplant that propels the vehicle.

In general, the series hybrid propulsion system has yet to find acceptance in gasoline and diesel electric passenger vehicles and light trucks. Part of the reason may be the fact that this architecture is heavier and more costly than the parallel alternative; however, in large vehicles such as locomotives, where weight is less of an issue, the series architecture is used extensively, in particular to improve the overall efficiency of the internal combustion engine operations.

### 2.3.4 Series-parallel configuration

Series-parallel hybrids incorporate power-split devices allowing for power paths from the engine to the wheels that can be either mechanical or electrical. Typically, a combustion engine's torque output is minimal at lower angular speeds and hence, in a conventional vehicle, a larger engine is necessary for acceptable acceleration from standstill. An electric motor, on the other hand, exhibits maximum torque at standstill and so it is perfect to complement the engine's torque deficiency at low rotational rates. In a power-split hybrid, combining the thermal and the electric motor in a series-parallel configuration, allows to take advantage of the strengths of both the engine types; moreover, thanks to the presence of the electric motor, a smaller ICE can be used and operated in the favorable region of the brake specific fuel consumption map, significantly improving the overall efficiency of the vehicle. The typical configuration of a series-parallel hybrid is shown in below Figure 2.10.

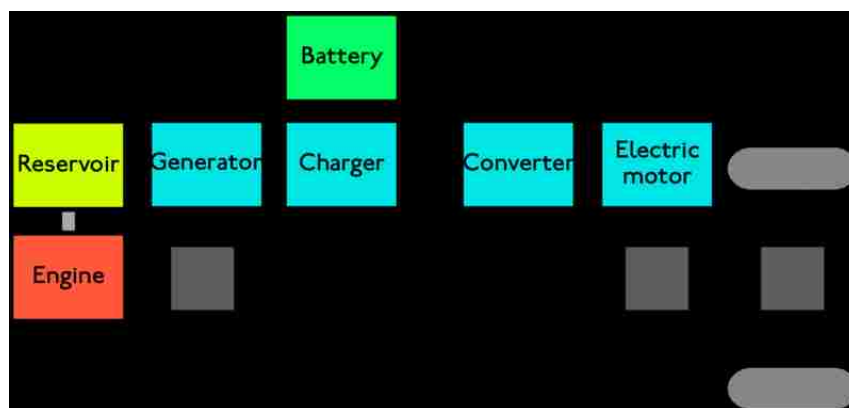


Figure 2.10 - Series-parallel hybrid configuration scheme [10]

### 2.3.4.1 The Toyota Hybrid Synergy Drive system

The Toyota Hybrid Synergy Drive system can be seen as a good model of this hybrid technology. As said before, in a standard car, the alternator (AC generator) and the starter (DC motor) are considered accessories that are attached to the internal combustion engine which normally drives a transmission to power the wheels and propel the vehicle. A battery is used only to activate the starter and, consequently, the ICE and to run ancillary accessories when the engine is not running; the alternator, instead, is used to recharge the battery and run the accessories when the engine is running.

The Toyota Hybrid Synergy Drive system, depicted in Figure 2.11, replaces the standard transmission, alternator and starter motor with:

- two powerful permanent magnet synchronous motors, a secondary starter/generator motor (MG1) and a primary drive/regeneration motor (MG2);
- the suitable associated power electronics;
- computerized control systems and sensors;
- a mechanical power splitter;
- an advanced high voltage battery pack (HVB).

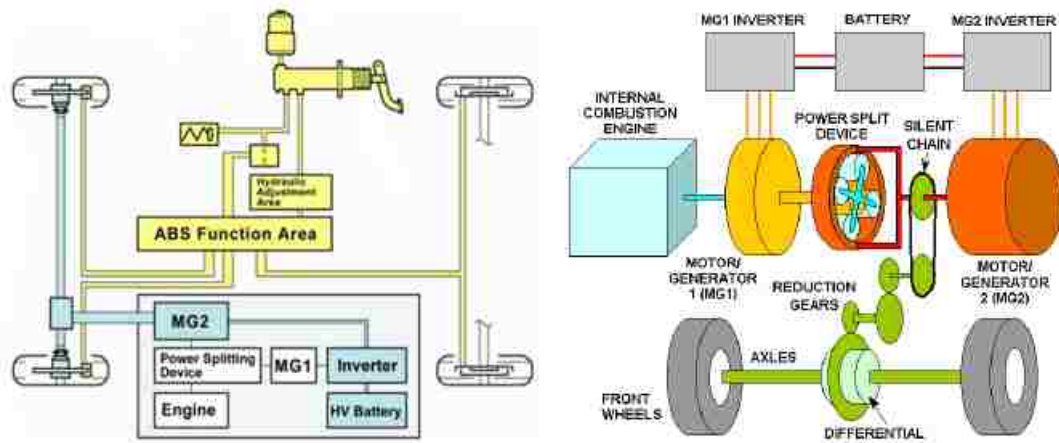


Figure 2.11 - Toyota Hybrid Synergy Drive system [13]

The MG1 serves as the engine starter motor and shares power with the ICE to drive the MG2 and to recharge the high voltage battery. The MG2, instead, drives the wheels and regenerates power for the battery pack, slowing down the vehicle through

regenerative braking actions: in general, the primary motor MG2 drives the wheels using the electrical power generated by the engine and by the MG1 activated by the battery while, during regenerative braking, the MG2 acts as a generator converting the kinetic energy of the vehicle into electricity and recharging the battery cells [14].

#### **2.3.4.2 Series-parallel hybrid strengths**

A primary advantage offered by a combination hybrid architecture is the relative simplicity of its transmission, characterized by the absence of clutches to engage and disengage, made possible by the mechanical power splitter device that constitutes a continuously variable transmission system. A second advantage is that the engine speed can be confined to a narrow range through the suitable control of the MG1, reaching the possibility to operate the ICE in the zone of highest efficiency. A third advantage is finally represented by the possibility to further downsize the engine, thanks to the presence of two electric machines.

On the other hand, a disadvantage of the combination architecture is the relatively high complexity of having two AC drive systems integrated into a unique transmission, along with their dedicated inverters and controllers [4]. This represents nearly twice the power electronics content of a parallel and series hybrid. In this regard, manufacturers of the power split hybrid architecture continue to search for ways to further minimize the electric machine and the power electronics content: the electric machines need to have high power density and the power electronics must be downsized because of the little volume available within the engine compartment.

### **2.4 Degrees of hybridization**

The hybrid electric vehicle technology, classified in the previous sections considering the drivetrain configuration, can be further divided from a different point of view, taking into account the hybridization degree of the investigated vehicle and, hence, the intensity of the “electric side” of the power contribution and of the various hybrid features. A typical classification is presented in the following list, that is going to be described in details in the next sections:

- micro hybrids, provided with a basic start-stop function of the ICE;

- mild hybrids, offering the same features of the micro hybrids plus an electric power assist for acceleration and regenerative braking actions;
- full hybrids, characterized by the mild technology and by the possibility for a total electric launch;
- plug-in hybrids, that function as full hybrid but with the possibility to recharge the battery pack thanks to a connection with the electrical grid;
- battery electric vehicles, that rely only on the batteries for their operations and are not provided with the internal combustion engine.

In Table 2.1, for each hybrid type described in the list above, is reported the specific cost of the battery pack and of the whole electric propulsion and transmission system, indicating moreover the percentage of fuel efficiency gain introduced by all the different configurations.

**Table 2.1 - Costs and fuel efficiency gains introduced by the new vehicles' electric system [15]**

	<b>Battery Cost, \$</b>	<b>Total Cost, \$</b>	<b>Fuel Efficiency Gain, %</b>
Micro Hybrid	100	600	5-10
Mild Hybrid	600	1,600	10-20
Full Hybrid	1,200	2,200	25-40
PHEV	6,000	8,000	40-65
EV	11,000	11,000	100

### **2.4.1 Micro hybrids**

Although not strictly hybrids, since the electricity from the battery is not used to propel the car, the micro hybrid vehicles are provided with the start-stop function that enables a modest reduction in CO<sub>2</sub> emissions and fuel consumption. When the car comes to a halt, the internal combustion engine is shut down and then, when the driver presses the accelerator, it is activated again thanks to an advanced alternator, which is powered by the 12 V battery.

Shutting down the ICE when stopped, a certain fuel consumption and emissions level reduction (in the range of 5% to 10%) is experienced by the vehicle, in particular if it is spending significant amount of time waiting at traffic lights or in queue in typical city traffic jams. For a manual transmission vehicle, the start-stop function is activated stopping the car, depressing the clutch, moving the gear lever to neutral and releasing the clutch; the engine restarts when the clutch is depressed again, prior to selecting a gear to move the vehicle. At the same time, the ICE may also restart if there is a power demand from, among the others, the air conditioning system that hence, in HEVs, should be redesigned to function properly also when the engine is turned off, for example through the use of an electric motor.

#### **2.4.2 Mild hybrids**

A mild hybrid uses the same start-stop system of the micro hybrids but it is characterized, moreover, by the possibility to take advantage from the torque boost and regenerative braking actions performed by the electric machine. Mild hybrids cannot be powered by the electric motor alone but they show considerable fuel economy and emission improvements [16].

Mild hybrids, like the Honda ECO Assist™ vehicles, are equipped with a three-phase electric motor mounted within the engine compartment between the engine and transmission, allowing the ICE to be turned off whenever the car is braking or stopped and to be restarted quickly when requested by the driver. Accessories can continue to run thanks to the electrical power generated by the electric machine that, moreover, is used for regenerative braking actions and to propel the vehicle at low gears and angular speeds, when the efficiency of the engine is dramatically low.

Typical mild hybrid solutions are represented by the ISG technology, in particular in its belt driven configuration, that offers the start-stop functionality, a modest assist for acceleration and captures energy during braking, leading to a 27% improvement in combined fuel efficiency.

### **2.4.3 Full hybrids**

Full hybrid vehicles can be powered by the only electric motor, the only combustion engine or both. Normally, when starting and driving at low speeds, the car is silently powered by the electric motor only, with a null fuel consumption and CO<sub>2</sub> emission. The combustion engine then intervenes at higher speeds and, when needed, it is sustained by the electric motor that provides extra power and torque. A full hybrid system intelligently selects the most appropriate power source and captures a significant amount of energy through regenerative braking actions to charge the high voltage battery, which activates the powerful electric motor placed along the drivetrain.

The Toyota Prius, Toyota Camry Hybrid, Ford Escape Hybrid, Ford Fusion Hybrid, Ford C-Max Hybrid, Lincoln MKZ Hybrid and Kia Optima Hybrid, are examples of this type of hybridization technique and, typically, they use the series-parallel configuration and are equipped with a high capacity battery pack. Fuel economy improvements can reach, in these vehicles, values near the 80% [17].

### **2.4.4 Plug-in hybrids**

A plug-in hybrid electric vehicle (PHEV) has two defining characteristics: it can be connected to the electrical grid to recharge its battery pack and can be moved for a notable distance and time using the only electric motion. Their driveline can be parallel or series designed and, in general, they use an internal combustion engine to turn a generator which, in turn, supplies current to an electric motor, which then puts in rotation the vehicle's wheels. Examples of series full hybrid vehicles include the Chevrolet Volt and the Fisker Karma, while the Honda Insight, Civic and Accord are typical parallel full hybrids models; the Toyota Prius Plug-in Hybrid operates finally with a series-parallel configuration.

Regardless of its architecture, a plug-in hybrid may be capable of charge depleting and charge sustaining modes. In the first case, the vehicle operates thanks to the energy supplied by the high voltage battery pack while, in the second case, that is activated after the battery has reached its minimum state of charge (SOC) threshold, the ICE is used to restore the energy content of the battery modules; combinations of these two operating modes are termed blended or mixed modes [18]. More specifically, the



charge depleting mode allows a fully charged PHEV to operate exclusively on electric power (all-electric range) until its battery state of charge is depleted to a predetermined threshold, at which the vehicle's internal combustion engine is engaged; the charge sustaining mode, instead, combines the operation of the two vehicle power sources in such a manner that the vehicle is operating as efficiently as possible allowing the battery recharge to a target SOC level.

#### **2.4.5 Battery electric vehicles**

A battery electric vehicle (BEV) is an electric vehicle (EV) propelled by one or more electric motors, activated by the chemical energy stored in rechargeable battery packs; BEVs derive all their power from the battery and thus they are not provided with an internal combustion engine. Battery electric cars are becoming more and more attractive with the advancement of new battery technology (lithium-ion solutions), characterized by higher energy density levels that allow to obtain greater accelerations and a longer autonomy range. The main problem of BEVs is in fact represented by the specific energy content typical of the batteries that is considerably lower than the one of the fossil fuels used to power conventional vehicles; moreover, the autonomy and recharge times of the battery packs represent two important issues to take into account. On the other hand, electric cars have the potential of significantly reducing city pollution thanks to their environmentally friendly operations characterized by a null fuel consumption and by a null emission of noxious and greenhouse gases; these considerations are leading world governments to sustain the development of BEVs through major investments.

#### **2.5 The battery**

As can be pointed out after the analysis of the previous sections, a basic requirement for hybrid and battery electric vehicles is a portable source of electrical energy, which has to be converted to mechanical by means of an electric motor to obtain the vehicle propulsion. Electrical energy is typically obtained through conversion of the chemical energy stored in devices such as batteries and fuel cells; a flywheel is an alternative portable source in which energy is stored in mechanical form to be converted

into electrical when requested by the whole vehicle system. The research of a portable electrical energy source capable of effective and efficient operations, represents the biggest obstacle in commercialization of HEVs and BEVs.

In Table 2.2, is shown a comparison of the specific energy (energy per unit mass) of the available energy sources actually used all over the world: after a rapid analysis of the numerical data listed below, it is possible to note that the specific energy content of the batteries is the least important one and leads to the necessity of use a highly heavy battery pack to generate notable quantities of energy.

**Table 2.2 - Nominal energy density of different sources [19]**

<b>Energy Source</b>	<b>Nominal Specific Energy (Wh/kg)</b>
Gasoline	12,500
Natural gas	9350
Methanol	6050
Hydrogen	33,000
Coal (bituminous)	8200
Lead-acid battery	35
Lithium-polymer battery	200
Flywheel (carbon-fiber)	200

The various battery types are usually compared in terms of descriptors and the desirable features of batteries typically used for EV and HEV applications are high specific power, high specific energy, high charge acceptance rate for recharging and regenerative braking actions, long calendar and cycle life. Battery technology has been undergoing extensive research and development efforts over the past 30 years, but there is not yet a battery type that can deliver an acceptable combination of power, energy, and life cycle for high volume production vehicles.

### **2.5.1 BEV and HEV battery design requirements**

First of all, it has to be underlined that while for battery electric vehicles the interest is to maximize the energy content of the battery pack in order to obtain an extended driving autonomy, for hybrid vehicles the dominant concern is instead to increase the power amount that can be delivered by the battery when requested by the driver, to perform the instantaneous cranking of the ICE or to obtain a torque boost during accelerations. The battery voltage is another important parameter to consider during the HEV and BEV design: the intense power and energy contributions of the electric machine, activated by the battery, render the conventional 14 V systems (that use 12 V batteries) not suitable for hybrid and pure electric applications. Dealing with HEVs, a new 42 V standard has been proposed in recent years in order to satisfy the increased electric power demand and to make possible to realize many hybrid technologies; at the same time, higher voltage systems have also been implemented, introducing advantages and drawbacks that are going to be described in the next paragraphs.

Knowing that the product of the battery current and voltage defines the power level of the device, for a fixed battery level a low voltage system requires higher currents. Moreover, knowing that the electric connections present a finite resistance and that the electric power losses are directly proportional to the this resistance and to the squared power of the electric current magnitude, it is possible to state that low voltage systems are characterized by higher power losses than the high voltage systems, if the same connectors and wires are used. At the same time, if the two systems are characterized by the same amount of power losses, the high voltage system offers the opportunity to use cheaper connectors that have a lower cross sectional area (and hence a lower resistance).

Furthermore, the voltage level has a relevant influence on the characteristics requested to the inverter. The power electronic transistor best suited for low voltage applications are the MOSFETs (metal-oxide-semiconductor field-effect transistor) that, however, cannot withstand too high current levels that ultimately lead to performance deterioration. The necessity to introduce higher current limits that can be tolerated by the transistors, imposes the use of particular power MOSFETs, that are limited in availability and very expensive, or the implementation of costly structures constituted by a great number of standard MOSFETS placed in parallel. For high voltage applications, higher

than 200 V [20], the IGBT (insulated-gate bipolar transistor) power semiconductor devices are more suitable, because they are specifically designed to efficiently handle high voltage levels. Moreover, the IGBTs are produced in large quantities with advanced fabrication techniques and so they are cheaper and more available than the MOSFET transistors [21].

Considering what has been explained in the two previous paragraphs, high voltage systems seem to be a better solution for hybrid electric vehicle applications than low voltage systems. At the same time, the safety requirements must be also taken into account in this perspective: high voltage systems can have, in fact, dangerous effects on human body and for voltages exceeding a 65 V DC threshold it is necessary to prevent direct electrical contacts between people and circuits. As a consequence, high voltage systems require a complete electrical insulation of the wires and of any other circuit components that might come in contact with people; this finally results in increased complexity and cost.

### **2.5.2 Battery basics**

A general overview of the battery structure is necessary to better understand how they work and how they can be integrated on a vehicle system. The batteries, in this regard, are made of unit cells “containing” the chemical energy that will be converted into electrical; these electrolytic cells are connected in series to form one battery module, enclosed in a coating and electrically linked one with the others. A battery pack is a collection of these individual battery modules, organized in series and parallel combinations to deliver the desired voltage and energy to the power electronic drive system [19].

The energy stored in a battery is the difference in free energy between chemical components in the charged and discharged states. This available chemical energy in a cell is converted into electrical energy only on demand, using the basic components of a unit cell, which are the positive and negative electrodes, the separators, and the electrolytes. The electrochemically active ingredient of the positive or negative electrode is called the active material; chemical oxidation and reduction processes take place at the two electrodes, thereby bonding and releasing electrons, respectively. The electrodes must be

electronically conducting and are located at different sites, divided by a separator, as shown in Figure 2.12. During battery operation, chemical reactions at each of the electrodes cause electrons to flow from one pole to another; however, the current flow in the cell is sustainable only if electrons generated in the chemical reactions are able to flow through an external electrical circuit that connects the anode and the cathode. The connection points between the electrodes and the external circuit are called the battery terminals and the external circuit ensures that most of the stored chemical energy is released only on demand and is utilized as electrical energy by an external load. It must be mentioned that only in an ideal battery the current flows only when the circuit between the electrodes is completed externally; unfortunately, many batteries allow a slow spontaneous discharge (self-discharge) due to diffusion effects, that decrease their long-term energy storage capability.

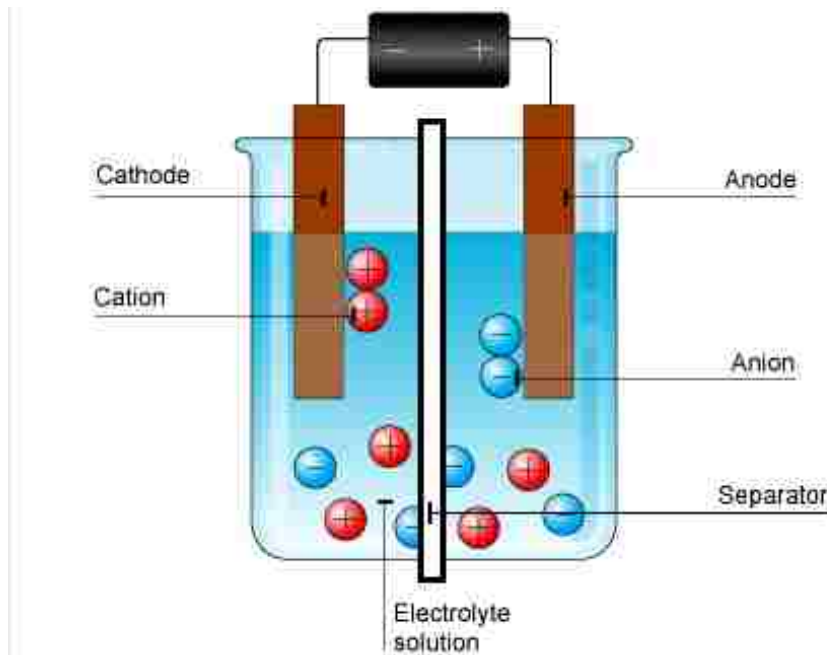


Figure 2.12 - Typical battery basic scheme [22]

The components of the battery cell are described in the following detailed list, focusing the attention on their purposes and typical operations.

- Positive electrode: it is an oxide or sulfide, capable of being reduced consuming electrons from the external circuit during cell discharge.

- Negative electrode: it is a metal or an alloy that is capable of being oxidized during cell discharge, generating electrons in the external circuit; examples of negative electrodes are lead (Pb) and cadmium (Cd).
- Electrolyte: it is the medium that permits ionic conduction between the positive and negative electrodes of a cell. The electrolyte must have high and selective conductivity for the ions that take part in electrode reactions, but it must be a nonconductor for electrons in order to avoid the self-discharge phenomenon.
- Separator: it is the electrically insulating layer of material that physically separates electrodes of opposite polarity [19]. Separators must be permeable to the ions of the electrolyte and may also have the function of immobilizing the electrolyte; present day separators are made from synthetic polymers.

### **2.5.3 Battery types**

There are two basic types of batteries: primary batteries and secondary batteries. Batteries that cannot be recharged and are designed for a single discharge phenomenon are known as primary batteries; batteries that can be recharged through a current flow that takes place in a reversal direction are known as secondary batteries. The batteries used for BEVs and HEVs are all secondary batteries, because they are recharged during certain operating conditions of the vehicle; in this regard, the major types of rechargeable batteries considered for BEV and HEV applications are:

- lead-acid (Pb-acid);
- nickel-cadmium (Ni-Cd);
- nickel-metal hydride (NiMH);
- lithium-ion (Li-Ion);
- lithium-polymer (Li-P).

Specific energy and power characteristics of the different battery technologies are often summarized in the similar-Ragone plot, reported in Figure 2.13. The Li-ion and NiMH technologies show the best performance and, for this reason, are at present days the most used in BEV and HEV applications.

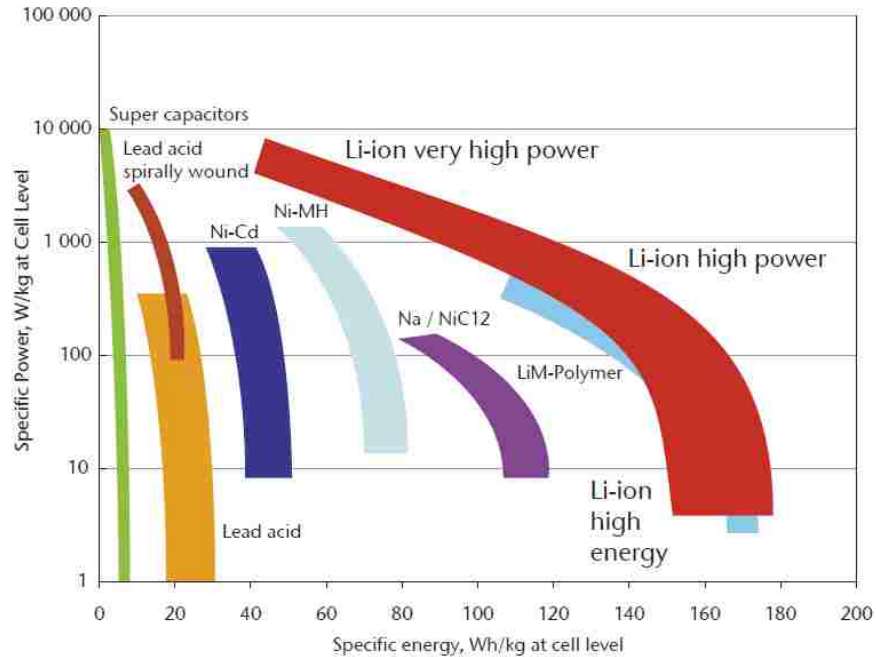


Figure 2.13 - Specific power and energy of different battery types [7]

### 2.5.3.1 Lead-acid battery

Lead-acid batteries have been the most popular choice of batteries for BEVs and HEVS for long time; they can be designed to be high powered and are inexpensive, easy to manufacture, safe and reliable. However, low specific energy, poor cold temperature performance and short calendar and cycle life represent negative aspects typical of the Pb-acid battery technology [19].

Lead-acid batteries are constituted by a sponge metallic lead anode, a lead dioxide ( $\text{PbO}_2$ ) cathode and an aqueous sulfuric acid ( $\text{H}_2\text{SO}_4$ ) electrolyte. The cell reactions imply the formation of water and above a certain voltage, called gassing voltage, this water dissociates into hydrogen and oxygen and must be replaced [23]. This is a heavy limitation that was solved with valve regulated lead-acid (VRLA) batteries in which hydrogen and oxygen are converted back into water, which no longer needs to be replaced. Lead-acid batteries are widely used within the 12 V network of conventional vehicles but also in some HEV applications, mainly due to their low cost, robustness and reliability.

A typical Pb-acid battery shows a specific energy and power of about 40 Wh/kg and 100 W/kg. The maximum possible number of discharge/charge cycles allowed sets

around 900 unities and the main advantages offered by this type of cells are the low cost, the high recycling facility and the easiness of the production process. The high charge time, the high temperature sensitivity and, finally, the high tendency of undergoing self-discharge reactions represent the weaknesses of this technology [24].

### **2.5.3.2 Nickel-cadmium battery**

Nickel-cadmium (Ni-Cd) batteries are examples of alkaline batteries in which the electrical energy is derived from the chemical reaction taking place between metals and oxygen in an alkaline electrolyte medium. The Ni-Cd battery employs a nickel oxide positive electrode, a metallic cadmium negative electrode and a potassium hydroxide (KOH) electrolyte [19]. The advantages of Ni-Cd batteries with respect to the Pb-acid ones are superior performance in cold climates, longer life, excellent reliability and low maintenance requirements. The biggest drawbacks, instead, are represented by a high cost and by the toxicity of the cadmium. Moreover, the insufficient power typically delivered by the Ni-Cd batteries constitutes an important reason for not considering this technology for BEV and HEV applications. Moreover, Ni-Cd cells are also affected by the so-called "memory effect", a temporary loss of capacity which occurs when the module is recharged without being fully discharged and can cause the battery life to be shortened [23].

The Ni-Cd batteries are usually characterized by a specific energy and power amount of about 50 Wh/kg and 150 W/kg. The maximum possible number of cycles of discharge/charge allowed sets around 2000 unities and the typical charge time is substantially lower than the one of lead-acid cells [24]. As said before, the high costs and the cadmium toxicity represent the main disadvantages offered by this battery type.

### **2.5.3.3 Nickel-metal hydride battery**

The nickel-metal hydride technology is typically used in the design of the battery packs of hybrid electric vehicles actually in production. In NiMH batteries, the positive electrode is a nickel oxide similar to the one used in a Ni-Cd battery, while the negative electrode is a metal hydride where hydrogen is stored. The concept of NiMH batteries is based on the fact that fine particles of certain metallic alloys, when exposed to hydrogen



at certain pressures and temperatures, absorb large quantities of the gas to form metal hydride compounds; furthermore, the metal hydrides are able to absorb and release hydrogen many times without deterioration.

The capacity of NiMH modules is significantly higher than that of Ni-Cd, with notable value of specific energy and power. Hence, the NiMH batteries have penetrated the market in recent years at an exceptional rate; in Japan, NiMH battery packs produced by Panasonic (Primearth) EV Energy Company are being used in the Toyota Prius models, the most widespread example of HEV. Nickel-metal hydride batteries have a considerably long life cycle if compared to the lead-acid cells, are safe and capable of high performance. The disadvantages of this technology are the relatively high cost, higher self-discharge rate, poor charge acceptance capability at elevated temperatures and low recharge efficiency [19].

Nickel-metal hydride batteries of the last generation can show an incredibly high value of specific power of 1300 W/kg, at a satisfying amount of specific energy (70 Wh/kg). The maximum possible number of cycles of discharge/charge allowed is of 2000 unities. The charge time is substantially low, the maintenance is quite easy and the environmental impact of the materials used for this battery type is not a big issue. The main problem is represented by the not negligible self-discharge rate [24].

#### **2.5.3.4 Lithium-ion battery**

The lithium-ion batteries have a graphite anode in which lithium ions are intercalated, filling the interstitial spaces of the crystal. The cathode is a lithium oxide component and the electrolyte is a lithiated liquid solution [23]. Lithium-ion batteries have high specific energy, high specific power, high energy efficiency and show good performance at high temperatures, a longer life and a low self-discharge characteristic. Moreover, the Li-ion modules are easily recyclable, can be manufactured in small size and light weight, have an improved charge efficiency and do not suffer the “memory effect”; all these characteristics make Li-ion batteries highly suitable for BEV and HEV applications. However, to make them commercially convenient, further developments are needed to improve their cycle life and to determine a reduction of costs.

As previously said, Li-ion batteries have high values of specific energy and power, around 200 Wh/kg and 300 W/kg, and the maximum number of discharge/charge cycles settles around 1200. The low weight, low volume and low self-discharge rate characteristics, together with the possibility to use a wide number of design solutions, represent the main strengths of this battery technology. The main weaknesses of this system are represented by the high reactivity of the lithium and by the considerable production costs of the cells.

### **2.5.3.5 Lithium-polymer battery**

The lithium-polymer batteries are considered solid state batteries, because their electrolytes are solids; the most common polymer electrolyte is the polyethylene oxide compounded with an appropriate electrolyte salt [19]. These lithium modules have the potential for higher specific energy and power and, thanks to the presence of the solid polymer that replace the more flammable liquid electrolyte, can work at temperatures above 60 °C. The use of solid polymers also has a great safety advantage in case of vehicle accidents and allows to form a battery of any size or shape to suit the available space within the BEV/HEV chassis. The other key characteristics of the Li-P cells are the good cycle and calendar life.

### **2.5.4 Battery key parameters**

Battery performance and cost are essential aspects that must to be taken into account for the development of battery and hybrid electric vehicles; in this regard, in the following sections, the most important factors necessary to identify the strengths and weaknesses of an investigated battery device are presented and described in details.

#### **2.5.4.1 Ampere-hour capacity**

The Ampere-hour (Ah) capacity represents the total charge amount that can be discharged from a fully charged battery under specified conditions. The rated Ampere-hour capacity, in particular, is the nominal capacity of a fully charged new battery under the conditions predefined by the manufacturer; a typical nominal condition, for example,

can be defined at a temperature of 20 °C and at a 1/20 C-rate of discharge [25]. It can be used also the Watt-hour capacity to represent the capacity of the battery: it is defined as the product between the Ah Capacity and the Voltage level of the cell. Physically, the theoretical capacity of a cell is determined by the amount of active materials and can be expressed as the total quantity of electricity involved in the electrochemical reaction [26].

#### **2.5.4.2 C-rate**

It is used to represent a charge or discharge rate (current magnitude) equal to the capacity of a battery deliverable in one hour. For a 1.6 Ah battery, C refers to a charge or discharge of the cell at 1.6 A; correspondingly, 0.1C is equivalent to 0.16 A rate, and 2C to a current of 3.2 A [25].

#### **2.5.4.3 Specific energy**

Also called gravimetric energy density, it is used to define how much energy a battery can store per unit mass. It is expressed in Watt-hours per kilogram and represents a very important parameter to take into account since it directly determines the distance the vehicle can drive in a charge depleting mode, as well as the mass of the battery pack [27].

#### **2.5.4.4 Specific power**

Also called gravimetric power density of a battery, it is defined as the peak power per unit mass. It is expressed in Watts per kilogram and gives indications about the torque boost performance that characterize a given HEV.

#### **2.5.4.5 Energy and power densities**

Also referred to as the volumetric energy and power densities, are defined as the ratio between the nominal battery energy or power and the related battery volume. Their units of measure are Wh/l and W/l and they indicate how much the battery has to be voluminous to generate the requested energy and power amounts.

#### **2.5.4.6 Internal resistance**

It is the overall equivalent resistance within the battery; it is different for charging and discharging events, may vary as the operating condition changes and determines the amount of power dissipated during time for Joule effect.

#### **2.5.4.7 State of charge (SOC)**

It is defined as the remaining capacity of a battery compared to its initial state of charge and is affected by the module operating conditions such as the load current and temperature [28]. It can be seen as the equivalent of a fuel gauge for the battery pack in a battery or hybrid electric vehicle; its mathematical expression is presented by Equation 2.1.

$$SOC = \frac{RemainingCapacity}{RatedCapacity} \quad (2.1)$$

The state of charge represents a critical condition parameter for battery management; accurate gauging of SOC is very challenging but, at the same time, necessary to obtain healthy and safe operation of the batteries.

#### **2.5.4.8 Depth of discharge (DOD)**

The depth of discharge is used to indicate the percentage of the total battery capacity that has been discharged and, hence, it is defined as the one's complement of the battery state of charge.

#### **2.5.4.9 State of health (SOH)**

It can be defined, through Equation 2.2, as the ratio of the maximum charge capacity of an aged battery to the maximum charge capacity that characterized the battery when it was new [25]. It is a very important parameter used to indicate the degree of performance degradation of a battery and to estimate the battery remaining lifetime.

$$SOC = \frac{AgedEnergyCapacity}{RatedEnergyCapacity} \quad (2.2)$$

#### **2.5.4.10 Cycle life**

It indicates the number of discharge/charge cycles the battery can handle at a specific DOD (normally 80%) before it fails to meet specific performance criteria. The actual operating life of the battery is affected by the charging and discharging rates and by other conditions such as the temperature. Obviously, the higher is the DOD and the shorter is the cycle life; to achieve a higher cycle life, hence, a larger battery can be used for a lower DOD during normal operations.

#### **2.5.4.11 Calendar life**

The calendar life is the expected life span of the battery under storage or periodic cycling conditions; it can be defined as the ability of the battery to withstand degradation over time. It is strongly related to the temperature and must be the highest possible to increase the calendar life of the entire BEV/HEV system.

#### **2.5.4.12 Efficiency**

The efficiency of the battery is the ratio between the electrical energy supplied by the accumulator during discharge and the electrical energy supplied to the accumulator during its recharge [29]. An accumulator, in fact, cannot deliver during discharge all the energy that it has absorbed during charge, since part of this energy is converted into heat or lost because of leakage currents taking place within the internal structure of the cell. The efficiency of common lead-acid batteries is about the 80%.

### **2.5.5 Battery state of the art**

As can be seen from Figure 2.13, rechargeable batteries extend over a wide range of specific power and energy densities and, among the different electrochemistry solutions presented in the previous sections, the NiMH and Li-Ion cells offer the most advanced performance that make them suitable for battery and hybrid electric vehicle applications. In particular, given their high power content, the NiMH batteries are well suited for HEVs

in which notable amount of power are requested by the electric motor to perform the start-stop function and, in particular, the torque boost actions during passing maneuvers. The Li-Ion batteries, instead, are well suited for typical BEV applications thanks to their high energy content that allows to propel the vehicle for long distances and times in a charge depleting mode.

Figure 2.14 gives details about the typical specific energy and energy density contents that characterize the most diffused battery types and, from its analysis, it can be seen that the NiMH and Li-Ion solutions represent again the most promising ones. However, NiMH batteries are considered to have reached their maximum potential and, for the future, experts do not expect further significant technical improvements and cost reductions [30]. Car makers are hence moving to Li-ion batteries, especially because they offer energy densities higher than what NiMH batteries do and, moreover, they are also characterized by significantly lower self-discharge rates [27].

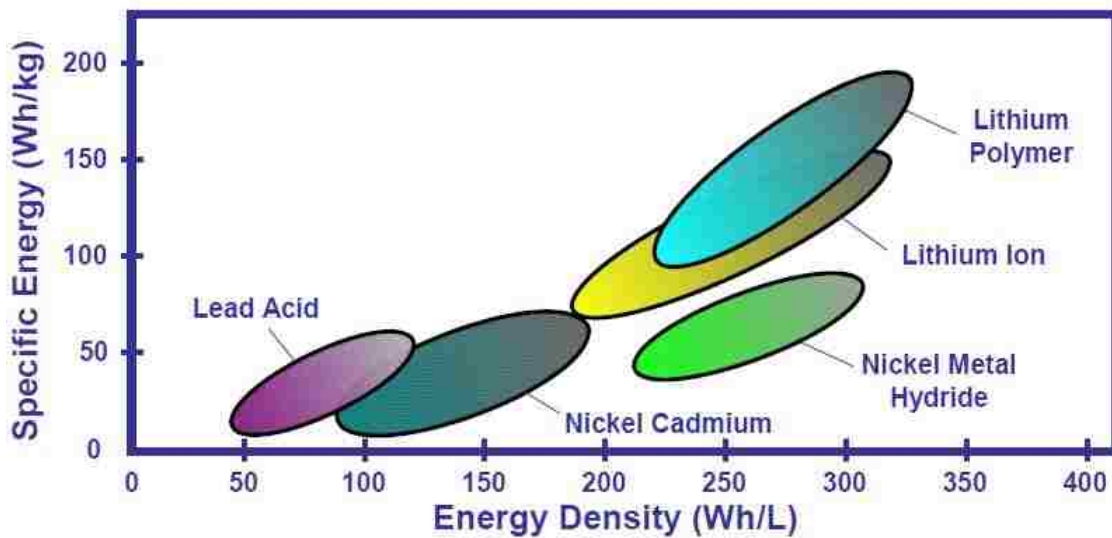


Figure 2.14 - Specific energy and energy density of different battery types [31]

Therefore, in the near future, intensive research and development activities are going to characterize the Li-Ion battery technology field, in order to obtain further performance improvements and cost reductions.

Following Table 2.3 finally proposes typical ranges of values assumed by the previously analyzed battery key parameters in modern hybrid, battery and plug-in hybrid electric vehicle applications.

**Table 2.3 - Typical values of the battery key parameters for HEV, BEV and PHEV applications [27]**

	HEV	BEV	PHEV
AER (miles)	0	150-200	10-60
Material	NiMH	Li-ion	Li-ion
Total capacity (kWh)	1.3	30-60	4-30
Specific energy (Wh/kg)	46	110-160	110-160
Energy density (Wh/l)	200-350	400-600	400-600
Peak power (kW)	27-35		40-100
Specific power (W/kg)	1300	1500	500-1500
Battery pack weight (kg)	29 <sup>(2)</sup>	200-500	70-190
Calendar life (years)	10-15	10-15	10-15
Deep cycle life (number of cycles)			>2500
Specific cost (€/kWh)	600		750-1500

### 2.5.6 Battery integration and control systems

A significant amount of research and development is being performed around the world to improve the attributes and performance of the batteries used for BEV and HEV technologies. However, the advanced performance of the battery modules must be supported by well suited integration solutions and advanced electrical and thermal control systems. Electrical management includes the measure and control of the most important battery operational and health indicators and properties that, definitely, have to maintain their magnitudes within specific ranges. At the same time, thermal management is a must because as the battery is used during time, its modules undergo significant heating phenomena and the high temperatures generation could lead to significant safety and working problems. In this regard, the battery pack management system is used to monitor and control the voltage differences between the cells and their specific temperature values; it ensures that the modules are not allowed to exceed the manufacturer's specified voltage and temperature limits [32].

### **2.5.6.1 Battery thermal control**

Given the specific field of study analyzed by this thesis project, particular attention must be addressed for the analysis of the battery thermal management system, critical in achieving the desired performance in low and high temperature environments. High temperatures, in particular, degrade the life of the batteries, while cold temperatures reduce their power and energy capabilities [33]; in general, battery temperature influences the availability of discharge power (for start up and acceleration), the charge acceptance capability during regenerative braking actions and, finally, also the life of the modules [32]. Therefore, ideally, batteries should operate within a temperature range that is optimum for performance and life: the desired operating temperature range is different depending on the electrochemistry solution but usually settles between 20 and 30 °C. A thermal management system is thus needed to either heat or cool the batteries in cold and high temperature climates. To cool down the batteries, air or liquid cooling systems are considered that have to reject the heat generated by the modules outside the vehicle. One important factor in thermal management is not only to maintain the maximum battery temperature below the prescribed limits, but also to maintain the highest possible uniformity of temperature between the cells in order to obtain balanced operations of the pack.

### **2.5.6.2 Desired attributes of a thermal management system**

The goal of a thermal management system is to keep the battery pack at an optimum average temperature with an even thermal distribution between the modules, as indicated by the battery manufacturer. Moreover, the thermal management system must be compact, lightweight, low cost and easily to package inside the vehicle; in addition, it must be reliable and accessible for maintenance. In general, a thermal management system may use the air or a liquid to maintain the battery pack at the specified temperature and it may be passive (only the ambient environment is used) or active (a built-in source provides heating and cooling depending on the actual battery temperature) [34].



### **2.5.6.3 Battery cooling concepts**

Designing a battery thermal management system for given BEV and HEV battery specifications starts with answering a sequence of questions, related to the heat quantity that must be removed from a pack, to the allowable temperature limits that the modules can reach, to the kind of heat transfer fluid that is needed [35]. On the basis of the answers given to these questions, a specific cooling concept is chosen and implemented on the vehicle to ensure the correct high voltage battery behaviour.

#### **2.5.6.3.1 Air cooling and liquid cooling systems**

The choice of the heat transfer medium has a significant impact on the performance and cost of the battery thermal management system. Figures 2.16 and 2.17 relate to typical battery forced air cooling systems while Figures 2.18, 2.19 and 2.20 refer to high voltage modules liquid cooling systems. If the coolant is a liquid fluid, it could flow through discrete tubes running around each module, inside a jacket that encloses the cells, directly in contact with the modules (submerged in the fluid) or inside a plate located on a specific surface of each cell. If the liquid is not in direct contact with the battery, such as in tubes or jackets, the heat transfer medium could be a water-glycol solution; instead, if the modules are submerged in the heat transfer liquid, it must be dielectric, such as silicon-based or mineral oils, to avoid any electrical shorts [34].

Using the air as the heat transfer medium may be the simplest approach, but it may not be as effective as the liquid coolant solution. The rate of heat transfer between the walls of the battery modules and the coolant depends in fact on the thermal conductivity, viscosity, density and velocity of the fluid; in particular, for the same coolant flow rate, the heat transfer phenomenon is more intense in case of direct contact liquid fluids such as oils because of their thinner boundary layer and higher thermal conductivity. However, because of oil's higher viscosity and associated higher pumping power, a lower flow rate usually circulates in the cooling system, making the oil overall heat transfer coefficient not really higher than the air one. Indirect contact liquids such as water-glycol solutions generally have lower viscosity and higher thermal conductivity than most oils, resulting in higher overall heat transfer coefficients. However, because the heat must be conducted through walls of the jacket/container or fins, indirect contact effectiveness decreases.

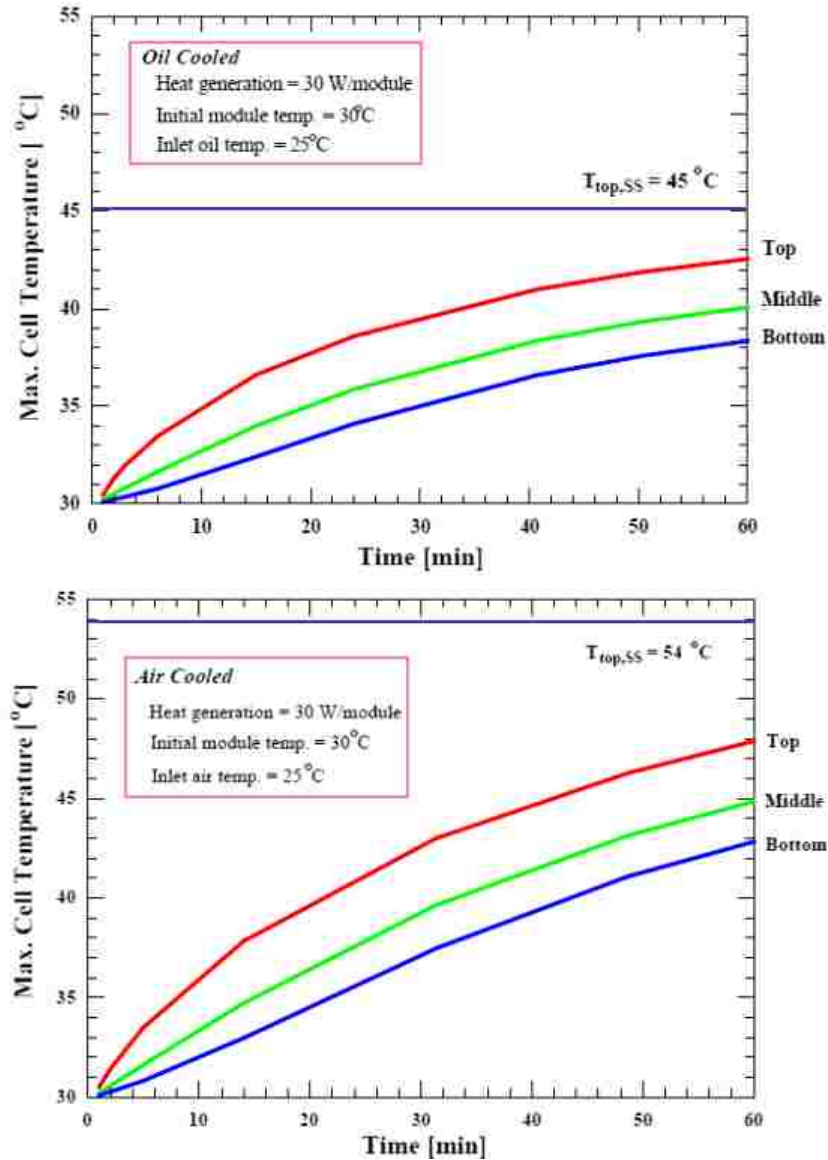


Figure 2.15 - Transient and steady state comparison of the oil and air cooling solutions [34]

Some studies have been conducted to compare the air and oil liquid cooling solutions for VRLA modules enclosed in a battery pack; a mass flow rate of 50 g/s at 25 °C has been chosen both for the air and the oil and the test has been realized for 1 hour, detecting the time trend of the temperature by means of thermocouples vertically placed on the bottom, middle and top points of the cells [34]. Figure 2.15 shows the maximum temperature time evolution acquired at the three different locations for the air cooling and oil cooling solutions, respectively. As expected, it is possible to note that the modules in the oil cooling case are cooler and reach the steady state condition much more quickly

than in the air cooling configuration because of the higher heat transfer rate of the liquid coolant.

### 2.5.6.3.2 Active and passive cooling systems

Because of cost, mass and space considerations and their use in mild climates, battery packs in early BEV and HEV models did not use heating or cooling units but disposed the heat generated by the batteries to the environment simply blowing ambient air across the modules using dedicated fans, as depicted in Figure 2.16.

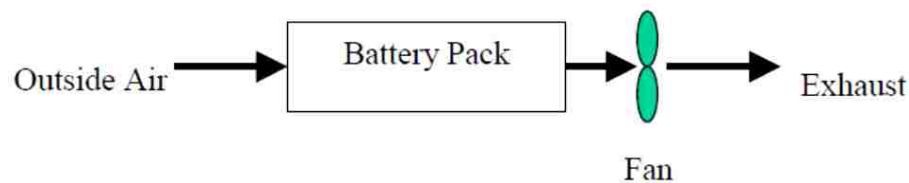


Figure 2.16 - Passive cooling, outside air ventilation [34]

Current production HEVs, as the Toyota Prius and Honda Insight, use instead cabin air for the cooling and heating actions of the battery pack, as can be seen from Figure 2.17; although the ambient air is cooled and heated by the vehicle air conditioning or heating systems, this solution is still considered to be passive since the coolant is drawn from the external environment. Figure 2.18, instead, shows a passive liquid system that uses outside ambient air for heat rejection.

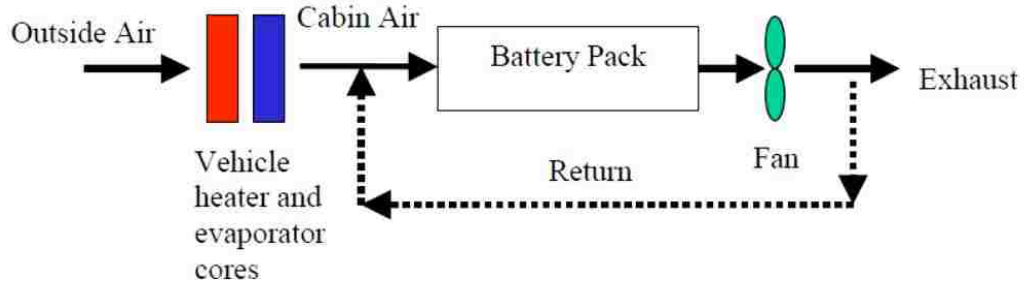


Figure 2.17 - Passive cooling/heating, cabin air ventilation [34]

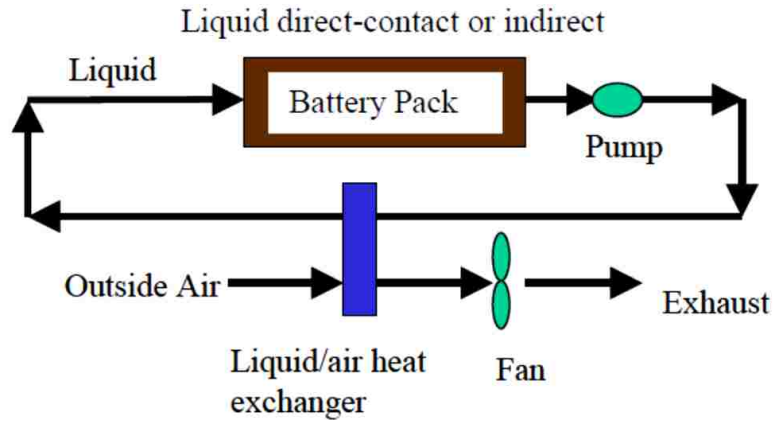


Figure 2.18 - Passive cooling, liquid circulation [34]

For all these passive systems, the ambient air must have a mild temperature (between 10 and 35 °C) to allow the correct functioning of the thermal management system; otherwise the pack performance worsens in very cold or very hot conditions.

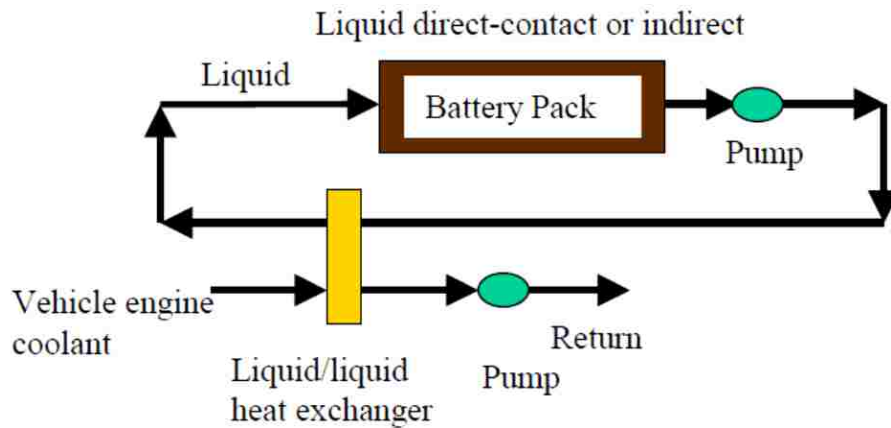


Figure 2.19 - Active moderate cooling/heating, liquid circulation [34]

To obtain a more advanced thermal control of the battery pack, roughly independent on the ambient temperature level, active systems as the ones depicted in Figures 2.19 and 2.20 are employed using active components such as evaporators, engine radiator and electric or fuel-fired heating cores.

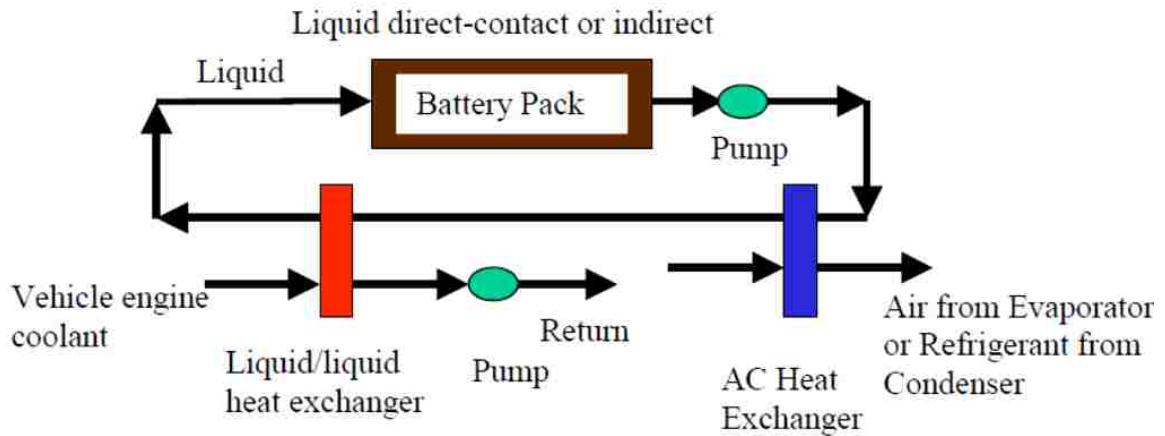


Figure 2.20 - Active moderate cooling/heating, liquid circulation [34]

### 2.5.6.3.3 Cooling only and cooling/heating systems

Since at cold temperatures, lower than 0 °C, the energy and power capability of most batteries drastically diminish, dedicated heating systems are installed on BEVs and HEVs that operate in colder climates. All batteries suffer in cold temperatures because their electrochemical processes slow down and their overall internal resistance increases [33]. In Figure 2.21 is reported the result of a study conducted by the US National Renewable Energy Laboratory (NREL) that shows an example of loss of power capability of a NiMH battery determined by a temperature decrease.

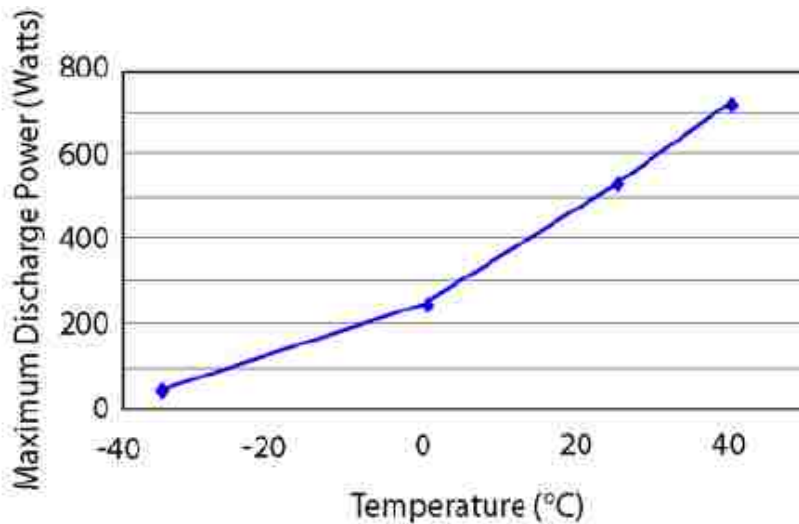


Figure 2.21 - Maximum discharge power dependence on temperature of a Panasonic prismatic 6.5 Ah NiMH module [33]

Hence, although all vehicles suffer in performance at very cold temperatures, BEVs and HEVs may suffer even more because of poor battery performance, leading to consumer rejection. Therefore, at very cold temperatures, high voltage batteries must be preheated to achieve acceptable power and energy performance. In BEVs there is no engine to be used to warm up the battery pack, so the heat rejected from the electric motor and the power electronics and the electricity taken from the battery could be used to perform an electric heating action; otherwise, a fuel-fired heater could be considered; for HEVs, instead, the heat from the engine could be used to obtain an effective battery heating.

#### **2.5.6.3.4 Series and parallel cooling systems**

Finally, there are two methods for distributing the coolant, the air for example, into a battery pack for cooling purposes. The first method is series cooling, where the air enters from one end of the pack and leaves from the other, exposing all the modules to the whole air mass flow rate. The second method is parallel cooling, where the total air mass entering the pack is split into equal portions and each portion flows over a single module. Depending on the size and geometry of the cells, series-parallel combination could be also configured [36]. Several studies have been performed in this regard and it has been found that a parallel airflow provides a more even temperature distribution among the modules in the pack, improving its thermal performance [37].

#### **2.5.6.4 Usefulness analysis of battery thermal management systems**

To conclude, it is important to underline that several virtual predicting studies and experimental tests have been performed to demonstrate the usefulness of a battery thermal management system, necessary to obtain improved battery life and performance. Applying joint thermal and degradation models to specific cells, the effect of the thermal management on battery life under several climate, drive cycle, control and coolant source scenarios have been investigated [38]. Preliminary results suggest that a correct thermal management can increase the life of the modules by 5% to 53%, depending on the operating conditions of the entire vehicle. Hence, the stringent need for a battery thermal management system seems to be evident and, in this regard, all the most important

worldwide battery and hybrid electric vehicle automotive companies, together with their suppliers, are working to find and design the best possible thermal system solutions.

## **2.6 Existing thermal models for HEV's engine and battery**

As stated in the first chapter, the final target of the thesis is to design two models, capable of simulating the thermal behaviour of the engine and battery devices equipping a HEV; in this regard, it is important to analyze the actual scenario related to the ICE and HVB modeling techniques, in order to be able to individuate the most important novelties introduced by the new software that have been created.

First of all, it must be underlined that, probably, every automotive company uses specific engine and battery thermal models, that have been designed by the research and development teams and are protected by confidentiality clauses. From this point of view, it would be impossible to describe existing thermal models but, after a careful literature analysis, some important concepts have been isolated that are useful to understand the current state of the art of this modeling technologies.

Starting from the ICE analysis, it can be stated that tools simulating the heat exchange phenomena taking place between the various engine components during different operating conditions are widespread and currently employed by many automotive companies. They are used to study the thermal behaviour of different engines tested over a specific driving cycle and, usually, are created for specific ICE families and technologies. Depending on the accuracy level offered by the software, more or less engine electronic controls are simulated and more or less sub-systems are described in details, such as the injectors, thermostat, supercharger and so on. In general, ICE thermal models have been strongly developed in the last years by the automotive companies; they are characterized by high levels of accuracy but are not so flexible in describing the behaviour of different engine types, diversified on the basis of their major operational and architectural facets.

Concluding with the HVB analysis, it must be pointed out that this technology has been strongly studied and investigated only in recent times and, in this regard, the battery virtual thermal models are not so advanced as it happens for the engine case. In particular,

the battery cells thermal modeling techniques follow two different main conceptual schemes:

1. when a high processing power is available and a detailed characterization is necessary, finite element method techniques are used that carefully describe the thermal state of each point of the HVB modules;
2. when a basic thermal analysis is requested that involves low computational constraints, the heat exchange phenomena are simulated considering a constant temperature of the battery cells, externally imposed by the user.

At this point, it is clear that these techniques lay on the opposite sides of an imaginary scale that gives a grade to the accuracy level offered by the investigated HVB thermal model. This scale, in particular, is not provided with an intermediate step capable of simulating the temperature of the cells during time, considering the battery in its whole structure and without performing severe finite element method calculations. Considering a current profile exciting the modules second per second, it would be useful to design a model aimed at predicting the time evolution of the HVB temperature depending on the thermal, electrochemical and geometrical characteristics of the battery pack. This type of model, in this way, would represent the intermediate step between the two extremes listed above, capable of thoroughly describe the various battery heat exchange phenomena at a basic level without involving too high hardware computational constraints.



## CHAPTER 3

### DESIGN AND METHODOLOGY

#### 3.1 Chrysler HEV prediction model

When a company is working to produce a new vehicle model, all the departments involved in the project must be aligned with the guidelines that define the target performance and characteristic of the new car that is going to be produced. The company, in fact, has to outline the main features that the new model has to offer to the customers and, during all the design stages, the different departments have to ensure that these dictates are met by the project.

In particular, in the early design stages, it is necessary to have the possibility to predict the performance and features that are going to define the final operating characteristics of the new model. From a mechanical, thermal, electric and electronic point of view, all the development teams must have a clear idea about the performance that the final automotive product is going to offer to the market. Hence, a careful and accurate prediction of these performance, must be done during the early design stages in order to analyze if the requirements indicated by the company direction will be effectively matched by the new vehicle. To give an idea of what could be these requirements, it is helpful to list the following ones: fuel economy, noxious emission levels, CO<sub>2</sub> emission level, power and torque offered by the vehicle at different engine rotational speeds and so on.

To have the possibility to predict what will be the future mechanical, thermal, electric and electronic behaviour of the new vehicle, some virtual models are necessary realize the appropriate simulations: using the highest possible number of inputs to better characterize the computation of the simulated output variables, these software will give thorough indications related to the performance and features that the new model is going to present. One of the most important aspect that has to be simulated relates to the power/torque performance and fuel consumption of a vehicle; these aspects, in fact, are the most important factors that a customer evaluates during his buying decision: the lower

is the vehicle consumption and the higher are the vehicle performance, the higher is the interest aroused by the vehicle in the possible customers.

The software used at Chrysler to simulate the overall behaviour of the new HEVs during the early design stages, is a proprietary model realized in Matlab® and Simulink® which was started around 2003 by three of the most important worldwide automotive companies. It was created to evaluate performance and fuel consumption of a conventional vehicle and, in the last years, it was modified by the Electrified Powertrain department in Chrysler to expressly predict the final behaviour of the new HEV models designed by the company. The model allows to study the different electrified powertrain alternatives, with the final purpose to evaluate the best possible solution that can be developed to obtain the desired performance and fuel economy. The software provides a library for the selection of the powertrain components that are modeled in detail, from the engine to the wheels, on the basis of their real mechanical, thermal, electric and electronic behaviours. The energy conservation is granted by the model thanks to energy balance equations present in each powertrain subsystem and the efficiency of the components is simulated for every operating condition addressed by the vehicle.

The general mode of operation of the model is based on the possibility to simulate the behaviour of the new HEV while running a certain driving cycle. In this way, during the early design stages, the new HEV model can be virtually tested along a given driving profile, studying the instantaneous magnitude of all its operating characteristics, for example of its driving performance, fuel economy and emission levels. The starting point necessary to run the simulations is, in this way, represented by the upload in the Matlab® base file, that manages all the input variables, of the various profiles defining the overall characteristics of the cycle.

### **3.1.1 Brief description of the driving cycles**

A driving cycle is a series of data points representing the linear speed of a vehicle during time; vehicles can be studied while running a driving profile both really, performing the test on a dynamometer, or virtually, using simulation tools. Driving cycles are produced by different countries and organizations to assess the performance of vehicles and the levels of their fuel consumption and polluting emission [39]. Fuel

consumption and emission tests are performed on chassis dynamometers, collecting and measuring tailpipe emissions and detecting the overall performance of the vehicle. On the other hand, driving cycles can be used also in vehicle simulations. More specifically, they are used in propulsion system simulations that are based on the use of tools and simulators designed specifically to model the drive system of the car, predicting the performance of its internal combustion engine, transmission, electric drive system, batteries, fuel cells and so on.

The driving cycles have been defined by the different countries to represent typical driving conditions and situations of their transportation background; this makes possible to really analyze or virtually simulate the performance of vehicles that are going to be used mainly in a specific country and so in specific road traffic conditions. Hence, the data collection from the test road is the most important activity to create a trusty driving profile, highly representative of the real traffic and driving conditions of the country. The test roads can be of various types, for example they can represent a typical city or highway situation, and the test road data measuring activity must be performed in a thorough way to allow a precise reproduction of the test road characteristics on the chassis dynamometer or on the computer simulator. In practice, the whole idea is to bring the road to the test lab (the dynamometer) or to the simulation software.

Finally, it has to be underlined that the drive cycles can be further classified into two different types:

1. Transient drive cycles: the speed changes a lot based on typical on-road driving conditions; the US Environmental Protection Agency (EPA) Federal Test Procedure (FTP-75) belongs to this type of profile.
2. Modal drive cycles: they involve protracted periods at constant speeds; the New European Driving Cycle (NEDC) is included in this type of profile.

It must be pointed out that, for all the studies performed in this thesis project, the driving cycles that have been used and investigated are the NEDC and the city driving program, or FTP-72, of the FTP-75 cycle, that are described with more details in the following sections.

### 3.1.1.1 New European Driving Cycle

The New European Driving Cycle is a driving profile designed to assess the emission levels and fuel economy of passenger cars (excluding light trucks and commercial vehicles), in a typical traffic condition and usage of a car in Europe [40]. It consists of four repeated ECE R15 Urban Driving Cycles (UDC) and an Extra-Urban Driving Cycle (EUDC).

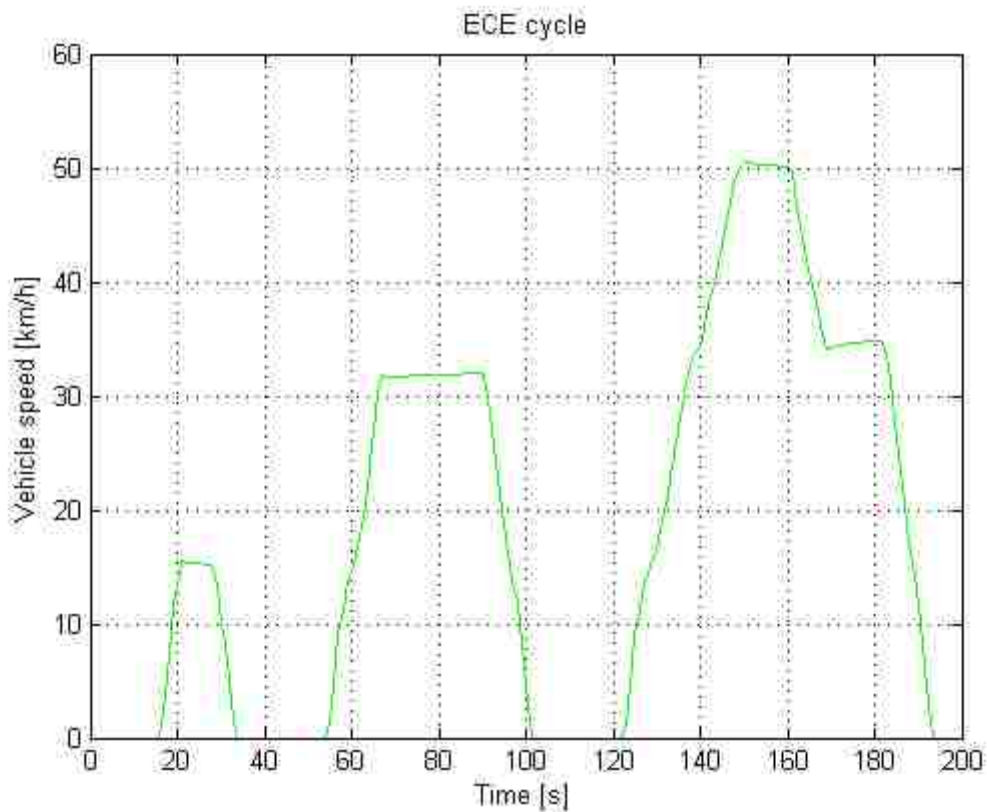


Figure 3.1 - Vehicle speed profile of the ECE driving cycle

The cycle must be performed with a cold startup, at typically 25 °C, with the only engine placed on a dynamometer and connected to an electric break or with the whole vehicle placed on a roller test bench. An electrical machine is used to simulate the resistances due to aerodynamic drag and to the vehicle inertia: for each vehicle configuration, a standard procedure is applied to simulate the resistances acting at every speed value thanks to a reverse torque applied to the drive wheels. A fan is coupled to the dynamometer or to the roller bench to provide the engine and vehicle air intakes with an

airflow matching the current speed. The test is conducted with all the ancillary loads (air conditioning compressor and fan, lights, heated rear window and so on) turned off [40].

### 3.1.1.1.1 Cycle main characteristics

The Urban Driving Cycle, also known as ECE R15 cycle, has been designed to represent typical driving conditions of busy European cities: it is characterized by low engine load, low exhaust gas temperature and a maximum speed of 50 km/h; its speed profile is depicted in Figure 3.1. The cycle ends in 195 seconds after a theoretical distance of 1013 meters, then it repeats four consecutive times. The total duration is of 780 seconds (13 minutes) over a theoretical distance of 4052 meters, with an average speed of 18.68 km/h.

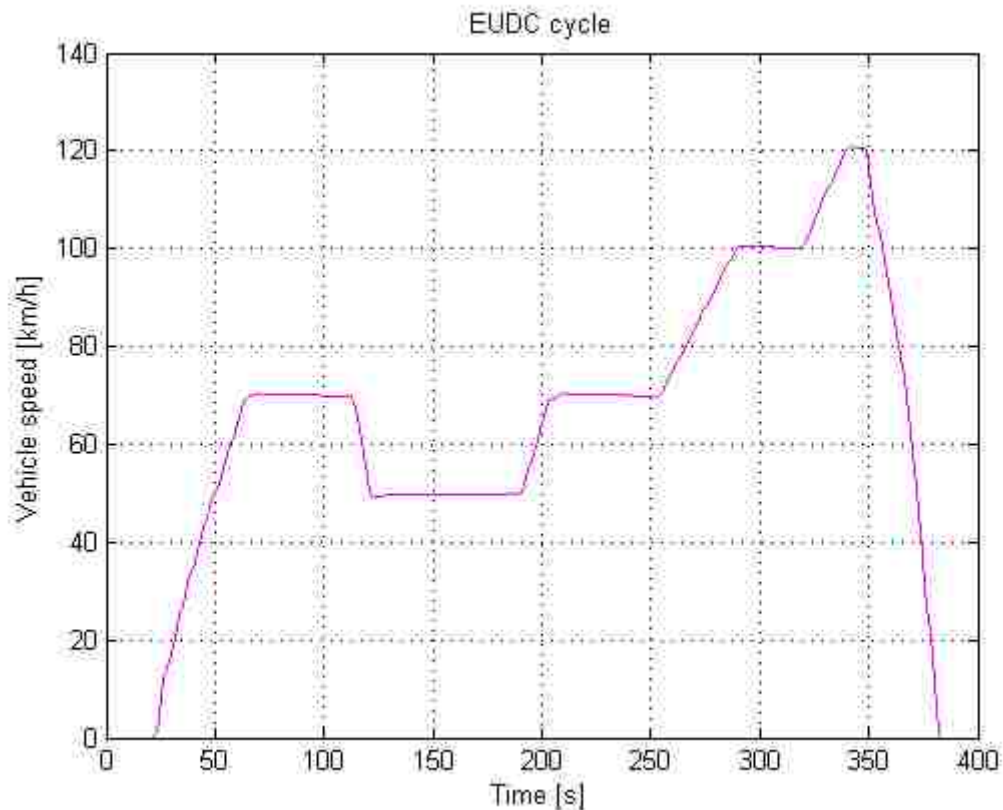


Figure 3.2 - Vehicle speed profile of the EUDC driving cycle

The Extra-Urban Driving Cycle (EUDC), instead, has been designed to represent a more aggressive, high speed driving mode; its speed profile is depicted in Figure 3.2. The maximum speed of the EUDC cycle is of 120 km/h, the total duration is of 400 seconds (6 minutes and 40 seconds), the theoretical distance is of 6944 meters and the average speed of 63.44 km/h.

Finally, the combined cycle covers a theoretical distance of 10996 meters, for a total amount of time of 1180 seconds with an average speed of 33.69 km/h. Its speed profile is shown in Figure 3.3 and its overall characteristics are listed in Table 3.1.

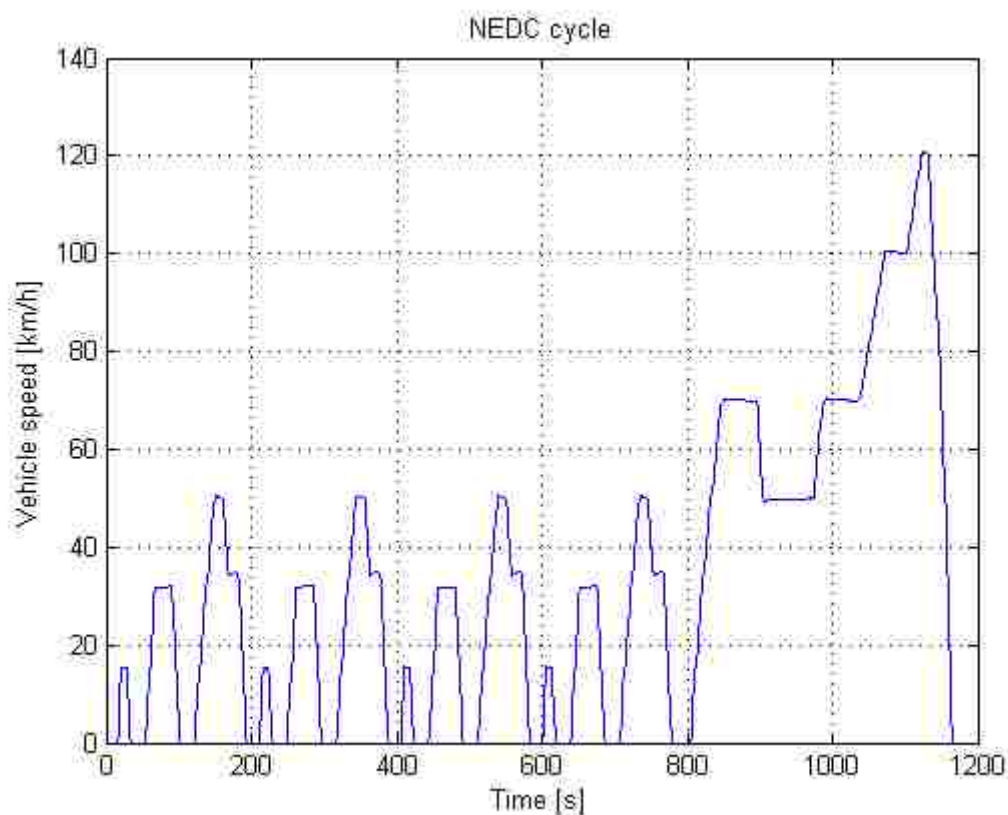


Figure 3.3 - Vehicle speed profile of the NEDC driving cycle

### 3.1.1.1.2 Criticism

The New European Driving Cycle was conceived at a time when vehicles were lighter and less powerful. As can be seen from Figure 3.3, the test offers a driving speed pattern with low accelerations, constant speed cruises and many idling events but, in practice, the transient accelerations events are usually much steeper and more dynamic

because of the power surplus of modern engines [40]. A new version of the driving cycle should also be realistic towards the daily use of ancillary units and functions which tend to be fitted to modern vehicles and used for long periods by the driver and passengers.

**Table 3.1 - NEDC driving cycle main characteristics**

<b>Time</b>	1180 s
<b>Distance</b>	10.996 km
<b>Maximum speed</b>	120 km/h
<b>Average speed</b>	33.69 km/h
<b>Maximum acceleration</b>	1.06 m/s <sup>2</sup>
<b>Maximum deceleration</b>	-1.39 m/s <sup>2</sup>
<b>Average acceleration</b>	0.54 m/s <sup>2</sup>
<b>Average deceleration</b>	-0.79 m/s <sup>2</sup>
<b>Idle time</b>	257 s
<b>Number of stops</b>	13

### **3.1.1.2 EPA Federal Test Procedure**

The EPA Federal Test Procedure, commonly known as FTP-75, is a series of tests defined by the US Environmental Protection Agency in order to measure the emissions levels and fuel economy characteristics of passenger cars (excluding light trucks and heavy-duty vehicles). One of the test included in the FTP-75 is the city driving program, or FTP-72, that constitutes the initial part of the whole speed profile of the EPA procedure. Another test is represented by the Highway Fuel Economy Driving Schedule (HWFET), that can be added at the end of a typical city cycle and represents extra-urban driving conditions; it is going to be described in the next chapter before presenting the analysis of the results.

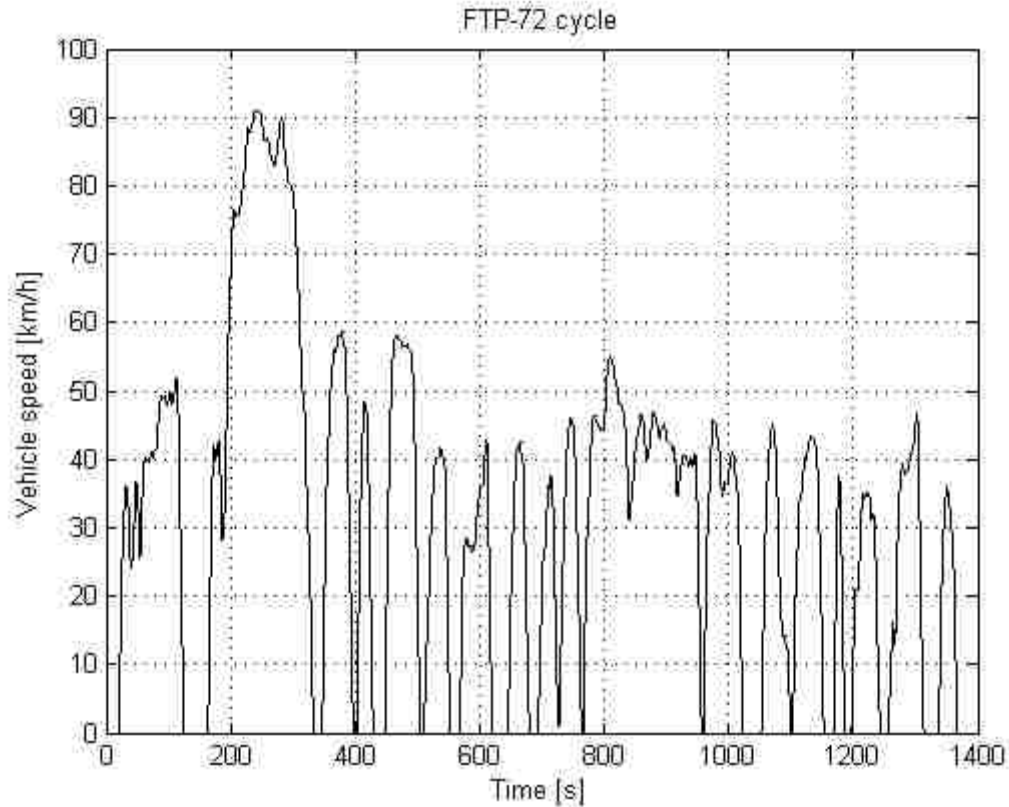


Figure 3.4 - Vehicle speed profile of the FTP-72 driving cycle

### 3.1.1.2.1 FTP-72

The city driving program is based on the Urban Dynamometer Driving Schedule (UDDS), that defines a typical urban profile to be done starting with a cold engine and making 17 stops over a period of 1369 seconds and a distance of 12 km, with an average speed of 31.5 km/h and with a top speed of 91.2 km/h [41]. The cycle is constituted by a “cold start” phase, that lasts for the first 500 seconds, and by a “transient” phase, that covers approximately the remaining 900 seconds. The speed profile of the cycle is represented in Figure 3.4 and its overall characteristics are listed in Table 3.2.



**Table 3.2 - FTP-72 driving cycle main characteristics**

<b>Time</b>	1369 s
<b>Distance</b>	12 km
<b>Maximum speed</b>	91.2 km/h
<b>Average speed</b>	31.5 km/h
<b>Maximum acceleration</b>	1.48 m/s <sup>2</sup>
<b>Maximum deceleration</b>	-1.48 m/s <sup>2</sup>
<b>Average acceleration</b>	0.50 m/s <sup>2</sup>
<b>Average deceleration</b>	-0.58 m/s <sup>2</sup>
<b>Idle time</b>	244 s
<b>Number of stops</b>	17

### 3.1.2 Chrysler HEV prediction model features

After the general analysis of the main characteristics of the NEDC and FTP-75 driving cycles, it is necessary to continue the description of the simulation tool used in the Electrified Powertrain department at Chrysler to predict the performance and fuel economy of the new HEV models during the early design stages. As stated in chapter 3.1.1, the model allows to evaluate the different electrified powertrain alternatives, in order to individuate the best possible solution in terms of mechanical, thermal, electric and electronic design that can lead to the desired performance and fuel economy.

Figure 3.5 shows the main Simulink® interface of the model the user deals with, depicting all its main blocks and connections: as can be seen, the drive cycle characteristics, and in particular its specific speed profile, are the inputs of the model.

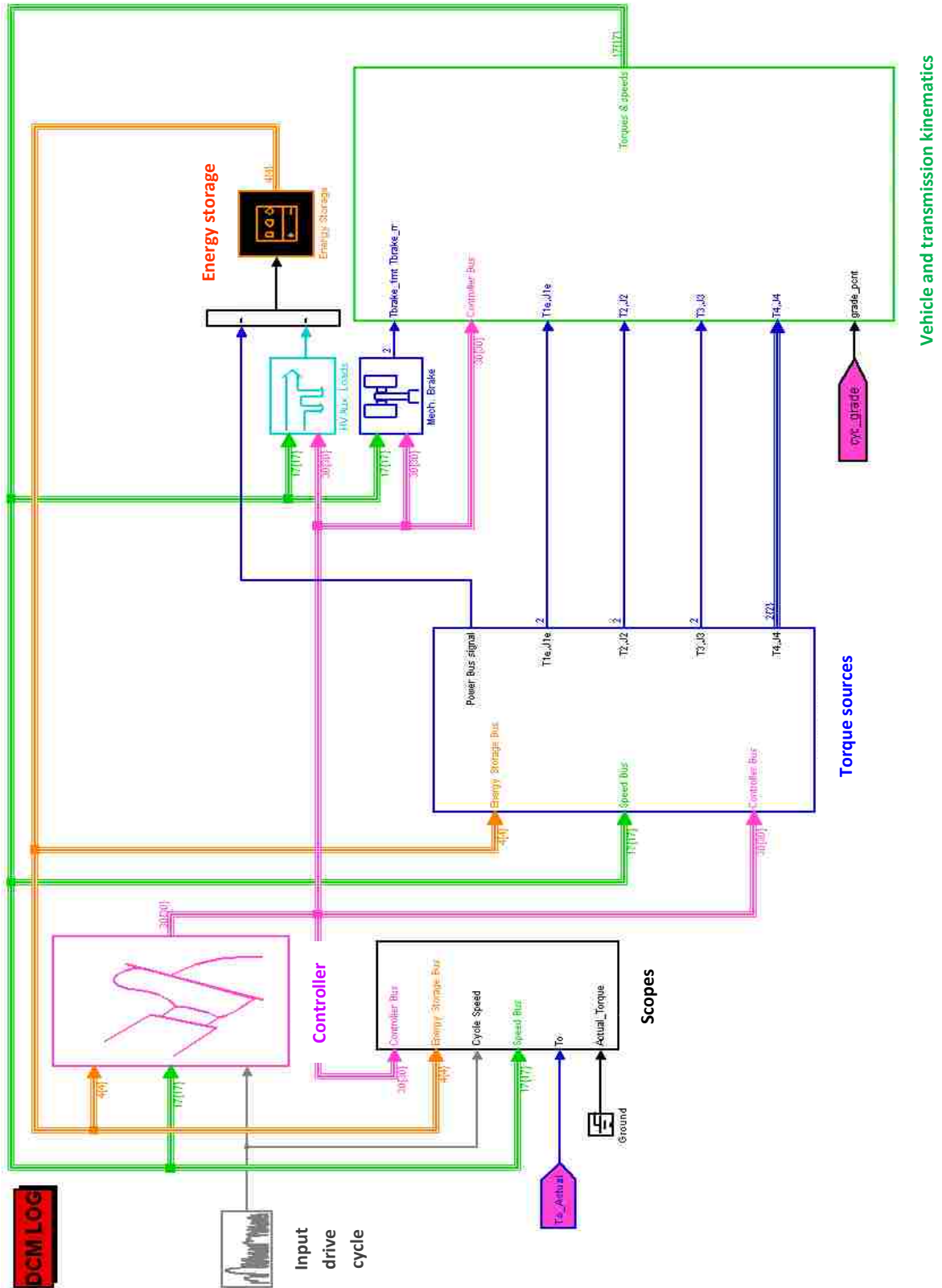


Figure 3.5 - Main control Simulink® interface of the Chrysler HEV prediction model

Figure 3.5 shows the main Simulink® interface of the model the user deals with, depicting all its main blocks and connections: as can be seen, the drive cycle characteristics, and in particular its specific speed profile, are the inputs of the model. The “controller” block evaluates the torque and power requested in order to run the vehicle at the speed specified instantaneously in the cycle and the final outputs of the model are the fuel economy and emissions level predictions, in addition to the power and torque trend expressed with respect to the driving cycle time. Instant per instant, the model considers the speed magnitude indicated by the driving cycle and, in order to compute the necessary power and torque that the vehicle has to deliver to cover this speed value, the tool calculates the instantaneous values of the resistances that counteract the vehicle motion. The aerodynamic resistance, the tire rolling resistance, the climbing resistance, the resistance due to the friction of the toothed gears engaged in the gearbox, the resistance due to the driveline downstream of the gearbox and, finally, the resistance due to possible remaining torque of the braking system, are computed with a coastdown procedure: the “controller” calculates the suitable coast function and coefficients based on the losses in the system, which are included in the “vehicle and transmission kinematics” block. Moreover, depending on the ancillary loads that can be activated during the driving profile by the driver or the passengers, the model defines the auxiliary power and torque requests that the vehicle has to deal with.

For a HEV, the “torque sources” block splits the output power request between the two available power sources, engine and electric machine, with the purpose of finding the optimum operating point of the engine, minimizing the losses in the system and obtaining the best fuel consumption. In this way, during the virtual running of the driving cycle, thorough predictions of the performance of the HEV can be done and, moreover, the design activity can be updated and modified in order to allow the vehicle to operate as long as it can in the optimum operating condition. In particular, the “controller” is characterized by two levels of optimization, called static and dynamic: during the static optimization, the “controller” defines the best operating point for the internal combustion engine at a specific time instant, on the basis of the requested power, and defines also the related power generation division between the engine and the electric machine; after that,

the dynamic optimization defines the most efficient path for the engine transient in order to reach the static optimum, starting from the current operating point.

### **3.1.3 Chrysler HEV prediction model strengths**

The main possibility offered by the model is represented by the prediction of the performance, fuel economy and emissions level of the investigated HEV, during its early design stages. At the same time, the tool performs an optimization activity determining the optimum operating conditions in which the vehicle components and sub-systems have to operate. In this way, the development teams can update and modify the design procedure of the HEV, in such a way it can meet these optimum conditions during its whole life, once it will be produced by the company.

Moreover, one the most important characteristics of this model is represented by the possibility to reproduce every operating aspect of the investigated HEV during the early design stages, on a real time basis. The instantaneous operating conditions of the vehicle transmission, engine, electric machine and battery are in fact simulated by the software for every instant of the driving cycle. Moreover, a real time optimization can be realized with the tool thanks to the “controller” optimization activity described in the previous section. This important feature offered by the model, allows the HEVs development teams to identify:

1. the best gear pattern that the gearbox has to present with respect to the different speed values indicated by the driving profile;
2. the best engine start-stop control to be performed during the various idle conditions;
3. the best battery energy/power ratio that affects the decision about what battery chemistry and voltage level have to be chosen.

Finally, the fact that the software considers and computes a lot of variables in order to predict the final performance and fuel economy of the HEV, ensures a high level of accuracy of the prediction activity and, moreover, also of the optimization phase.

### **3.1.4 Chrysler HEV prediction model weaknesses**

One of the most relevant concerns that has to be taken into account while dealing with prediction tools, is related to the level of accuracy of the predictive method implemented and used by the model. The logical and computational procedure created on Matlab® and Simulink® must represent in the best possible way the real behaviour of the investigated HEV, in such a way that every mechanical, thermal, electric and electronic variable is determined accurately and precisely. In order to do that, every powertrain component has to be simulated by the software taking into account all the variables that can affect its behaviour and performance. Moreover, all the mathematical and physical links existing between a given variable and all the other ones defining the system architecture, must be logically represented by the Simulink® software; the tool, finally, has to compute every physical quantity taking into account all of its dependences on the other ones with the final purpose to give, as outputs, results close to what will be the real behaviour of the whole hybrid electric vehicle system, once it will be really on the road.

Taking into account what has been stated in the previous paragraph, a thorough analysis of the actual architecture of the model must be performed in order to highlight if some physical and/or mathematical connection between the variables defined in the tool is missed. If, for example, a certain quantity *A* that physically depends on the quantity *B*, among other, is not defined in the Simulink® tool with respect to the actual value of *B*, its accuracy level will be inevitably objectionable. Hence, to consider the outputs of the model as sensitive data with a high level of fidelity, is necessary that every physical links existing in the real world between the variables of the system must be logically represented by the software and implemented in the Matlab® and Simulink® files.

In this regard, two important aspects are not considered by the Chrysler model at the moment; both of them refer to the thermal behaviour of the whole HEV system, in particular the internal combustion engine and the battery that gives energy to the electric machine. More precisely, the simulation tool does not compute the temperature of the ICE coolant and, at the same time, it does not compute also the instantaneous temperature of the cells of the HEV battery pack. The mechanical efficiency of the engine, decisive in the fuel economy and performance analysis, strongly depends on the temperature of the coolant and so this temperature has to be carefully determined by the model that, actually,

it is not provided with a computational path that can allow this type of calculation. Moreover, the temperature of the cells, constituents of the battery pack, must be computed with a high level of accuracy because on it depends the state of charge of the battery and also the value of its internal resistance.

#### **3.1.4.1 Internal combustion engine coolant temperature**

Not all the work transferred to the piston from the gases burnt inside the cylinder is available at the drive shaft for actual use; a certain portion of the work which is not available is usually termed friction work. The friction work, or power, is a sufficiently large fraction of the work, or power, delivered by the fresh mixture burning and so it is of great practical importance in engine design. Friction losses affect the maximum brake torque and the minimum brake specific fuel consumption directly: often, the difference between a good and a bad engine design is determined by the quantity of frictional losses that determines the mechanical efficiency.

A large part of the friction losses appears as heat in the engine coolant and oil, that has to be removed by the radiator and oil cooler system. Thus, friction losses strongly influence the size and the operating conditions of the coolant systems that, finally, have a great impact on the performance and fuel economy of the investigated HEV, tested with the simulation model in the early design stages. The instantaneous values of the temperature of the coolant and oil, determine in fact the working performance of the engine affecting the amount of work necessary to overcome the resistance to relative motion of all its moving parts: this includes the friction between the piston rings and skirt and the cylinder wall; the friction in the wrist pin, crankshaft and camshaft bearings; the friction in the valve mechanism and in the gears, pulleys and belts of the transmission and engine accessories.

Hence, it is clear that the Simulink® model used at the moment by the Electrified Powertrain department teams at Chrysler, must be modified introducing a new computational path that allows to determine the trend during time of the temperature of the coolant of the internal combustion engine of the investigated HEV. In this way, once the model will be updated, it will be possible to consider the magnitude of the coolant temperature during all the instants of the driving cycle used for the simulation, predicting

with a considerably higher level of accuracy the performance and fuel economy of the tested vehicle. This because, taking into account the instantaneous temperature of the engine coolant, the effective amount of friction work and power during time can be determined.

#### **3.1.4.2 High voltage battery temperature**

The performance and fuel economy of a hybrid electric vehicle are strongly linked to the operation of its electrical source of power, the electric motor, and energy storage device, the battery. Dealing with mild hybrids, the battery has a voltage of more than 60 Volts and can be called “high voltage battery”: delivering power, when the driver is asking for an assist from the electric machine, and receiving power, during the recharge phases, the battery is characterized by a current flow that generates heat for the Joule effect, as stated by Equation 3.1.

$$P_{diss} = R \cdot I^2 \quad (3.1)$$

The term  $P_{diss}$  represents the power dissipated as heat by the battery,  $R$  is the internal resistance of the battery, that depends on its electrochemistry, and  $I$  is the magnitude of the current that is flowing during battery operations. Hence, as the current flows through the cells that constitute the battery pack of the HEV, their temperature tends to increase, affecting the behaviour of the whole energy storage device. In fact, battery temperature influences the life of the device and the availability of discharge power (for startup and acceleration), energy and charge acceptance during energy recovery from regenerative braking, affecting finally the overall vehicle drive-ability and fuel economy [42]. Therefore, ideally, batteries should operate within a temperature range that is optimum for their performance and life: the desired operating temperature range is different for different battery types (with different electrochemistry) and, usually, is between 20 and 30 °C.

In general, higher temperatures improve the rate at which the battery can be charged or discharged; however, the battery’s number of recharges and its total time in service decrease if it operates for too long time in hot climates [43]. Lower temperatures lead to

slower charge and discharge operations because of a decrease in the conductivity of the ionic conductors used in electrolytes, separators and electrodes: an overall increase of internal resistance is experienced by the battery, whose operating cycles become sluggish. At the same time, lower temperatures tend to extend the cycle and calendar life of the battery because, in colder climates, the internal chemical degradation reactions are slowed down. Hence, it is possible to underline that at higher temperatures the degradation reactions accelerate and cause a reduction of the overall charging efficiency of the battery: in order to reach a certain state of charge, an increased amount of energy must be delivered. Finally, it can be stated that the overall behaviour of a battery is strongly affected by its temperature that, directly or indirectly, defines the rates of charge and discharge cycles, the magnitude of the internal resistance, the cycle and calendar life, the charging efficiency and, moreover, the open circuit voltage (that depends on the SOC).

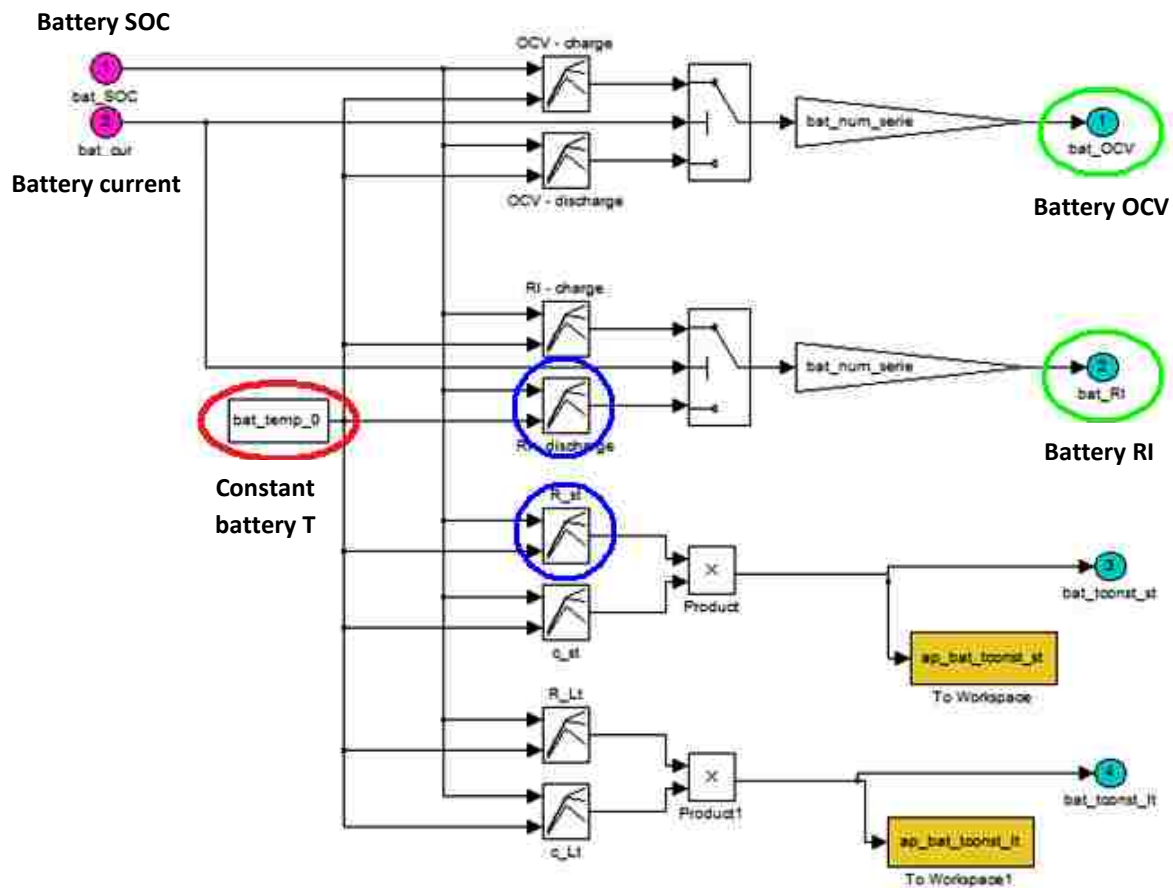


Figure 3.6 - Multi-points map interpolation system computing of the HVB open circuit voltage and internal resistance



Considering what has been described in the previous paragraphs, it is clear the necessity to compute instant per instant the actual temperature of the cells of the battery pack and so, in general, the actual temperature of the HEV battery. In this way, every quantity defining the behaviour of the electrical energy source can be computed by the model with a high level of accuracy, making possible to obtain thorough and precise final predictions about the performance and fuel economy of the investigated HEV. Unfortunately, at the moment, the Chrysler tool does not compute the instantaneous value of the battery temperature during the simulations but, on the contrary, asks to the user to insert a fixed value for the battery temperature that is taken as constant for the whole driving cycle. In this way, the state of charge of the battery and its internal resistance are computed with respect to this temperature input value decided by the user and so their accuracy is not satisfactory. A new computational loop should be added to the actual model, in order to calculate the time trend of the battery temperature during the whole driving cycle: knowing the actual temperature of the battery, its SOC, internal resistance, open circuit voltage and other temperature-dependent variables, can be determined more precisely.

In Figure 3.6, highlighted in the red circle, it is shown a “Constant” block of Simulink®, where the user can input the constant value of the battery temperature that will be considered during the whole simulation. This value is going to be used, among the others, as an input for the multi-point maps (indicated in the blue circles) that define, for example, the magnitude of the internal resistance and open circuit voltage of the battery (highlighted in the green circles). Considering, for the sake of simplicity, the internal resistance, it is possible to state that, if it is computed from a multi-points map that has four inputs, including the battery temperature, if this temperature is a constant then the resistance calculation is not as precise as it should be. To improve the resistance definition, the solution is to use as an input of its multi-points map, the instantaneous value of the battery temperature computed thanks to a new designed Simulink® loop that takes into account the thermal behaviour of the battery pack. Calculating, instant by instant, the values of the temperature of the cells, the “Constant” block in the red circle can be replaced by the variable output of the new computational loop: the final benefit

will be represented by a more precise and trusty definition of the battery internal resistance.

#### **3.1.4.3 Necessity for an update of the Chrysler HEV prediction model**

Considering what has been underlined in the two previous sections, an effective update of the tool used in the Electrified Powertrain department at Chrysler, to simulate and predict the performance and fuel economy of hybrid electric vehicles, is necessary. In fact, the design of suitable new logical and computational loops in the Simulink® model will give the possibility to compute the actual time trend of the temperature of the internal combustion engine coolant and of the cells of the battery pack. It can be seen how the importance of the main objective of the thesis project has a really high relevance both from a company and scientific research point of view: the company will benefit from the operative results of the project, if successful, with an updated model capable of more accurate and precise predictions and simulations while, at the same time, the scientific audience will appreciate two new physical models created to compute the ICE coolant and battery cells temperature time trend for HEV applications.

The work will be considered successful by the company if, at the end of the design process of the ICE and battery thermal models, they will be integrated in the overall simulation tool allowing it to obtain more accurate final results and performance and fuel economy predictions. Thanks to the new thermal models, the software will have, in fact, the possibility to deal with the actual instantaneous values of the engine coolant and battery cells temperature: in this way, a precise and effective computation of the friction work and power of the engine and, moreover, of the temperature-dependent quantities that define the behaviour of the battery, will be possible. Finally, this possibility will lead to an overall improvement of the accuracy level of the results generated by the whole model.

From a research perspective, the two new thermal models, whose design is the main purpose of this work, will represent an innovation if they will be characterize by the possibility to determine the actual temperature of the engine coolant and of the battery with respect to a high number of input variables and considering every physical aspect that characterizes the thermal behaviour of this entities. Searching through the modern

literature, there are not too much information related to similar already existing thermal models but, from papers and conferences' proceedings, it is possible to note that all the studies that have been done in these specific areas do not deal with a comprehensive background and with a high number of input variables that can allow to simulate with high precision the time trend of the engine coolant and battery temperature for hybrid electric vehicles.

### **3.2 Brief description of the Matlab® and Simulink® virtual platforms**

Matlab® (matrix laboratory) is a numerical computing environment, developed by MathWorks, that allows matrix manipulations, plotting of functions and data and implementation of algorithms. Simulink®, instead, is a graphical programming language tool for modeling, simulating and analyzing multidomain dynamic systems; its primary interface is constituted by a graphical block diagramming tool and by a customizable set of block libraries [44]. It offers tight integration with the rest of the Matlab® environment and, usually, it is run executing a Matlab® script.

For the purposes of this thesis project, a deep knowledge of the Matlab® and Simulink® environment is necessary because the Chrysler simulation tool is totally developed using these computing platforms: its operations are based on the execution of a base file, written in Matlab® with the suitable script, and of a simulation loop, implemented on Simulink® with the suitable logical blocks. The Matlab® file manages the creation of the input variables of the model, that are stored in a “Workspace”, and the Simulink® file uploads all these variables and operates on them processing all the calculations defined by the logical loop that has been created. In order to design the two new thermal models (related to the ICE and to the battery pack) that will be integrated in the basic software, a deep knowledge of the programming languages, of both Matlab® and Simulink®, is necessary to transpose on the virtual plan the physical theory at the base of the thermal behaviour of the engine and of the battery pack. Hence, the first step is represented by the creation of the correct mathematical and physical background and theory that manage and describe the heat exchange phenomena of the two HEV's devices; the second step consists in “writing” this theory using a new language, the computer's one. In this way it is possible to design on Matlab® and Simulink® two thermal models

that virtually predict the behaviour of the HEV's engine and battery pack, simulating the physical theory that regulates the heat generation and transfer phenomena.

The main feature offered by Simulink® is the possibility to run simulations during time, determining the time variations of the desired outputs, whose trend can be plotted with respect to time at the end of the computation. In this way, the variables of interest can be calculated instant per instant on the basis of the given inputs expressed as two-columns vectors: the first column contains increasing time values while the second one contains the related magnitudes of the quantity described by the vector. For this work, the input variables are the driving cycle characteristics that are taken from Excel® files and stored in the “Workspace” by the Matlab® script in order to be used afterwards by the two new Simulink® models. For example, as it will be carefully described in the next sections, some of the driving cycle characteristics are represented by the instantaneous values of:

1. vehicle linear speed;
2. engine rotational speed;
3. engine torque;
4. exhaust gases temperature;
5. radiator inlet and outlet temperatures;
6. engine coolant mass flow rate;
7. battery pack coolant mass flow rate;
8. fuel mass flow rate;
9. ambient temperature;
10. current flowing through the high voltage battery (considering mild hybrids);
11. engine inlet fresh charge temperature.

All the quantities contained in the Excel file representing the characteristics of the driving cycle are experimental quantities, detected during the test of already existing vehicles on the chassis dynamometer, or simulated quantities, generated by suitable simulators that virtually reproduce the behaviour of new vehicle models asked to follow the linear speed profile indicated by the cycle.

### 3.2.1 Basic structure of the Matlab® and Simulink® files of the new thermal models

In order to create the desired thermal models for the engine and battery of a hybrid vehicle, a suitable code writing and tool design activity has to be done. The first step consists in the creation of a Matlab® base file that manages the creation of vectors expressing all the driving cycle quantities with respect to time. After the execution of the Matlab® script, all these vectors are created from the Excel® database and stored in the “Workspace” of the program, ready for future use. At this point, the connection between the Matlab® and Simulink® files takes place: in fact, once the Matlab® base file’s script has been executed, the Simulink® model can be activated, pressing the “play button” on the main interface, as depicted in Figure 3.7, and starting in this way the simulation. Once the simulation has been started, the Simulink® computational loop begins to work, managing all the input variables uploaded from the Matlab® “Workspace” with the various mathematical and logical blocks that have been taken from the libraries.

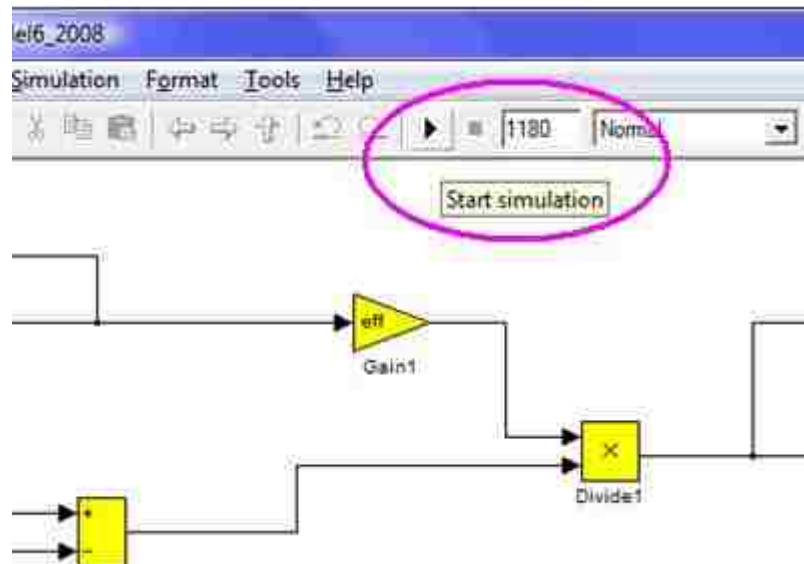
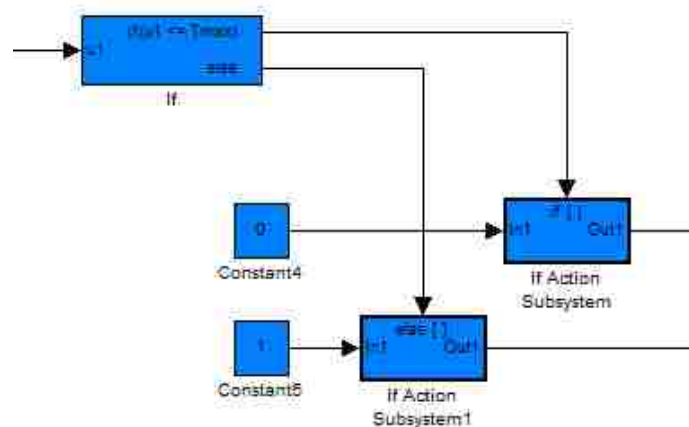


Figure 3.7 - Start simulation button of the main Simulink® interface

The Simulink® models have to be carefully designed, using the suitable blocks to reproduce the physical theory at the base of the thermal phenomena that characterize the engine and battery behaviour. At the end of the simulation, the model gives as outputs the desired investigated quantities, in the form of vectors expressed with respect to time that can be plotted in graphs. All these outputs have been determined processing the inputs of

the model that, passing through the various computational blocks, are combined to satisfy all the equations written during the physical theory study phase. Both the Simulink® files related to the engine and the battery thermal models, include some sub-blocks, as will be explained in the following sections, that contain complex calculation procedures: the Simulink® platform, in fact, gives to the user the possibility to organize the progressive logical and computational step in separated sub-blocks, in order to obtain a final model's interface easier to manage for the user.

Moreover, from the Simulink® libraries, some “if/else” sub-blocks can also be taken and used inside the calculation loop, in order to impose some “if” conditions that might be necessary to describe mutually exclusive events. For example, in Figure 3.8 is depicted a typical “if/else” sub-block that, in this case, lets pass a 0 value in case the “if” condition is satisfied; on the contrary, is a 1 value that the block lets pass (the “else” condition is satisfied).



**Figure 3.8 - Typical “if/else” sub-block taken from the Simulink® library**

The final outputs of the overall logical and computational structure implemented on Simulink®, are vectors of elements expressed with respect to the time vector of the investigated driving cycle. If the two new models that have to be designed during the internship at Chrysler, to implement the prediction tool used by the Electrified Powertrain department, will be correctly built, their outputs will be the ICE coolant and battery cells temperature time trends. These trends, if correctly determined (as close as possible to the reality of the thermal phenomenon), will allow the simulation software to define the

temperature-dependent variables, that determine the ICE and battery behaviour, with a higher level of accuracy. At the moment, the actual simulation tool does not compute the engine coolant temperature and use a constant value for the battery temperature: dealing with time varying temperature values, if correctly computed, obviously determines an improvement of the predictive performance of the software.

### **3.3 Internal combustion engine cooling system model design**

The first model that has been designed during the internship at Chrysler, is the one describing the thermal behaviour of the engine. As stated before, the actual prediction tool used by the Electrified Powertrain development team is not provided with a computational block that determines the temperature of the engine coolant: in this way, the overall performance and operating conditions of the HEV's engine cannot be precisely simulated and the final results are not satisfying.

Hence, the first target of this work consists in the design of a model, implemented in Matlab® and Simulink®, that can compute, instant per instant, the temperature of the engine coolant during the virtual running of the given driving cycle performed by the investigated hybrid electric vehicle.

The final output of this new sub-model, that has to be integrated in the overall Chrysler prediction software, must be represented by the time trend of the engine coolant temperature, computed with respect to all the time-dependent variables specified by the driving cycle. When the investigated HEV is studied in its early design stages, while running the given driving cycle on the Chrysler simulation tool, the instantaneous value of the coolant temperature is computed thanks to new thermal sub-model and, finally, this value is used by the overall tool to determine the instantaneous value of the friction work and power generated by the engine.

The starting point is a blank paper, and so the design activity has to be performed without a previous base and path that can be followed. This is a disadvantage, because the objective of the thesis becomes more difficult to be achieved without a starting track to follow but, at the same time, it could be also an advantage, because the design can be realized without external limitations and constraints. The final target is therefore to realize an advanced thermal model that can compute the temperature of the ICE coolant

with respect to the highest possible number of input variables, in such a way that the calculation can be characterized by a high level of accuracy and precision. More specifically, if the temperature time trend is determined considering all the possible source of heat that characterize the engine, the final result will be the closest to the reality of the phenomenon.

To conclude, the first step of the design is represented by the creation of the physical and mathematical background theory that defines the heat transfer phenomena taking place between the engine and its coolant medium; the second step is instead represented by the transposition of the theoretical model on the Matlab® and Simulink® platforms, with the final creation of the operative engine thermal tool that can be finally integrated in the Chrysler prediction and simulation software.

### **3.3.1 Basic concepts about internal combustion engine operations**

Internal combustion engines operate thanks to the combustion of a fuel that occurs with an oxidizer (usually air) in a combustion chamber; the expansion of the high-temperature and high-pressure gases produced by combustion, apply a direct force to the reciprocating pistons of the engine allowing the rotation of its shaft, transforming in this way the chemical energy into useful mechanical energy.

Internal combustion engines are commonly used for mobile propulsion, since they can provide high power to weight ratios together with excellent fuel energy density. In this way, the overall weight of the propulsion system is not so high and allows a convenient application of this energy source on a land vehicle.





Figure 3.9 - Example of internal combustion engine [45]

All internal combustion engines base their operations on the combustion of a fossil fuel, that has to be ignited and provided with oxygen from the air in order to burn and create energy. The combustion process typically results in the production of a great quantity of heat that, finally, is partially transformed in mechanical energy that can move the vehicle. Significant amounts of heat are, unfortunately, lost by the engine in various forms and because of different phenomena and, in particular, a certain part of the combustion heat goes to the coolant medium. The coolant, cooperating with the engine radiator, has the important objective to maintain the engine temperature below a threshold of about 105 °C to avoid damages to the engine materials and lubricants. At the same time, the cooling system has to maintain the temperature of the engine above a certain limit, guaranteed by a minimum temperature of the coolant of about 85 °C, because at lower temperatures the wear of the moving parts of the engine accelerates and its overall efficiency decreases, causing higher fuel consumption and emissions levels.

The internal combustion engines used for hybrid applications work exactly in the same manner of the engine used for conventional vehicles; the only difference could be represented by lower displacement and dimensions because, thanks to the presence of the electric motor that generates additional energy and power, the engine can be downsized.

### 3.3.2 Driving cycle input data and creation of the Matlab® base file

First of all, in order to design the engine cooling system model, the physical theory that regulates the engine thermal behaviour must be implemented. The final objective of the new model, as stated in the previous section, is to compute the time trend of the engine coolant temperature on the basis of the time-dependent quantities that characterize the investigated driving cycles. The more are the quantities used to determine the final desired output, the higher is the physic relevance covered by the results: the thermal behaviour of the engine, in fact, depends on a lot of different variables that must be taken into account in the calculation loop of the Simulink® file that is going to be created. In this perspective, the inputs of the model have to be carefully analyzed before starting the design activity; in the Excel® file containing all the driving cycle characteristics, it is possible to individuate, among the others, the following important quantities that will cover a decisive role in the computation of the engine coolant temperature time trend:

1. engine rotational speed, expressed in rpm;
2. engine torque, expressed in Nm,
3. vehicle linear speed, expressed in km/h;
4. exhaust gas temperature, expressed in °C;
5. engine inlet fresh charge temperature, expressed in °C;
6. ambient temperature, expressed in °C;
7. cabin temperature, expressed in °C;
8. air mass flow rate going inside the cabin, expressed in kg/s;
9. engine coolant mass flow rate, expressed in kg/s;
10. radiator inlet coolant temperature, expressed in °C;
11. radiator outlet coolant temperature, expressed in °C;
12. fuel mass flow rate, expressed in kg/s.

All these quantities are expressed, instant per instant, with respect to the time vector of the driving cycle and are uploaded in the Matlab® base file and then saved in its “Workspace”. In order to be used by the Simulink® model, these variables must be allocated in two-columns vectors: the first column contains the progressive values of time defining the duration of the driving cycle, while the second column contains the values of the variable described by the vector itself.

### 3.3.3 Internal combustion engine cooling system model theoretical and virtual design

In this section, the implementation of the physical theory at the base of a model which can predict the coolant temperature of an internal combustion engine, during a given driving cycle, is studied in details. Moreover, the design activity realized using the Matlab® and Simulink® computer platforms, is thoroughly described to understand how the engine cooling system model has been created and how it works.

In a water cooled engine, the coolant temperature is regulated by a thermostat which is usually mounted between the engine and the radiator input: when the engine is cold, the thermostat is closed and the coolant bypasses the radiator in order to heat up the engine as quickly as possible; when the engine reaches its desired operating temperature, the thermostat opens and the coolant temperature is kept constant allowing the coolant to flow through the radiator. A careful study of the cooling system energy balance must be done, in order to write the correct equations that regulate the heat transfer phenomena between the engine and the whole vehicle system.

In order to compute the instantaneous temperature of the coolant, the heat that the coolant itself receives instant per instant from the overall heat quantity produced instantaneously by the fresh mixture burning must be determined. Hence, the different heat “consumptions” are subtracted from the heat produced inside the cylinders in order to obtain the heat that is going to the coolant, as described in Equation 3.2.

$$\dot{Q}_{coolant} = \dot{Q}_{combustion} - \dot{Q}_{exhaust} - P - \dot{Q}_{heater} - \dot{Q}_{surrounding} - \dot{Q}_{radiator} \quad (3.2)$$

Referring to the previous equation, it is necessary to underline that is not correct to use the word “heat” to define its terms but, instead, the concept of “heat rate” must be used: the heat rate represents, in fact, the rate at which the heat is exchanged between two or more entities and its unit of measure is the Watt, equal to the ratio between Joules and seconds. Deriving with respect to time a certain heat quantity ( $Q$ ), the corresponding heat rate can be computed ( $\dot{Q}$ ). In internal combustion engines, the produced energy comes from the combustion of the fuel that is ignited and burnt into the cylinders, thanks to the oxygen taken from the inlet air: this energy results in both mechanical energy and heat.

The different power and heat rate contributions that are contained in Equation 3.2 are described in the following list:

- $\dot{Q}_{combustion}$  is the heat rate generated by the combustion of the fuel inside the cylinders;
- $\dot{Q}_{exhaust}$  is the heat rate that is going to the exhaust gases exiting from the engine outlet manifolds;
- $P$  is the mechanical power generated at the engine crankshaft;
- $\dot{Q}_{heater}$  is the heat rate that is going to the cabin heater, to increase the temperature of the air entering in the cabin of the vehicle;
- $\dot{Q}_{surrounding}$  is the heat rate lost by the engine that is going to the surrounding air;
- $\dot{Q}_{radiator}$  is the heat rate dissipated by the engine coolant through the radiator when the thermostat is opened.

Knowing the heat that is going to the coolant during time, it becomes possible to calculate the instantaneous coolant temperature. In the following, the physical theories at the base of the different heat rate and power contributions are described and, moreover, the related logical and computational blocks implemented on Simulink® are carefully explained.

In Figure 3.10 is depicted the overall structure of the engine cooling system model implemented in Simulink®, with all the necessary blocks taken from the libraries to transpose all the equations describing the thermal phenomena to the computer level. Each heat rate and power contribution is computed with the suitable logical loop and, finally, the heat going to the coolant and its instantaneous temperature are determined during time.

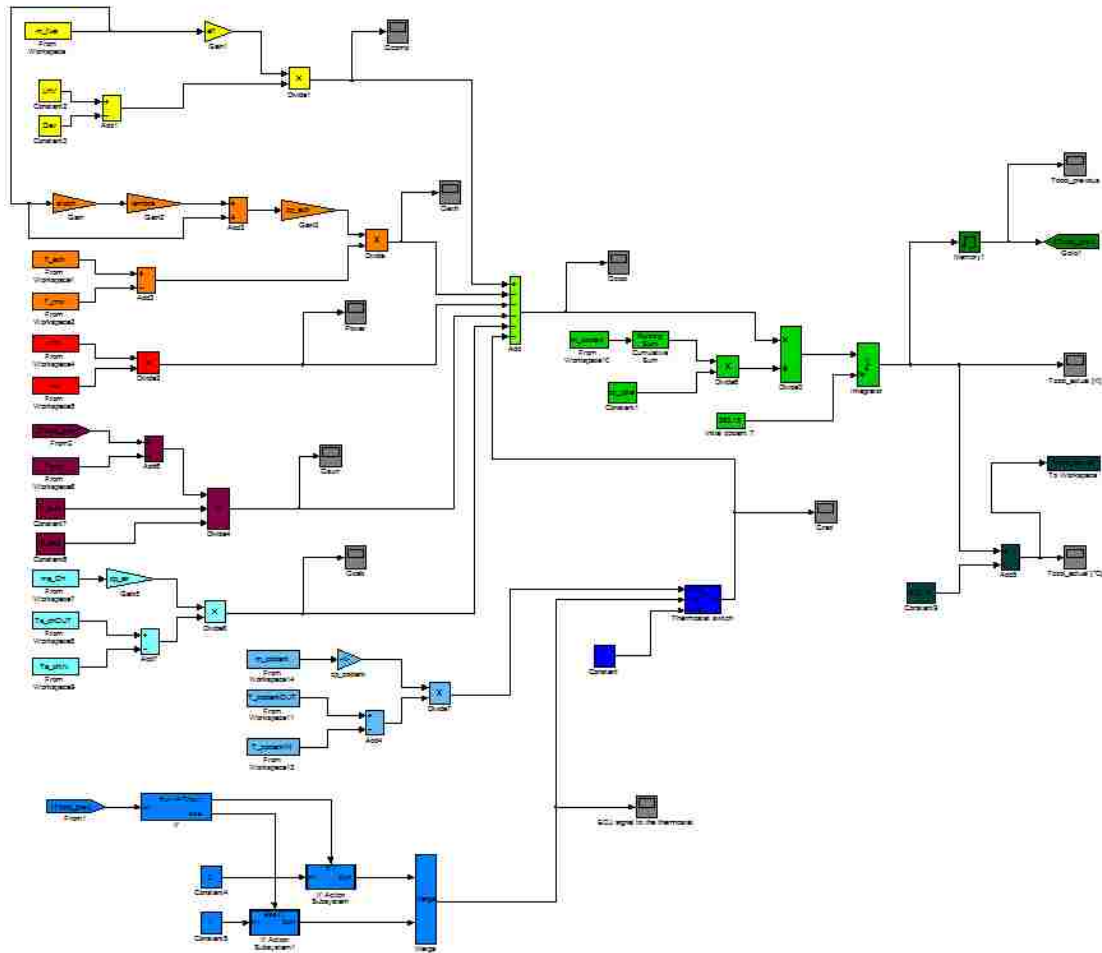


Figure 3.10 - Overall Simulink® structure of the internal combustion engine cooling system model

### 3.3.3.1 Combustion heat rate

All the energy that warms up the coolant comes from the fuel injected into the engine and burning inside the cylinders; the amount of heat generated in this way depends on the following factors:

- amount of fuel injected;
- lower heating value of the fuel;
- evaporation heat of the fuel;
- efficiency of the combustion.

The heating value of a substance is the amount of heat released during the perfect combustion of a specified amount of it and it is a characteristic of each substance. The lower heating value (*LHV*) determination assumes that the water generated during a

combustion process is in the vapor state at the end of the combustion, as opposed to the higher heating value (*HHV*) which assumes that all the water produced is in a liquid state after the combustion process. For a conventional diesel fuel sold in the United States, the *LHV* is of 42.791 MJ/kg [46]. The heat of vaporization ( $Q_{ev}$ ), instead, represents the energy required to transform a given quantity of a substance from a liquid into a gas at a given pressure (often the atmospheric one) and, for a typical diesel fuel, it is equal to 250 kJ/kg [47].

Uploading from the Matlab® “Workspace” the instantaneous quantity of fuel mass flow rate that is burning in the cylinders during the driving cycle and multiplying it for the difference between the fuel *LHV* and heat of vaporization, the amount of heat rate generated instantaneously can be obtained. This quantity is computed for a perfect burning event in which all the chemical energy of the fuel is converted into heat; in reality, a combustion efficiency ( $\eta_{combustion}$ ) must be taken into account to calculate the real quantity of heat rate generated, instant per instant, during the driving cycle. The combustion efficiency of a recent gasoline or diesel engine varies between approximately 0.96 and 0.97 [48] and there are several reasons why not all the injected fuel chemical energy is converted into heat. First of all, the mixture in the cylinder is never perfectly homogeneous and this means that not all the fuel molecules can react with the oxygen in the air and therefore will leave the cylinder as unburned hydrocarbons; in rich conditions, this effect is worsened while, in lean conditions, misfire and incomplete combustion can occur. A part of the fuel is also going into the crevices of the cylinder and remains there unburned; the fuel can also be absorbed by the oil layer on the walls where, in addition, the flame quenching leaves an unburned layer of hydrocarbons.

Equation 3.3 represents the computation procedure necessary to determine the heat rate instantaneously generated by the combustion of the fuel injected in the cylinders ( $\dot{m}_{fuel}$ ), considering its lower heating value (*LHV*), its heat of vaporization ( $Q_{ev}$ ) and the efficiency of the combustion ( $\eta_{combustion}$ ).

$$\dot{Q}_{combustion} = \dot{m}_{fuel} \cdot \eta_{combustion} \cdot (LHV - Q_{ev}) \quad (3.3)$$

Figure 3.11 represents the logical block implemented in Simulink® to compute the heat rate  $\dot{Q}_{combustion}$  during time and, moreover, Figure 3.12 depicts the time trend of this heat rate, calculated by the engine cooling system model while running a simulation of a segment B vehicle, equipped with a diesel engine, driving a NEDC cycle.

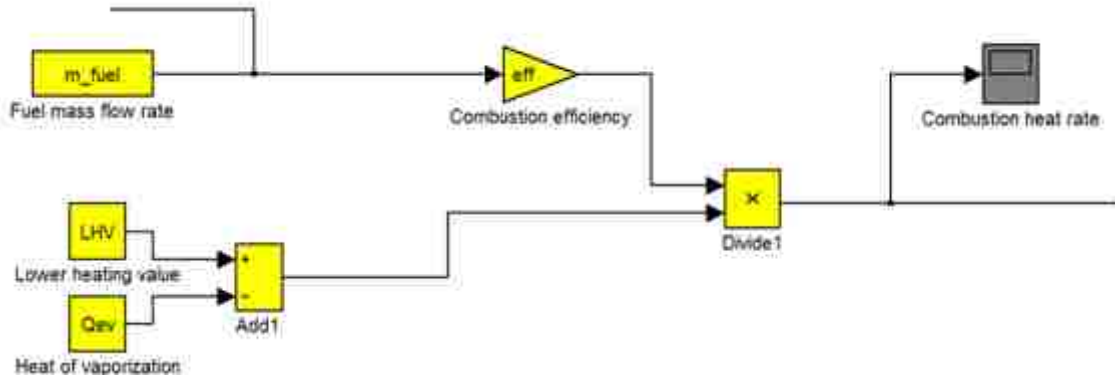


Figure 3.11 - Combustion heat rate computational block

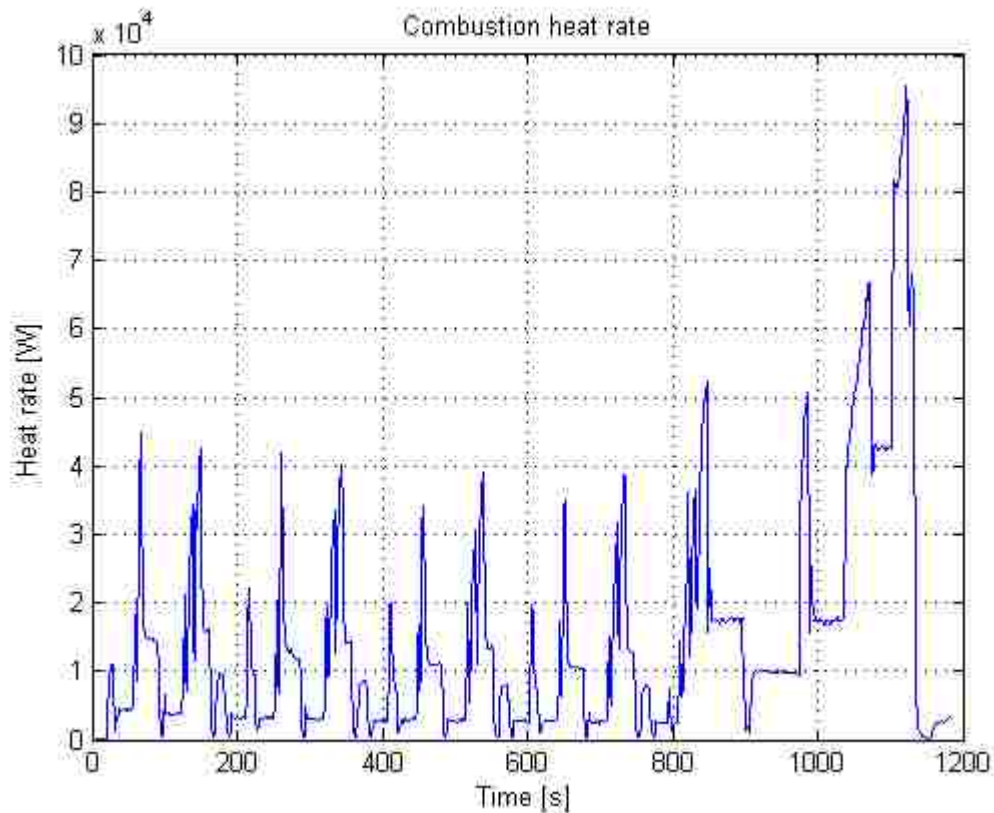


Figure 3.12 - Combustion heat rate time trend

### 3.3.3.2 Exhaust heat rate

To create a precise thermal model of the engine, it is strongly necessary to determine the amount of heat going out of the engine through the exhaust ports, that represents one of the main contributions of the heat losses; in fact, about the 20% of the total energy produced inside the cylinders by the burning charge is going to the exhaust. To calculate the heat going to the exhaust, it is required to know the exhaust gas flow rate and the temperature of the gases at the engine outlet manifolds, immediately after exiting the exhaust valves. The instantaneous fuel mass flow rate is known as a data from the Excel® file of the investigated driving cycle while the air mass flow rate entering the cylinders has to be computed; the exhaust gas instantaneous flow rate is represented by the sum of the fuel and air mass flow rate flowing inside the cylinders during time. In order to calculate the air mass flow rate ( $\dot{m}_{air}$ ), the fuel mass flow rate ( $\dot{m}_{fuel}$ ) has to be multiplied for the stoichiometric air-to-fuel ratio ( $\alpha_{stoich}$ ) that has been taken equal to 14.45 for a typical diesel fuel [49]; moreover, this product has to be further multiplied for the instantaneous value sent to the engine electronic control unit (ECU) by the lambda sensor ( $\lambda$ ), that detects the quantity of oxygen contained in the exhaust gases: if the value of the signal is greater than 1, the fresh mixture injected is in a lean condition, on the contrary, if the value of the signal is lower than 1, the fresh mixture is in a rich condition. The instantaneous values of the air mass flow rate entering the cylinders are hence computed through Equation 3.4.

$$\dot{m}_{air} = \dot{m}_{fuel} \cdot \alpha_{stoich} \cdot \lambda \quad (3.4)$$

At this point, summing the fuel flow rate and the air mass flow rate instantaneous values, it is possible to compute the exhaust gases mass flow rate ( $\dot{m}_{exhaust}$ ) that is flowing in the outlet manifolds instant per instant. This quantity, finally, has to be multiplied by the specific heat of the exhaust gases ( $c_{p_{ex}}$ ) and by the instantaneous magnitude of the difference between the temperature of the exhaust ( $T_{exhaust}$ ) and the temperature of the fresh charge ( $T_{fresh}$ ): these temperatures are uploaded from the Matlab® base file, where they are stored in the “Workspace” while the exhaust specific heat has been taken equal to 1063 J/(kg·K) [50]. In this way, the heat lost during time by



the engine through the exhaust ports ( $\dot{Q}_{exhaust}$ ) can be computed, as stated in Equation 3.5.

$$\begin{aligned} \dot{Q}_{exhaust} &= \dot{m}_{exhaust} \cdot c_{p\_ex} \cdot (T_{exhaust} - T_{fresh}) = (\dot{m}_{fuel} + \dot{m}_{air}) \cdot c_{p\_ex} \cdot (T_{exhaust} - T_{fresh}) = \\ &= \dot{m}_{fuel} \cdot (1 + \alpha_{stoich} \cdot \lambda) \cdot c_{p\_ex} \cdot (T_{exhaust} - T_{fresh}) \end{aligned} \quad (3.5)$$

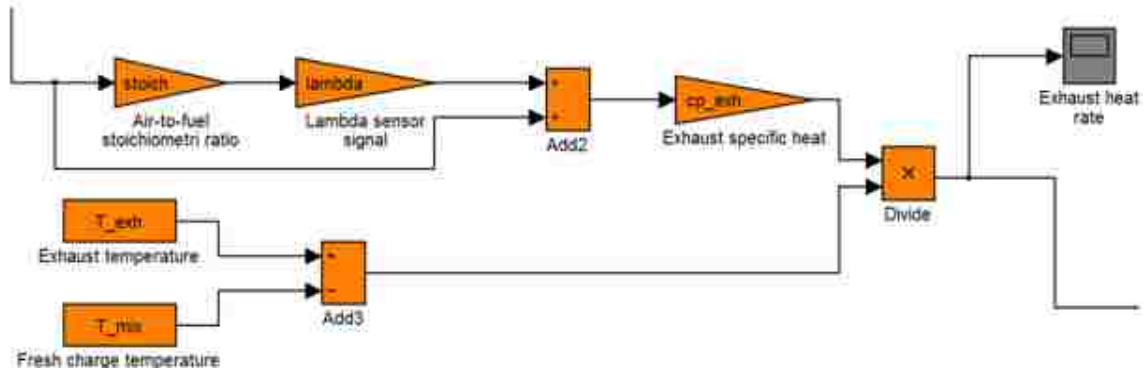


Figure 3.13 - Exhaust heat rate computational block

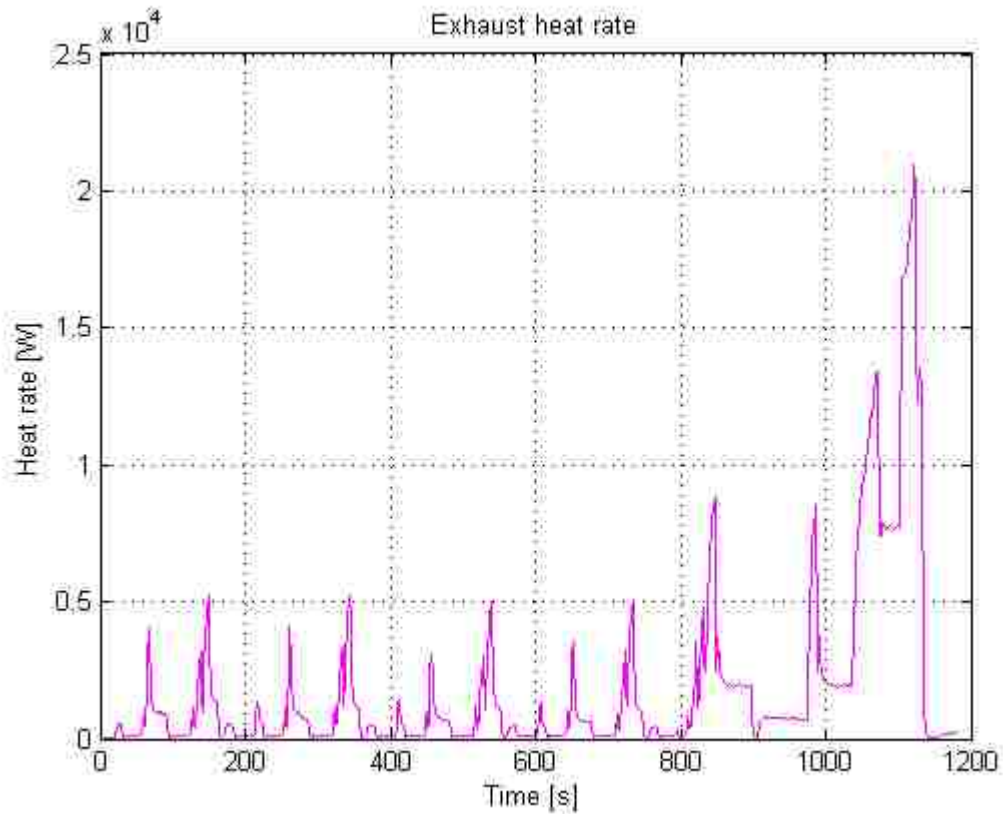


Figure 3.14 - Exhaust heat rate time trend

In Figure 3.13 is showed the logical block implemented in Simulink® to compute the heat rate  $\dot{Q}_{exhaust}$  during time, on the basis of Equation 3.5. Moreover, Figure 3.14 depicts the time trend of this heat rate, calculated by the engine thermal model while running a simulation of a segment B vehicle, equipped with a diesel engine, driving a NEDC cycle.

### 3.3.3.3 Mechanical power

The mechanical power that is generated during time at the engine crankshaft must be computed and subtracted to the combustion heat rate, to continue with the final calculation of the heat amount acquired instantaneously by the coolant. The definition of this power ( $P$ ) is explained in Equation 3.6, where the engine angular speed ( $\omega$ ) is multiplied by the torque generated at the crankshaft ( $T$ ), instant per instant.

$$P = \omega \cdot T \quad (3.6)$$

The instantaneous values of the engine angular speed and torque are taken from the Excel® file of the driving cycle; the torque is expressed in Nm while the speed is expressed in rpm and so, for the power calculation, it must be converted through the Matlab® script in rad/s as defined by Equation 3.7.

$$\omega = n \cdot \frac{2\pi}{60} \quad (3.7)$$

During engine braking, the torque is characterize by negative values and so, because the engine angular speed is always greater than zero (the engine shaft can obviously rotate only in one direction), the power generated is negative and increases the amount of heat going to the coolant. This “brake torque” in fact, caused by friction, is turned into heat and warms up the coolant that experiences an increase of temperature during the engine braking periods.

In Figure 3.15 is represented the Simulink® calculation block that computes the mechanical power generated by the engine at the crankshaft during time, as explained by Equation 3.6. Figure 3.16 depicts instead the trend during time of the mechanical output,

determined by the engine thermal model while running a simulation of a segment B vehicle, equipped with a diesel engine, driving a NEDC cycle.

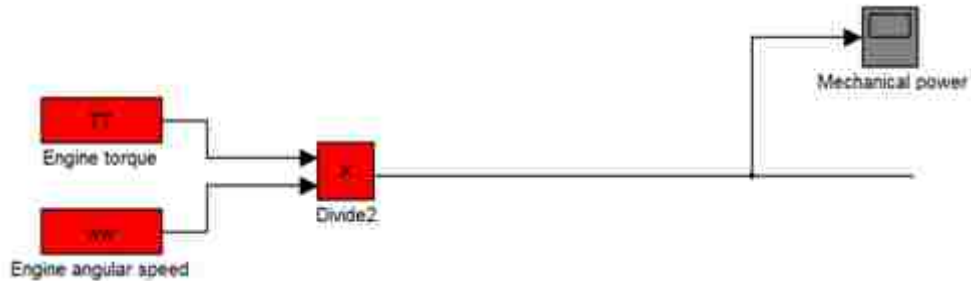


Figure 3.15 - Mechanical power computational block

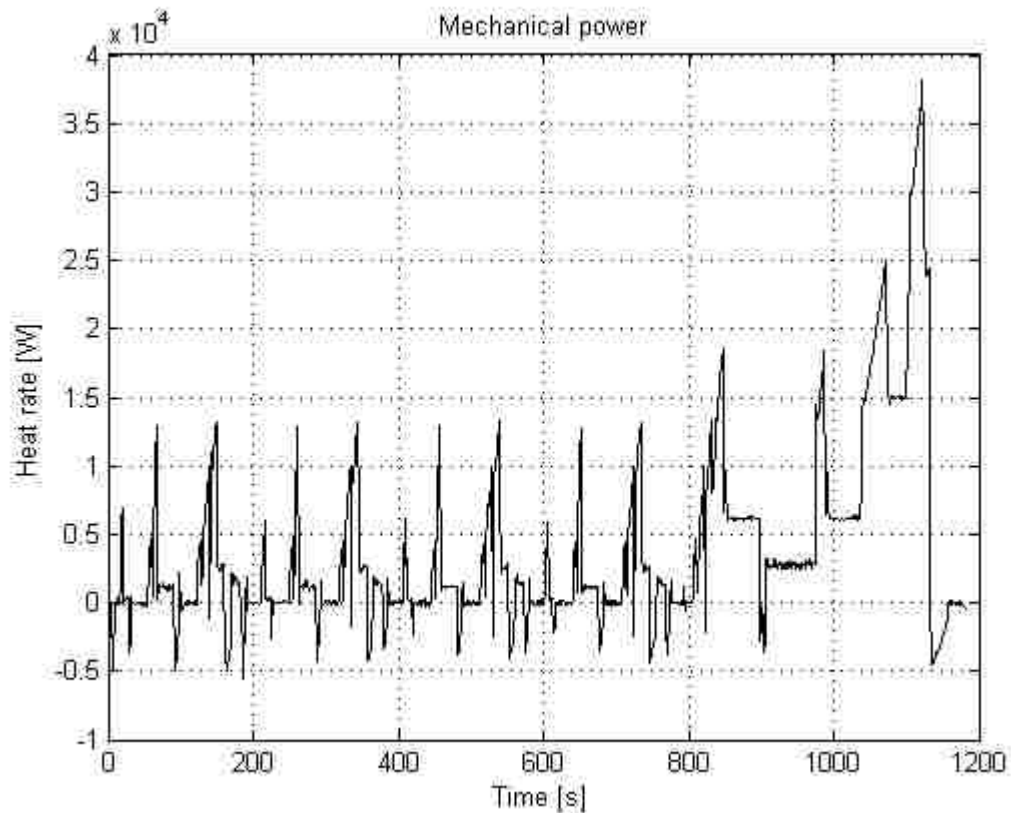


Figure 3.16 - Mechanical power time trend

As stated before, during the engine braking periods, characterized by a negative “brake torque”, the mechanical power generated by the engine assumes negative values, leading to an increase of the engine coolant temperature.

### 3.3.3.4 Cabin heater heat rate

As described before, a careful estimation of the heat withdrawn from the coolant by the cabin heater must be done. This because, when the driver or the passengers desire to get warm the vehicle cabin, the engine coolant flows through the so-called cabin heater providing it with part of its heat. The air entering the cabin, passing through the cabin heater, is in fact heated thanks to the heat rate taken from the engine coolant whose temperature, in this way, decreases. The layout of the heating system is showed in Figure 3.17 where “B” is the blower, “E” is the evaporator and “H” is the heater core [48]. The air entering the device, aspirated by the blower, first goes through the evaporator that cools it down in order to dry it; then, a part of the air is directed to the heater core to be warmed up and, finally, the cold and warm air are mixed through a throttle valve in order to obtain the requested cabin temperature.

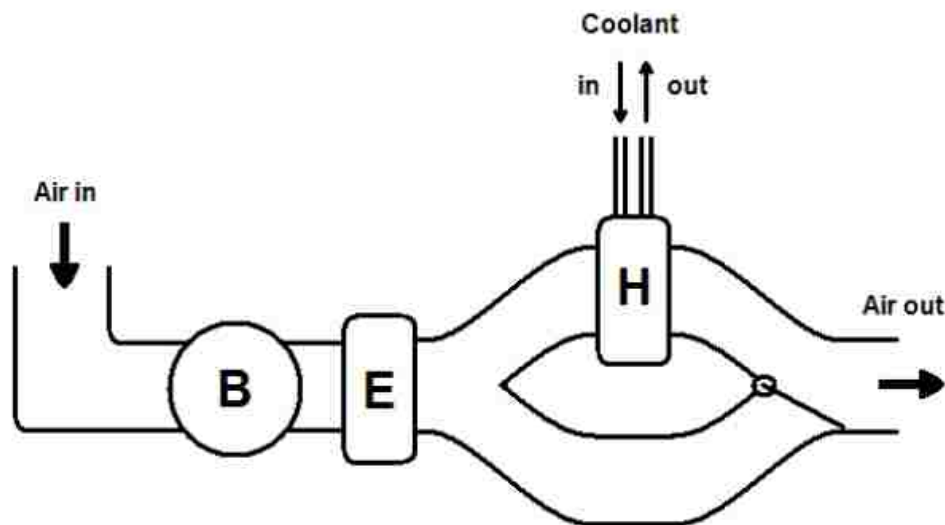


Figure 3.17 - Cabin heating system layout [48]

Knowing, from the driving cycle data, the time trend of the temperature inside the cabin ( $T_{cabin}$ ), defined on the basis of the ideal occupants needs, and of the ambient temperature ( $T_{amb}$ ), it is possible to determine the instantaneous temperature gradient experienced by the air across the cabin heater. In fact, the temperature of the air at the inlet of the device is equal to the ambient temperature while, at the outlet of the device, the temperature of the air is the same of the cabin. Multiplying this temperature difference, instant per instant, for the specific heat of the air ( $c_{p\_air}$ ) and for the

instantaneous value of the air mass flow rate going through the heater ( $\dot{m}_{air\_CH}$ ), the cabin heater heat rate can be finally determined. The specific heat of the air has been taken equal to 1006.1 J/(kg·K) [51] while, for the air mass flow rate computation, Equation 3.8 has been used and implemented in the Matlab® base file.

$$\dot{m}_{air\_CH} = \rho_{air} \cdot A_{CH} \cdot \frac{v}{3.6} \quad (3.8)$$

The variable  $A_{CH}$  represents the cross section of the cabin heater, through which all the air entering in the device has to flow, whose value has been obtained from the Thermal and NVH department at Chrysler while  $v$ , instead, indicates the vehicle linear speed, expressed in km/h and taken from the driving cycle Excel® file. For all the calculations, the air density ( $\rho_{air}$ ) has been taken equal to 1.225 kg/m<sup>3</sup> [52]. Because the air enters the cabin heater from the outside through the front-end, its volume flow rate depends on the vehicle linear speed and, in particular, can be computed during time as the product between this speed (expressed in m/s) and the cross section of the cabin heater (expressed in m<sup>2</sup>); finally, multiplying the air volume flow rate (expressed in m<sup>3</sup>/s) for the air density (expressed in kg/m<sup>3</sup>), the air mass flow rate can be computed (expressed in kg/s).

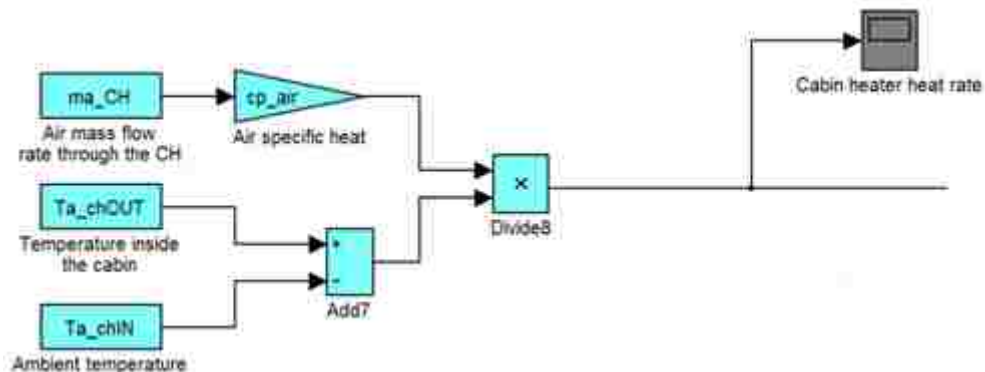
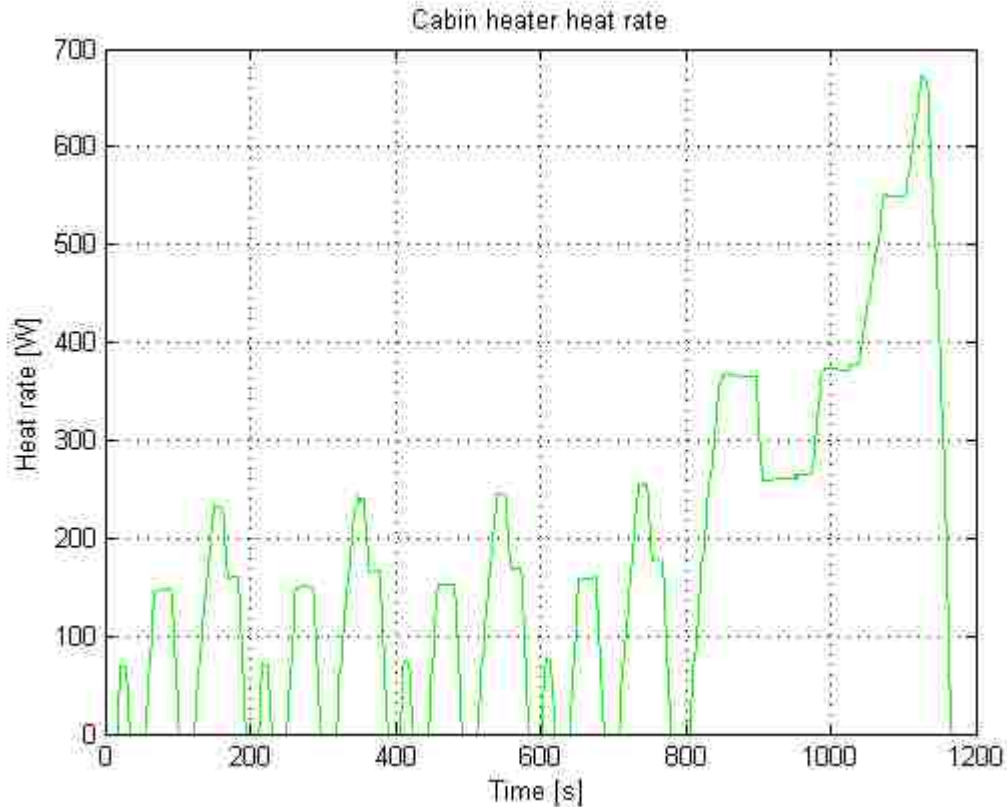


Figure 3.18 - Cabin heater heat rate computational block



**Figure 3.19 - Cabin heater heat rate time trend**

Figure 3.18 depicts the logical block that has been implemented in Simulink®, in order to compute the cabin heater heat rate that, instantaneously, is taken from the engine coolant to warm up the external air entering in the vehicle cabin. In Figure 3.19, instead, is showed the trend during time of this heat rate, determined by the engine thermal model while running a simulation of a segment B vehicle, equipped with a diesel engine, driving a NEDC cycle.

Since the temperature inside the cabin, during a typical NEDC driving cycle, does not vary a lot during time and the same happens for the ambient temperature, the temperature gradient experienced by the air across the heater is quite constant. In this way, the time trend of the cabin heater heat rate mainly depends on the instantaneous values of the air mass flow rate flowing through the heater that directly depends, in turn, on the vehicle linear speed defined by the cycle. Hence, the heat rate taken from the engine coolant by the cabin heater has a profile similar to the one of the vehicle linear speed, as can be seen from Figure 3.19.

### 3.3.3.5 Surroundings heat rate

Because the temperature of the engine block, during the driving cycle, is obviously higher than the temperature of the ambient, a spontaneous heat transfer takes place between the engine and the surrounding air. This heat transfer phenomenon has two components: the convection and the radiation that, however, is negligible with respect to the first contribution (it usually starts to be relevant with temperatures strongly higher than the ones typical of engine devices) and so it is not considered in the model. To compute the instantaneous amount of heat that the engine dissipates for convection with the surrounding air “touching” its surface, Equation 3.9 has been written and implemented in the tool.

$$\dot{Q}_{surrounding} = U_{surrounding} \cdot A_{eng} \cdot (T_{cool\_prev} - T_{amb}) \quad (3.9)$$

Considering the only convection contribution, to compute the heat exchanged by the engine walls and the external ambient, it would be necessary to consider the difference between the temperature at the engine walls and the temperature of the ambient air. But, since the driving cycle data do not provide this temperature, it is not possible to compute the surroundings heat rate following this strategy.

The solution is to consider the temperature of the engine coolant and not of the engine walls, taking into account that a certain amount of heat is going from the coolant to the external surface of the engine and, from this surface, to the surroundings. In this way, the heat lost by the engine to the ambient can be determined using the temperature gradient existing between the coolant and the external air but, at this point, attention must be paid in considering the correct heat transfer coefficient ( $U_{surrounding}$ ).

Taking into account the temperature difference between the engine wall and the air, the air convective heat transfer coefficient has simply to be used but, taking into account the temperature difference between the coolant and the air, a more complicated heat transfer coefficient has to be considered, that accounts also for the heat conduction that takes place across the engine walls.

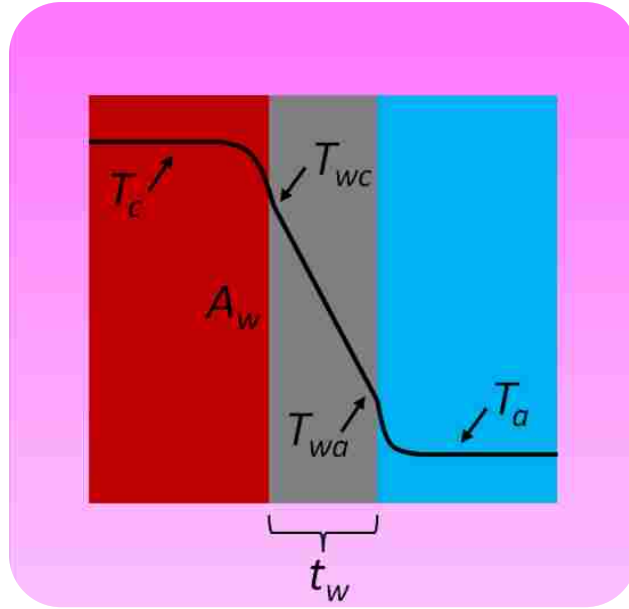


Figure 3.20 - Engine wall, cooling medium and surrounding ambient simplified view

Figure 3.20 shows a simplified view of the engine wall, in grey, of the cooling medium, in red, and of the ambient air, in cyan; moreover, the black line represents the general trend of the temperature of the different parts of the engine: the coolant is hotter than the engine coolant-side surface, the engine coolant-side surface is hotter than the engine ambient-side surface and, finally, the engine ambient-side surface is hotter than the surrounding air. In order to compute the spontaneous heat transfer rate between the coolant and the ambient, the three different heat transfer phenomena existing between the coolant and the inner surface of the engine (convection), between the inner and outer surfaces of the engine (conduction) and, finally, between the outer surface of the engine and the surroundings (convection) must be taken into account. For a steady-state one-dimensional heat flow and considering the engine wall having thickness  $t_w$  and surface  $A_w$ , the following equations can be written.

$$\dot{q} = \dot{q}_{conv} = h_c \cdot (T_c - T_{wc}) \quad (3.10)$$

$$\dot{q} = \dot{q}_{cond} = \frac{k_w}{t_w} \cdot (T_{wc} - T_{wa}) \quad (3.11)$$

$$\dot{q} = \dot{q}_{conv} = h_a \cdot (T_{wa} - T_a) \quad (3.12)$$



Equations 3.10, 3.11 and 3.12 compute the heat flux  $\dot{q}$  that, for convection and conduction, is flowing from the engine coolant to the ambient air, passing through the engine wall. The terms contained in the equations are explained in the following list:

- $h_c$  is the convective heat transfer coefficient of the coolant, equal to 3000 W/(m<sup>2</sup>·K) [53];
- $k_w$  is the conductivity of the engine wall, equal to 63.18 W/(m·K) for a cast iron element [54];
- $h_a$  is the convective heat transfer coefficient of the air, equal to 100 W/(m<sup>2</sup>·K) [55];
- $t_w$  is the engine wall thickness, whose value has been received from the Thermal and NVH department at Chrysler;
- $T_c$  is the temperature of the coolant;
- $T_{wc}$  is the temperature of the engine coolant-side surface;
- $T_{wa}$  is the temperature of the engine ambient-side surface;
- $T_a$  is the temperature of the surrounding ambient.

Therefore, considering the overall system as a series of thermal resistances and rewriting the previous three equations as follows, it is possible to compute the overall heat transfer coefficient that exists between the engine coolant and the surroundings and that takes into account both the convective and conductive heat transfer phenomena.

$$T_c - T_{wc} = \dot{q} \cdot \frac{1}{h_c} \quad (3.13)$$

$$T_{wc} - T_{wa} = \dot{q} \cdot \frac{t_w}{k_w} \quad (3.14)$$

$$T_{wa} - T_a = \dot{q} \cdot \frac{1}{h_a} \quad (3.15)$$

Equations 3.13, 3.14 and 3.15 have to be summed up side by side, obtaining Equation 3.16; then, knowing that the heat flux  $\dot{q}$  must be multiplied for the surface  $A_w$  to obtain the heat rate  $\dot{Q}$ , Equation 3.17 can be finally derived: among its terms, it is possible

to individuate the overall heat transfer coefficient  $U_{surrounding}$  that has been obtained combining the convective and conductive heat transfer coefficients of the overall system.

$$T_c - T_a = \dot{q} \cdot \left( \frac{1}{h_c} + \frac{t_w}{k_w} + \frac{1}{h_a} \right) \quad (3.16)$$

$$\dot{Q} = \dot{q} \cdot A_w = \left( \frac{1}{h_c} + \frac{t_w}{k_w} + \frac{1}{h_a} \right)^{-1} \cdot A_w \cdot (T_c - T_a) = U_{surrounding} \cdot A_w \cdot (T_c - T_a) \quad (3.17)$$

At this point, following the thermodynamic theory that has been explained in the previous paragraphs, it is possible to implement Equation 3.9 in the engine thermal model. The overall heat transfer coefficient ( $U_{surrounding}$ ) computation is realized on the basis of Equation 3.17 in the Matlab® base file, the value of the external surface ( $A_{eng}$ ) of the investigated HEV's engine is a data obtained from the Thermal and NVH department and, finally, the instantaneous values of the ambient temperature are given by the Excel® file of the driving cycle. Once the overall heat transfer coefficient has been determined, the surroundings heat rate can be calculated considering the temperature of the engine coolant and not the temperature of the engine wall that, as said before, it is not given as a driving cycle data and, at the same time, can be determined only experimentally. For what concern the temperature of the engine coolant, instead, it must be remembered that its time trend is the unknown of the problem and that, at the end of the computations, it will be given as the simulation output by the engine thermal model; because it is computed instantaneously during the driving cycle simulation, to determine the heat rate going to the surroundings at a given instant, the coolant temperature computed at the instant before ( $T_{cool\_prev}$ ) can be used. In order to compute the coolant temperature at the moment immediately preceding the actual instant considered by the driving cycle, the “Memory” block has to be used, as described in the following sections.

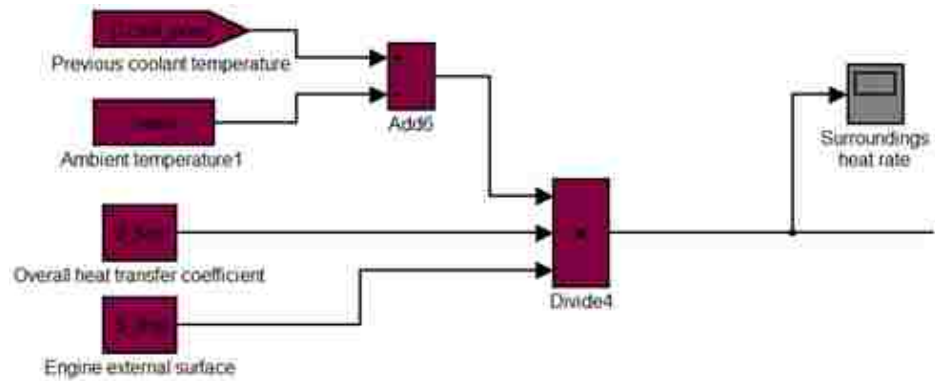


Figure 3.21 - Surroundings heat rate computational block

In Figure 3.21, the logical block implemented in Simulink® to compute the heat rate  $\dot{Q}_{surrounding}$  during time can be analyzed. Moreover, in Figure 3.22, the time trend of this heat rate can be studied: it is calculated by the engine cooling system model while running a simulation of a segment B vehicle, equipped with a diesel engine, driving a NEDC cycle.

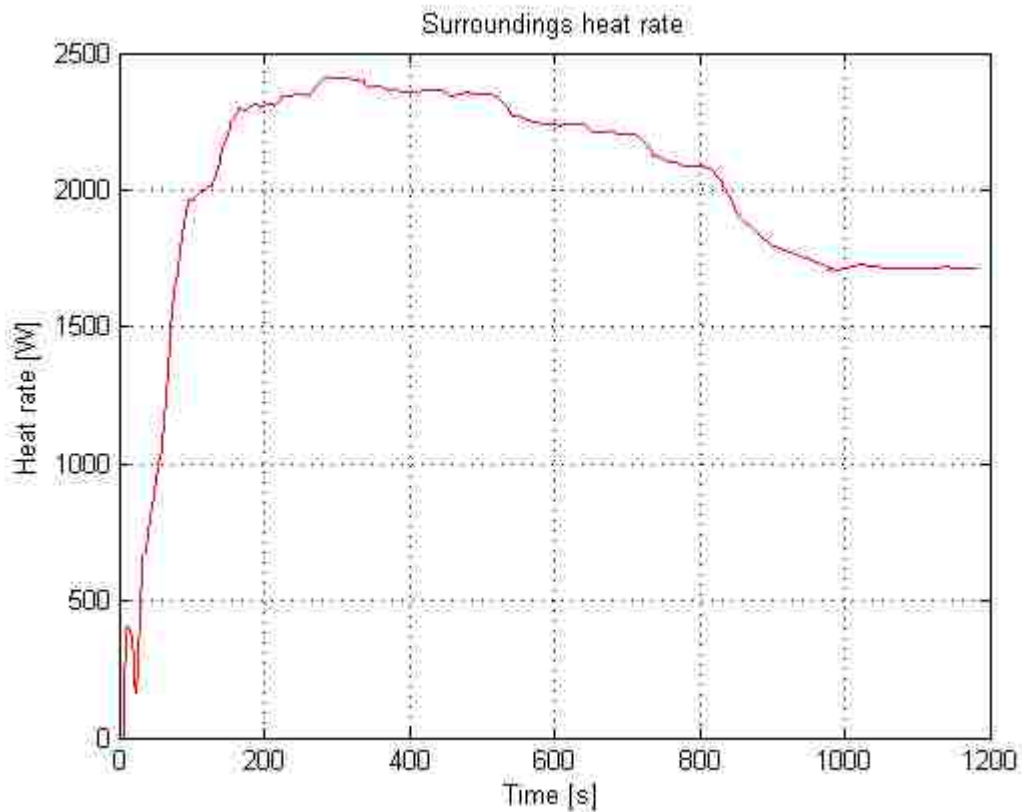


Figure 3.22 - Surroundings heat rate time trend

To conclude, it is important to underline that the main difficulty encountered during the design of this part of the engine thermal model, is represented by the estimation of the overall heat transfer coefficient existing between the engine coolant and the surrounding ambient air; anyway, thanks to a thorough study of the thermodynamic theories at the base of the convective and conductive heat transfer phenomena, the computation of  $U_{surrounding}$  has been possible. Moreover, also the outer surface of the engine is difficult to determine because of the complex geometry of the whole engine bay; fortunately, this vital information has been received from the Thermal and NVH department where, with dedicated studies and technologies, the external surfaces of different engine models can be determined.

### **3.3.3.6 Radiator heat rate**

The last term that has to be subtracted to the heat quantity generated during time by the combustion of the fresh charge, in order to compute the heat rate going to the coolant, is represented by the heat that the coolant itself dissipates to the external environment through the radiator. To maintain the coolant temperature, as well as the engine one, within the desired range optimum for the engine operations, the radiator is necessary to regulate the amount of heat that, instant per instant, the coolant exchanges with the environment; the radiator, in fact, has the purpose to let the coolant dissipate the heat received from the engine and, in order to correctly set this heat quantity, it works coupled with a thermostat that adjusts the coolant flow to the radiator.

The radiator, usually, is an air-to-liquid finned heat exchanger that works with the coolant circulating inside the tubes moved by a pump and the air flow passing outside the tubes, through the fins, thanks to the motion of the vehicle and to the operation of the fan mounted at the front-end. It should be characterized by a high power density, and so by the possibility to reject a high quantity of heat with a relatively small frontal area, by a permanent resistance to corrosion and by low production costs; it is generally made of copper or aluminum and its typical constructive scheme, in the U-pattern or multi-passage configuration, is represented in Figure 3.23.

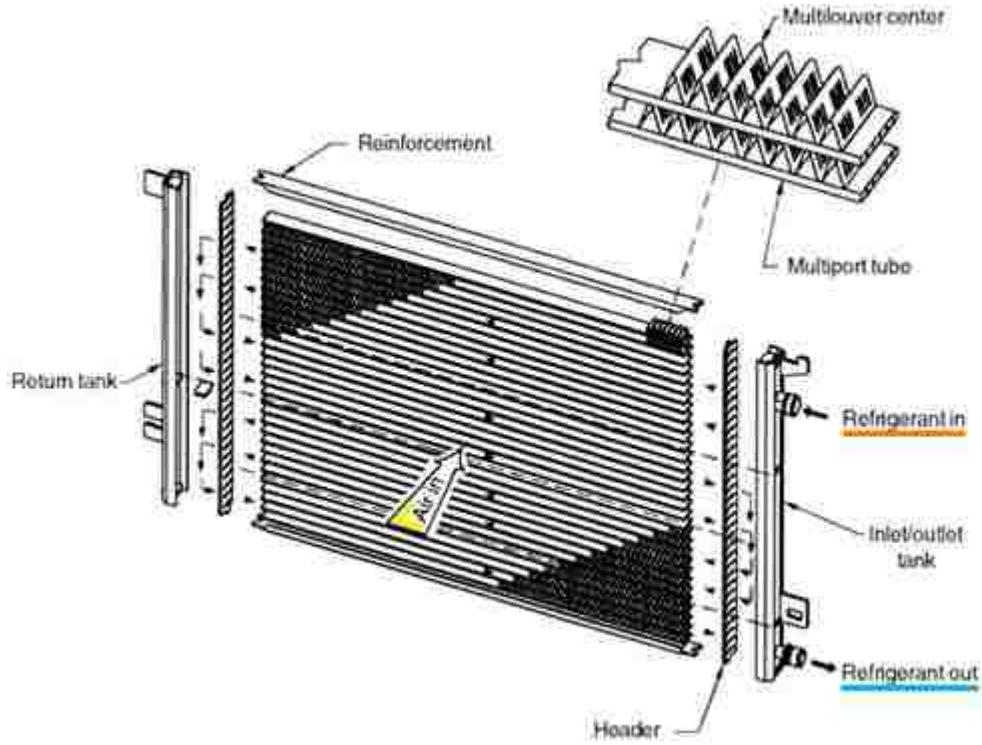


Figure 3.23 - U-pattern radiator constructive scheme [56]

In order to compute the heat rate ( $\dot{Q}_{radiator}$ ) that is instantaneously rejected by the coolant, flowing through the radiator tubes, to the external air, flowing across the tubes, the formula presented in Equation 3.18 has to be used. The term  $\dot{m}_{cool}$  represents the instantaneous coolant mass flow rate flowing in the engine cooling system, given as a driving cycle data, while the term  $c_{p\_cool}$  represents the coolant specific heat, equal to 3740 J/(kg·K) [53]. Inside the brackets, the term  $T_{rad\_IN}$  represents the coolant temperature experimentally measured at the inlet section of the radiator, while the term  $T_{rad\_OUT}$  represents the coolant temperature at the outlet of the exchanger.

$$\dot{Q}_{radiator} = \dot{m}_{cool} \cdot c_{p\_cool} \cdot (T_{rad\_IN} - T_{rad\_OUT}) \quad (3.18)$$

At this point, careful attention must be paid considering that the engine coolant does not always flow through the radiator during vehicle operations. This because the engine cooling circuit is provided with a thermostat that controls the coolant flow rate entering the radiator, in order to maintain the temperature of the coolant inside the engine roughly constant, regardless of the requested engine power: in order to do that, the balance

between the heat introduced into the cooling circuit by the engine and the heat transferred to the surroundings by the coolant, has to be guaranteed. To ensure that the coolant is heated up rapidly, the thermostat remains closed at the engine switch on; in this way, instead of flowing through the radiator, the coolant is fed through a bypass circuit where the heat from the engine warms up the coolant very rapidly. Only when the coolant temperature is close to the optimum, the thermostat opens and lets the coolant flow to the radiator in a measured way; when the maximum temperature has been reached, the thermostat fully opens allowing the maximum coolant flow rate to the radiator to prevent overheating. Both in case of a conventional wax thermostat and of an advanced map-controlled or electrically heated wax thermostat, the coolant flow regulation system can work in three different operating ranges:

1. thermostat closed, the coolant only flows through the engine thanks to the bypass circuit and is rapidly heated;
2. thermostat open, the entire volume of coolant flows via the radiator and the maximum cooling capacity available is utilized;
3. thermostat control range, a part of the coolant volume flows through the bypass circuit while the other one flows through the radiator.

In general, once the coolant reaches its maximum allowed temperature, the thermostat fully opens in order to let the coolant flow to the radiator and to maintain its temperature permanently close to the optimum value. With conventional wax thermostat, the opening temperature is permanently set, independently of the engine working conditions; however, performance-optimized modern engines require advanced thermostat whose opening temperature is fixed during time by the engine electronic control unit (ECU) on the basis of the actual working conditions. For example, in the partial load conditions, when the engine efficiency is lower and the fuel consumption reaches its maximum, the opening temperature of the thermostat can be set in such a way that the coolant temperature stands at approximately 100 °C to 110 °C: increasing the temperature of the coolant, the engine friction decreases and, in this way, a fuel consumption reduction about the 3% can be obtained.

To implement in the Simulink® model the working principle of the thermostat, an “if/else” sub-block has been imported from the library and the following condition has

been imposed: if the instantaneous temperature of the coolant, computed by the model at the previous iteration, is lower than the maximum temperature that the coolant is allowed to reach (set by the user), then a “signal 0” is generated and sent to the thermostat switch; on the contrary, if the actual temperature of the coolant, computed by the model, is higher than the maximum temperature that the coolant is allowed to reach, then a “signal 1” is generated and sent to the switch of the thermostat. In case the switch receives a “signal 0”, the thermostat remains closed and no heat is dissipated by the coolant through the radiator, while in case a “signal 1” is received by the switch, the thermostat opens and the coolant deliver to the environment a certain heat rate, computed by Equation 3.18.

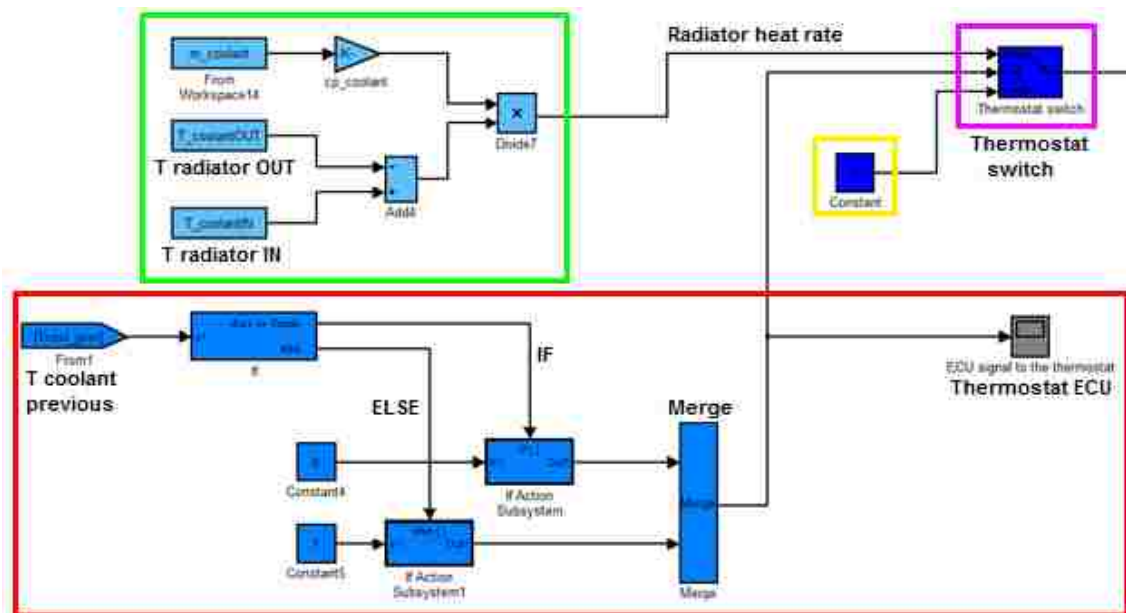
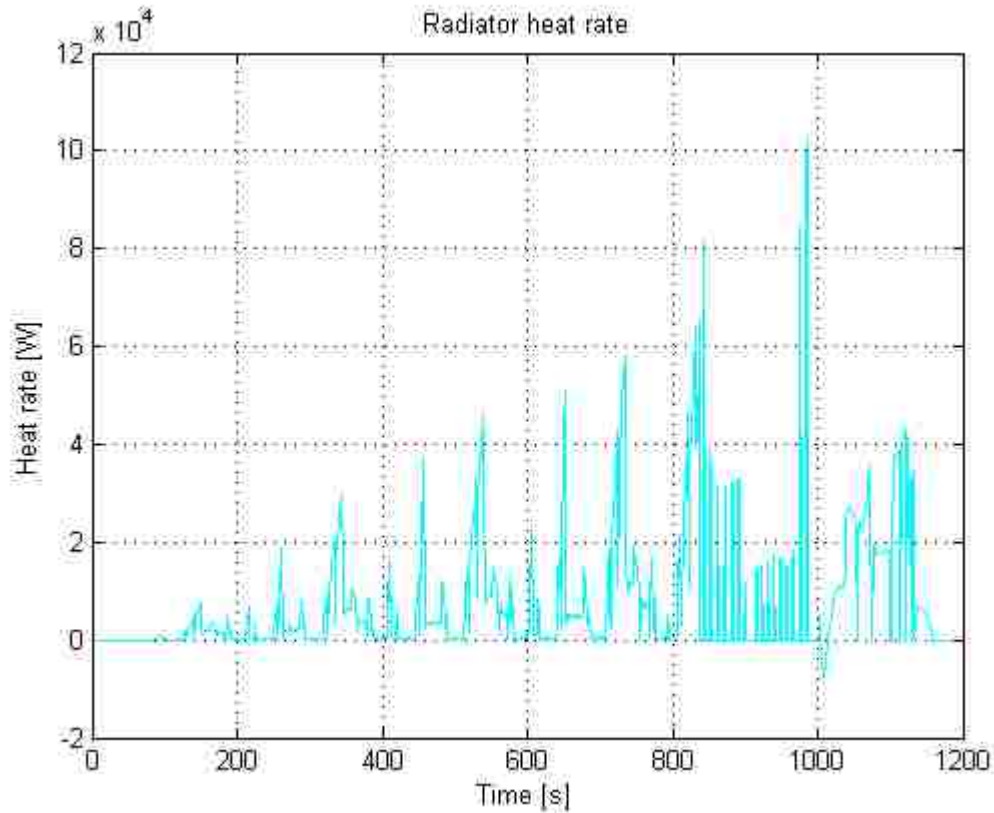


Figure 3.24 - Radiator heat rate computational block

In Figure 3.24 it can be seen the overall logical block implemented in Simulink® to represent the behaviour of the thermostat and of the radiator: in the red frame is represented the “if/else” sub-system that, on the basis of the actual coolant temperature and of the maximum allowed coolant temperature set by the user, generates the ECU signals to be sent during time to the thermostat switch, highlighted in the magenta frame; in the green frame, instead, is represented the logical block necessary to compute the heat rate  $\dot{Q}_{radiator}$  as described by Equation 3.18 and, finally, in the yellow frame is highlighted a “Constant” block equal to zero that represents the null amount of heat

dissipated by the coolant through the radiator if the thermostat is closed. Activating the engine cooling system model to run a simulation of a segment B vehicle, equipped with a diesel engine, driving a NEDC cycle, the  $\dot{Q}_{radiator}$  time trend depicted in Figure 3.25 is obtained; Figure 3.26, instead, shows the trend of the binary signal that is generated by the engine ECU during time and sent to the thermostat switch.



**Figure 3.25 - Radiator heat rate time trend**

As can be seen from both the Figures 3.25 and 3.26, the thermostat opens only after some seconds from the beginning of the driving cycle; this because, when the engine is switched on, its temperature is equal to the ambient temperature and it takes a certain time to rise until the value at which the thermostat begins to open. When the engine coolant reaches that temperature, it starts flowing through the radiator dissipating heat to the external environment.

Finally, it must be pointed out that, since the coolant mass flow rate going to the radiator depends on how much the thermostat is opened, the values of this flow rate given



by the Excel® file of the driving cycle must be determined, experimentally or virtually, considering this phenomenon; in case this condition is not respected, a suitable function that correlates the coolant mass flow rate flowing through the radiator to the engine angular speed (and so to the engine operating conditions) must be defined. In order to do that, the engine rotational speed ( $n$ ) must be multiplied for a suitable factor  $w_m$ , given by the Thermal and NVH department, that is peculiar for each type of engine and allows to obtain the radiator coolant flow rate ( $\dot{m}_{cool\_rad}$ ) corresponding to a specified speed value, as described by Equation 3.19.

$$\dot{m}_{cool} = w_m \cdot n \quad (3.19)$$

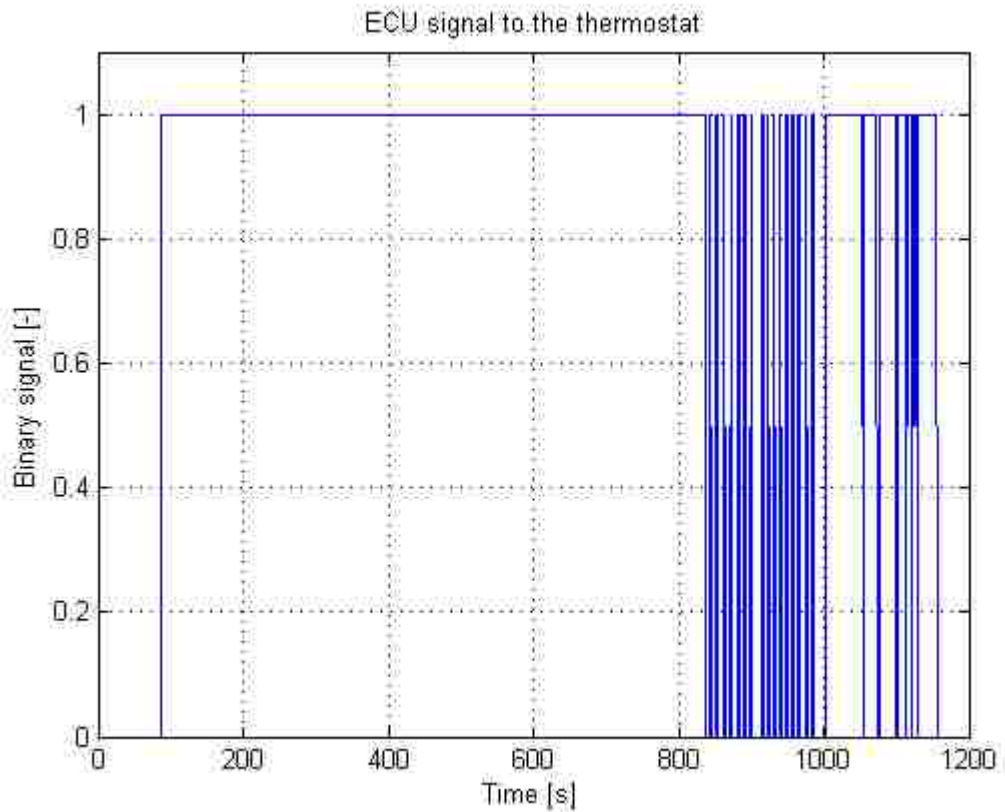


Figure 3.26 - ECU signal to the thermostat time trend

### 3.3.3.7 Coolant heat rate

At this point, once all the heat rate contributions have been determined, the instantaneous heat quantity acquired by the engine coolant can be obtained. The

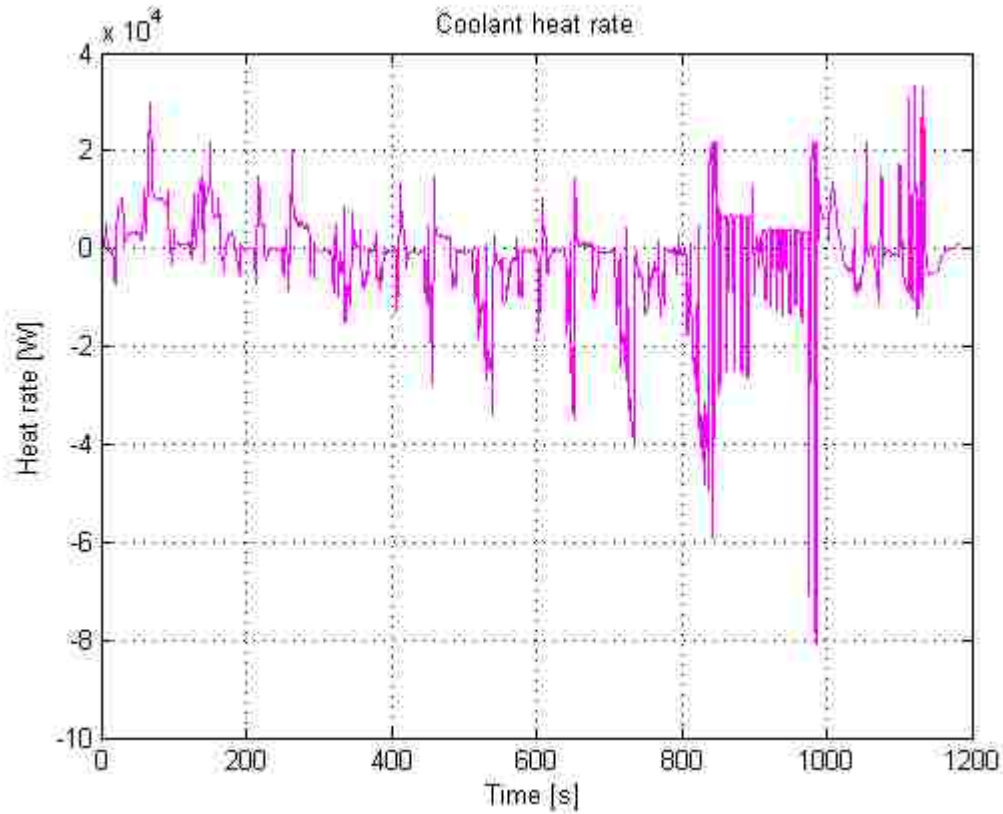
mechanical power going to the wheels, the heat rate going to the exhaust, the heat rate exchanged with the cabin heater, the heat rate dissipated to the surroundings and, finally, the heat rate lost through the radiator, must be subtracted to the heat quantity produced inside the cylinders by the fresh mixture burning. The result of this subtraction is represented by the heat rate acquired by the engine coolant during time, whose trend is depicted in Figure 3.27.

Moreover, the instantaneous heat quantity going to the coolant is expressed by Equation 3.20 as the product between the coolant mass flow rate ( $\dot{m}_{cool}$ ), the coolant specific heat ( $c_{p\_cool}$ ) and the temperature gradient experienced by the coolant during two consecutives instants of the driving cycle.

$$\dot{Q}_{coolant} = \dot{m}_{cool} \cdot c_{p\_cool} \cdot (T_{cool\_actual} - T_{cool\_prev}) \quad (3.20)$$

Once the coolant heat rate ( $\dot{Q}_{coolant}$ ) is determined by the engine cooling system model for every iteration, the instantaneous actual temperature of the coolant can be finally computed; in this way, at the end of the simulation, the engine coolant temperature time trend is obtained. It must be remembered that the purpose of the design activity was to develop a Simulink® model capable of determining the temperature of the engine coolant during time, for a given HEV model equipped with a specified internal combustion engine, tested on a certain driving cycle.

The mechanical efficiency of the engine, in fact, that is decisive in the fuel economy analysis, strongly depends on the temperature of the coolant: if the newly created engine thermal model is successful in determining this temperature, than the level of accuracy of the overall Chrysler simulation tool can increase, giving more accurate results and predictions related to the performance and fuel economy of the new hybrid models.



**Figure 3.27 - Coolant heat rate time trend**

Analyzing Figure 3.27, it can be seen how the coolant heat rate results negative in many different time periods: this because, in certain conditions, the resultant coolant heat rate is not going to the coolant, increasing its temperature, but is taken away from the coolant, whose temperature starts decreasing. This happens, in particular, if the engine coolant temperature is too high and so the thermostat is fully open and directs all the coolant flow to the radiator that, finally, removes a considerable quantity of heat from the coolant itself. Dividing, instant per instant, the coolant heat rate showed in Figure 3.27 for the specific heat of the coolant and for its instantaneous mass rate flowing in the engine cooling system, the temperature gradient  $T_{cool\_actual} - T_{cool\_prev}$  can be finally obtained.

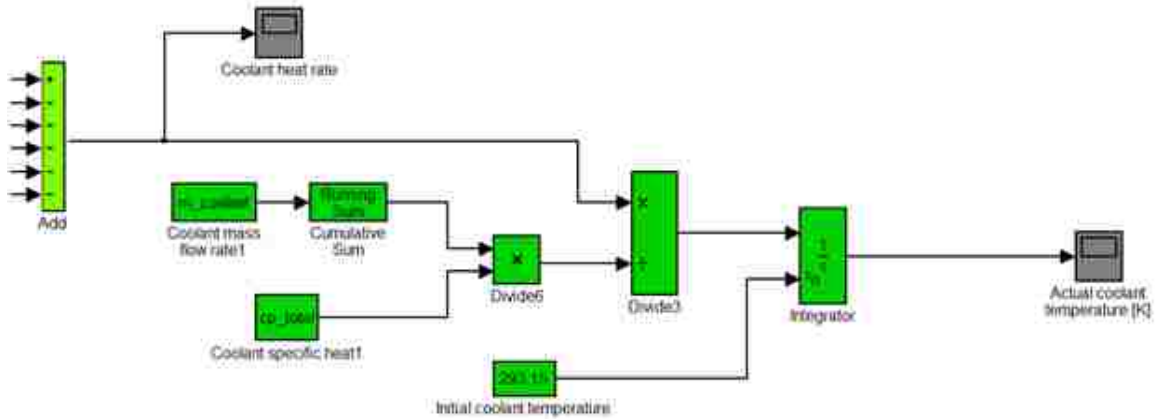


Figure 3.28 - Coolant temperature computational block

The Simulink® block that performs this computation is represented in Figure 3.28 where it is possible to note the presence of a “Running Sum” block, whose purpose is to compute the cumulative sum during time of the coolant mass rate that flows through the system. Since each driving cycle considers that the engine is off at the beginning of the test, there is not any liquid flow in the engine cooling system at that moment and then, time after time, the quantity of coolant circulating in the engine continuously grows in a cumulative way.

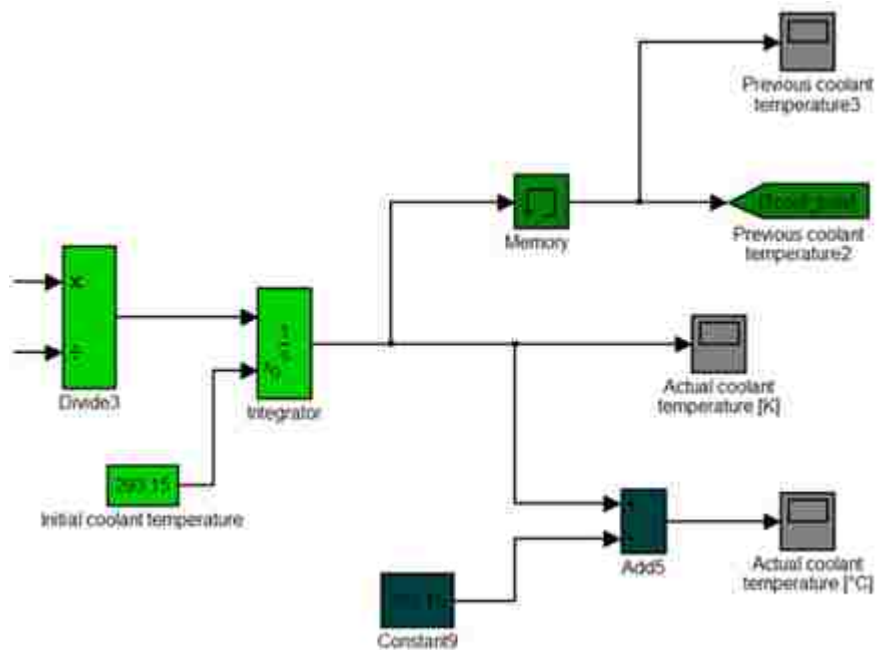


Figure 3.29 - Coolant temperature computational block (detail)

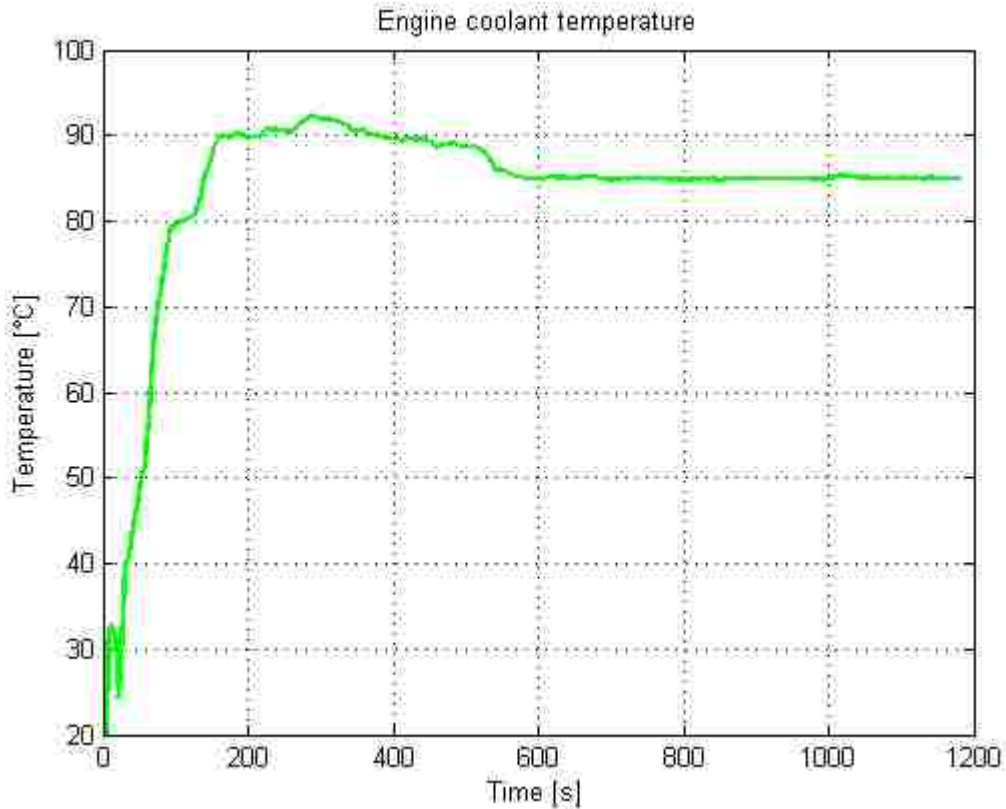
Taking into account this consideration, the instantaneous temperature gradient of the coolant is determined and sent to the “Integrator” block that, knowing the initial temperature of the coolant (set by the user and usually equal to the ambient temperature) finally determines the unknown of the problem: the coolant temperature time trend during the driving cycle. The coolant temperature is obviously computed in degrees Kelvin and, as showed in Figure 3.29, it can be translated in degrees Celsius; moreover, the coolant temperature determined at the previous iteration ( $T_{cool\_prev}$ ) is obtained thanks to the “Memory” block and then sent to the radiator and surroundings heat rate computational blocks.

### **3.3.4 Internal combustion engine cooling system model simulation running**

After the detailed description of the architecture of the engine cooling system model that has been designed during the internship at Chrysler, a general overview of its operating mode has to be depicted in order to better understand how the program can run a simulation. The first step consists in the upload of the driving cycle characteristics in the Matlab® “Workspace”, performed thanks to the Matlab® base file’s code execution. The driving cycle data have been obtained from the Thermal and NVH department and are experimental data, in case the investigated vehicle is in production, or simulation data, in case the investigated vehicle is in the early design stages. Once all the data from the driving cycle have been stored in the Matlab® base file, together with the physical and thermal characteristics of the overall engine system, the Simulink® file can be activated to run the simulation and to find, at the end of the process, the engine coolant temperature time trend.

The Simulink® tool, once the simulation has been started by the user, combines the input data coming from the Matlab® “Workspace” and begins the instantaneous computation of the six heat rate and power contributions: the heat from combustion, the heat going to the exhaust, the mechanical power, the heat going to the cabin heater, the heat dissipated to the surroundings and, finally, the heat exchanged by the coolant through the radiator. Instant per instant, the software computes these variables and subtracts the last five contributions described right now to the combustion heat rate, in order to find the heat that goes during time to the coolant. From the previous pictures, it is

possible to underline that the less influential contributions are represented by the cabin heater and surroundings' heat rate. Once the coolant heat rate is computed for every instant of the driving cycle, the tool determines the temperature gradient experienced by the coolant during that instant and finally, thanks to the “Integrator” block, calculates the actual temperature of the engine coolant.



**Figure 3.30 - Engine coolant temperature time trend**

Figure 3.30 represents the final result obtained through the model when running a simulation of a segment B vehicle, equipped with a diesel engine, driving a NEDC cycle: the trend of the engine coolant temperature is showed during time and, through an accurate analysis of its shape and magnitude, the thermal behaviour of the engine can be studied now with a higher level of detail.

From a thorough study of Figure 3.30, it can be said that the obtained result well reflects the reality of the thermal phenomenon characterizing the engine behaviour. The coolant temperature, in fact, experiences a sharp increase at the beginning of the driving

cycle when the engine needs to be warmed up in the shortest possible time; the thermostat is closed and the coolant is fed through a bypass circuit, circulating in this way only through the engine where it is rapidly heated. Then, when the temperature reaches high magnitudes, more than 90 °C, the thermostat fully opens and lets the coolant flow through the radiator, in such a way it dissipates a considerable amount of heat to the external environment; hence, the temperature of the coolant starts decreasing and reaches the value of 85 °C that, for this specific case, has been set by the user as the optimum engine temperature. At this point, the thermostat continuously regulates its opening range, in order to maintain the coolant at this optimum thermal state represented by the temperature of 85 °C set by the user before running the simulation. The engine thermal model validation procedure will be described in the next chapter but, from a preliminary analysis of the results presented in this section, it can be pointed out that the model gives as output a reasonable engine coolant temperature time trend, satisfying the initial expectations and matching the reasons for which the software has been created.

### **3.3.5 New features introduced by the internal combustion engine cooling system model**

The engine thermal model developed for the Electrified Powertrain research team at Chrysler, as underlined before, has been designed starting from a blank paper with the final purpose to create a software capable of determining the temperature time trend experienced by the engine coolant during a virtual running of a given driving cycle. The reason why this model has to be realized is that the Chrysler simulation tool used to predict the performance and fuel economy of new HEV models, does not take into account the actual temperature of the engine coolant in the computation of the variables characterizing the engine behaviour as, for example, the friction work. The friction work generated by the engine, in particular, affects the maximum brake torque and the minimum brake specific fuel consumption, determining the mechanical efficiency of the engine; the friction losses, moreover, strongly depend on the instantaneous values of the temperature of the engine coolant and oil that, in fact, determine the amount of work necessary to overcome the resistance to relative motion of all the moving parts of the engine. From this perspective, it is clear that the prediction tool used at Chrysler must be

provided with a new sub-model that can compute the engine coolant temperature, in order to better simulate the behaviour of the engine and to finally obtain more precise and accurate predictions.

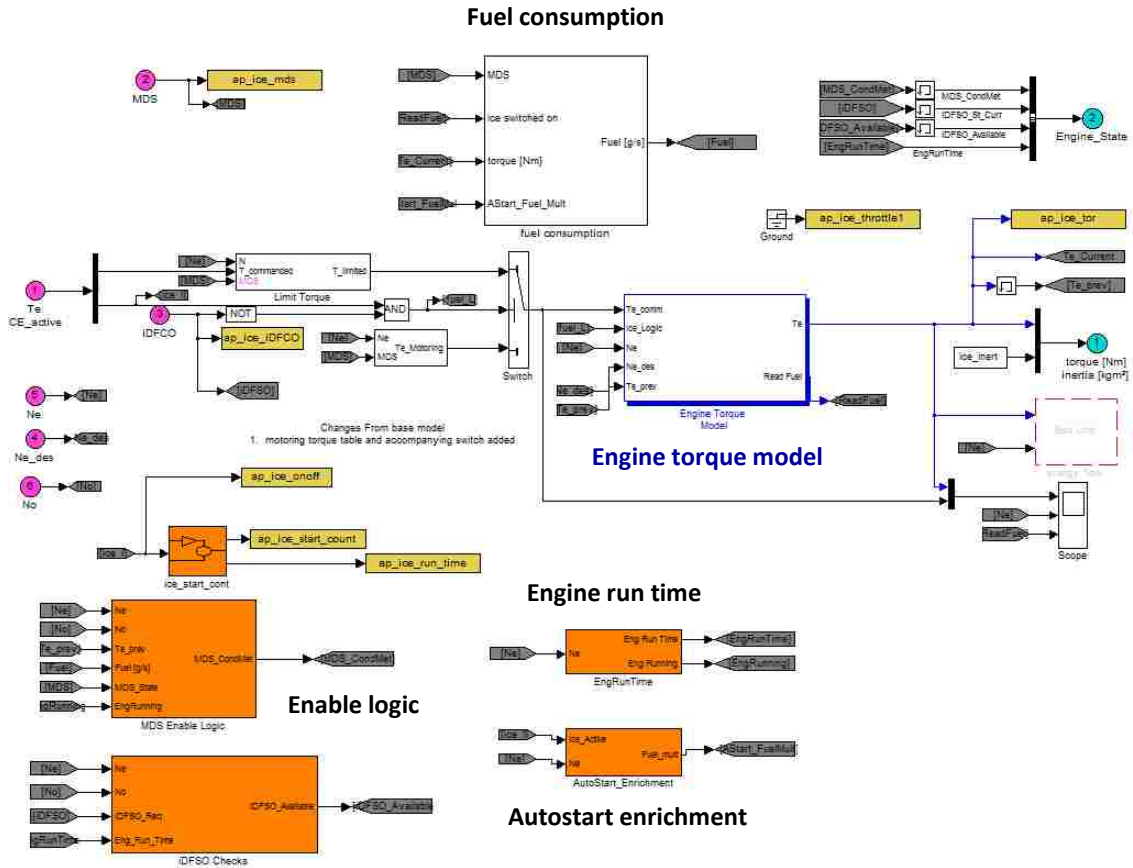


Figure 3.31 - Internal combustion engine sub-block enclosed in the Chrysler HEV prediction model

The new engine thermal model allows the coolant temperature computation and so it can be integrated in the overall simulation software in order to improve the engine thermal aspects definition. After the integration, in fact, the Chrysler tool is provided with a logical structure capable of determining the coolant temperature during the investigated driving cycle and, at this point, all the quantities that depend on this temperature can be computed with new formula that consider also the coolant thermal state. The friction work, for example, strongly depends on the engine coolant temperature and so, now, it can be determined with respect to it acquiring a higher level of precision. In Figure 3.31 is represented a global view of the engine sub-block enclosed in the Chrysler software: analyzing all the variables contained in the model, it is clear that the engine coolant



temperature is not considered. Thanks to the integration of the new engine thermal model, this quantity is now determined and used to improve the performance of the simulation tool.

From a company perspective, it is clear that the level of importance and innovation covered by the engine thermal model is considerably high: this because it has been created from a blank paper and integrated in the Chrysler prediction tool, offering a brand new possibility to improve the accuracy level of the simulations. Thanks to its features, in fact, the engine coolant temperature can now be determined and used in the overall prediction software to simulate the engine behaviour in a more precise way. From a research perspective, on the other hand, the innovation degree of the engine model must be studied from a completely different point of view, trying to understand what are the aspects that make it a novelty. From various literature researches, it has been tried to individuate papers and documents describing similar models and tools, in order to make a comparison between them and the engine model created during this project. In this regard, there are not already existing software that perform its same task and that have its same final purpose but, in general, it has been pointed out that the following aspects determine definitely the novelty introduced by the engine cooling system model.

- High number of inputs: the Simulink® model operates on a high number of variables (listed in the previous sections) that are created by the Matlab® script, working on the data uploaded from the driving cycle information Excel® file. These variables represent the physical and thermal aspects that characterize the behaviour of the investigated engine and are suitably combined by the model to finally obtain the engine coolant temperature time trend during the driving cycle. Because this output temperature is determined by the tool with respect to such a high number of input quantities, the accuracy level of the result is considerably high and satisfactory from the overall simulation and prediction perspective of the program.
- Analysis of many different heat contributions: since the coolant temperature is determined directly from the heat rate going instantaneously to the coolant, this heat quantity must be determined in the most precise way. In order to do that, all the heat contributions really affecting the engine behaviour have to be subtracted

from the combustion heat rate to determine the effective amount of heat that goes to the coolant during the driving cycle. As briefly described in the previous sections, the five heat contribution logical blocks implemented in the model depict an engine thermal scenario that well matches the real characteristics of such a type of phenomena.

- Flexibility of the model: this is probably the most important and innovative characteristic of the tool. The engine model can work with whatever driving cycle and engine type that the user wants to investigate; given the input characteristics of the driving cycle and of the engine, in fact, the tool starts and proceeds with the computations and generates as output the engine coolant temperature time trend. This result is obtained for every type of engine and every type of driving cycle that the user wants to simulate, without the need for modifications of the architecture of the software. The input variables determine the resultant trend of the coolant temperature and they can refer to any type of engine (fuel type, stroke number, cylinder arrangement, displacement and so on) and driving cycle (NEDC, FTP-75, 10-15 mode, JC08 and so on).
- Thermostat representation: the coolant mass flow rate time trend is given as an input from the driving cycle data and refers to the quantity of coolant that flows instantaneously through the engine cooling system. This quantity, however, does not refer to the coolant flow inside the radiator because, in this case, it is regulated by the thermostat operations that define the amount of coolant directed into the radiator tubes. One of the most important feature of the program is the possibility to represent the thermostat behaviour, considering the radiator heat rate only when the thermostat is open and so the coolant dissipates heat at the front-end. The Simulink® model represents the thermostat working conditions considering that it is open or closed depending on the actual coolant temperature and, moreover, determines the coolant flow rate going through the radiator with respect to engine angular speed and so with respect to the engine operating conditions. Finally, for each simulation, the user can impose the optimum temperature that the coolant should have during vehicle operations, regulating in this way the working characteristics of the thermostat.

Analyzing all these points, it is clear that, despite the complexity of the field of study, the engine cooling system model represents an innovative software both from a company and a research perspective: its features make possible to improve the performance of the Chrysler HEV prediction tool and to introduce some novelties in the panorama of the engine thermal models.

### **3.4 Battery cooling system model design**

For the analysis and study that are going to be addressed in the following sections of the thesis, a mild hybrid vehicle concept is considered and, because of that, a high voltage battery (HVB) storing device (with a nominal voltage higher than 60 V) has to be taken into account. During vehicle operations, the HVB is crossed by a certain amount of electric current that, as described by Equation 3.1, determines a power dissipation for the so-called Joule effect. This power dissipation leads to an increase of the temperature of the battery cells and, finally, determines the actual behaviour of the vehicle battery pack: in fact, the battery temperature influences the availability of discharge power (for startup and acceleration), the life of the device and, moreover, the energy and charge acceptance during the regenerative braking events. High temperatures improve the charge and discharge rates of the battery but, at the same time, lower the total number of recharges and the total service time. Low temperatures, instead, lead to slower charge and discharge operations, to an overall increase of the battery internal resistance and to an extended calendar life because, in colder climates, the chemical degradation reactions are slowed down. Therefore, ideally, batteries should operate within an optimum temperature range that, usually, sets between 20 and 30 °C. To conclude with a very important concept, it has to be highlighted that the behaviour of a battery is strongly affected by its temperature that, among the others, defines the rates of charge and discharge, the value of the internal resistance, the charging efficiency, the cycle and calendar life and, finally, the SOC-dependent open circuit voltage.

Hence, it is clear that in order to thoroughly describe the behaviour of the HVB of the investigated HEV, the actual temperature of the cells of the battery pack must be computed during the simulations run by the Chrysler prediction tool. Unfortunately, at the moment, this tool does not calculate the instantaneous value of the battery temperature

during the simulated driving cycle but simply takes into account for the whole analysis a fixed value for the battery temperature decided by the user. In this way, the battery behaviour cannot be described in an accurate and satisfactory way and so a new thermal sub-model should be added to the Chrysler software, in order to calculate the time trend of the battery temperature during the whole driving cycle and to narrowly determine all the temperature-dependent battery variables. As for the engine cooling model, the starting point for the design activity is a blank paper that has to be filled with theories, equations and programming codes, with the final task of obtaining a battery thermal model capable of computing the time trend of the battery temperature during a virtual driving cycle, considering the characteristics of the cooling system used to control the thermal state of the cells.

In order to realize an advanced battery cooling model, that can describe in the best possible way the thermal behaviour of the HVB of the investigated hybrid vehicle, all the physical aspects regulating the cells cooling phenomenon must be taken into account: starting from the computation of the power dissipated for Joule effect by the HVB during vehicle operations, the temperature trend of the battery is determined on the basis of the cooling solution adopted by the HEV. The higher is the number of inputs considered by the model and the higher is the resultant precision level of the final results, represented by the battery and coolant temperature time trend during the driving cycle. Taking into account the overall architecture of the battery pack cooling system, the characteristics of the coolant, the physics of the coolant flow through the cells, the structural features and thermal properties of the battery and, finally, the boundary conditions of the problem, an advanced battery cooling system model can be designed and integrated in the Chrysler simulation tool, determining an improvement of the accuracy level of the final performance and fuel economy predictions.

### **3.4.1 Battery pack geometric characteristics and cooling solutions**

A battery pack is a set of any number of individual battery cells that may be configured in series or parallel to deliver the desired voltage, capacity and power density; components of a battery pack include the individual cells and the interconnects which provide the electrical conductivity between them. In HEVs, the battery pack has the

purpose to contain the cells constituting the electric energy storage device, to isolate and protect them from the external environment and, finally, to allow their correct and suitable cooling. In Figure 3.32 is showed the external view of the nickel-metal hydride battery pack of the Toyota Prius 2<sup>nd</sup> generation, whose location inside the vehicle is depicted in Figure 3.33 and compared with the location of the battery pack of the Prius 1<sup>st</sup> generation.



**Figure 3.32 - Toyota Prius 2nd generation NiMH battery pack [14]**

Careful studies are done to choose the best possible location of the battery pack, in order to maintain the desired vehicle dynamic configuration that is strongly affected by the weight of the HVB. The Toyota Prius design and development teams have proposed different solutions during the years, in order to characterize the new Prius models with continuously improved battery pack constructive configuration and advanced location options that can ensure the correct management of the pack without worsen the dynamic performances of the vehicle. In this regard, the battery pack has to be realized and located inside the vehicle in such a way it is characterized by:

- a suitable damping behaviour, necessary to attenuate the vibration and pulse components coming from the road through the wheels and suspensions that can affect the structural integrity of the device;
- a correct cooling system configuration, necessary to ensure the best thermal behaviour of the battery and defined by the disposition of the cells inside the pack;

- a complete electromagnetic isolation from the external environment, necessary to avoid dangerous alterations in the behaviour of the cells.

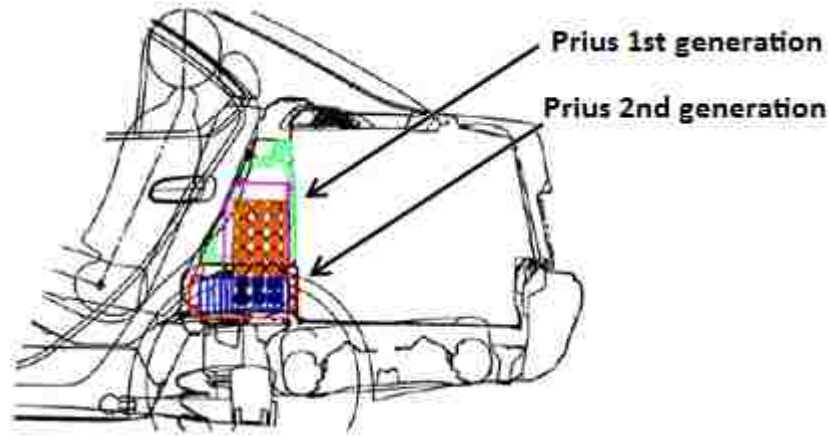
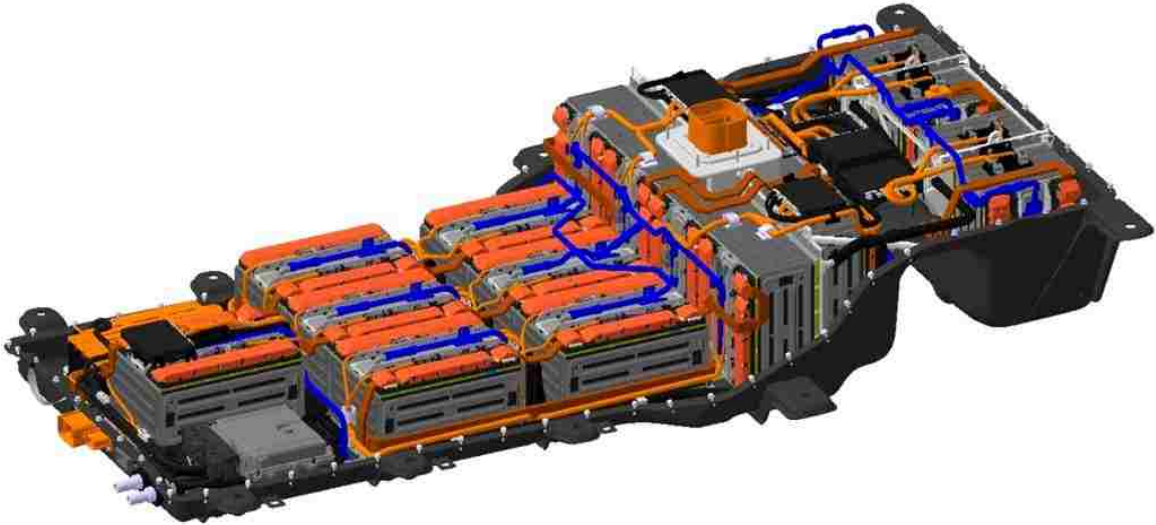


Figure 3.33 - Toyota Prius 1<sup>st</sup> and 2<sup>nd</sup> generation battery pack location [57]

Speaking about the cooling system configuration, there are two methods for distributing the air or the liquid coolant mixture inside the battery pack between the cells. The first method is series cooling, where the coolant medium enters from one end of the pack and leaves it from the other, exposing the several modules to the same amount of coolant; the second method is parallel cooling, where the same total coolant flow rate is split into equal portions, and each portion flows over a single module. After several experimental studies, it has been demonstrated that a parallel cooling solution provides a more even temperature distribution among the cells contained in the pack; the most effective battery cooling systems rely, therefore, on the parallel configuration because it is important to achieve a uniform temperature distribution between the modules, to ensure that they can work in the same controlled thermal state. In this regard, the Toyota Prius (full hybrid electric vehicle) uses a pure parallel air distribution system and also the new FIAT 500e (battery electric vehicle) uses a pure parallel cooling configuration realized with a liquid coolant.

Figure 3.34 shows a CAD picture of the FIAT 500e battery pack, provided with the representation of the thermal plates, battery modules, battery management system devices, high and low current networks. The cooling solution implemented for this battery

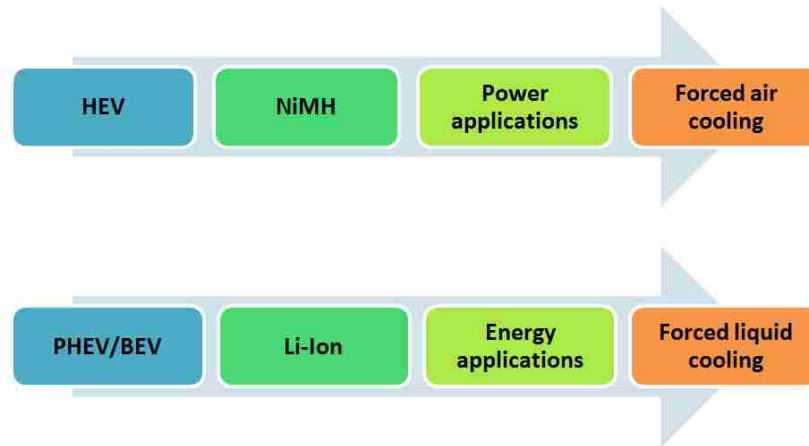
system is a parallel configuration realized with a water-glycol liquid coolant mixture that flows in plate heat sinks placed in contact with the cells.



**Figure 3.34 - FIAT 500e battery pack [58]**

The choice of the heat transfer medium has a significant impact on the performance and cost of the battery thermal management system; usually the heat transfer medium is represented by air, liquid fluid, phase change material or any combination of them. Heat transfer with air is achieved by blowing the air across the modules, while heat transfer with liquid could be achieved either through tubes placed around each module, submerging the cells in a dielectric fluid for direct contact or placing the modules on a liquid cooled plate heat sink. If the liquid is not in direct contact with the cells, such as in tubes or jackets, the cooling medium can be a water-glycol solution; instead, if the modules are submerged in the heat transfer liquid, it must be dielectric, such as silicon-based or mineral oils, to avoid any electrical short circuits. Using the air as the cooling medium may be the simplest approach, but it may not be as effective as a liquid cooling solution; the rate of heat transfer between the walls of the cells and the coolant depends in fact on the thermal conductivity, viscosity, specific heat, density and velocity of the fluid. For the same coolant mass flow rate, the heat transfer for direct contact liquids such as oils is much higher than with air because of the thinner boundary layer and higher fluid thermal conductivity; however, because of oil's higher viscosity and associated higher

pumping power, a lower flow rate is usually employed, making the oil overall heat transfer coefficient only 1.5 to 3 times higher than the one characterizing the air cooled solution. Indirect contact liquid mediums such as water-glycol mixtures, generally have lower viscosity and higher thermal conductivity than most oils, resulting in higher overall heat transfer coefficients; however, because the heat must be conducted through the walls of the tubes, the indirect contact effectiveness decreases.



**Figure 3.35 - HVB cooling solutions**

Figure 3.35 gives an idea of what are, at the current status of the hybrid and electric vehicles market, the cooling solutions actually used to manage and control the thermal state of the HVBs. Hybrid electric vehicles (HEVs) are equipped with high-power nickel-metal hydride (NiMH) batteries, capable of providing and storing high charge quantities in very short periods of time, when the driver is asking the electric motor for a torque boost and during intensive regenerative braking actions. On the other hand, plug-in hybrids (PHEVs) and battery electric vehicles (BEVs) are equipped with high-energy lithium-ion (Li-ion) batteries, capable of storing considerably high quantities of electric charge for long periods of time, in order to propel the vehicle over long distances even working in all-electric range. The cooling solutions adopted for the two cases are different: for HEVs, the NiMH batteries are cooled with a forced air solution, that maintains the cells in a controlled thermal state during the continuous alternating charge and discharge cycles; for PHEVs and BEVs, instead, the Li-ion batteries are cooled with a



liquid solution, in order to maintain the modules of the battery pack at the optimum working temperature with an even distribution.

### 3.4.2 Battery cooling system model implementation and background theory, system configuration

Since the most widespread battery pack cooling solution, in the actual HEVs market, is represented by the parallel configuration, it has been decided to found the battery cooling system model design on such a type of modules location. The battery pack has been treated as composed by a variable number of cells disposed in parallel and cooled by equal portions of coolant, whose flow rate is evenly distributed between them. Dealing with mild and full hybrids, the air has been chosen as the basic cooling medium for the design activity; anyway, in the next chapter, simulations run considering a 50-50 water-glycol coolant medium are also described to study the influence of the coolant type on the battery temperature time trend. Prismatic cells have been considered but, at the same time, the model can work also taking into account pouch cells and cylindrical cells: the different geometries influence the heat transfer phenomenon between the modules and the coolant but the software has the possibility to operate in both the cases, simply implementing some corrections inside the script of the Matlab® base file depending on the investigated cells design.

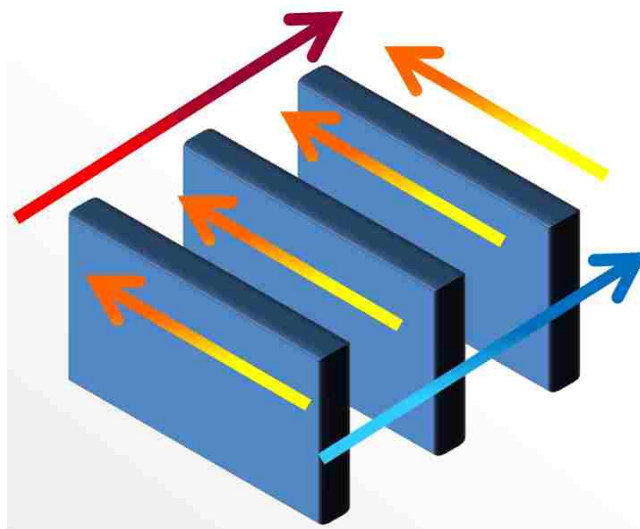
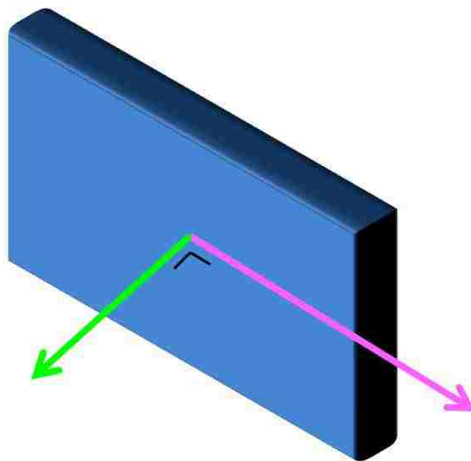


Figure 3.36 - Battery pack modules constructive configuration considered for the design of the battery thermal model

The constructive configuration of the battery pack and cells considered during the design of the battery thermal model, is showed in Figure 3.36; the three blue parallelepipeds represent three modules of the pack and the colored arrows give indications about the path followed by the coolant between the cells. The blue arrow depicts the coolant flow along the entrance side of the pack, where it is warmed up by the cells thanks to a heat transfer phenomenon taking place along the longitudinal direction; the yellow arrows, instead, stand for the coolant flow developing around the modules along their major surface, where it is warmed up by the heat exchanged along the transverse direction; finally, the red arrow shows the coolant flow along the exit side of the pack, where is warmed up by a heat transfer that develops along the longitudinal direction. Since the coolant considered for the design activity is the air, its flow around and between the cells takes place in direct contact with the modules; the same scenario takes place if a dielectric liquid coolant is considered that submerges the modules and flows in direct contact with their surfaces. As stated in the previous lines, the heat transfer takes place between the cells inside the battery pack and the coolant along two different directions, the longitudinal and the transverse ones, as showed in Figure 3.37 where a single module is depicted and the heat transfer directions are highlighted: the longitudinal direction is represented by the fuchsia arrow while the transverse one is represented by the perpendicular green arrow.



**Figure 3.37 - Battery pack module and heat transfer directions**

Analyzing together Figures 3.36 and 3.37, the dynamic of the overall heat transfer phenomenon that defines the thermal behaviour of the battery pack can be well understood: the coolant (air or dielectric liquid) enters the pack at one of its major sides that covers for its whole length, meanwhile it splits between the different passages that run parallel to the major surfaces of the modules and, finally, it merges together again on the opposite major side of the pack from where it leaves the device, with a temperature obviously higher than the one that it has at the entrance. The heat exchanged during vehicle operations between the cells and the battery coolant is determined by the Joule effect that takes place inside the modules conducting electric current: the product between the internal resistance of the cells and the squared magnitude of the current flowing through them, determines the amount of power instantaneously dissipated as heat and transmitted to the coolant whose task is, precisely, to maintain the modules at their optimum operating temperature. To conclude, the battery cooling system model design, that is going to be described in the following sections, is based on a parallel cooling configuration of the battery pack, on a prismatic geometry of the cells and, finally, on the use of air as the cooling medium.

### **3.4.3 Battery cooling system model implementation and background theory, thermodynamic and flow studies**

As a starting point, before going through the detailed description of the battery thermal model design, a thorough analysis of the inputs of the tool has to be realized. All this inputs are managed by the Matlab® base file and stored in the “Workspace”, from where they are uploaded by the Simulink® model and elaborated by its logical blocks to finally obtain the battery and coolant temperature time trends. As for the engine cooling model, the simulations refer to specific driving cycles that determine the operations of the HVB through the definition of the magnitude of the electric current that is flowing during time through the cells. In the following list, all the inputs of the model are introduced and preliminary described:

- magnitude of the electric current ( $I$ ) flowing through the cells during the driving cycle;
- driving cycle time ( $t$ ), necessary to define the time trend of the electric current;

- internal resistance of the cells ( $R_c$ ), that determines the amount of heat dissipated for Joule effect;
- density of the cooling medium ( $\rho_{coolB}$ ) used to cool down the modules of the battery pack;
- thermal conductivity of the coolant ( $k_{coolB}$ );
- specific heat of the coolant ( $c_{p\_coolB}$ );
- dynamic viscosity of the coolant ( $\mu_{coolB}$ );
- coolant mass flow rate entering the battery pack ( $\dot{m}_{coolB\_TOT}$ );
- number of cells ( $N_c$ ) constituting the battery pack;
- cell width ( $w$ );
- cell height ( $h$ );
- cell length ( $l$ );
- transverse distance between two adjacent cells ( $d$ );
- mass of a single cell ( $m_c$ );
- specific heat of the cells ( $c_{p\_c}$ );
- copper current collector thickness ( $th_{copper}$ );
- copper current collector thermal conductivity ( $k_{copper}$ );
- aluminum current collector thickness ( $th_{aluminum}$ );
- aluminum current collector thermal conductivity ( $k_{aluminum}$ );
- separator thickness ( $th_{sep}$ );
- separator thermal conductivity ( $k_{sep}$ );
- temperature of the coolant and of the cells at the beginning of the simulation.

All these inputs depend on the investigated case of study and have to be provided as specific characteristics of the driving cycles, specific thermophysic properties of the battery coolant, specific electric and geometrical characteristics of the cells and of the battery pack. After a suitable elaboration performed by the code written in the Matlab® base file, the various inputs are ready to be uploaded in the Simulink® model and then combined to obtain the desired outputs, represented by the battery and coolant temperature time trends.

### 3.4.3.1 Types of fluid flow regime

It is known that a heat transfer phenomenon taking place between a solid body and a fluid flowing around it, strongly depends on the type and characteristics of the fluid motion. In particular, the thermal scenario and the physical mechanism that regulate the heat transfer between the two entities are determined by the specific motion of the fluid that, generally, can be laminar or turbulent. Laminar flow occurs when a fluid moves at low velocities and tends to flow in parallel layers, without lateral mixing; there are no cross currents perpendicular to the direction of flow, nor eddies or swirls of fluids. In laminar flow, the motion of the particles is highly ordered and occurs in straight lines parallel to the surface touched by the moving fluid. The viscous forces, finally, are dominant over the inertia forces. Turbulent flow, instead, is a flow regime characterized by high speed values of the stream, chaotic property changes and rapid variations of pressure and velocity in space and time. Self-sustained and irregular speed fluctuations occur in all directions and a large presence of variable-size eddies is experienced along the fluid flow direction; due to the effect of the eddies, a large-scale mixing takes place between the fluid particles and enhances the transport of momentum, energy and heat between the fluid and the surfaces that it touches during its flow.

When a fluid is flowing through a closed channel such as a pipe or between two flat plates, either the types of flow may occur depending on the velocity of the fluid; since a basic and clear distinction between the laminar and turbulent flows is difficult to realize simply on the basis of the speed of the fluid, a dimensionless number has been introduced to clarify the operating distinction. This number, known as the Reynolds number ( $Re$ ), gives a measure of the ratio between the inertia forces and the viscous forces, quantifying their relative importance for given flow conditions. Laminar flow occurs at low Reynolds numbers, where the viscous forces are dominant and the fluid motion is smooth; turbulent flow occurs instead at high Reynolds numbers and is dominated by the inertia forces, which tend to produce chaotic eddies, vortices and a general flow instability. The Reynolds number can be defined for a number of different situations where a fluid is in relative motion with a surface; its definition depends on the properties of the moving fluid and on the geometry of the system and is described by Equation 3.21.

$$\text{Re} = \frac{\rho \cdot u \cdot L}{\mu} = \frac{u \cdot L}{\nu} \quad (3.21)$$

Every term contained in Equation 3.21 has to be described in details, in order to better understand the meaning of the Reynolds number:

- $\rho$  is the density of the fluid, expressed in  $\text{kg/m}^3$ ;
- $u$  is the mean velocity of the fluid, expressed in  $\text{m/s}$ ;
- $\mu$  is the dynamic viscosity of the fluid, expressed in  $\text{kg/m}^3$ ;
- $\nu$  is the kinematic viscosity of the fluid, expressed in  $\text{m}^2/\text{s}$ .

A separate mention must be done for the term  $L$  that symbolizes a linear dimension characteristic of the investigated system: for flows in circular pipes,  $L$  is represented by the diameter of the pipes; dealing with flow in noncircular tubes and channels, instead,  $L$  is represented by an equivalent diameter defined as the hydraulic diameter ( $D_h$ ). This variable has a relevant role when performing dimensional analysis of fluid dynamics problems and when studying the main characteristics of an investigated flow regime and, specifically, it is defined by Equation 3.22 where  $A_c$  represents the cross sectional area of the channel and  $P_w$  is the related wetted perimeter.

$$D_h = \frac{4A_c}{P_w} \quad (3.22)$$

At this point, once the meaning of the Reynolds number has been understood in details, its properties can be used to make a clear distinction between the laminar and turbulent flows; experiments, in fact, confirm that the Reynolds number magnitude defines if a given flow is laminar or turbulent. Usually, it exists a certain value of the Reynolds number at which, approximately, the flow regime is considered transitional; before that value the flow regime is considered laminar, after that the regime becomes turbulent.

In a boundary layer flow over a flat plate, the instability occurs for Reynolds numbers of about  $5 \cdot 10^5$  while, for internal flows in a circular or noncircular channel, the transitional regime takes place for Reynolds numbers of about 3500. Since this theoretical analysis has to be referred to the case of the coolant flow around the cells of the HEV

battery pack, a fluid flow inside a noncircular channel must be taken into account; hence, the distinction between the laminar and the turbulent flows has to be done for Reynolds number values of about 3500. In particular, experimental observations show that, for fully developed internal flows, the laminar regime is experienced when the condition  $Re < 2300$  is satisfied while, when the condition  $Re > 4000$  takes place, the turbulent regime characterizes the flow. The design activity of the battery thermal model, in this regards, has been developed imposing the condition that the value of 3500 must be considered as the discriminating between the laminar and the turbulent flows.

### **3.4.3.2 Nusselt number and convective heat transfer coefficient**

Moreover, given the properties of the fluid and the geometric characteristics of the system, the Reynolds number is defined by the speed of the fluid that, in this way, covers a decisive role in the definition of the flow regime and, in turn, of the heat transfer phenomena taking place between the fluid and the walls of the channel in which it is moving. The heat transfer rates, in fact, vary considerably depending on the nature of the flow: with laminar flows, heat transfer to or from the wall varies with distance from the leading edge of a boundary layer, remaining under specified thresholds; turbulent flows, instead, can give rise to heat transfer rates which are much larger than those of laminar flows, caused by turbulent fluctuations and sharp mixing that enhance the transport of energy and heat.

Hence, since the heat transfer phenomena strongly depend on the type and characteristics of the fluid motion, the battery thermal model requested by the Electrified Powertrain department at Chrysler to improve the performance of its prediction tool, must be provided with a function dedicated to the determination of the flow regime that characterizes the coolant motion inside the battery pack. In order to do that, the strategy is to implement in the Simulink® model a computational block able to determine the instantaneous values of the Reynolds number, given as inputs the density, viscosity, mean speed of the coolant and, finally, the hydraulic diameter of the channels in which the coolant itself is flowing.

Considering, instant per instant during the simulation, the actual value of the Reynolds number calculated by the model, it can be determined if the coolant flow

regime is laminar or turbulent and, in this way, characterize in a thorough way the heat transfer phenomenon. As stated before, the flow regime type influences the heat transfer phenomenon because of a different depth of heat transport of the fluid: physically, this condition has a direct impact on the computation of another dimensionless number, whose knowledge is necessary for the further determination of the convective heat transfer coefficient existing, for this study, between the battery coolant and the surfaces of the modules constituting the HVB battery pack.

This dimensionless number is known as the Nusselt number ( $Nu$ ) and it is defined as the ratio between the convective and conductive heat transfers across a given surface; a low Nusselt number is characteristic of a laminar flow experiencing a limited amount of convective heat transfer while a high Nusselt number corresponds to a turbulent flow with a more active heat convection.

$$Nu = \frac{h_f \cdot L}{k} = \frac{h_f \cdot D_h}{k} \quad (3.23)$$

As described by Equation 3.23, the Nusselt number depends on the convective heat transfer coefficient of the fluid ( $h_f$ ), expressed in  $W/(m^2 \cdot K)$ , on the thermal conductivity of the fluid ( $k$ ), expressed in  $W/(m \cdot K)$ , and finally on the characteristic length ( $L$ ) of the physical device through which the fluid is flowing, usually represented by the hydraulic diameter ( $D_h$ ).

The fluid considered for the development of the battery cooling system model is the air, as described in the previous sections, and the channels through which it flows while cooling down the battery are determined by two major surfaces of two adjacent cells and by the top and bottom covers of the battery pack. Hence, the dimensions of the rectangular ducts are represented by the height of the modules ( $h$ ) and by the distance existing between two adjacent cells ( $d$ ), as can be seen in Figure 3.38.



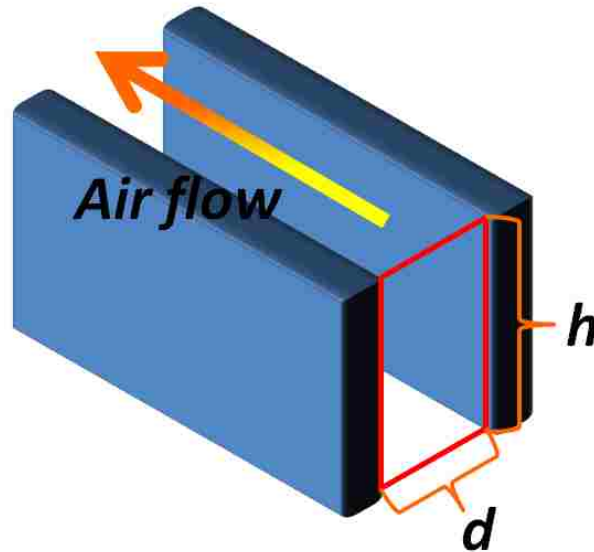


Figure 3.38 - Constructive and geometric characteristics of the battery cooling ducts

Using Equation 3.22, it is possible to compute the hydraulic diameter of the channels through which the air flows while cooling down the modules of the battery pack: taking into account the geometrical variables highlighted in Figure 3.38, Equation 3.24 is obtained.

$$D_h = \frac{4A_c}{P_w} = \frac{4(d \cdot h)}{2(d+h)} = 2 \frac{d \cdot h}{d+h} \quad (3.24)$$

Moreover, also the value of the thermal conductivity is known and, for the air, it is equal to 0.0262 W/(m·K); at this point, the unknowns of the system are represented by the Nusselt number ( $Nu$ ) and by the air convective heat transfer coefficient ( $h_f$ ). This coefficient actively determines the mechanism of the heat transfer between the air and the cells, as it is described in the following paragraphs, and so it has to be defined in the most precise possible way depending on the actual flow regime that is characterizing the air motion between the cells during the driving cycle. The battery cooling model, in this regard, has been designed not using a constant value for the convective heat transfer coefficient taken from the experimental tables but computing, instant per instant, the value of this coefficient from Equation 3.23: in that formula, the hydraulic diameter and the conductivity of the coolant are known (from the coolant properties and the geometry

of the system) and the Nusselt number can be determined through suitable empirical theories that vary on the basis of the flow regime of the coolant. In this way, if the newly designed software defines, instant per instant, the type of flow (laminar or turbulent) of the air in the battery pack and, consequently, uses different formula to determine the Nusselt number, finally the convective heat transfer coefficient is continuously computed as a function of the flow regime type and describes the heat transfer phenomenon with a high level of accuracy. In this regard, the logical steps followed by the battery model to determine the actual characteristics of the heat transfer between the cells and the coolant are listed in the following:

1. the tool uploads the data related to the properties of the coolant, to its mean speed and to the geometry of the system;
2. knowing these data, the software computes the instantaneous value of the Reynolds number, using Equation 3.21;
3. comparing the obtained Reynolds number with its limit value for the transitional flow regime, the model defines if the actual flow regime of the coolant is laminar or turbulent;
4. on the basis of the flow regime type, the tool computes the value of the Nusselt number using the theories developed for the laminar or the turbulent flow;
5. once the Nusselt number has been obtained, the software uses Equation 3.23 to calculate the actual convective heat transfer coefficient;
6. the heat quantity exchanged between the cells and the coolant is computed using the convection coefficient that has been obtained (passing before through the definition of the overall heat transfer coefficient).

Step number five presented in the list above is implemented in the Simulink® file through Equation 3.25, directly derived from Equation 3.23 and from the knowledge of the hydraulic diameter of the investigated channel geometry.

$$h_f = \frac{Nu \cdot k}{L} = \frac{Nu \cdot k}{D_h} = \frac{Nu \cdot k}{2} \cdot \frac{d+h}{d \cdot h} \quad (3.25)$$

From Equation 3.25, it can be clearly pointed out that the convective heat transfer coefficient is linear function of the Nusselt number that, depending on the type of flow regime of the battery coolant, has to be computed in different ways.

#### **3.4.3.2.1 Nusselt number determination, laminar flow**

If the coolant is flowing between the cells of the battery pack with low speed values and, in this way, its Reynolds number is lower than 3500, the flow regime is considered laminar. For fully developed laminar flows in ducts of constant cross sectional area, the Nusselt number is constant and depends on the flow passage geometry and on the thermal boundary conditions, described as follows.

- T condition: the wall temperature of the duct is constant both axially and peripherally throughout the passage length.
- H1 condition: the wall temperature of the duct is constant at any cross sections in the peripheral direction while the heat transfer rate is constant along the axial direction.
- H2 condition: the wall heat transfer rate is constant in the axial direction as well as in the peripheral direction.

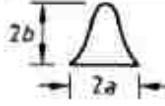
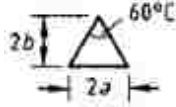
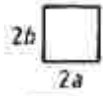

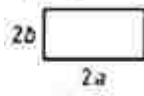

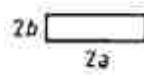
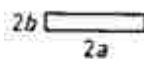
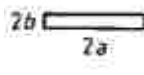

Hence, once the flow passage geometry (and in particular its aspect ratio) has been defined together with the thermal boundary condition characterizing the overall system, the Nusselt number is determined as constant using Table 3.3 or similar [56].

#### **3.4.3.2.2 Nusselt number determination, turbulent flow**

If the coolant is flowing between the cells of the battery pack with high speed values and, in this way, its Reynolds number is higher than 3500, the flow regime is considered turbulent. For fully developed turbulent flows in smooth ducts of constant cross sectional area, the Nusselt number depends on the Reynolds and Prandtl numbers and can be computed using the simplified Petukhov and Popov correlation [56], described by Equation 3.26.

$$Nu = 0.023 \cdot Re^{0.8} \cdot Pr^{0.4} \quad (3.26)$$

Table 3.3 - Nusselt number constant values for laminar flow regimes [56]

Geometry ( $L/D_h > 100$ )	Aspect Ratio	$Nu_{H1}$	$Nu_{H2}$	$Nu_T$
	$\frac{2b}{2a} = \frac{\sqrt{3}}{2}$	3.014	1.474	2.39
	$\frac{2b}{2a} = \frac{\sqrt{3}}{2}$	3.111	1.892	2.47
	$\frac{2b}{2a} = 1$	3.608	3.091	2.976
		4.002	3.862	3.34
	$\frac{2b}{2a} = \frac{1}{2}$	4.123	3.017	3.391
		4.364	4.364	3.657
	$\frac{2b}{2a} = \frac{1}{4}$	5.331	2.94	4.439
	$\frac{2b}{2a} = \frac{1}{6}$	6.049	2.93	5.137
	$\frac{2b}{2a} = \frac{1}{8}$	6.490	2.94	5.597
	$\frac{2b}{2a} = 0$	8.235	8.235	7.541

The Prandtl number ( $Pr$ ) is a dimensionless number, determined as the ratio between the momentum diffusivity and the thermal diffusivity of a given fluid. In heat transfer problems, the Prandtl number controls the relative thickness of the momentum and thermal boundary layers: when the Prandtl number is small, it means that the heat diffusion is very rapid if compared to the momentum diffusion. Hence, for fluids as liquid metals, characterized by Prandtl numbers ranging approximately between 0.001 and 0.03, the thermal diffusion occurs at a greater rate with respect to the momentum diffusion (the opposite happens for high-viscosity oils whose Prandtl number varies between 100 and 40000). The Prandtl number definition is showed in Equation 3.27, where  $\nu$  represents the kinematic viscosity of the fluid (expressed in  $m^2/s$ ) and  $\alpha$  its thermal diffusivity (expressed in  $m^2/s$ ); finally, the Reynolds number is determined multiplying the dynamic

viscosity of the fluid by its specific heat and dividing this product for the value of the thermal conductivity.

$$\text{Pr} = \frac{\nu}{\alpha} = \frac{\frac{\mu}{\rho}}{\frac{k}{\rho \cdot c_p}} = \frac{\mu \cdot c_p}{k} \quad (3.27)$$

### 3.4.3.2.3 Convective heat transfer coefficient determination

Coming back to the analysis of the Nusselt number determination procedure, now it is possible to understand how the battery cooling model has to be designed in order to thoroughly characterize the study of the heat transfer that takes place between the cells and the air flowing around them. In this regard, it is clear the necessity to implement in the model an “if/else” sub-system that, instant per instant, determines if the flow regime of the coolant (air) inside the battery pack is laminar or turbulent: if the air flow is laminar, then the Nusselt number is imposed as constant and its value is taken from Table 3.3 on the basis of the aspect ratio of the channels in which the coolant is moving; if the air flow is turbulent, on the contrary, then the Nusselt number is determined instantaneously through Equation 3.26. Once the model has computed the value of  $Nu$ , the procedure described in Equation 3.25 is activated and the instantaneous value of the convective heat transfer coefficient is determined: this value depends, in this way, on the Nusselt number that, in turn, depends on the flow regime type that the coolant shows at the investigated instant of the simulation. To conclude, time after time during the driving cycle chosen to simulate the battery thermal behaviour, the battery cooling system model computes the actual values of the convective heat transfer coefficient in order to define the heat transfer phenomenon, instant per instant, with respect to the flow regime type.

### 3.4.3.3 Overall heat transfer coefficient determination

For the implementation of the overall battery thermal model, as it was for the study of the surroundings heat rate during the engine cooling system model design, attention must be paid to the dynamics of heat transfer that characterize the battery cells and the coolant flowing between them. The final purpose of the battery thermal model, as highlighted in the previous sections, is to determine the temperature time trend of the

cells during an investigated driving cycle that determines the amount of current flowing through the cells to fulfill the requests of the driver. To compute, instant per instant, the temperature of the HVB of the considered hybrid vehicle, the amount of heat exchanged between the modules of the battery pack and the coolant must be accurately determined. In this regard, the heat transfer phenomenon taking place between the cells and the coolant is defined by a conductive path, between the middle section of the cells and their external surfaces, and by a convective path, between the outer surfaces of the cells and the coolant in which they are submerged. Calculating the heat transfer rate with respect to the temperature difference existing between the modules' medium point and the coolant, an overall heat transfer coefficient  $U$  must be considered in order to take into account both the conduction and convection of heat that characterize the battery thermal behaviour. Given  $T_B$  as the temperature of the battery taken at the medium point of the cells,  $T_s$  as the temperature of the cells taken at their surface and, finally,  $T_{cool}$  as the temperature of the air that is cooling down the cells during vehicle operations, Equations 3.28 and 3.29 can be written.

$$\dot{q} = \dot{q}_{cond} = \frac{k_B}{t_B} \cdot (T_B - T_s) \quad (3.28)$$

$$\dot{q} = \dot{q}_{conv} = h_{cool} \cdot (T_s - T_{cool}) \quad (3.29)$$

Moreover, knowing that the heat flux  $\dot{q}$  multiplied by the surface of the cells  $A$  gives as output the heat rate  $\dot{Q}$ , it is possible to rewrite and combine Equations 3.28 and 3.29 to obtain the final formula represented by Equation 3.32. The term  $k_B$  represents the thermal conductivity of the battery, while the term  $t_B$  represents its thickness considered from the medium point to the external surface of the cells.

$$T_B - T_s = \dot{q} \cdot \frac{t_B}{k_B} \quad (3.30)$$

$$T_s - T_{cool} = \dot{q} \cdot \frac{1}{h_{cool}} \quad (3.31)$$

$$\dot{Q} = \dot{q} \cdot A = \left( \frac{t_B}{k_B} + \frac{1}{h_{cool}} \right)^{-1} \cdot A \cdot (T_B - T_{cool}) = U \cdot A \cdot (T_B - T_{cool}) \quad (3.32)$$

Furthermore, the heat transfer characteristics have to be determined also on the basis of the direction considered for the thermal exchange phenomenon (these directions are the longitudinal and transverse ones, represented by the fuchsia and green arrows in Figure 3.37). Since the cells of the HVB are not constituted by a unique homogeneous material but, instead, by a series of different layers, their thicknesses and thermal conductivities have to be carefully combined in order to determine the overall heat transfer coefficients along the longitudinal ( $U_L$ ) and transverse ( $U_T$ ) directions. A nickel-metal hydride or lithium-ion battery cell, in fact, has many parallel thin battery layers across its length and so, in the thermal analysis of the cell, it is important to take into account this constructive detail to compute the real conductivity of the device, both longitudinally and transversely.

The cell has to be described as containing several equivalent battery layers placed one after the other and represented by the anode current collector, the separator and the cathode current collector: the battery thermal model has been designed, in this way, modeling the prismatic modules as complex layered structures and not as simple homogeneous parallelepipeds composed by a unique type of material. Because of this layered structure, the thermal behaviour of the cell has to be characterized by the effective thermal properties that regulate the heat transfer phenomenon along the longitudinal and the transverse directions; the thermal conductivities at the component interfaces should be determined based on the mutual arrangement of the different layers. connections of the components. For series connections, the composite thermal conductivity is given by Equation 3.33 while, for parallel connections, the expression for the composite thermal conductivity becomes the one of Equation 3.34 [59].

$$k = \frac{\sum_i L_i}{\sum_i (L_i / k_i)} \quad (3.33)$$

$$k = \frac{\sum_i (L_i \cdot k_i)}{\sum_i L_i} \quad (3.34)$$

The terms  $L_i$  and  $k_i$  are the thickness and the thermal conductivity of the layer  $i$  respectively. The battery layers are showed in Figure 3.39, where the black arrow indicates the longitudinal direction of the battery geometry: the three colored parallelepipeds represent in a simplified way the three different types of layers included in the battery modules, whose length ( $l$ ) is constituted by approximately forty sets of them.

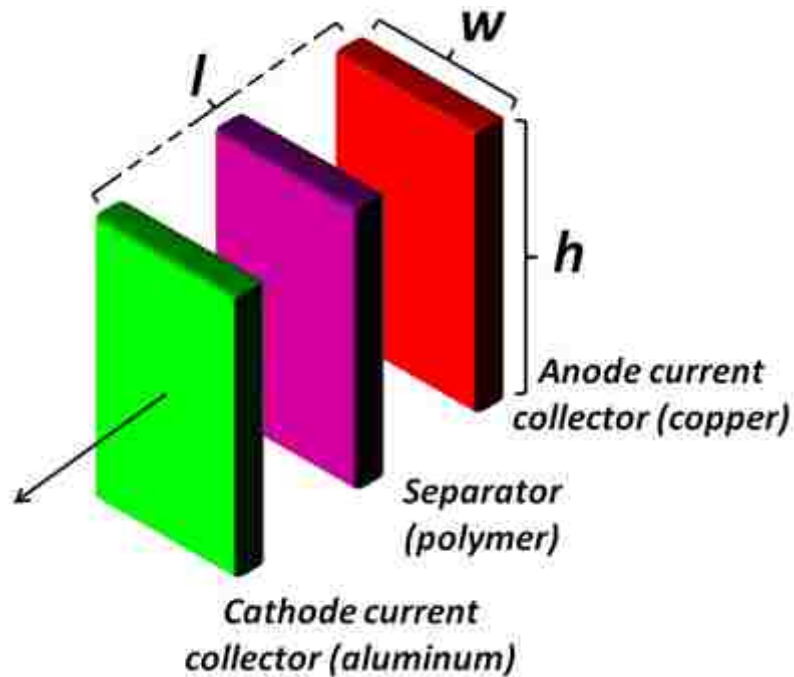


Figure 3.39 - Different layers constituting the internal layered structure of a cell

The red parallelepiped refers to the anode current collector, usually made of copper; the purple one refers to the polymer separator (polyethylene/polypropylene), a permeable membrane placed between the anode and the cathode to prevent electrical short circuits and to allow the transport of the ionic charges; the green parallelepiped, finally, refers to the cathode current collector, usually made of aluminum.



**Table 3.4 - Thicknesses and thermal conductivities of the different layers constituting the battery module structure**

Layer	Thermal conductivity	Thickness
Anode current collector (copper)	$k_{an} = 573 \text{ W/(m}\cdot\text{K)}$	$L_{an} = 12 \text{ }\mu\text{m}$
Separator (polymer)	$k_{sep} = 0.35 \text{ W/(m}\cdot\text{K)}$	$L_{sep} = 21 \text{ }\mu\text{m}$
Cathode current collector (aluminum)	$k_{cat} = 214 \text{ W/(m}\cdot\text{K)}$	$L_{cat} = 20 \text{ }\mu\text{m}$

The thickness and thermal conductivity of each of these layers are described in Table 3.4, while Equations 3.35 and 3.36 computes the longitudinal and transverse thermal conductivities of the HVB cells considered for the development of the battery thermal model ( $n_l$  is the number of layers contained in a single module).

Substituting the thermal conductivity and thickness values contained in Table 3.4 in the following equations, the longitudinal and transverse cell thermal conductivities are computed. It can be seen that the longitudinal conductivity is about two orders of magnitude lower than the transverse one: this because, along the longitudinal direction, a hypothetical heat flow has to pass completely through the separator layers, without the possibility to take a low thermal resistance path; on the other hand, along the transverse direction, a hypothetical heat flow can pass through the only current collector layers, encountering a low thermal resistance lane.

$$k_L = \frac{\sum_i L_i}{\sum_i (L_i / k_i)} = \frac{n_l \cdot (L_{an} + L_{sep} + L_{cat})}{n_l \cdot \left( \frac{L_{an}}{k_{an}} + \frac{L_{sep}}{k_{sep}} + \frac{L_{cat}}{k_{cat}} \right)} = \frac{(12 + 21 + 20)}{\left( \frac{12}{573} + \frac{21}{0.35} + \frac{20}{214} \right)} = 0.8817 \frac{W}{m \cdot K} \quad (3.35)$$

$$k_T = \frac{\sum_i (L_i \cdot k_i)}{\sum_i L_i} = \frac{n_l \cdot (L_{an} \cdot k_{an} + L_{sep} \cdot k_{sep} + L_{cat} \cdot k_{cat})}{n_l \cdot (L_{an} + L_{sep} + L_{cat})} = \frac{(12 \cdot 573 + 21 \cdot 0.35 + 20 \cdot 214)}{(12 + 21 + 20)} = 210.6292 \frac{W}{m \cdot K} \quad (3.36)$$

At this point, using the longitudinal and transverse thermal conductivities computed for the cells of the battery pack, it is possible to determine the overall longitudinal and transverse heat transfer coefficients through Equations 3.37 and 3.38.

$$U_L = \left( \frac{t_{BL}}{k_L} + \frac{1}{h_{cool}} \right)^{-1} \quad (3.37)$$

$$U_T = \left( \frac{t_{BT}}{k_T} + \frac{1}{h_{cool}} \right)^{-1} \quad (3.38)$$

The terms  $t_{BL}$  and  $t_{BT}$  represent the overall longitudinal and transverse thickness respectively, defined from the medium point of the cell to the external surfaces normal to the longitudinal and transverse direction respectively: following Equations 3.39 and 3.40 express these thickness with respect to the cell geometric measures. Finally, studying Equation 3.37 and 3.38, it must be underlined that the term  $h_{cool}$  refers to the actual value of the convective heat transfer coefficient, determined instant per instant on the basis of the flow regime type of the coolant, as thoroughly described in the previous section: the overall heat transfer coefficients, in this way, vary instantaneously during the driving cycle depending on the actual value of  $h_{cool}$  computed by the program.

$$t_{BL} = \frac{l}{2} \quad (3.39)$$

$$t_{BL} = \frac{w}{2} \quad (3.40)$$

At this point, once the longitudinal and transverse overall heat transfer coefficients have been determined, it is possible to study the amount of heat exchanged instantaneously by the cell with the coolant that is flowing around it. Considering that the overall heat transfer coefficients take into account that the heat transfer phenomenon takes place through conduction and convection, the temperature difference that has to be considered for the calculation relates to the temperature inside the cell and the temperature of the coolant. Equation 3.41 is generally valid and has to be developed along the longitudinal and transverse directions, for all the four surfaces of each module.

$$\dot{Q} = U \cdot A \cdot (T_B - T_{cool}) \quad (3.41)$$

Considering Figure 3.36, that clearly depicts the coolant motion inside the battery pack between the cells, the assumptions made for the analysis and design activities can be studied. It has been imposed that the temperature of the coolant along the whole inlet side of the pack (blue arrow, parallel to the transverse direction) has to be considered equal to the inlet temperature of the coolant: this assumption is not so restrictive because, as it can be seen from Equations 3.35 and 3.36, the longitudinal thermal conductivity of the cells is very low compared to the transverse one and so the heat quantity that warms up the coolant along the battery inlet side length is not sufficiently high to determine a considerable increase of the coolant temperature. The same assumption has been done for the whole exit side of the pack (red arrow, parallel to the transverse direction) but, obviously, this time the temperature of the coolant has been taken equal to its outlet temperature. Referring to the inlet and outlet temperatures of the coolant, it has to be underlined that the inlet one is imposed by the user or by the boundary operating conditions of the investigated driving cycle, while the outlet one has to be computed by the model during the simulation. Finally, studying the coolant path parallel to the major surfaces of the modules (yellow arrow, parallel to the longitudinal direction), the temperature of the coolant has been treated as increasing from the inlet to the outlet value thanks to the transverse heat transfer phenomena taking place during time. Since the transverse heat transfer occurs homogeneously along the length of the cell, it can be computed considering the temperature difference existing between the module, whose temperature is considered at the longitudinal and transverse midpoint of the prismatic structure, and the coolant, whose temperature is considered at the midpoint along the longitudinal direction (the one followed by the coolant between two adjacent modules). The final assumption relates to the fact that this temperature of the coolant has been considered as the arithmetic mean between the coolant inlet and outlet temperatures: this because, since the heat exchange takes place linearly along the longitudinal direction, then the temperature of the coolant increases linearly from the inlet side to the outlet side of the battery pack. Hence, considering a single cell surrounded by the coolant, the following Equations 3.42, 3.43, 3.44 and 3.45 can be written to compute the heat rate that the cell itself dissipates during time along the longitudinal and transverse directions, for

each of its four lateral surfaces (the top and bottom surfaces are directly connected with the battery pack casing and so they are not touched by the coolant).

$$\dot{Q}_{L1} = U_L \cdot A_{L1} \cdot (T_B - T_{cool\_IN}) \quad (3.42)$$

$$\dot{Q}_{T1} = U_T \cdot A_{T1} \cdot (T_B - T_{cool\_M}) \quad (3.43)$$

$$\dot{Q}_{L2} = U_L \cdot A_{L2} \cdot (T_B - T_{cool\_OUT}) \quad (3.44)$$

$$\dot{Q}_{T2} = U_L \cdot A_{T2} \cdot (T_B - T_{cool\_M}) \quad (3.45)$$

The first heat rate ( $\dot{Q}_{L1}$ ) refers to the heat transfer taking place along the longitudinal direction across the cell surface ( $A_{L1}$ ) facing the inlet side of the battery pack; the coolant inlet temperature ( $T_{cool\_IN}$ ) has hence to be taken into account. The second and fourth heat rates ( $\dot{Q}_{T1}$  and  $\dot{Q}_{T2}$ ) refer instead to the heat transfers taking place along the transverse direction across the major cell surfaces ( $A_{T1}$  and  $A_{T2}$ ) that extend along the length ( $l$ ) of the modules; the coolant temperature at the midpoint of the cell length ( $T_{cool\_M}$ ), supposed to be equal to the arithmetic mean of the coolant inlet and outlet temperatures, has hence to be considered. Finally, the third heat rate ( $\dot{Q}_{L2}$ ) refers to the heat transfer that takes place along the longitudinal direction across the cell surface ( $A_{L2}$ ) facing the outlet side of the battery pack; the coolant outlet temperature ( $T_{cool\_OUT}$ ) has hence to be taken into account. The geometric characteristics of the modules are given as input data and so the areas of the cell surfaces are known, at the same time also the inlet temperature of the coolant is defined as an input data while, finally, the overall heat transfer coefficients are computed instantaneously (on the basis of the actual value of the convective heat transfer coefficient) by the battery thermal model during the simulation, as previously described. In this way, the unknowns of the system are represented by the battery temperature  $T_B$  and by the coolant outlet temperature  $T_{cool\_OUT}$ , analyzed in details in the following list.

- Battery temperature: it is considered at the core of the modules and so at their midpoint along both the longitudinal and transverse directions. It is correct to

define the battery temperature equal to the temperature of each cell because, as long as all the cells are crossed by the same electric current magnitude during the driving cycle, considering the amount of coolant flowing around a single cell gives the same result as considering the whole coolant entering the battery pack and cooling down all the modules of the system. The thermal phenomenon taking place between the whole HVB and the global quantity of coolant flowing inside the pack, has the same characteristics and gives rise to the same temperature changes of the thermal phenomenon taking place between a single cell and the specific portion of coolant flowing around it. The time trend of the battery temperature has to be determined by the model as the final output of the simulations investigated by the user.

- Coolant outlet temperature: it is determined by the overall heat transfer phenomena that takes place between the cells and the coolant across the various surfaces of the modules. The heat rate dissipated by the cells during time for the Joule effect, computed through Equation 3.1, causes an increase of the coolant temperature; the coolant, in fact, in order to cool down the modules to maintain their temperature in the optimum range for the operating conditions, acquires the heat delivered by the cells and leaves the battery pack at a temperature higher than the one it has at the inlet manifold. Since the outlet temperature of the coolant has a direct impact on the computation of the heat rates, it has to be determined during time by the battery cooling system model, as it is for the temperature of the modules.

#### **3.4.4 Battery cooling system model implementation and background theory, software creation**

Now that the background theory related to the fluid flow and heat transfer phenomena has been studied, the implementation and design activity of the battery thermal model can be described and analyzed in details. As for the engine cooling system software, also the structure of the Simulink® file of the battery model is going to be described step by step, in relation to the main logical sub-blocks that define its operating features.



Figure 3.40 shows the overall structure of the Simulink® file of the battery cooling system model that, it must be remembered, has been designed to compute the time trend of the battery temperature and of the coolant outlet temperature given the investigated hybrid electric vehicle, the thermal and geometrical characteristics of its high voltage battery, the thermal physical properties of the coolant used to cool down the battery pack and, finally, the profile of the current flowing through the battery modules during the considered driving cycle.

#### 3.4.4.1 Reynolds and Prandtl numbers computation

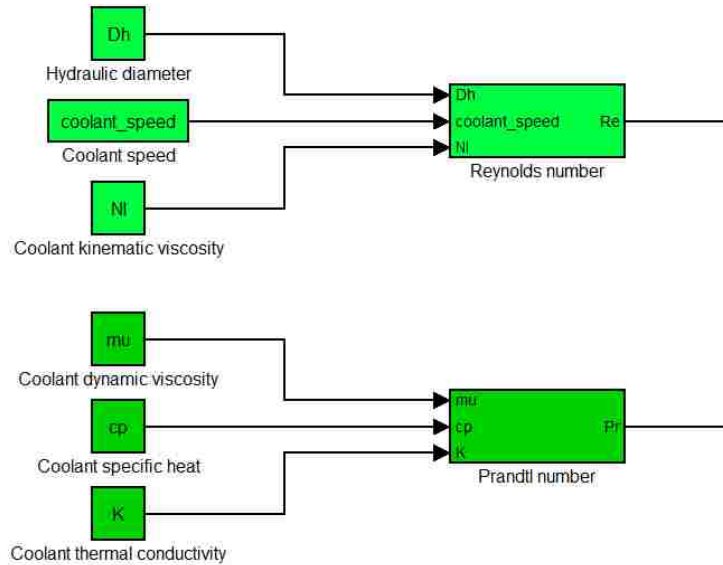
Taking into account the studies developed and discussed in the previous sections, it has to be underlined that, in order to compute the temperature of the HEV battery and of the coolant at the outlet section of the battery pack, it is necessary to consider if the heat transfer between the cells and the coolant occurs in case of laminar or turbulent cooling medium flow regime.

To determine the actual flow type of the coolant, the instantaneous Reynolds number values have to be computed through Equation 3.21 and compared with the discriminating value of 3500; at this point, once the coolant flow regime has been defined, the Nusselt number must be calculated using the Petukhov and Popov correlation, in case of turbulent flow, while it must be taken as constant from Table 3.3, in case of laminar flow. The Petukhov and Popov correlation, described by Equation 3.26, is based on the knowledge of the Prandtl number that, in this way, has to be determined by the model together with the Reynolds number.

The logical sub-blocks of the Simulink® file that manage the computation of these two dimensionless groups are represented in Figure 3.41, where the inputs coming from the Matlab® “Workspace” are represented by:

- the hydraulic diameter ( $D_h$ ) of the channels in which the coolant flows cooling down the cells, determined for the studied case by Equation 3.24;
- the instantaneous speed of the coolant ( $u_{coolB}$ ), determined instantaneously through Equation 3.46 presented below;
- the coolant kinematic viscosity ( $\nu_{coolB}$ ), computed as the ratio between the coolant dynamic viscosity ( $\mu_{coolB}$ ) and the coolant density ( $\rho_{coolB}$ );

- the coolant specific heat ( $c_{p\_coolB}$ );
- the coolant dynamic viscosity ( $\mu_{coolB}$ );
- the coolant thermal conductivity ( $k_{coolB}$ ).



**Figure 3.41 - Reynolds and Prandtl numbers computational block (external view)**

All the inputs listed above relate to the thermophysical properties of the considered coolant and to the geometrical characteristics of the investigated battery system: they are saved or computed by the Matlab® base file of the model and, subsequently, they are uploaded on Simulink® in order to be combined and elaborated for the purposes of the simulation. As far as the instantaneous speed of the coolant is concerned, it is determined by the Matlab® code through Equation 3.46 considering the time-dependent values of the coolant mass flow rate that are given as a vector from the driving cycle characteristics.

$$u_{coolB} = \frac{\dot{m}_{coolB}}{(\rho_{coolB} \cdot d \cdot h)} \quad (3.46)$$

Dividing the instantaneous coolant mass flow rate ( $\dot{m}_{coolB}$ ) for the density of the coolant ( $\rho_{coolB}$ ) and the cross sectional area of the cooling duct, computed as the product of the height of the cells ( $h$ ) and the distance between two adjacent modules ( $d$ ), the instantaneous magnitude of the coolant speed is obtained. Once the inputs of the



Reynolds and Prandtl numbers computational blocks have been uploaded from the Matlab® “Workspace”, they are elaborated inside the two blocks to compute the two dimensionless numbers using Equations 3.21 and 3.27, as depicted in Figures 3.42 and 3.43.

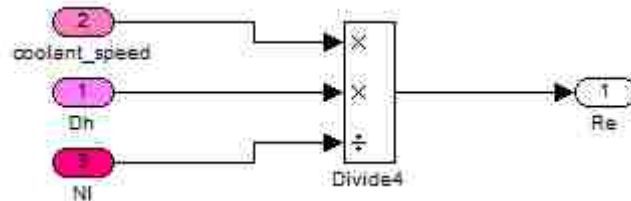


Figure 3.42 - Reynolds number computational block (internal view)

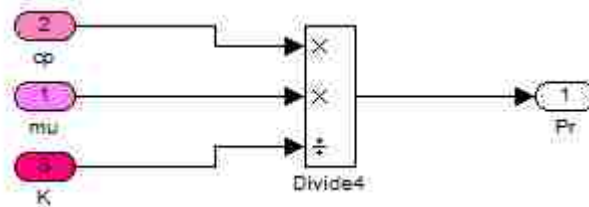
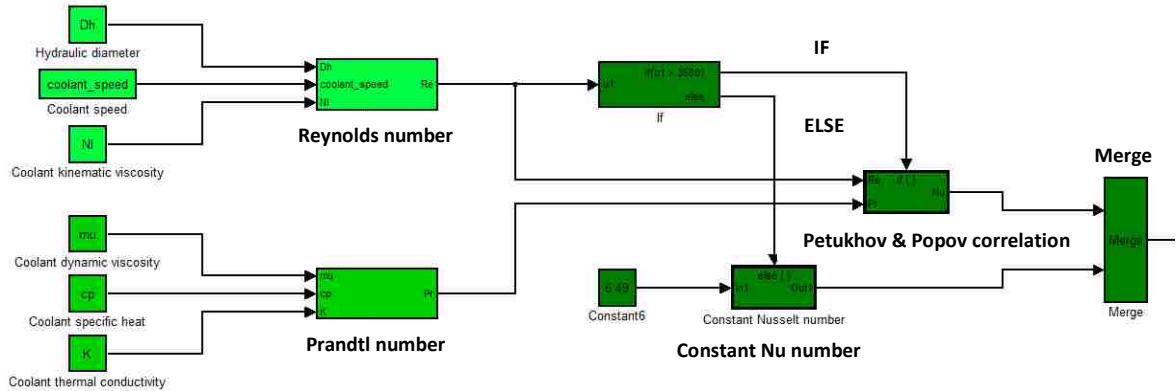


Figure 3.43 - Prandtl number computational block (internal view)

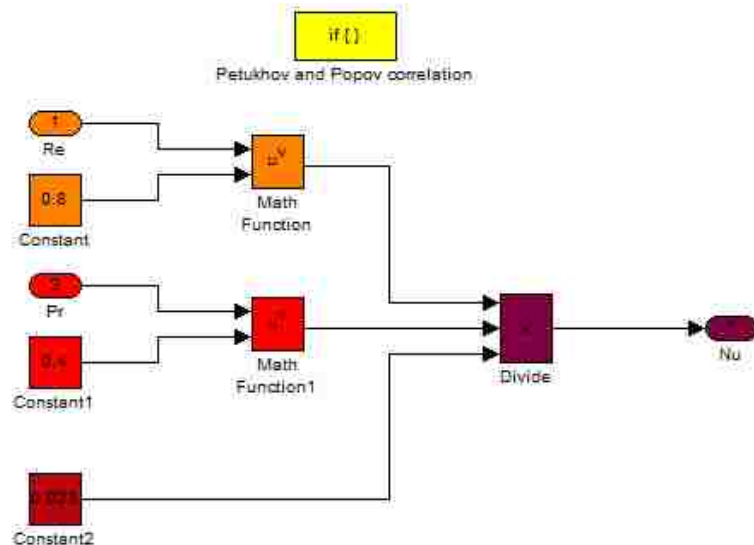
### 3.4.4.2 Nusselt number computation

Once the Reynolds number has been computed, instant per instant during the driving cycle, it becomes the input of the “if/else” condition necessary to determine the actual type of coolant flow regime, as depicted in Figure 3.44. In case the “if” condition is satisfied, and this happens when the Reynolds number is higher than the limit value of 3500 (imposed by the user on the basis of theoretical passages explained in the previous sections), then the flow regime is assumed to be turbulent and the Nusselt number computation takes place using the Petukhov and Popov correlation.



**Figure 3.44 - Logical block responsible for the determination of the flow regime type and for the computation of the Nusselt number**

The Reynolds and Prandtl numbers computed by the model become the inputs of the “if” condition sub-block, where they are combined through Equation 3.26 to calculate the actual Nusselt number magnitude; the logical blocks used to implement on Simulink® the Petukhov and Popov function are represented in Figure 3.45.



**Figure 3.45 - Internal view of the logical block implementing the Petukhov and Popov correlation**

On the contrary, in case the “else” condition is satisfied, and this happens when the Reynolds number is lower than the discriminating value of 3500, then the regime is assumed to be laminar and, because of this, the Nusselt number is imposed as constant using the suitable value taken from Table 3.3 on the basis of the geometry of the cooling duct. In this way, during a simulation, the outputs of the “if/else” sub-block are

represented by the instantaneous values of the Nusselt number, determined during time by the software on the basis of the actual type of flow of the coolant; in order to obtain a unique time-dependent vector for  $Nu$ , the mutually exclusive outputs of the “if/else” sub-block have to be merged by the program using the “Merge” logical block imported from the Simulink® library. At the end of this logical loop, built and implemented during the battery thermal model design, a time-dependent vector containing the instantaneous values of the coolant Nusselt number is obtained that can be used to compute the convective heat transfer coefficient ( $h_{cool}$ ) magnitudes during time.

### 3.4.4.3 Convective heat transfer coefficient computation

Considering a given instant of the driving cycle, from the Nusselt number value that is given as output by the “Merge” logical block, it is possible to compute the corresponding coolant convective heat transfer coefficient magnitude, using Equation 3.25. Hence, a time-dependent vector containing all the instantaneous values of  $h_{cool}$  is computed by the program, through the logical loop depicted in Figure 3.46.

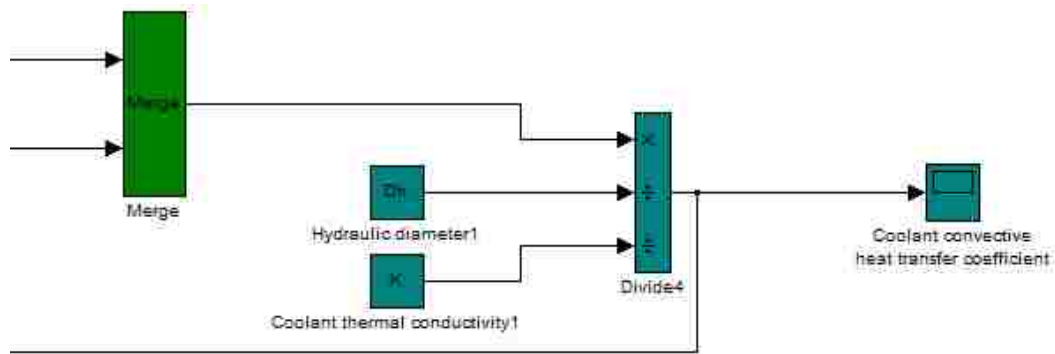


Figure 3.46 - Convective heat transfer coefficient computational block

As thoroughly described before, the actual value of the convective heat transfer coefficient of the coolant actively determines the characteristics and dynamics of the heat transfer phenomena taking place between the battery cells and the cooling medium. This because the instantaneous magnitude of  $h_{cool}$  is determined from the Nusselt number that, in turn, directly depends on the type of flow that characterizes the coolant. In this regard, it has to be remembered that the flow regime type of the coolant has a sharp influence on

the amount of heat that the coolant itself and the surface over which it is flowing can exchange: in case of turbulent flow, the swirling regions of the fluid, called eddies, transport an amount of energy and heat higher than the one that can be involved in case of a laminar, highly ordered flow. The chaotic motion of the fluid, in fact, enhances the convective heat transfer which is influenced by the number of fluid molecules that, in a given period of time, are in contact with the surface over which the fluid flow is taking place. If the coolant flow regime is turbulent, the large-scale mixing and swirling phenomena lead to an increased amount of fluid particles touching instantaneously the surface of the cooling duct and, finally, to an overall increase of the convective heat transfer between the coolant and the battery modules (whose surfaces constitute the walls of the cooling channels). Physically, the enhanced convective heat transfer that characterizes the turbulent flow regimes is determined by a high value of the convective heat transfer coefficient ( $h_{cool}$ ) obtained, in turn, from a high value of the coolant Nusselt number computed by the tool: comparing, in fact, for the same boundary conditions, two different Nusselt numbers obtained for a laminar and a turbulent flow types, the turbulent one is certainly the highest. Coming back to the description of the battery thermal model architecture, once the instantaneous value of  $h_{cool}$  is computed on Simulink®, it is sent to the sub-block responsible for the calculation of the longitudinal and transverse overall heat transfer coefficients.

#### **3.4.4.4 Overall heat transfer coefficients computation**

At this point, once the instantaneous value of the convective heat transfer coefficient has been determined, it is sent to the sub-block created specifically for the calculation of the overall longitudinal and transverse heat transfer coefficients that have to be computed through Equations 3.37 and 3.38. From Figure 3.47 it is possible to see that only one input is going, instant per instant, to the overall heat transfer coefficient computational block and this input is represented by the coolant convective coefficient, calculated by the software at the previous logical step. The other variables necessary to determine during time the values of  $U_L$  and  $U_T$  are uploaded in Simulink® from the “Workspace” of the Matlab® base file and, as depicted in Figure 3.48, are represented by

the ratios between the modules thicknesses and thermal conductivities computed along the longitudinal and transverse directions.

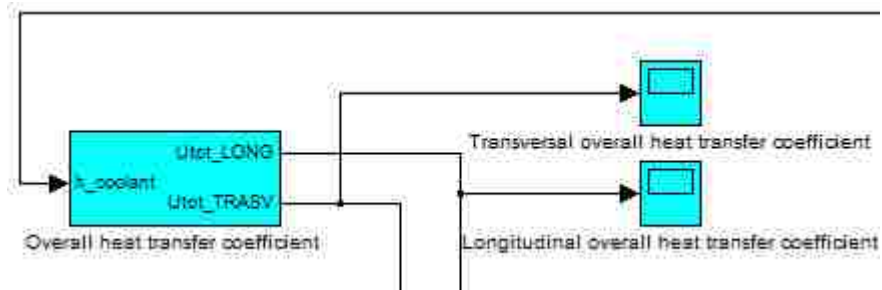


Figure 3.47 - Longitudinal overall and transverse heat transfer coefficients computational block (external view)

Adding these ratios to the reciprocal of the convective heat transfer coefficient and, finally, raising to the -1 power both the sums, the longitudinal and transverse overall heat transfer coefficients are calculated by the battery thermal model, as can be seen from Figure 3.48 where the logical structure implemented inside the sub-block of Figure 3.47 is represented.

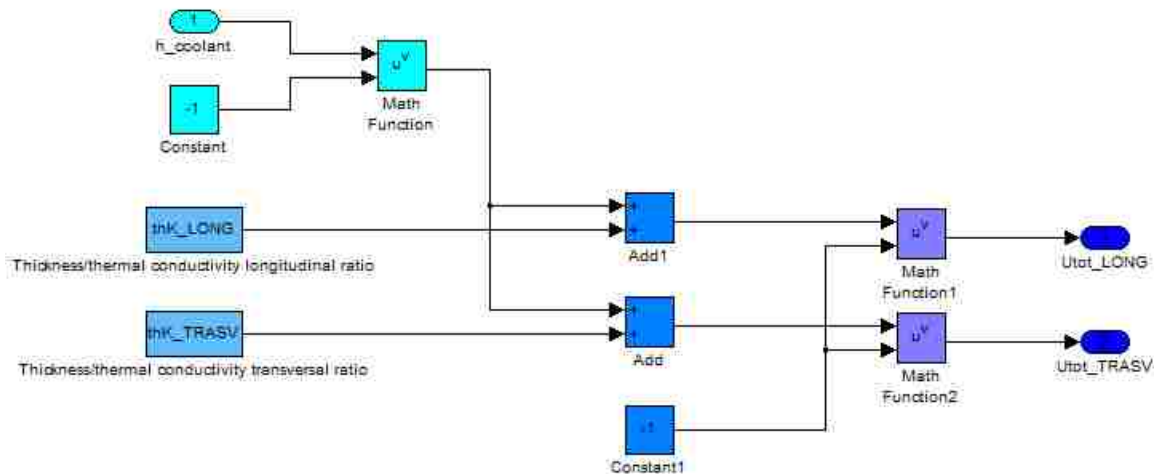


Figure 3.48 - Longitudinal overall and transverse heat transfer coefficients computational block (internal view)

After the overall heat transfer coefficients calculation, the software has determined all the thermodynamic quantities needed to proceed with the computation of the temperature time trend of the battery and of the coolant at the outlet section of the pack. It could be useful to resume what are the main variables generated by the upper level of the

battery thermal model Simulink® file that, at this point, are going to become the inputs of the lower computational level that has the purpose to actively determine the two unknowns of the problem.

- Reynolds number ( $Re$ ): its instantaneous values are computed through Equation 3.21 by the logical loop depicted in Figure 3.42. The Reynolds number depends on the coolant kinematic viscosity and on the hydraulic diameter of the cooling duct that are fixed quantities for the investigated case of study; moreover  $Re$  depends also on the coolant speed that, on the contrary, varies during time depending on the actual value of the coolant mass flow rate.
- Prandtl number ( $Pr$ ): it is constant and depends on the coolant type considered for the simulation. In fact, it is determined by the values of the dynamic viscosity, specific heat and thermal conductivity of the coolant that are fixed quantities for every type of fluid taken into account. Equation 3.27 defines the Prandtl number computation and the related logical block implemented on Simulink® is depicted in Figure 3.43.
- Nusselt number ( $Nu$ ): it is a quantity that depends on the flow regime of the coolant and that, because of this, is computed by the Simulink® model through an “if/else” condition necessary to determine if the coolant flow type is laminar or turbulent. In case of a laminar flow, the value of  $Nu$  is imposed as constant by the program and its magnitude is defined on the basis of the geometry of the cooling channels; in case of turbulent flow, on the contrary, the value of  $Nu$  is computed using the Petukhov and Popov function of Equation 3.26, logically implemented as represented in Figure 3.45, that gives as output a  $Pr$  value variable during time on the basis of the instantaneous value of  $Re$ .
- Convective heat transfer coefficient ( $h_{cool}$ ): it is determined by the battery thermal model implementing Equation 3.25 with the logical structure depicted in Figure 3.46. The magnitude of  $h_{cool}$  varies during time since it depends on the actual value of the Nusselt number that, as stated in the previous point, is a time-dependent quantity.
- Overall heat transfer coefficients ( $U_L$  and  $U_T$ ): they are determined along the longitudinal and transverse directions of the battery modules, using Equations

3.37 and 3.38. Figure 3.48 represents the logical loop used to compute their instantaneous values that are varying during time on the basis of the actual magnitude of  $h_{cool}$ . The values of  $U_L$  and  $U_T$  finally determine the amount of heat exchanged between the battery cells and the coolant flowing around them during the investigated driving cycle; hence, their thorough calculation is necessary to describe in a precise way the heat transfer phenomena that regulate the thermal behaviour of the battery pack of the hybrid electric vehicle considered for the study.

Once the overall heat transfer coefficients have been computed by the model, they become two important inputs of the main sub-blocks constituting the architecture of the Simulink® file and responsible for the calculation of the battery temperature and coolant outlet temperature time trends. These two blocks represent the major pillars of the battery thermal model and their theoretical and logical structures are going to be studied in details in the following sections, focusing the attention on the milestones placed during the design process.

#### 3.4.4.5 Coolant outlet and battery temperatures computation

Once the overall thermal characteristics of the battery have been carefully determined, together with the dynamics of the heat transfer phenomenon taking place between the cells and the investigated cooling medium, the operating sub-blocks of the model intended for the calculation of the coolant outlet and battery temperatures can be designed. As stated in the previous sections, in order to proceed with the computation of the two unknowns, a single module is studied as an independent object considering the amount of coolant flowing around it ( $\dot{m}_{coolB}$ ); as described by Equation 3.47, this coolant portion is computed by the model starting from the knowledge of the overall coolant mass flow rate ( $\dot{m}_{coolB\_TOT}$ ) and of the number of cells contained in the battery pack ( $N_c$ ), given as input data from the driving cycle and battery characteristics.

$$\dot{m}_{coolB} = \frac{\dot{m}_{coolB\_TOT}}{N_c} \quad (3.47)$$

Moreover, it has to be underlined again that the HVB temperature has been defined as equal to the temperature of each single module because, as long as all the cells are crossed by the same electric current magnitude during the driving cycle, considering the amount of coolant flowing around a single cell gives the same result as considering the total coolant rate entering the battery pack and cooling down all the modules of the system. Considering this important assumption, it is possible to formulate the theoretical and mathematical background that regulates the thermal phenomena taking place between a single prismatic module of the pack and the cooling air flowing around it. A condition of thermal equilibrium between the two entities has to be imposed, considering that part of the power dissipated during time by the cell (for Joule effect) is exchanged with the coolant while the other part remains stored inside the module increasing its temperature, and so the temperature of the whole battery pack; Equations 3.48 and 3.49 describe this condition and, finally, allow to determine the time trend of the two unknown investigated temperature. The amount of heat acquired by the cooling air generates an increase of the coolant temperature and, at the same time, leads to a reduced and controlled increase of the temperature of the modules that has not to exceed specific limits.

$$\dot{Q}_L + \dot{Q}_T = \dot{m}_{coolB} \cdot c_{p\_coolB} \cdot (T_{cOUT\_actual} - T_{cOUT\_prev}) \quad (3.48)$$

$$P_{diss} - \dot{Q}_L - \dot{Q}_T = m_c \cdot c_{p\_c} \cdot (T_{B\_actual} - T_{B\_prev}) \quad (3.49)$$

Underlining again that the thermal transfer is considered between a single module and the coolant portion flowing on its surfaces, the main variables contained in the previous Equations 3.48 and 3.49 are described in the following list:

- $P_{diss}$  is the power dissipated for Joule effect by the module;
- $\dot{Q}_L$  and  $\dot{Q}_T$  are the heat rate exchanged between the module and the coolant (air) along the longitudinal and transverse directions, respectively;
- $c_{p\_coolB}$  and  $c_{p\_c}$  are the specific heats of the cooling air and of the cell, respectively;
- $\dot{m}_{coolB}$  is the portion of coolant mass flow rate moving around a single module;



- $m_c$  is the mass of the module that, for such a type of theory, is considered as a permanent value of a hypothetical constant flow rate;
- $T_{cOUT\_actual}$  is the unknown instantaneous value of the actual temperature of the coolant at the outlet section of the battery pack;
- $T_{cOUT\_prev}$  is the instantaneous value of the outlet temperature of the coolant considered at the previous instant of the simulation;
- $T_{B\_actual}$  is the unknown instantaneous value of the actual temperature of the module and, hence, of the whole battery pack;
- $T_{B\_prev}$  is the instantaneous value of the temperature of the module considered at the previous instant of the simulation.

At this point, once all the main system variables have been described, it is possible to detail and analyze deeper the physical and logical structures of the two main sub-blocks of the battery thermal model, responsible for the calculation of the two unknown investigated temperatures.

#### 3.4.4.5.1 Coolant outlet temperature

Previous Equation 3.48 can be further developed expressing the heat rates  $\dot{Q}_L$  and  $\dot{Q}_T$  as the products of the overall heat transfer coefficient, the surface of the module and the temperature difference between the cell and the coolant, considered along the longitudinal and the transverse directions respectively. Taking into account Equations 3.42, 3.43, 3.44, 3.45 and the geometric characteristics of the modules of the HEV battery pack, it is possible to derive following Equation 3.50 that expresses the amount of heat acquired instantaneously by the cooling medium from a cell of the HVB.

$$\begin{aligned} \dot{Q}_L + \dot{Q}_T &= [U \cdot A \cdot (T_B - T_{cool})]_L + [U \cdot A \cdot (T_B - T_{cool})]_T = \\ &= [w \cdot h \cdot U_L \cdot (T_B - T_{cool\_IN}) + w \cdot h \cdot U_L \cdot (T_B - T_{cool\_OUT})] + [2 \cdot h \cdot l \cdot U_T \cdot (T_B - T_{cool\_M})] \end{aligned} \quad (3.50)$$

The overall heat transfer coefficients values are the instantaneous ones computed by the upper level of the battery thermal model during the simulation, for both the heat transfer directions, while the surfaces of the cells are determined on the basis of the dimensions of the modules specified for the investigated battery pack. Equation 3.50 is

implemented in the tool in order to determine the instantaneous values of the unknown coolant temperature at the outlet section of the battery pack ( $T_{cool\_OUT}$ ) but, in order to do that, the software needs further information since also another unknown,  $T_B$ , is contained in the formula. Combining Equations 3.48 and 3.50 and expressing the unknown temperatures of the coolant and the battery with respect to the specific investigated instant of the simulation, Equation 3.51 can be obtained and finally transposed into the Simulink® model.

$$\begin{aligned} w \cdot h \cdot U_L \cdot (T_{B\_prev} - T_{cool\_IN}) + w \cdot h \cdot U_L \cdot (T_{B\_prev} - T_{cOUT\_prev}) + 2 \cdot h \cdot l \cdot U_T \cdot (T_{B\_prev} - T_{cool\_M}) = \\ = \dot{m}_{coolB} \cdot C_{p\_coolB} \cdot (T_{cOUT\_actual} - T_{cOUT\_prev}) \end{aligned} \quad (3.51)$$

The battery temperature is considered at the previous instant of the simulation ( $T_{B\_prev}$ ) and its value is known as an output of the battery temperature computational sub-block; the coolant outlet temperature of the left-hand member of the formula is considered, in the same way, at the previous instant of the simulation ( $T_{cOUT\_prev}$ ) and its value is known since determined at the previous iteration by the coolant outlet temperature computational sub-block. Using Equation 3.52 to express the coolant temperature at the medium point along the length of the module and, moreover, considering the temperature gradient of the right-hand member of Equation 3.51 as the instantaneous increase of the coolant outlet temperature, the model can be finally built upon Equation 3.53.

$$T_M = \frac{T_{cool\_IN} + T_{cool\_OUT}}{2} = \frac{T_{cool\_IN} + T_{cOUT\_prev}}{2} \quad (3.52)$$

$$\begin{aligned} T_{cOUT\_actual} - T_{cOUT\_prev} = \\ = \frac{w \cdot h \cdot U_L \cdot (2 \cdot T_{B\_prev} - T_{cool\_IN} - T_{cOUT\_prev}) + 2 \cdot h \cdot l \cdot U_T \cdot \left[ T_{B\_prev} - \left( \frac{T_{cool\_IN} + T_{cOUT\_prev}}{2} \right) \right]}{\dot{m}_{coolB} \cdot C_{p\_coolB}} \end{aligned} \quad (3.53)$$

The overall internal logical structure of the coolant outlet temperature computational sub-block is depicted in Figure 3.49: every operating block has been

suitably chosen from the Simulink® library to virtually implement Equation 3.53 and to determine, instant per instant, the investigated temperature difference  $T_{cool\_OUT\_actual} - T_{cool\_OUT\_prev}$ .

The cyan dot highlighted in Figure 3.49 represents the point of the logical loop at which the coolant temperature gradient is computed; after that, this instantaneous temperature gradient is sent to an “Integrator” block (represented in the orange frame) that finally determines the coolant outlet temperature time trend during the driving cycle. The starting value of the coolant temperature at the outlet section of the battery pack is set by the user and it is equal to the inlet temperature value, usually set at the ambient level. Moreover, the coolant outlet temperature determined at the previous iteration ( $T_{cool\_OUT\_prev}$ ) is obtained thanks to the “Memory” block (highlighted in the green frame) and then sent inside the logical loop (thanks to the “Goto” and “From” blocks represented in the magenta frames), to allow the operating implementation of Equation 3.53.

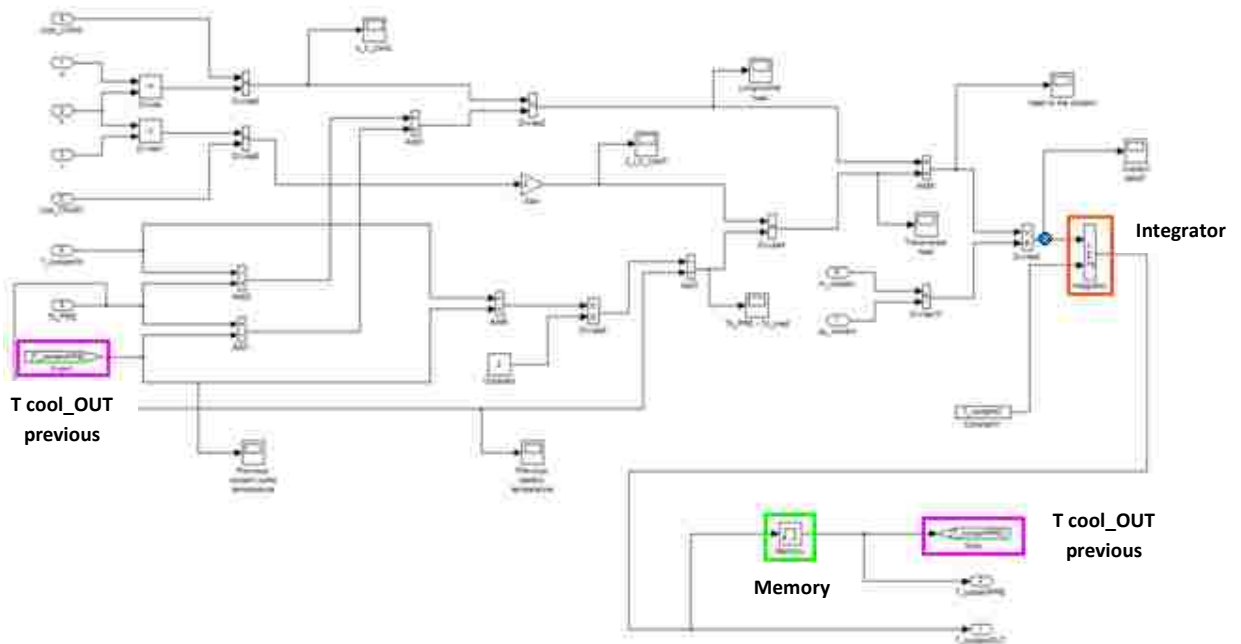
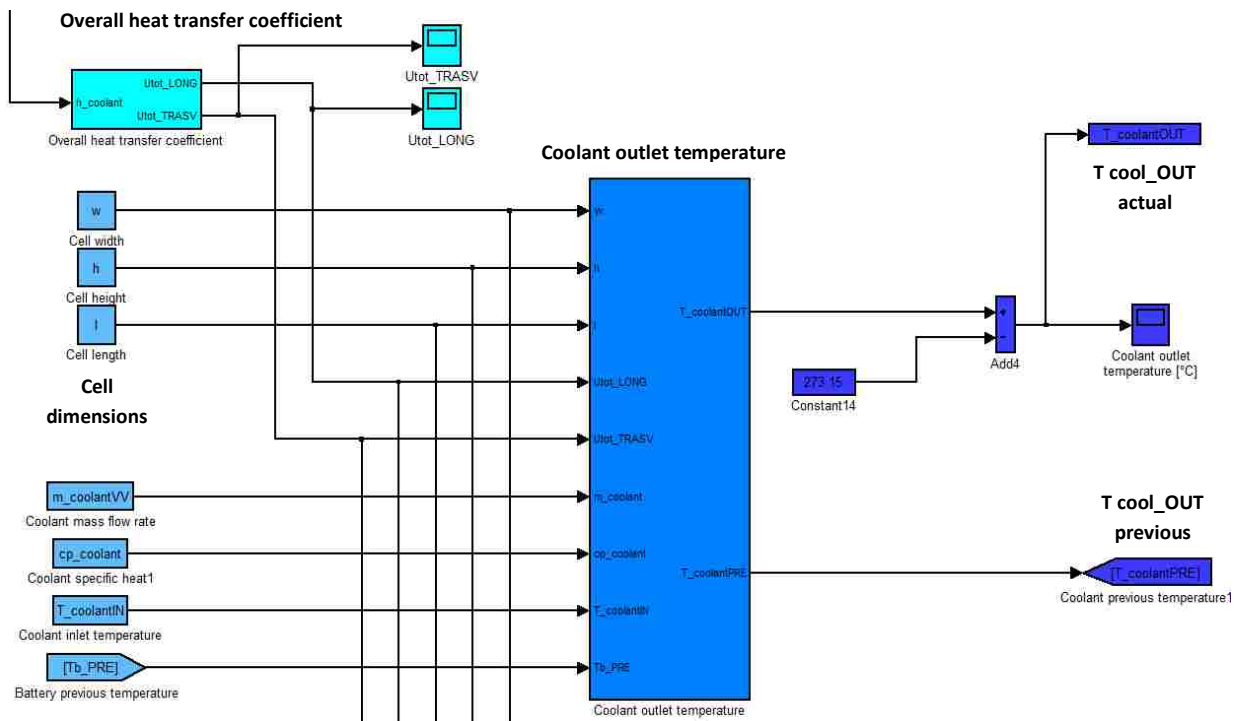


Figure 3.49 - Overall structure of the coolant outlet temperature computational block (internal view)



**Figure 3.50 - Overall structure of the coolant outlet temperature computational block (external view)**

Above Figure 3.50 depicts the external view of the coolant outlet temperature computational sub-block, presented in Figure 3.49, and its careful analysis is necessary in order to better understand what are the inputs of the block and from where they are derived inside the model: the longitudinal and transverse overall heat transfer coefficients are computed in the upper level of the software and are necessary to define the overall characteristic of heat transfer phenomenon; the width, height and length of the cells are given as inputs from the Matlab® base file “Workspace” and determine the geometry of the modules; the coolant mass flow rate depends on the cooling system setup and is intended as the instantaneous mass of coolant flowing between the cells during time (hence, its overall quantity increases instant per instant as the air begins to flow inside the battery pack); the coolant specific heat is a coolant property and it is stored in the Matlab® “Workspace”; the coolant inlet temperature is set by the user when the simulation is activated and, usually, it is equal to the ambient temperature; the battery previous temperature, finally, refers to the value of the battery temperature already computed by the model at the previous iteration (inside the battery temperature computational sub-block). The outputs of the sub-block depicted in Figure 3.50 are

instead represented by the instantaneous values of the coolant temperature at the outlet section of the HEV battery pack, considered both at the actual and previous iterations during the simulation execution: the values of  $T_{cOUT\_actual}$  are sent to the Matlab® platform to be studied and presented graphically as desired, while, on the other hand, the values of  $T_{cOUT\_prev}$  are continuously sent to the battery temperature computational sub-block allowing the battery temperature calculation.

### 3.4.4.5.2 Battery temperature

As it has been done for Equation 3.48, also Equation 3.49 can be further developed expressing the heat rates  $\dot{Q}_L$  and  $\dot{Q}_T$  with respect to the external surfaces of the cell, to the overall heat transfer coefficients and to the temperature differences existing between the module and the coolant, considered both along the longitudinal and the transverse directions. Taking into account the main passages explained in the previous section to obtain Equation 3.50 and, moreover, considering the amount of power dissipated as heat by the battery for Joule effect, following Equation 3.54 can be derived.

$$\begin{aligned} P_{diss} - \dot{Q}_L - \dot{Q}_T &= P_{diss} - [U \cdot A \cdot (T_B - T_{cool})]_L - [U \cdot A \cdot (T_B - T_{cool})]_T = \\ &= P_{diss} - [w \cdot h \cdot U_L \cdot (T_B - T_{cool\_IN}) + w \cdot h \cdot U_L \cdot (T_B - T_{cool\_OUT})] - [2 \cdot h \cdot l \cdot U_T \cdot (T_B - T_{cool\_M})] \end{aligned} \quad (3.54)$$

Equation 3.54 expresses the amount of heat that, during time, is accumulated inside the cells of the battery pack after that a certain portion of the Joule effect power is exchanged with the cooling medium. As for Equation 3.50, still now the overall heat transfer coefficients values are the instantaneous ones calculated by the upper level of the software during the simulation, while the surfaces of the modules are defined by the geometry of the investigated HEV battery. Combining Equations 3.49 and 3.54 and expressing the unknown temperatures of the coolant and the battery on the basis of the specific iteration considered during the simulation, Equation 3.55 can be finally obtained and then transposed into the Simulink® model.

$$\begin{aligned} P_{diss} - w \cdot h \cdot U_L \cdot (T_{B\_prev} - T_{cool\_IN}) - w \cdot h \cdot U_L \cdot (T_{B\_prev} - T_{cOUT\_prev}) - 2 \cdot h \cdot l \cdot U_T \cdot (T_{B\_prev} - T_{cool\_M}) = \\ = m_c \cdot c_{p\_c} \cdot (T_{B\_actual} - T_{B\_prev}) \end{aligned} \quad (3.55)$$

The coolant inlet temperature ( $T_{cool\_IN}$ ) is known and fixed by the user (usually set at the ambient level), while the coolant temperature at the outlet section of the battery pack is considered at the previous instant of the simulation ( $T_{cOUT\_prev}$ ) and its value is known since determined at the previous iteration by the coolant outlet temperature computational sub-block. The battery temperature terms of the left-hand member of the formula are considered, in the same way, at the previous instant of the simulation ( $T_{B\_prev}$ ) and, in this way, they have already been computed by the battery temperature sub-block. Using again Equation 3.52 to express the coolant temperature at the medium point along the length of the module and, moreover, considering the temperature gradient of the right-hand member of Equation 3.55 as the instantaneous increase of the battery temperature, the model can be finally built upon Equation 3.56.

$$T_{B\_actual} - T_{B\_prev} = \frac{P_{diss} - w \cdot h \cdot U_L \cdot (2 \cdot T_{B\_prev} - T_{cool\_IN} - T_{cOUT\_prev}) - 2 \cdot h \cdot l \cdot U_T \cdot \left[ T_{B\_prev} - \left( \frac{T_{cool\_IN} + T_{cOUT\_prev}}{2} \right) \right]}{m_c \cdot c_{p\_c}} \quad (3.56)$$

Equation 3.1 has to be used to compute the amount of power dissipated as heat by the battery, given as the product of the internal resistance of the cells and the squared power magnitude of the electric current flowing through the HVB during the driving cycle (and defined as a driving cycle characteristic). The overall internal structure of the battery temperature computational sub-block is depicted in Figure 3.51: every logical block has been suitably chosen from the Simulink® library to virtually implement Equation 3.56 and to determine, instant per instant, the investigated temperature difference  $T_{B\_actual} - T_{B\_prev}$ .

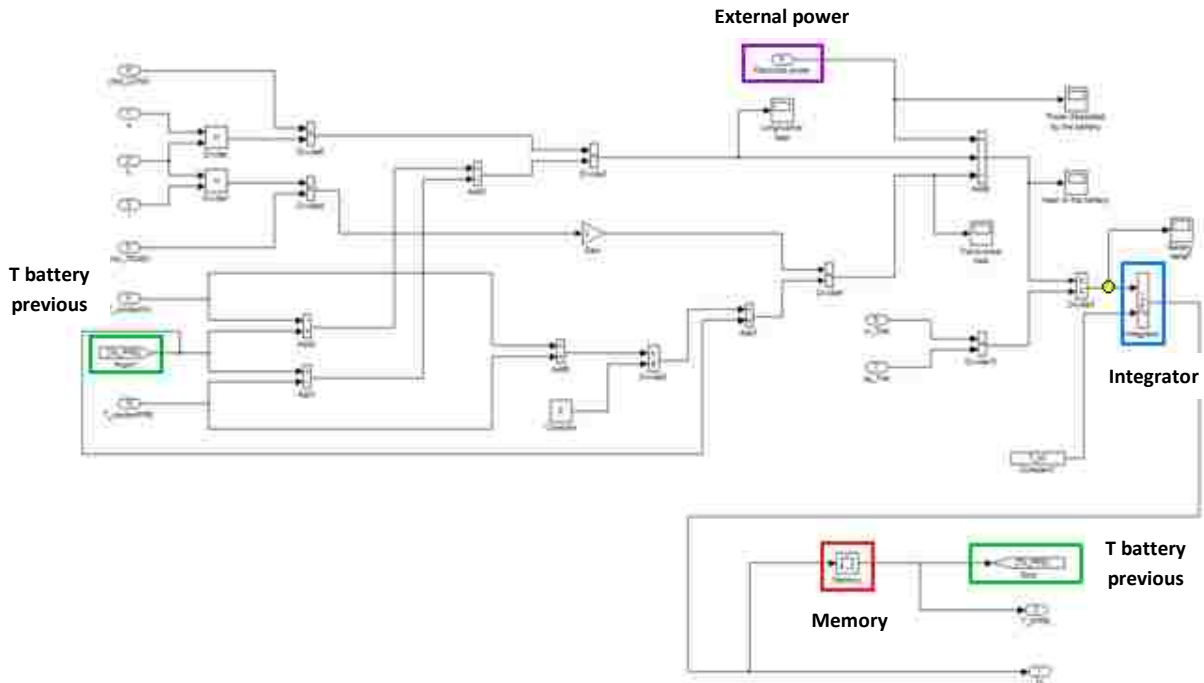


Figure 3.51 - Overall structure of the battery temperature computational block (internal view)

The yellow dot highlighted in Figure 3.51 represents the point of the logical loop at which the battery temperature gradient is calculated; afterwards, this instantaneous temperature gradient is sent to an “Integrator” block (represented in the light blue frame) that finally computes the battery temperature time trend during the driving cycle. The starting value of the battery temperature, necessary to perform the integrative action, is set by the user and it is usually chosen as the ambient temperature value. Moreover, the battery temperature determined at the previous iteration ( $T_{B\_prev}$ ) is obtained thanks to the “Memory” block (highlighted in the red frame) and then sent inside the logical loop (thanks to the “Goto” and “From” blocks represented in the green frames), to allow the operating implementation of Equation 3.56. Finally, the dissipated power contribution represents the main input of the battery computational sub-block (highlighted in the purple frame) and, determined instant per instant, it strongly affects the characteristic time trend of the battery temperature.

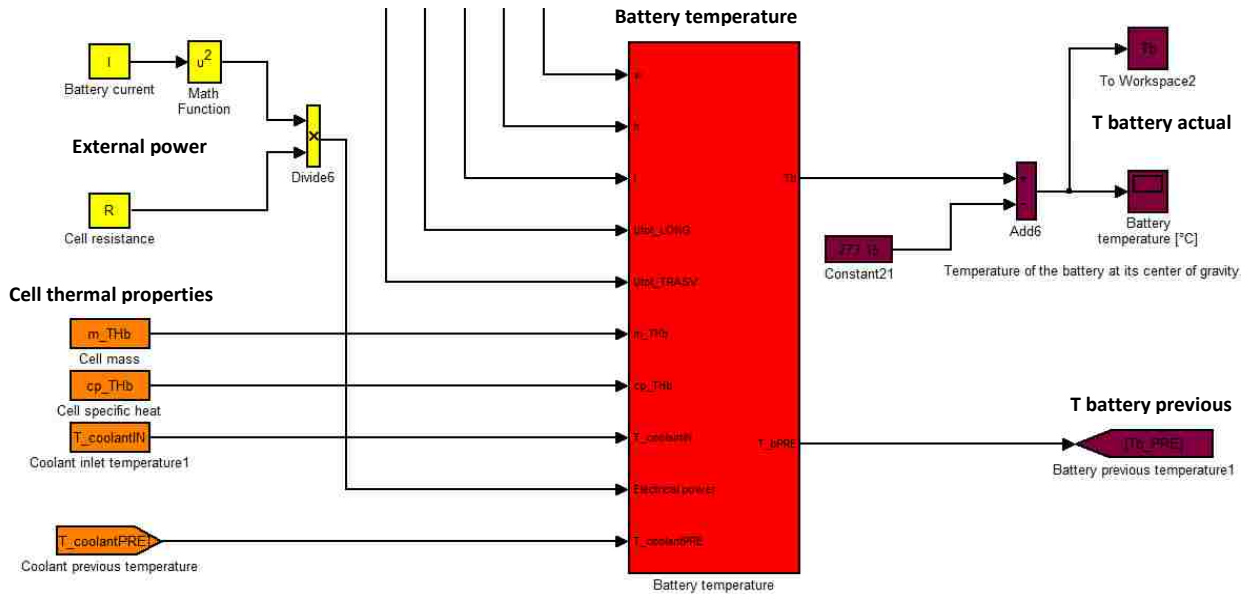


Figure 3.52 - Overall structure of the battery temperature computational block (external view)

The external view of the battery temperature computational sub-block is depicted in Figure 3.52 and its careful analysis is necessary to better understand the meaning of the inputs of the block and their origin inside the model. As for the coolant outlet temperature block, also in this case the longitudinal and transverse overall heat transfer coefficients are two of the main inputs of the logical loop; moreover the width, height and length of the modules are necessary again to virtually implement the computational model, determining the geometry of the cells; finally, the coolant inlet temperature still represents one of the inputs and it is set again by the user depending on the boundary conditions of the test. Continuing the inputs analysis, the coolant mass flow rate ( $\dot{m}_{coolB}$ ) and specific heat ( $c_{p\_coolB}$ ) are now substituted by the mass ( $\dot{m}_c$ ) and specific heat ( $c_{p\_c}$ ) of the battery modules, whose values have been received from the thermal experts of the Electrified Powertrain department at Chrysler. The coolant previous temperature input, moreover, refers to the value of the coolant temperature at the outlet section of the battery pack already computed by the model at the previous iteration (inside the coolant outlet temperature computational sub-block). The yellow block structure has been finally implemented to compute the overall power amount dissipated during the driving cycle by the cells: the current leaving the modules to actuate the electric machine (charge depleting mode) and the current going to the modules during the regenerative braking actions (charge sustaining mode), generate a power dissipation for Joule effect that strongly



influences the time trend of the battery temperature determined at the end of the simulation. The outputs of the sub-block depicted in Figure 3.52 are instead represented by the instantaneous values of the battery temperature, considered both at the actual and previous iterations during the simulation execution: the values of  $T_{B\_actual}$  are sent to the Matlab® platform in order to be studied and presented graphically as desired, while, on the other hand, the values of  $T_{B\_prev}$  are continuously sent to the coolant outlet temperature computational sub-block allowing the coolant temperature calculation at the outlet manifold of the battery pack.

### **3.4.5 Battery cooling system model simulation running**

After the thorough description of the architecture and theoretical background of the battery cooling system model that has been designed during the internship at Chrysler, an overview of its operating mode has to be depicted in order to better understand how the program can run a simulation. The first step consists in the upload of the driving cycle battery current profile in the Matlab® “Workspace”, performed thanks to the Matlab® base file’s code execution. Depending on the investigated driving cycle, a specific current profile characterizes the battery because, since the operations performed by the “electric side” of a hybrid vehicle are strongly determined by the speed and acceleration characteristics of the driving path, is exactly the driving cycle that defines the battery level of excitation. Moreover, all the geometric and constructive variables related to the investigated HEV battery pack have also to be stored in the Matlab® “Workspace”: their knowledge is necessary to allow the software to correctly model the actual geometry of the cells, their disposition inside the pack and, at the same time, the characteristics of the cooling ducts and the resulting distribution of the coolant flow. These variables are mainly represented by the modules dimensions, by the distance existing between two adjacent modules and by the overall number of cells that constitute the battery pack. Furthermore, the geometric and material characteristics of the layered structure of the modules must be well known and have to be correctly described by the Matlab® base file: since the software models the battery cells not as simple prismatic bodies made of a unique homogeneous material but, on the contrary, as prismatic structure composed by a series of different layers, the thermal and geometric properties of these layers have to be

thoroughly taken into account to describe the thermal phenomena taking place between the whole battery and the cooling medium along the longitudinal and transverse directions. Then, also the magnitudes of the internal resistance, weight and specific heat of the modules have to be known and used as inputs for the Matlab® base file, in order to completely characterize the thermal and electrical behaviour of the cells. Finally, vital data related to the type and quantity of coolant considered for the simulation have to be uploaded by the model: the instantaneous amount of coolant flow rate and the thermophysical properties of the coolant (density, viscosity, specific heat, thermal conductivity) must be carefully defined by the user before activating the simulation. In this regard, it is important to underline again that the battery thermal model has been principally designed for an air cooled solution typical of a mild and full hybrid NiMH battery pack, whose modules are touched directly by the cooling air without the need for external shells and coatings.

Once all the necessary input data have been stored in the Matlab® base file, the Simulink® model can be activated to run the simulation and to find, at the end of the process, the battery temperature time trend during the investigated driving cycle. The Simulink® tool, once the simulation has been started by the user, suitably combines the input data coming from the Matlab® “Workspace”, completing the computational procedure at the upper and lower levels of the model. The software calculates, first of all, the time-dependent Reynolds number and recognizes the type of flow regime of the coolant; at this point, depending on the flow characteristics, the battery model computes the magnitude of the Nusselt number, necessary to determine the actual convective heat transfer coefficient of the coolant; knowing the value of  $h_{cool}$  it is possible then to calculate the longitudinal and transverse overall heat transfer coefficients, at the end of the upper computational level of the model. Finally, the suitable variables computed by the tool become the inputs of the two main sub-blocks intended for the calculation of the coolant outlet temperature and battery temperature time trends: these two blocks, implemented upon Equations 3.53 and 3.56 respectively, combine and elaborate all the quantities treated by the model and allow to reach the desired results.

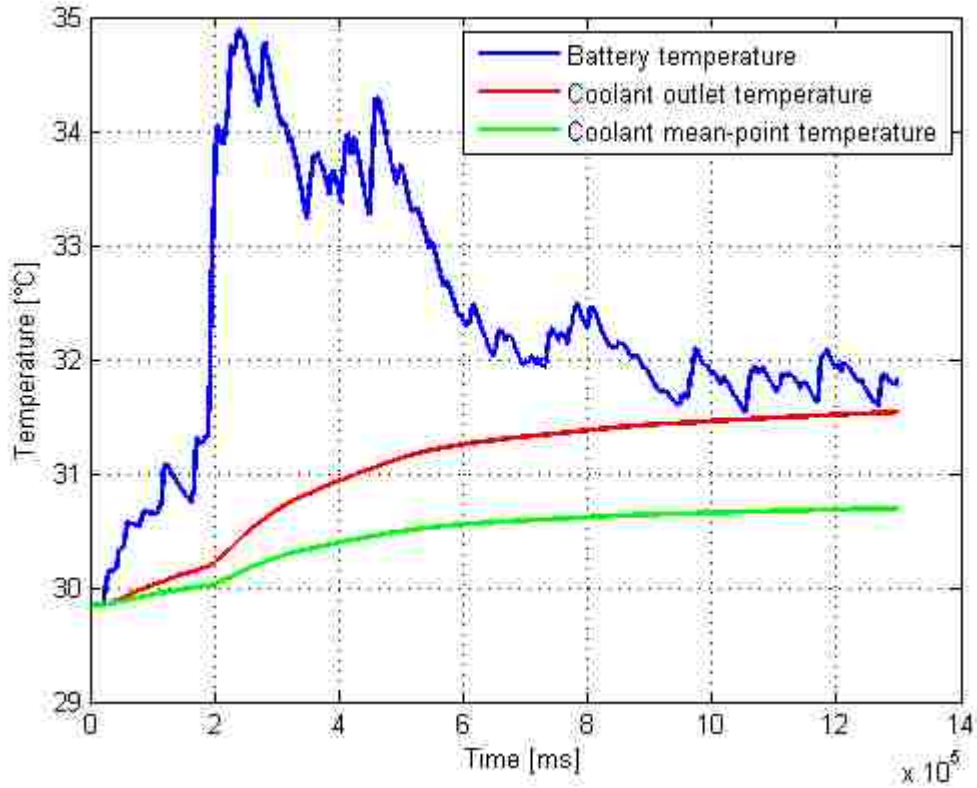


Figure 3.53 - Battery and coolant temperature time trends (FTP-72 driving cycle)

Table 3.5 - Boundary conditions and main characteristics of the simulation (FTP-72 driving cycle)

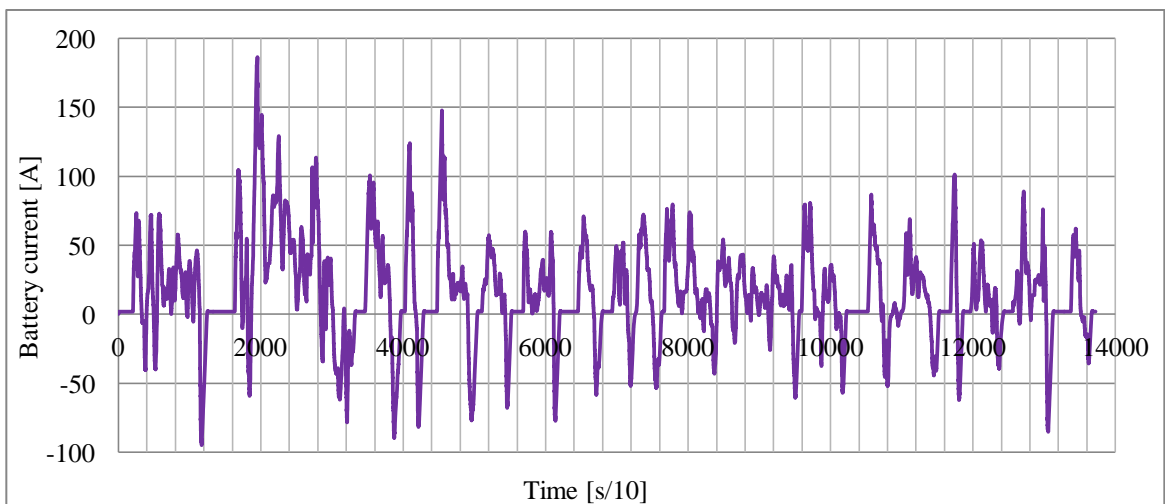
<b>Cell width</b>	12.5 mm
<b>Cell height</b>	85 mm
<b>Cell length</b>	120 mm
<b>Number of cells</b>	72
<b>Distance between two adjacent cells</b>	5 mm
<b>Battery internal resistance</b>	2.9 mΩ
<b>Cell mass</b>	0.24 kg
<b>Cell specific heat</b>	980 J/(kg·K)
<b>Total coolant (air) mass flow rate</b>	100 cfm
<b>Ambient temperature</b>	30 °C

Figure 3.53 is a typical output of the battery thermal model and it depicts the battery and coolant outlet temperature time trends determined by the software during an EPA city driving program (FTP-72), performed by a hybrid electric vehicle equipped with an air

cooled battery; the main characteristics and boundary conditions of the current simulation are listed in Table 3.5. While the blue curve represents the battery temperature, the red and green ones refer respectively to the coolant temperature considered at the outlet section of the battery pack and at the medium point along the cell length.

From a detailed analysis of Figure 3.53, it can be seen how the most important battery temperature increase takes place around second 200, when a 4 °C gradient is experienced by the modules. Then, thanks to the cooling action performed by the air, the temperature of the battery shows a notable decrease that, at steady state, leads to a thermal condition fluctuating around 32 °C.

At the beginning of the driving cycle, the outlet temperature of the coolant is equal to the temperature of the battery and settles at the ambient level while, as soon as the electric current starts flowing through the cells that dissipate heat for Joule effect, the coolant begins a continuous warm up until a steady state temperature of about 31.5 °C. It is important to underline that, at a steady state condition, is reasonable and expected that the thermal states of the battery and the coolant (at the outlet manifold) are approximately the same: in fact the two entities must be in a condition of thermal equilibrium at the end of the simulation, once the energy transients are finished, and the heat transfer phenomena are such that the cooling air can ensure the thermal control of the battery pack.



**Figure 3.54 - Battery current profile (FTP-72 driving cycle, charge depleting mode)**

In order to give validity to the temperature time trend depicted in Figure 3.53, a study of the power amount dissipated instantaneously by the battery modules for Joule effect can be done. Above Figure 3.54 represents the battery current profile typical of the EPA FTP-72 city driving program in a charge depleting mode that, thanks to Equation 3.1, allows to obtain the dissipated power time trend depicted in Figure 3.55. While the electric current magnitude can be both positive and negative depending on the operation mode of the battery (charge depleting or sustaining), the amount of power dissipated as heat within the cells is obviously always positive and, for the investigated driving cycle, is characterized by a strong peak around second 200 when the current reaches its maximum value of 186.25 A.

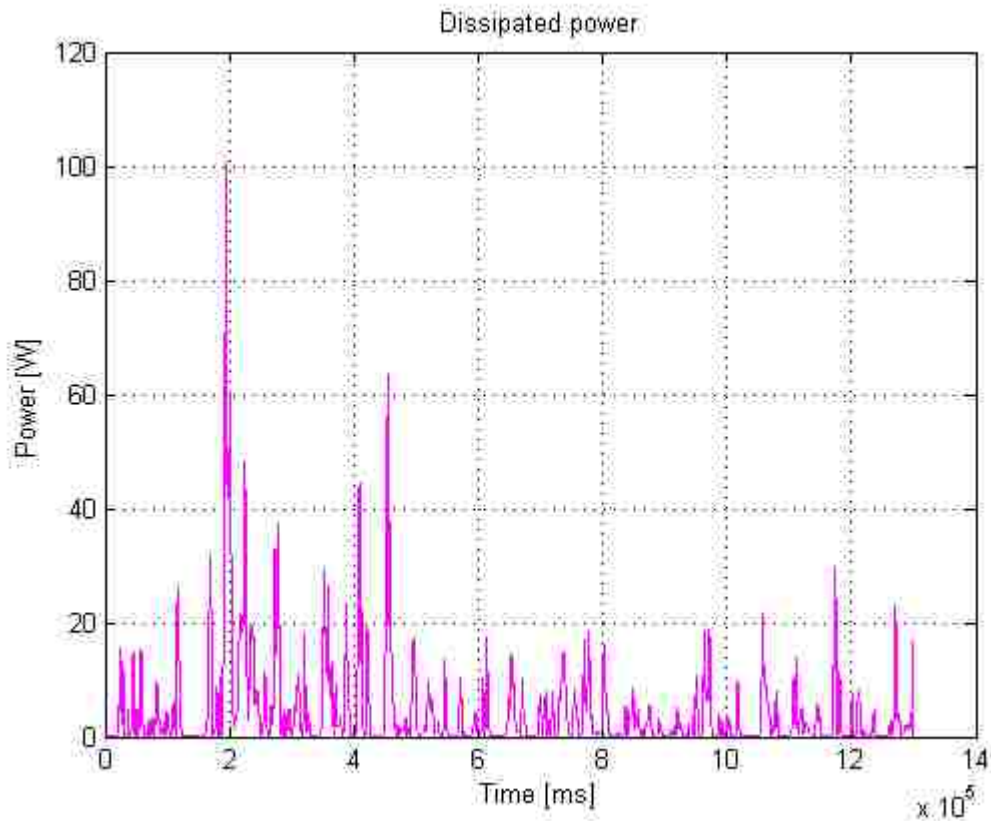


Figure 3.55 - Dissipated power time trend (FTP-72 driving cycle)

Furthermore, approximately after second 500, the dissipated power does not exceeds anymore the magnitude of 30 W and remains under a 20 W limit for most of the remaining time; moreover, from about second 500, the battery temperature becomes

definitively lower than 33 °C and the increase of the coolant outlet temperature becomes less sharp and more flat than before. Hence, from a comparison of Figures 3.53 and 3.55, it can be stated that the battery temperature trend meets the expectations evoked by the picture above and, finally, this can be seen as a positive aspect that gives validity to the performance of the battery thermal model.

To conclude, coming back to the model architecture analysis, it is important to underline that the two main computational sub-blocks work closely together during the whole simulation: the operations of the battery temperature block, for example, become possible only thanks to the knowledge of the coolant outlet temperature already computed at the previous iteration ( $T_{cOUT\_prev}$ ) by the coolant temperature block; this temperature, as described before, becomes an input of the battery sub-block and it is necessary to implement Equation 3.56 inside the block itself. The same happens, if the roles were reversed, for the logical implementation of Equation 3.53 which needs the knowledge of the battery temperature computed at the previous iteration ( $T_{B\_prev}$ ) by the coolant outlet temperature sub-block: the values of this temperature are continuously sent inside the battery computational block to allow the determination of the battery temperature time trend for the investigated driving cycle.

### **3.4.6 New features introduced by the battery cooling system model**

As explained in the previous sections, the design of a cooling system model capable of describing the thermal behaviour of a high voltage battery that equips a mild or full hybrid electric vehicle, covers an incredible importance for the Electrified Powertrain department teams at Chrysler. These research and project teams conduct thorough studies in order to predict the performance and fuel economy of the new model of hybrid vehicle in their early design stages, when the physical product is not yet available to perform experimental analysis and tests. Unfortunately, the prediction tool actually used at Chrysler to realize these predictive studies and simulations is not provided with a computational loop that allows to determine the battery temperature; the software is used to examine the overall behaviour of a given HEV virtually running a certain driving profile but, as said before, it is not able to determine the battery temperature time trend during the investigated cycle. Since, during vehicle operations, the HVB is crossed by a

certain amount of electric current that generates a power dissipation for Joule effect, the battery cells temperature changes during time, experiencing a considerable increase of its value; this battery temperature increase, in the end, determines the actual behaviour of the vehicle battery pack and so it has to be carefully taken into account. In fact, the availability of discharge power (for startup and acceleration), the life of the battery and, moreover, the energy and charge acceptance during the regenerative braking events, are strongly influenced by the temperature of the device. High temperatures improve the rates of charge and discharge but, at the same time, cause a reduction of the total number of life cycles and, consequently, of the total service time. Low temperatures, instead, slow down the charge and discharge operations, lead to an overall increase of the modules internal resistance and, moreover, to an extended calendar life: this because, in colder climates, the chemical degradation reactions are countered and slackened. Therefore, it can be underlined that the behaviour of a battery is strongly affected by its temperature that determines the charge and discharge rates, the internal resistance magnitude, the charging efficiency, the calendar life and, finally, the SOC-dependent open circuit voltage. At this point, it is clear that the actual temperature time trend experienced by the HEV battery during the investigated driving cycle must be computed during the simulations run by the Chrysler prediction tool that, at the moment, simply takes into account for the whole analysis a fixed value for the battery temperature imposed by the user. Hence, the Chrysler software has to be absolutely modified and provided with a new thermal sub-model, capable of calculating the time trend of the battery temperature during the whole driving cycle and to narrowly determine all the temperature-dependent battery variables. Once the new thermal model is added to the basic structure of the overall Chrysler tool, the level of accuracy of the predictive results obtained by the program is certainly higher than before, thanks to an improved modeling of the “electric side” of the overall HEV system and, in particular, of the thermal characteristics of its electric energy storage device.

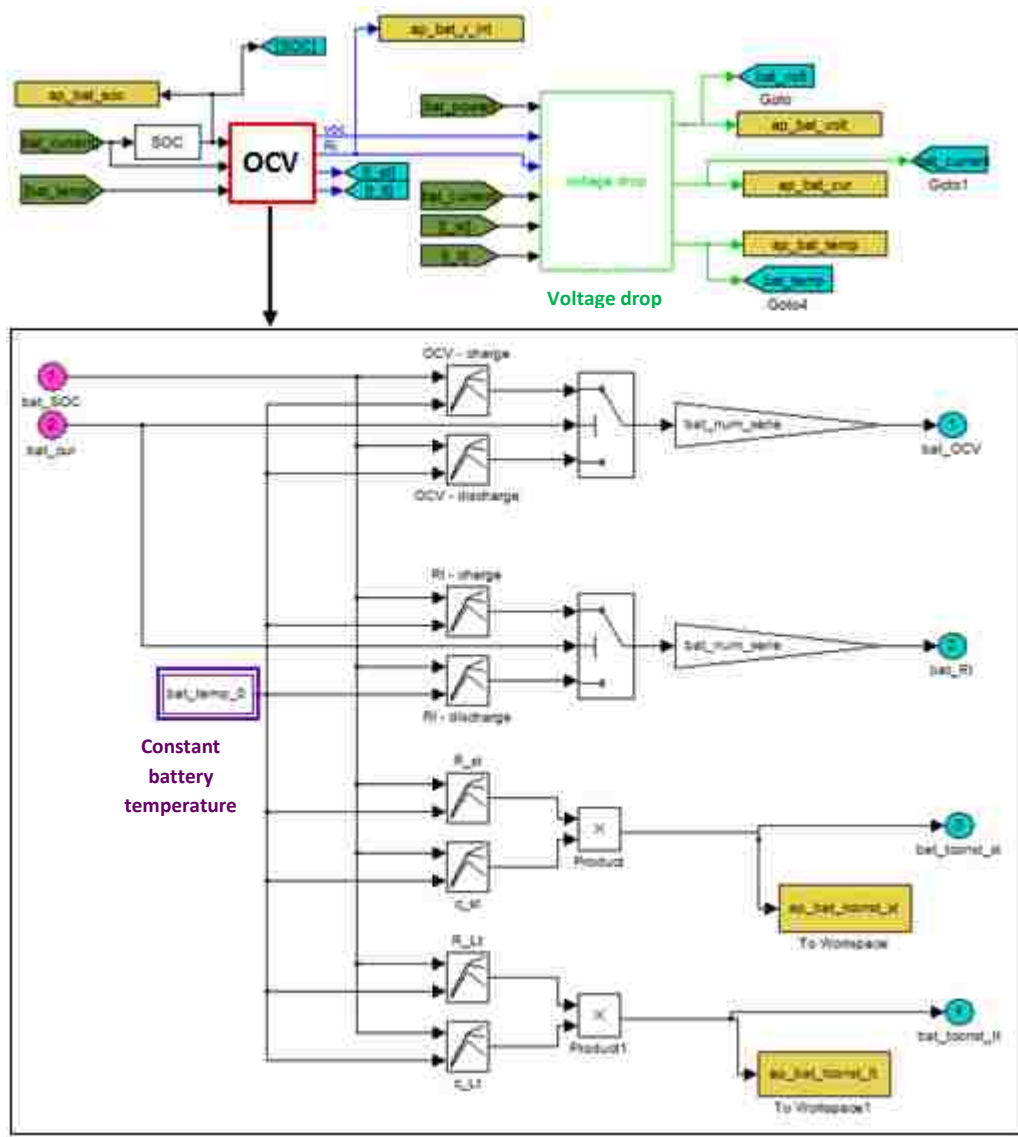


Figure 3.56 - HVB “OCV” channel of the original Chrysler HEV prediction model

Figure 3.56 represents one of logical channels that are used by the Chrysler prediction software to model the HVB of the hybrid electric vehicle; the overall battery tool is definitely wider and more complicated but the portion showed in Figure 3.56 is the one responsible for determining, during the driving cycle, the actual values of the battery internal resistance and open circuit voltage that, among the others, depend on the thermal state of the battery. The logical loop contained in the red box “OCV” is depicted inside the black frame and it performs the internal resistance and open circuit voltage computation, interpolating multi-points maps stored in the Matlab® “Workspace” and dependent on the battery temperature and state of charge.



From a careful analysis of the “OCV” logical loop, it is possible to note that a purple frame highlights a “Constant” block in which the user can insert the constant temperature value that is going to characterize the battery thermal status for the whole simulation; in this way, the results of the multi-points maps lose the variability related to the knowledge of the actual battery temperature that, if treated as constant, cannot correctly define the electric behaviour of the battery.

Figure 3.57 represents the same logical channel depicted in Figure 3.56 and used by the Chrysler prediction software to model the HVB of the investigated HEV; this time, however, the picture is taken from the updated Chrysler software, after the introduction of the battery thermal sub-model. The logical loop contained in the light blue box “OCV” is depicted inside the black frame and it performs the internal resistance and open circuit voltage computation thanks to the interpolation of multi-points SOC-dependent and temperature-dependent maps stored in the Matlab® “Workspace”.

From a thorough analysis of the “OCV” logical loop, it is possible to note that now an orange frame highlights an “Inport” block that imports in the “OCV” system the instantaneous values of the battery temperature, computed during time by the new battery thermal model included in the overall Chrysler prediction software.

Now that the battery temperature is no more treated as constant during the driving cycle but, on the contrary, is determined instant per instant by the battery cooling system model that has been designed, the results of the multi-points maps are represented by values of internal resistance and open circuit voltage more accurate and reliable than it was for the original Chrysler model not already updated. Computing during time the actual value of the battery temperature, the definition of the temperature-dependent battery variables is obviously more precise and allows to obtain thorough final predictions about the performance and fuel economy of the investigated HEV.



The new battery thermal model has been integrated inside the “Voltage Drop” block of Figure 3.57, where the dissipated power amount is computed instant per instant starting from the knowledge of the battery internal resistance and current profile, related to the investigated driving cycle. The internal view of the “Voltage Drop” block is presented in Figure 3.58 where the purple box constitutes the external structure of the battery thermal model: its main input is represented by the power dissipated by the modules for Joule effect and its output, obviously, is represented by the battery temperature time trend. Inside the black frame, moreover, the overall Simulink® structure of the battery cooling system model is depicted once again to underline the high amount of input variables directly taken from the Matlab® base file.

In this way, during the simulation, the battery thermal model works together with the other logical channels of the overall prediction software and computes, instant per instant, the value of the battery temperature. This quantity is continuously sent to the blocks of the tool responsible for the calculation of temperature-dependent battery variables, in order to allow an improved computation that can be more accurate and effective.

Obviously, the validation of the new battery cooling system model is necessary to ensure the correctness of the resulting temperatures and this analysis is going to be performed in the next chapter; anyway, as a starting point, it must be underlined that unfortunately there is not the possibility to compare the battery temperature time trends obtained through simulations with experimental data coming from laboratory tests. This because, since the new thermal tool virtually shapes battery devices specifically intended for new mild or full hybrid models, there is not the possibility to perform experimental tests to detect the actual temperature of the battery pack: the vehicle project, in fact, is still in the early design stages, when a physical product is not yet available and only virtual simulations can be realized.

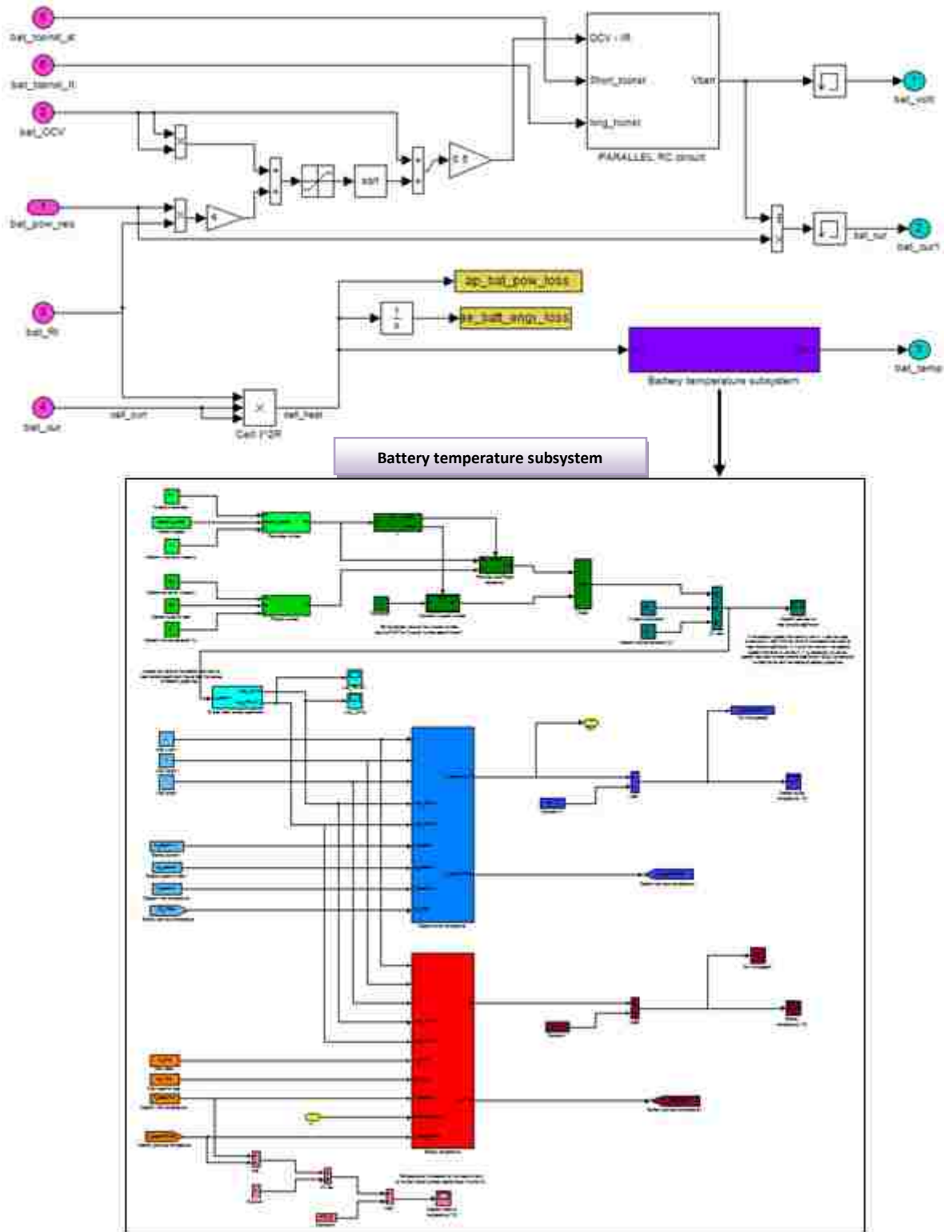


Figure 3.58 - HVB "Voltage Drop" block of the updated Chrysler HEV prediction model and internal view of the new thermal battery sub-model

However, the temperature gradient showed by the graphs obtained through the new battery simulation model are in the range that characterizes typical mild and full hybrid battery applications: considering both a charge depleting or sustaining condition, the simulated temperature magnitudes seem to be reasonable and reliable. Moreover, as described in the previous section, the battery temperature fluctuations correctly follow the dissipated power profile, given as input from the driving cycle and battery characteristics; this consideration gives further validity to the accuracy level of the new thermal model that, finally, computes temperature values capable of determining a more thorough temperature-dependent battery variables calculation.

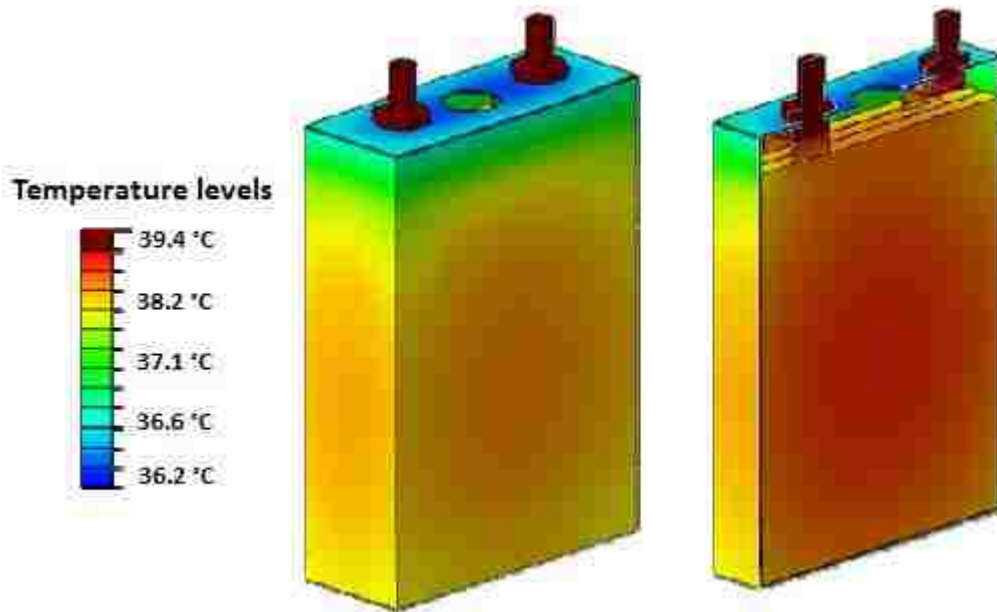
From a company perspective, it is clear that the level of innovation covered by the battery thermal model is considerably high: this because it has been created from a blank paper and integrated in the Chrysler prediction tool, offering a brand new possibility to improve the precision level of the simulations. Thanks to its features, in fact, the battery temperature can now be computed and used in the overall prediction tool to simulate the behaviour of the battery and of the whole vehicle “electric side” in a more accurate way. From a research and academic perspective, on the other hand, the innovation degree of the battery cooling system model must be studied from a completely different point of view, trying to understand what are the aspects that make it a novelty. From various literature researches, papers and documents describing similar models have been studied, making comparative analysis between them and the battery thermal model created during this project; taking into account the specific purposes at the base of the design of the compared tools, it has been pointed out that the following aspects determine definitely the novelty introduced by the battery cooling system model.

- High number of inputs: the Simulink® model operates on a high number of variables that are created by the Matlab® base file code, starting from the driving cycle information, from the cooling medium properties and from the battery constructive and electric specifications. These variables represent the thermoelectric aspects that characterize the behaviour of the investigated battery pack, cooled down by a specific coolant, and are suitably combined by the model to finally obtain the battery modules temperature time trend during the driving cycle. The input quantities mainly relate to the electric current profile that flows

through the cells, to the geometry of the battery pack and of the single modules, to the quantity of coolant flowing inside the device and, finally, to its thermal and physic properties. Because the resultant battery temperature is determined by the software with respect to such a high number of input quantities, the accuracy level of the result is considerably high and satisfactory from the overall simulation and prediction perspective of the program.

- Simplicity of the model: when the objective of a research work is to design a model that has to simulate the behaviour of a system from a given perspective, the first step of the project must be spent to define the desired precision level requested to the software. In fact, depending on the application of the model, its results must be characterized by different levels of accuracy and precision that, finally, determine the processing power necessary to activate and run the model itself. Dealing with thermal software, the most powerful and comprehensive expression is represented by the finite element method (FEM) solvers that use numerical techniques for finding solutions to boundary value problems; FEM encompasses all the methods for connecting many simple element equations over many small sub-domains, named finite elements, to approximate a more complex equation over a larger domain. A typical work out of the method involves dividing the domain of the problem into a collection of sub-domains, each of them represented by a set of element equations, followed by systematically recombining all sets of equations into a global system for the final calculation. Using this advanced technique to perform a thermal study of an investigated component, for example a prismatic HEV's battery cell, a complete description of its thermal state can be obtained through the definition of the temperature values over its whole volume and external surface. A typical output of this type of thermal analysis is represented in Figure 3.59 that depicts an external and internal views of a typical prismatic module, colored in different shades depending on the temperature levels [59]. At this point, it is clear that the result of a FEM analysis is characterized by a very high level of precision and accuracy but, at the same time, it requires the CAD file of the investigated component, a high power processing machine and, finally, long times of computation that make the FEM solvers not suitable to be

integrated in the overall Chrysler prediction software to study the thermal behaviour of the battery pack.



**Figure 3.59 - FEM thermal analysis of a typical battery prismatic module**

The model that has been designed during this study, on the contrary, offers the possibility to obtain information about the time-dependent temperature of the battery in a short period of time, generating results characterized by a satisfactory level of accuracy and precision, although not as thorough as the ones obtained through a FEM solver (that, anyway, are beyond the requests of the overall prediction tool). The complexity level of the battery thermal model is definitely not so high and this leads to a reduced time necessary to complete the simulations and, anyway, to a satisfactory precision of the obtained results. A complete three-dimensional analysis of the thermal behaviour of the modules, in fact, is not mandatory to obtain battery temperature results that can be used in the Chrysler prediction tool to determine the temperature-dependent variables of the hybrid vehicle “electric side”. A mono-dimensional analysis is sufficient to increase the accuracy level of the predictions since, at the moment, the battery temperature is considered as constant during the whole driving cycle; introducing an although simple computational procedure that determines the battery temperature during

time, the final results of the simulation are certainly more thorough and reliable than the ones obtained with the original simulation tool, not yet provided with the new battery thermal sub-model.

- Flexibility of the model: this is probably the most important and innovative characteristic of the tool. The battery model can work with whatever driving cycle, coolant type, battery constructive and electric characteristics that the user wants to investigate; individuated and specified all the input quantities of the case, in fact, the tool starts and proceeds with the simulation and generates as output the battery temperature time trend. This result is obtained for every type of battery, current profile and cooling medium that the user wants to study, without the need for modifications of the architecture of the software. The input variables determine in this way the resultant trend of the battery and coolant outlet temperatures and they are defined by the user before starting the simulation, depending on the specific case of study that he wants to investigate.
- Rapidity of the model: as already underlined before, an important aspect introduced by the battery model is the possibility to complete a simulation in a short period of time (less than 5 minutes) in order to quickly provide the battery temperature values to the overall prediction tool. Since the Chrysler software has to determine a lot of electric variables with respect to the temperature of the battery modules, it is important that the new thermal sub-model supplies as soon as possible the battery temperature results to the other logical channels of the prediction software. In this regard, the novelty introduced by the model at the end of this work, is represented by the possibility to generate precise and accurate results in reasonable times and without the need for high-power processing machine that are expensive to buy and maintain.
- Modules representation: one of the main objective of this work is to design a battery thermal model characterized by short computational times and, consequently, by precision and accuracy levels not so high, to avoid that the overall logical structure becomes too complicated. Anyway, the final results have to be obtained considering all the thermophysic mechanism that regulate the heat transfer phenomenon between the battery cells and the cooling medium. In



particular, the fact that the heat exchange takes place in different ways along the longitudinal and transverse direction of the battery pack and that, moreover, the modules are internally arranged as layered structures composed by consecutive sets of parallel layers, have to be taken into account. Because of this, the Matlab® and Simulink® files have been created in order to model the battery cells not as simple prismatic homogeneous entities, made up of a single material, but instead as complex bodies constitute by many sets of parallel layers having different thermal characteristics. Hence, even if the complexity level of the model is not so high, the characterization of the internal structure of the battery cells has been realized with an important level of detail, considering the different thermal conductivities of the anode current collector (copper), separator (polymer) and cathode current collector (aluminum) layers.

- Flow regime analysis: one of the most advanced features offered by the battery thermal model is represented by the possibility to individuate the type of flow regime of the coolant flowing between the cells. The new battery cooling system model, in fact, does not simply deal with the basic thermodynamic aspects of the heat transfer phenomenon but, at the same time, it studies and takes into account also the characteristics of the coolant flow inside the battery pack that have a strong influence on the thermal behaviour of the modules. The new battery sub-model, in fact, has been designed in order to consider all the physical variables that define the forced convection heat transfer phenomenon typical of an internal fluid flow configuration; computing during time the Reynolds number values, the battery thermal model is able to distinguish the flow regime type of the cooling air that could be laminar or turbulent. The knowledge of the flow regime characteristics is decisive in the calculation of the Nusselt number values and, in turn, of the convective heat transfer coefficient of the coolant that, finally, determines the instantaneous magnitudes of the longitudinal and transverse overall heat transfer coefficients. Since the amount of heat exchanged instantaneously between the battery cells and the coolant directly depends on the  $U_L$  and  $U_T$  values, their precise computation is necessary to thoroughly characterize the thermal behaviour of the battery pack during the investigated driving cycle;

because of this, it is clear that the flow regime analysis introduced by the new battery model covers an exceptional importance in studying the actual temperature time trend of the electric energy storage device of the investigated HEV.

From a final analysis of all these points, it is clear that, despite its basic level of sophistication, the battery cooling system model represents an innovative software both from a company and a research perspective. In particular, given the actual logical background of the overall Chrysler prediction tool, it performs a completely new computational action that allows to study and determine the battery temperature time trend during the investigated driving cycle. Knowing the actual instantaneous values of the HVB cells temperature, it becomes possible for the Chrysler model to thoroughly calculate all the temperature-dependent battery variables and to increase the accuracy level of the final predictive results related to the HEV performance and fuel economy. Moreover, in the panorama of the battery thermal model and computational software, there are not examples of basic tools capable of describing the thermal behaviour of a typical HVB HEV application without the necessity to use high-power processing machines. In fact, at the state of art, the most spread software intended to investigate the thermal performance of battery applications typical of mild and full hybrids, make use of FEM techniques asking for long times of computation and for high-power hardware. The battery thermal model that has been designed for this thesis project, instead, allows to reach the knowledge of the HVB temperature using ordinary-power processing machines and short times of computation; obviously, it gives less accurate results that relate to a mono-dimensional temperature analysis and not to a comprehensive three-dimensional analysis capable of describing the thermal state of the battery over its whole volume and surface. The temperature of the modules, in fact, is computed at their medium point along both the longitudinal and transverse directions without considering the thermal state of the other zones of the battery pack: this leads to a partial thermal characterization of the device but sufficient to give useful indications for the final purposes of the Chrysler prediction tool that, at the moment, consider the temperature of the cells as a constant imposed by the user. Moreover, despite the simplicity of the tool, the battery modules are carefully described as regards their internal layered structure and the heat transfer phenomena are carefully described depending on the considered heat exchange direction

and flow regime of the coolant; the number of input variables treated by the software is then considerably high, giving the possibility to compute, in any case, the battery temperature with a sufficient level of accuracy and precision. Finally, it can be pointed out that the battery thermal model introduces notable novelties from an academic point of view since it combines effectively a basic level of sophistication with the possibility to obtain even precise and thorough results, sufficient to increase the accuracy level of the predictive results of the Chrysler HEV simulation software.

## CHAPTER 4

### ANALYSIS OF RESULTS

#### 4.1 Introduction to the analysis of the results

In the previous chapter, the background theory at the base of the internal combustion engine and battery thermal models design has been carefully described: the equations representing the theoretical pillars of the tools have been studied and explained; the Matlab® base file code has been investigated together with the architecture of the Simulink® software, considered in its whole structure and regarding the specific logical channels and blocks; finally, preliminary simulations have been run by the models in order to evaluate their features and potential. Moreover, the novelty and innovation introduced by the two thermal models have been thoroughly evaluated and described, with the final purpose to understand if the technical and scientific content of the work is relevant and so if the internship activity could be seen as successful.

Certainly, from a company perspective, this project can be judged as highly satisfactory because, at the end of the models design and integration, the Chrysler HEV simulation software has become more accurate and reliable in predicting the performance and fuel economy of new hybrid models, investigated in the early design stages. From an academic perspective, instead, the attention is focused on the most important characteristics that make the two thermal models different and more advanced with respect to similar existing tools described in the literature. This important analysis and comparison has been conducted at the end of the previous chapter and it has highlighted that both the engine and battery thermal software can be considered as innovative and advanced but, first of all, they have to be thoroughly validated before being used to run simulations about the main characteristics of the investigated HEV models.

At this point, it is clear that a validation activity is necessary to prove the quality of the tools and to corroborate the principles of the design and the logic of their Simulink® architectures. The validation step has been performed after the design completion and before the software integration in the Chrysler prediction tool, and it is going to be

described in the following sections of the chapter. To complete the introduction of the validation activity, it must be remembered and underlined that the two cooling system software are intended to predict the thermal behaviour of engine and battery devices not already produced or equipping not already produced hybrid electric vehicles: this makes impossible to have experimental data through which implement a comparison between the real behaviour of the devices and their simulated performance and, in turn, this lead to the necessity to use general experimental indications and partially specific data, coming from real test procedures, to set up and complete the validation phase.

Moreover, the last important step of the project is represented by the simulation activity that has been done using the ICE cooling system model and, in particular, the battery thermal software as autonomous prediction tools, not integrated in the overall Chrysler model. One of the most interesting possibilities offered by the two newly designed sub-models is, in fact, their predisposition to be used alone to study the thermal performance of the investigated engine and battery pack considered as autonomous devices, not integrated in a vehicle system. High attention is going to be paid in this chapter to describe the simulation activities conducted with the two software, studying the input variables used for the analysis and the outputs obtained at the end of the logical computations that, finally, have been used to conduct a preliminary sensitivity study about the most important variables affecting the battery thermal behaviour.

#### **4.2 Internal combustion engine cooling system model simulation and validation phase**

A preliminary analysis of the main performance and features offered by the ICE cooling system model has been described in the previous chapter, using input data coming from a New European Driving Cycle test, driven by a segment B vehicle equipped with a diesel engine, and focusing the attention on the outputs generated by the whole software and by the single logical blocks of the Simulink® file. Afterwards, a thorough simulation has been conducted with the engine thermal model studying the case of a Chrysler Pentastar engine, tested on a dynamometer while running a UDDS and HWFET EPA cycles; this analysis has been conducted in a more precise way, because all the necessary input data have been received from the Thermal and NVH department at Chrysler with a

considerably high level of accuracy. The results of the simulation are going to be described in the following sections together with the validation procedure that has been realized referring to this particular engine device and driving cycle.

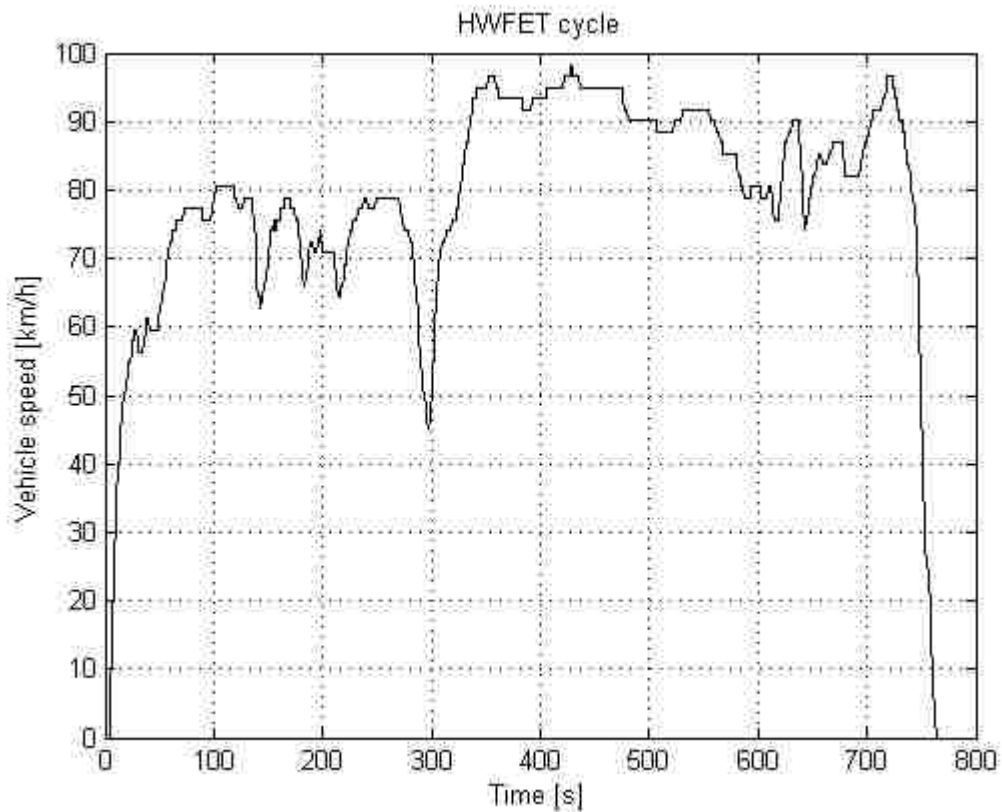
#### **4.2.1 Engine and driving cycle characteristics and input data**

The Chrysler Pentastar engine family is a series of aluminum die-cast cylinder block engines, with dual overhead cam and a 24-valve V6 technology, presented in 2009 at the New York Auto Show. The market launch has taken place in 2011 for Chrysler, Dodge and Jeep vehicles. The production investment announced by Chrysler was of \$2 billion, not including the product engineering but considering only the manufacturing process implementation. The engine was initially named “Phoenix”, it supports the cylinder deactivation, offers a dual variable valve timing but does not use an exhaust gas recirculation (EGR) valve [60].



**Figure 4.1 - Chrysler 3.6-L Pentastar engine [61]**

The Pentastar engines are made in Trenton, Michigan, USA, and Saltillo, Mexico, in three basic sizes: the 3.0-L, featuring the FIAT Multiair technology, the 3.2-L and the 3.6-L, characterized by different power ratings depending on the specific vehicle application (305 hp is the maximum power level, related to a Dodge Challenger application); more powerful single and twin turbocharged variants are planned for 2014, together with direct injection configurations. Figure 4.1 represents the external view of the Chrysler 3.6-L Pentastar engine considered for the simulation run by the ICE thermal model, whose results are going to be thoroughly described in the next sections.



**Figure 4.2 - Vehicle speed profile of the HWFET cycle**

The input data used to activate the ICE cooling system model relate to the engine depicted in Figure 4.1, tested on a dynamometer with a UDDS and a Highway Fuel Economy Driving Schedule (HWFET) profiles: the Urban Dynamometer Driving Schedule defines the city driving program, or FTP-72, included in the EPA Federal Test Procedure (FTP-75), that has been described in section 3.1.1.2.1 and, in particular, by

Figure 3.4 and Table 3.2; the HWFET profile, instead, represents the highway driving program included in the FTP-75 [41], whose speed pattern and main characteristics are shown and listed in Figure 4.2 and Table 4.1.

**Table 4.1 - HWFET driving cycle main characteristics**

<b>Time</b>	765 s
<b>Distance</b>	16.45 km
<b>Maximum speed</b>	96.40 km/h
<b>Average speed</b>	77.58 km/h
<b>Maximum acceleration</b>	1.43 m/s <sup>2</sup>
<b>Maximum deceleration</b>	-1.48 m/s <sup>2</sup>
<b>Average acceleration</b>	0.19 m/s <sup>2</sup>
<b>Average deceleration</b>	-0.22 m/s <sup>2</sup>
<b>Idle time</b>	3 s
<b>Number of stops</b>	1

The most important variables that are taken into account and elaborated by the Simulink® file of the tool are presented in the following list and, moreover, they derive from the Excel® file describing the driving cycle characteristics and created by the Thermal and NVH department teams, during the engine characterization activity.

1. Driving cycle time, expressed in seconds and necessary to create the time-dependent vectors that the Simulink® logical loops has to deal with.
2. Engine rotational speed, expressed in rpm.
3. Engine torque, expressed in Nm,
4. Vehicle linear speed, expressed in km/h and defining the velocity profile of the cycle chosen to describe a specific driving pattern.
5. Exhaust gas temperature, expressed in °C and taken at the cylinders outlet manifold.
6. Engine inlet fresh charge temperature, expressed in °C.
7. Ambient temperature, expressed in °C.
8. Cabin temperature, expressed in °C and defined on the basis of the specific requests of the driver and the passengers.



9. Air mass flow rate going inside the cabin, expressed in kg/s.
10. Engine coolant mass flow rate, expressed in kg/s and determined with respect to engine angular speed and so with respect to the engine operating conditions.
11. Radiator inlet coolant temperature, expressed in °C and considered at the radiator inlet port.
12. Radiator outlet coolant temperature, expressed in °C and considered at the radiator outlet port.
13. Fuel mass flow rate, expressed in kg/s.

As stated before, all these variables refer to the FTP-72 driving profile included in the EPA Federal Test Procedure, followed by the additional excitation velocity profile constituted by the HWFET highway driving program. In reality, the data received from the Thermal and NVH department refer to an updated profile in which a section of the FTP-72 has been repeated two times with the addition of a 10 minutes ICE stop. The engine thermal model system's response to this specific driving cycle is going to be studied and analyzed in the following sections, with suitable graphs obtained from the Matlab® base file used to elaborate the Simulink® outputs.

Proceeding with the input study, moreover, precise information related to the thermodynamic properties of the fuel, external air and engine coolant are necessary to run the simulation, together with the constructive and geometric characteristics of the cabin heater, thermostat and engine devices. All these variables have been described in section 3.3.3 while explaining the theory at the base of the engine cooling model design and, in particular, during the analysis of all the equations constituting the computational structure of the tool; some of them are specified in the following list.

1. air density;
2. air specific heat;
3. air convective heat transfer coefficient;
4. coolant density;
5. coolant specific heat;
6. coolant convective heat transfer coefficient;
7. fuel density;
8. exhaust gases specific heat;

9. stoichiometric air-to-fuel ratio;
10. combustion efficiency;
11. fuel lower heating value;
12. fuel heat of vaporization;
13. engine walls thermal conductivity;
14. engine walls thickness;
15. engine external surface;
16. cabin heater cross sectional area.

The magnitude of these variables has been defined through careful literature reviews and through meetings with the engineers working in the Thermal and NVH department at Chrysler. In particular, the support of the NVH teams has been necessary to correctly model on Simulink® the behaviour of the engine thermostat, that is difficult to study since it depends on the engine rotational speed and operating conditions.

#### **4.2.1.1 Thermostat working principles**

The thermostat has the objective to maintain the temperature of the coolant inside the engine roughly constant, regardless of the requested engine power, and to fix its value at the optimum level that ensure the best mechanical efficiency. In order to do that, the thermostat controls the coolant flow rate entering the radiator: at the engine switch on, the main cooling circuit remains closed and thermostat prevents the coolant to pass through the radiator but, instead, feed it through a bypass circuit where the heat from the engine warms up the coolant in a considerably short period of time. Then, when the coolant temperature is close to the optimum, the thermostat opens and allows the coolant flow to the radiator: regulating instant per instant its opening section, the thermostat defines the exact magnitude of the coolant mass flow rate such that the desired coolant temperature can be maintained.

The thermal control of the engine cooling system with a conventional wax thermostat is determined by the coolant temperature only that, in fact, defines the opening characteristics of the thermostat (fixed at a constant temperature) independently of the engine working conditions. On the contrary, advanced map-controlled wax thermostat can perform an electrical heating of the wax element changing, as desired, the opening

temperature of the thermostat and therefore the coolant temperature inside the cooling circuit. As a result, the engine can be operated at higher temperatures in partial load conditions, approximately between 100 °C and 110 °C, when the engine friction sharply decreases in case of high temperature values, leading to fuel consumption reduction up to about the 3%. On the other hand, under full load operations, the coolant temperature is reduced to approximately 80 °C in order to decrease the intake air temperature and, consequently, increase the engine volumetric efficiency. In this way, operating the electrically heated thermostat using the suitable ECU algorithms, the thermal control of the engine cooling system can be realized using characteristic maps dependent on the engine load and angular speed.

#### 4.2.1.2 Thermostat modeling

In particular, the Thermal and NVH teams at Chrysler have realized some studies and experimental analysis to determine the relationship existing between the engine angular speed and the coolant mass flow rate that the thermostat allows to flow to the radiator. Given different rotational speeds of the engine, the related amounts of coolant flowing through the radiator have been detected and stored in Excel® databases; in this regard, the database related to the 3.6-L Pentastar engine has been carefully studied in order to be able to model and implement in details the operating characteristics of the thermostat.

**Table 4.2 - Engine angular speed and radiator coolant volume flow rate**

<b>Angular speed [rpm]</b>	0	735.29	1470.59	2205.88	3676.47	4411.76	5919.12	<b>348.183</b>
<b>Coolant flow rate [US gpm]</b>	0	6.81	14.16	21.46	36.11	43.82	59.49	<b>3.499</b>

Above Table 4.2 represents some couples of values related to the engine angular speed and the respective coolant flow rate, expressed in gallons per minute. Knowing their series of values, it is possible to think about the two variables as approximated straight lines passing through the origin of a Cartesian coordinate system, whose abscissa axis represents the considered couple number and whose ordinate axis indicates the engine angular speed and coolant volume flow rate correspondent to the same couple. The

two lines are partially represented in Figure 4.3 (the maximum displayed amount of rotational speed has been fixed at 750 rpm to improve the resolution of the graph) and their angular coefficients have been suitably computed and indicated in the right-most cells of Table 4.2, filled in blue and red.

Hence, from the knowledge of Figure 4.3 and of the angular coefficients expressed in Table 4.2, it is possible to find the instantaneous magnitude of coolant flow rate passing through the radiator from the instantaneous value of the engine angular speed given as a driving cycle characteristic.

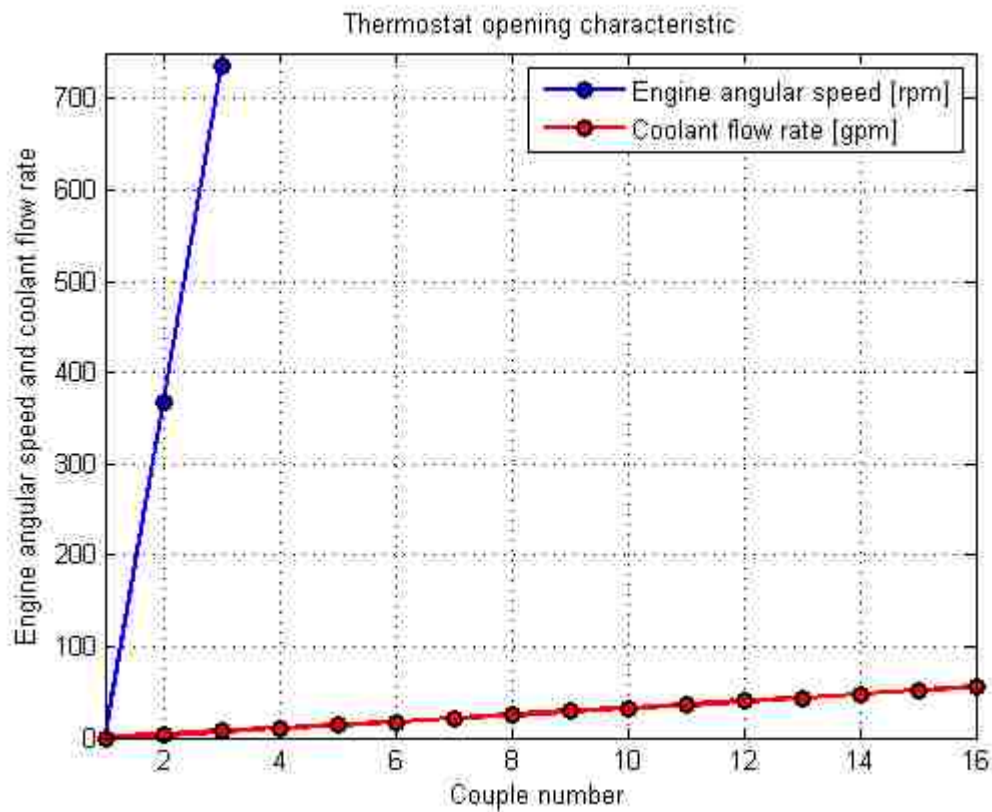


Figure 4.3 - Characteristic curves of the radiator coolant volume flow rate and engine angular speed

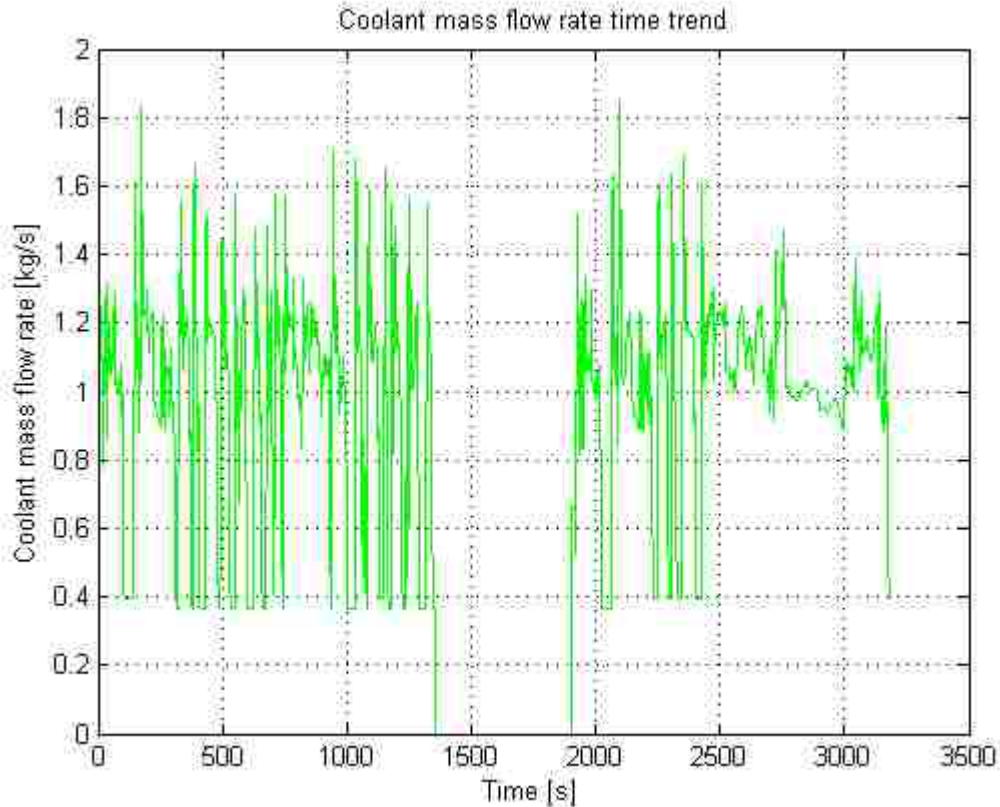
As written in Equation 4.1, it is necessary to divide the rotational speed of the engine ( $n$ ) for the angular coefficient of the blue line of Figure 4.3 ( $m_b$ ) and, then, to multiply the result for the angular coefficient of the red line of the same picture ( $m_r$ ): in this way, the coolant volume flow rate entering the radiator ( $\dot{V}_{coolR}$ ) can be determined for each value of the engine angular speed.

$$\dot{V}_{coolR} = n \cdot \frac{m_r}{m_b} \quad (4.1)$$

At this point it is clear that, using the instantaneous values of engine rotational speed, whose profile is known as a driving cycle characteristic, the correspondent magnitudes of the coolant volume flow rate can be determined. Moreover, since the final output of the engine thermal model, represented by the coolant temperature time trend during the investigated driving cycle, is computed by the Simulink® software using the coolant mass flow rate, its volume flow rate has to be suitably converted by the Matlab® base file code.

$$\dot{m}_{coolR} = \dot{V}_{coolR} \cdot C \cdot \frac{\rho_{cool}}{1000} \quad (4.2)$$

In Equation 4.2,  $\dot{m}_{coolR}$  represents the coolant mass flow rate flowing through the radiator that is obtained multiplying the coolant volume flow rate ( $\dot{V}_{coolR}$ ), expressed in gallons per minute, by the coefficient  $C$ , that converts the unit of measure from gpm to l/s, by the density of the coolant, expressed in  $\text{kg/m}^3$ , and finally dividing the result for 1000: in this way, the term  $\dot{m}_{coolR}$  is obtained and its unit of measure is the desired kg/s. In this way, uploading in the Matlab® “Workspace” the engine rotational speed values stored in the driving cycle Excel® file and finding from them the coolant volume and mass flow rates, implementing in the Matlab® script Equations 4.1 and 4.2, Figure 4.4 can be finally plotted to show the time trend of the coolant mass flow rate flowing in the cooling circuit of the engine depending on the thermostat operations that, in turn, depend on the load conditions of the ICE.



**Figure 4.4 - Coolant mass flow rate flowing in the engine cooling circuit**

Analyzing Figure 4.4, it is clear that the coolant mass flow rate flowing in the engine cooling circuit during the investigated driving cycle strongly depends on the operating conditions of the engine itself and, in particular, on the rotational speed of its crankshaft: the coolant flow rate profile, in fact, directly depends on the angular speed of the engine, whose trend is defined as the one that allows to finally obtain the overall vehicle linear speed profile of the FTP-72 and HWFET driving cycle (considered for the case of study). The linear speed characteristics of the whole cycle are going to be described in the next section, before presenting the results generated by the engine cooling model simulation, in order to better understand how the engine and the whole vehicle investigated during the study are going to be virtually excited by the model.

#### **4.2.2 Internal combustion engine cooling system model simulation phase**

Once all the variables introduced in the previous sections have been uploaded and stored in the Matlab® “Workspace” and, moreover, the operating characteristics of the

specific thermostat used for the current analysis have been modeled in the engine thermal software, the simulation can be activated in order to find the engine coolant temperature time trend that characterizes the investigated 3.6-L Pentastar ICE while running a FTP-72 and a HWFET driving cycle. As underlined in the previous chapter, the engine thermal tool can be used to run simulations related to every type of ICE model and to every type of driving profile, thanks to its considerable level of flexibility that makes it perfect to perform specific thermal analysis regarding different types of engine and driving cycle.

In particular, the ICE cooling system model can be used as an autonomous prediction tool that, not integrated in the overall Chrysler model, can run simulation on its own to analyze the thermal behaviour of the investigated engine, not considered as part of a whole hybrid electric vehicle system but intended as an independent device. In this regard, at the end of the model design and preliminary check stages, a thorough simulation has been conducted using the newly created software: a 3.6-L Pentastar engine has been investigated over a “modified” FTP-75 profile, constituted by both the city and highway driving programs, with the final purpose to study the time trend of the temperature of its cooling medium.

#### **4.2.2.1 Excitation driving profile**

The most important characteristic of a driving cycle is represented by the linear speed profile that has to be guaranteed to the vehicle by the engine; through specific test conducted on the dynamometer, all the variables affecting the ICE behaviour are determined in such a way that the engine can propel the vehicle at the specific speeds indicated by the driving profile. In this way, the Excel® files generated by the Thermal and NVH department teams during these studies are provided, among the others, with the fuel mass flow rate, torque and angular speed time trends that characterize the ICE when it has to move the vehicle at the speeds specified by the considered driving cycle. For the present simulation, it has been decided to study the thermal behaviour of a 3.6-L Pentastar engine, while running a FTP-72 city driving program, followed by a HWFET highway driving program. The overall linear speed pattern requested by the vehicle is depicted in Figure 4.5 and described in details in the next paragraph.

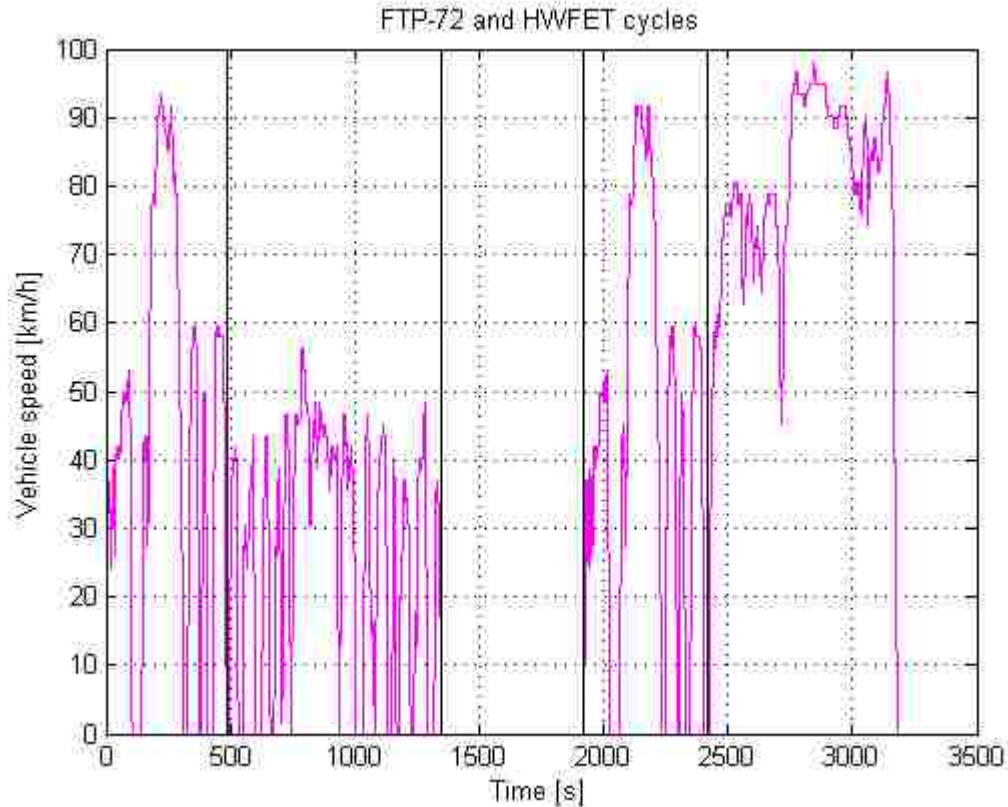


Figure 4.5 - Vehicle speed profile of the “modified” FTP-75 driving cycle

First of all, it has to be underlined that the last section of the profile, the one at the right of the fourth black vertical line, represents the HWFET driving cycle whose specific linear speed pattern is shown by Figure 4.2 and whose main characteristics are listed in Table 4.1. At the left of the second black vertical line, instead, it is possible to recognize the FTP-72 speed profile that has been described in section 3.1.1.2.1 and, in particular, by Figure 3.4 and Table 3.2: the cycle is characterized by a “cold start” phase (between the ordinate axis and the first black vertical line) of 505 seconds, over a projected distance of 5780 meters at 43.585 km/h of average speed and, then, by a “transient” phase of 864 seconds. Between the second and third lines, moreover, it is possible to note the presence of a 10 minutes ICE switch off phase, followed finally by a “hot start” phase which repeats the “cold start” one starting around second 1900. Hence, in order to sum up, it is possible to state that the overall driving profile considered for the present simulation is composed by a FTP-72 and a HWFET program, interspersed by a 10 minutes engine stop

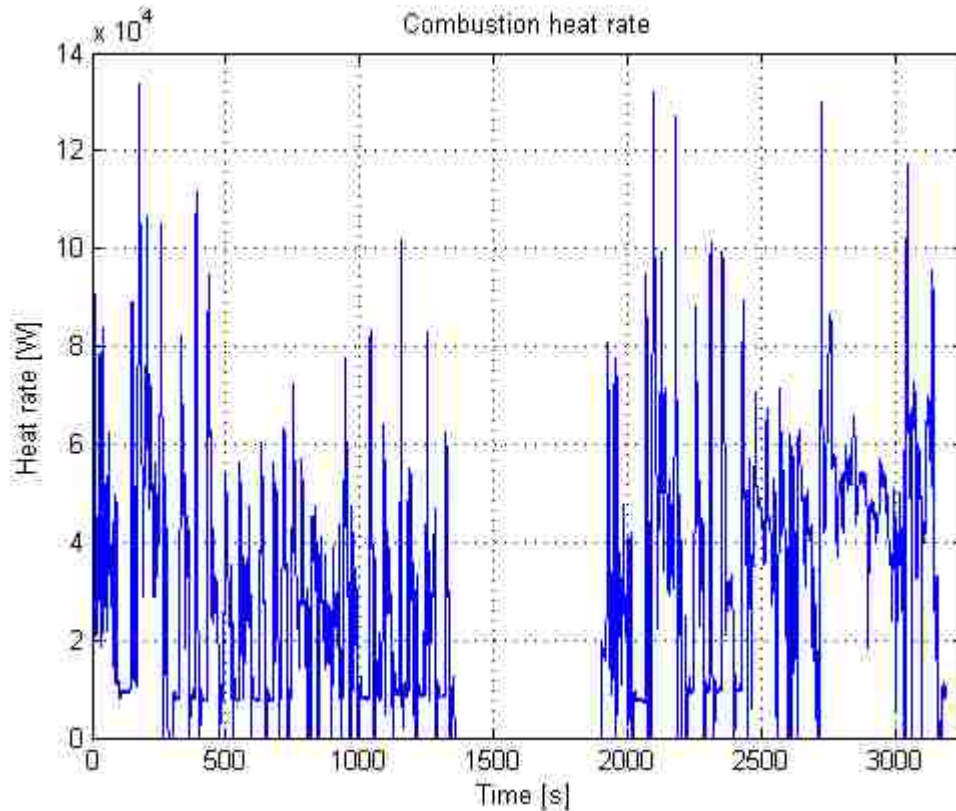


and by a “hot start” phase: the whole driving profile obtained in this way can be finally seen as a “modified” FTP-75 driving cycle.

Now that the characteristics of the investigated driving cycle have been described in details, it is possible to begin the analysis of all the results obtained through the simulation performed by the engine cooling system model, studying the time trend of the various heat rate contributions and of the sought engine coolant temperature. Placing appropriate “To Workspace” blocks on the specific logical channels of the engine thermal model Simulink® file, all the time trends of the investigated variables and quantities have been sent to the Matlab® “Workspace” in order to be plotted as desired by the user to facilitate their study and thorough analysis. Executing the Matlab® base file code and, then, activating the simulation on Simulink®, the software has suitably elaborated and combined all the input data coming from the driving cycle Excel® file and engine specifications, allowing the computation of all the unknown variables constituting the logical structure of the model.

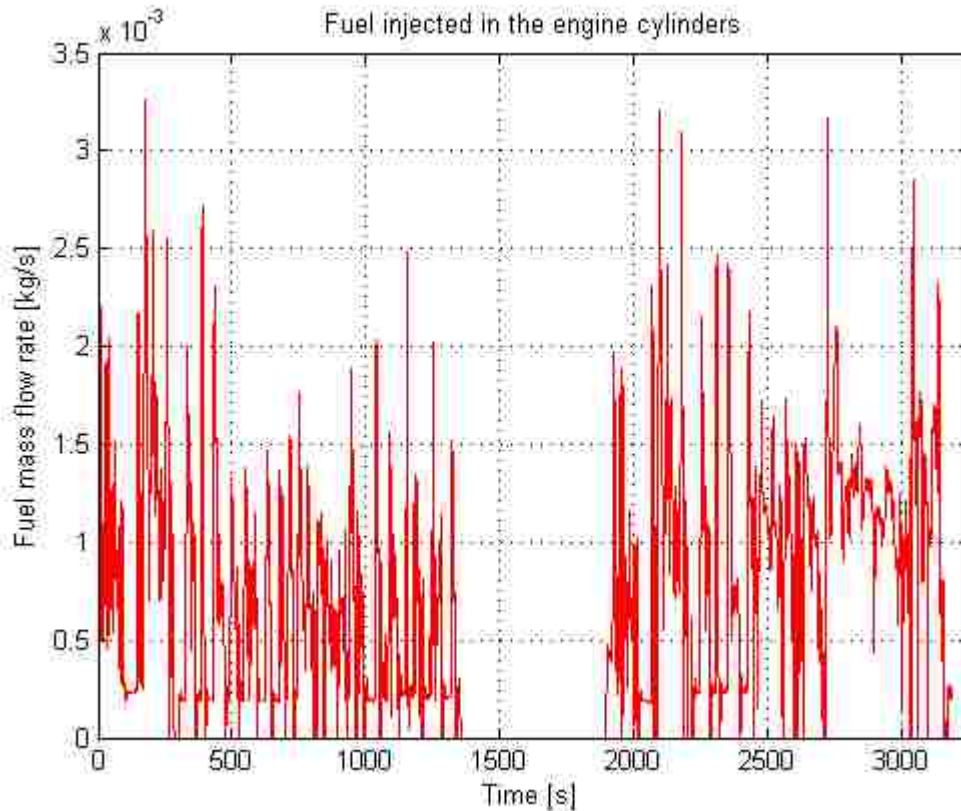
#### **4.2.2.2 Analysis of the combustion heat rate**

In order to move the vehicle at the linear speeds specified by the driving cycle, the engine has to burn during time specific quantities of fuel injected inside the cylinders: the fuel mass flow rate time trend is defined as a driving profile characteristic for the 3.6-L Pentastar engine and it refers to a typical gasoline sold in the United States. Given the fuel mass flow rate, the related amount of heat generated by its burning is computed by the software knowing the magnitude of the gasoline lower heating value and evaporation heat and, moreover, of the combustion efficiency typical of the investigated ICE. Uploading from the Matlab® “Workspace” the suitable value of these quantities, the Simulink® model computes the instantaneous heat rate generated by the combustion phenomenon that, for the current case of study, is depicted in Figure 4.6. Not considering the 10 minutes engine stop phase, a medium combustion heat rate of 33.157 kW can be found over the whole driving cycle and its magnitude is reasonable for the investigated engine and linear speed profile.



**Figure 4.6 - Combustion heat rate time trend**

In Figure 4.7 is shown the time trend of the fuel mass flow rate and, as can be seen from a comparison of Figures 4.6 and 4.7, it directly determines the combustion heat rate generated by the engine. Moreover, as expected, the fuel injected instantaneously inside the cylinders is directly linked to the magnitude of the vehicle speed and, because of this, its maximum values can be found during the “cold start” and “hot start” phases of the FTP-72 driving program and during the HWFET profile. Obviously, during the 10 minutes engine stop, a complete fuel cut-off takes place in order not to waste gasoline during the idle condition; moreover, during the highway driving program, the average vehicle speed is higher with respect to the rest of the cycle and, because there are not stopping events and the decelerations are not highly sustained, between second 2700 and 3050, the fuel mass flow rate is approximately always greater than the considerable value of 1 mg/s.



**Figure 4.7 - Fuel mass flow rate injected in the engine cylinders**

Since all the energy that warms up the coolant comes from the heat of combustion, its computation is necessary to determine the engine coolant temperature time trend: the amount of heat that, instant per instant, is going to the cooling medium is in fact calculated by the engine thermal model subtracting to the combustion heat rate all the heat “consumption” terms that are leaving the ICE and are not directed to its cooling circuit. All the calculations are more precise for this case of study than for the preliminary analysis, presented in the previous chapter, that was made during the design phase to check the mathematical and physical correctness of the model.

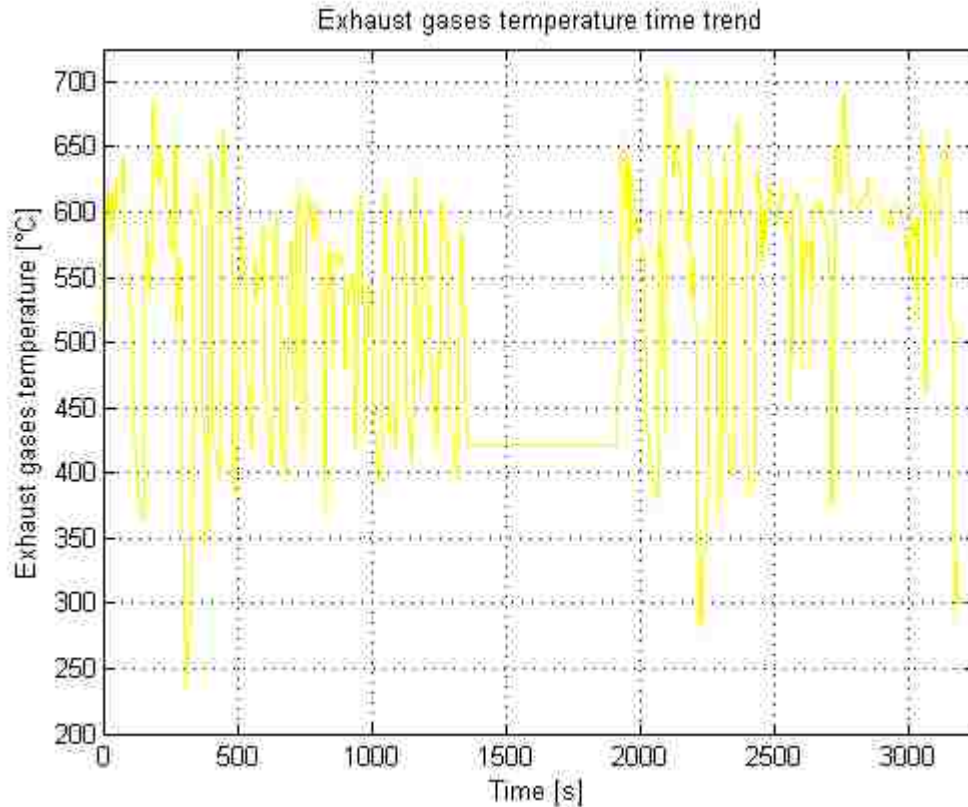
That analysis refers to a segment B vehicle, equipped with a diesel engine, driving a NEDC cycle and its input data have a limited validity since received from an external company with a not high level of detail: because of this, they can be used to check if the model is able to run simulations without computational errors and to obtain reasonable results. On the contrary, since the simulation investigated in this chapter has been realized with more precise and thorough input data obtained from the Thermal and NVH

department at Chrysler, the results of the current analysis can be analyzed in details to understand if the operations of the model are really founded on accurate scientific basis. The time trend and order of magnitude of all the model outputs is going to be carefully described with the final purpose to demonstrate the validity of the results generated at the end of the simulation.

#### **4.2.2.3 Analysis of the exhaust heat rate**

About the 20% of the whole energy produced by the engine thanks to the combustion of the fresh charge usually goes to the exhaust gases, generating the main contribution of the heat losses that characterize the ICE operations. Hence, the exhaust heat rate has to be carefully taken into account and computed during the simulation, implementing an appropriate logical loop that combines the exhaust gas flow rate, exhaust specific heat, fresh charge and exhaust temperatures as the necessary input variables. The mass flow rate of the exhaust can be simply computed as the sum of the instantaneous fuel mass flow rate, given by the driving cycle Excel® file, and the instantaneous air mass flow rate entering the cylinders, determined from the fuel quantity making use of the stoichiometric air-to-fuel ratio and of the logical signal sent from the lambda sensor to the engine ECU. Moreover, the specific heat of the exhaust gases is known from the literature while the temperatures at the inlet and outlet manifold of the engine have been detected through thermocouples during the driving cycle test of the engine on the dynamometer.

Since the exhaust specific heat is a constant property of the burnt gases and the temperature of the fresh charge is usually constant during the driving cycle, because set at the ambient level, the amount of heat that goes during time to the exhaust depends primarily on the mass flow rate and outlet temperature of the gases leaving the engine cylinders. In this regard, Figure 4.8 depicts the time trend of the exhaust gases temperature detected at the engine outlet manifolds, immediately after exiting the exhaust valve systems. The minimum and maximum temperature values are about 250 °C and 700 °C, respectively, while during the engine switch off phase the outlet manifold temperature has been maintained roughly on the value it had at the end of the FTP-72 “transient” phase, in order to be able to impose a later “hot start” around second 1900.



**Figure 4.8 - Exhaust temperature at the outlet manifold**

Figure 4.9, instead, shows the time trend of the exhaust heat rate computed by the engine thermal model during the simulation, in order to characterize the most important heat loss contribution for every second of the driving cycle. Calculating through the suitable Matlab® command the mean magnitude of the heat rate going to the exhaust during time, a value of 7.6275 kW is found (the engine idle period has not been taken into account): this quantity is quite high and suggests that it would be better not to waste the energy of the exhaust gases in the surrounding ambient but to use it in some ways. For example, in turbocharged engines, the energy of the exhaust is used to drive a compressor that forces more air, and proportionally more fuel, into the combustion chamber, leading to increased value of power produced by the ICE. From the data set plotted in Figure 4.8, it can be computed the mean value of the exhaust gases temperature whose magnitude settles at 788.213 °C: the energy content of such a high-temperature fluid is relevant and can be certainly used to activate ancillary loads on the vehicle or to give more power to

the driveshaft; it would be a wrong choice decide not to recover the thermal and kinetic energy of the exhaust before they leave the muffler.

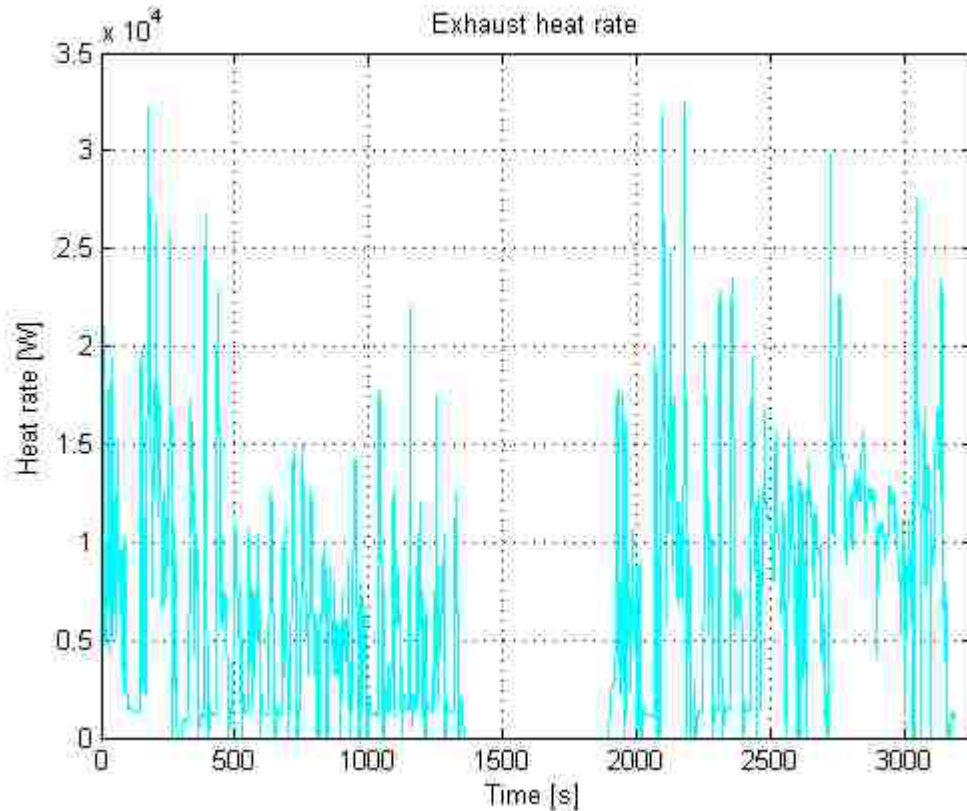


Figure 4.9 - Exhaust heat rate time trend

#### 4.2.2.4 Analysis of the mechanical power

Part of the combustion heat rate is obviously transmitted to the engine crankshaft in the form of mechanical power, given by the product between the rotational speed and the torque detected at the shaft. The instantaneous values of the engine angular speed and torque are given by the Excel® file of the driving cycle and, once uploaded in the Matlab® “Workspace” and Simulink® model, are suitably combined to compute the mechanical power time trend, depicted in Figure 4.10 for the 3.6-L Pentastar engine running the “modified” FTP-75 driving cycle. It has to be remembered that, during the engine braking actions, the crankshaft torque is characterized by negative values and so, because the engine angular speed is always greater than zero, the power generated is negative and leads to an increase of the heat amount that goes to the coolant. For the

investigated driving cycle, there are not frequent engine braking actions and, moreover, they are not so intense: hence, the coolant warm up caused by the “brake torque” is not relevant for the current case of study.

Comparing Figure 4.10 with Figure 3.15, it is possible to note that the engine braking actions performed during the NEDC cycle are more frequent than for the FTP-75 program, in which the decelerations are mainly realized using the mechanical brakes at the wheels. Moreover, the mean amount of power generated by the diesel engine during the ECE cycles is similar to the one generated by the Pentastar during the FTP-72 city driving program; on the contrary, the HWFET highway profile requests a lower power amount to the gasoline ICE than the one requested by the EUDC to the diesel one: this because the velocity profile of the EUDC cycle is highly sustained and reaches a maximum speed of 120 km/h.

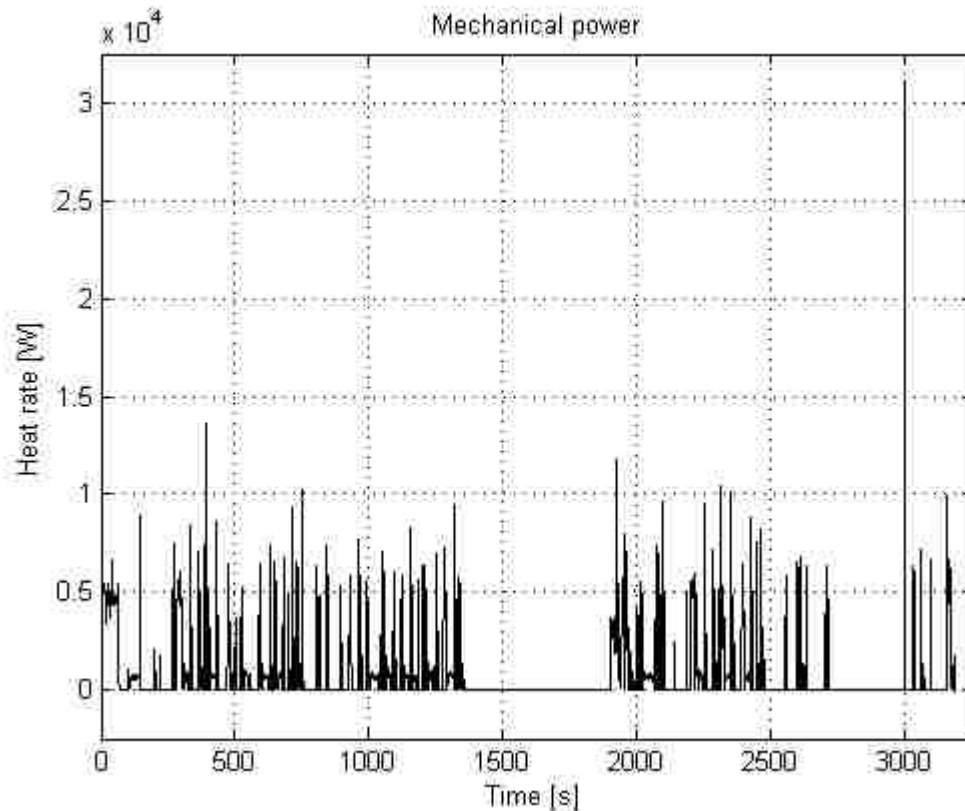


Figure 4.10 - Mechanical power time trend

#### 4.2.2.5 Analysis of the cabin heater heat rate

Another important contribution that has to be subtracted to the combustion heat rate in order to determine the heat amount going to the coolant, is represented by the cabin heater heat rate; it is directly withdrawn from the coolant and, even if its magnitude is not so high, a careful estimation of its value must be done. When the driver or the passengers desire to get warm the vehicle cabin, the engine coolant is directed through the cabin heater providing it with part of its heat; the air entering the cabin, passing through the cabin heater exchanger, is warmed up thanks to the heat rate taken from the engine coolant whose temperature, in this way, decreases. Knowing the time trend of the ambient and vehicle cabin temperatures, given as driving cycle data, it is possible to determine the instantaneous temperature gradient experienced by the air across the cabin heater and then, multiplying this temperature difference for the specific heat of the air and for the instantaneous value of the air mass flow rate going through the heater, the cabin heater heat rate can be finally determined; for the investigated engine and driving profile, its time trend is depicted in Figure 4.11.

Since the air mass flow rate flowing through the cabin heater is not directly given as an input data received from the Thermal and NVH department at Chrysler, it has to be calculated during time knowing the density of the air, the cross section of the cabin heater and the linear speed of the vehicle: since the air entering the cabin derives from the external ambient and passes through the front-end before going to the cabin heater, its time trend has the same shape of the vehicle linear velocity defined by the driving profile. Analyzing Figure 4.11, it is possible to note that the same time trend characterizes also the cabin heater heat rate and this is correct since the temperature gradient experienced across the heater during a typical FTP-75 driving program is quite constant: because of this, the heat rate magnitude is mainly determined by the air mass flow rate that, in turn, has a linear relationship with the linear velocity of the vehicle.

Even if the physical validity of the heat rate represented in Figure 4.11 is beyond doubt, its specific trend has been obtained considering a limiting assumption: all the air vents inside the cabin has been fully opened by the driver and the passengers, in such a way that all the air passing through the vehicle front-end enters the vehicle cabin during its motion. In theory, instead, the quantity of air entering the cabin is totally regulated by



the occupants who impose the opening section of the vents; hence, to better characterize the cabin heater heat rate computation, the engine thermal model could be updated with a new algorithm that takes into account the working profile of the vents on the basis of a specific trend representing the typical temperature feeling of the driver and the passengers.

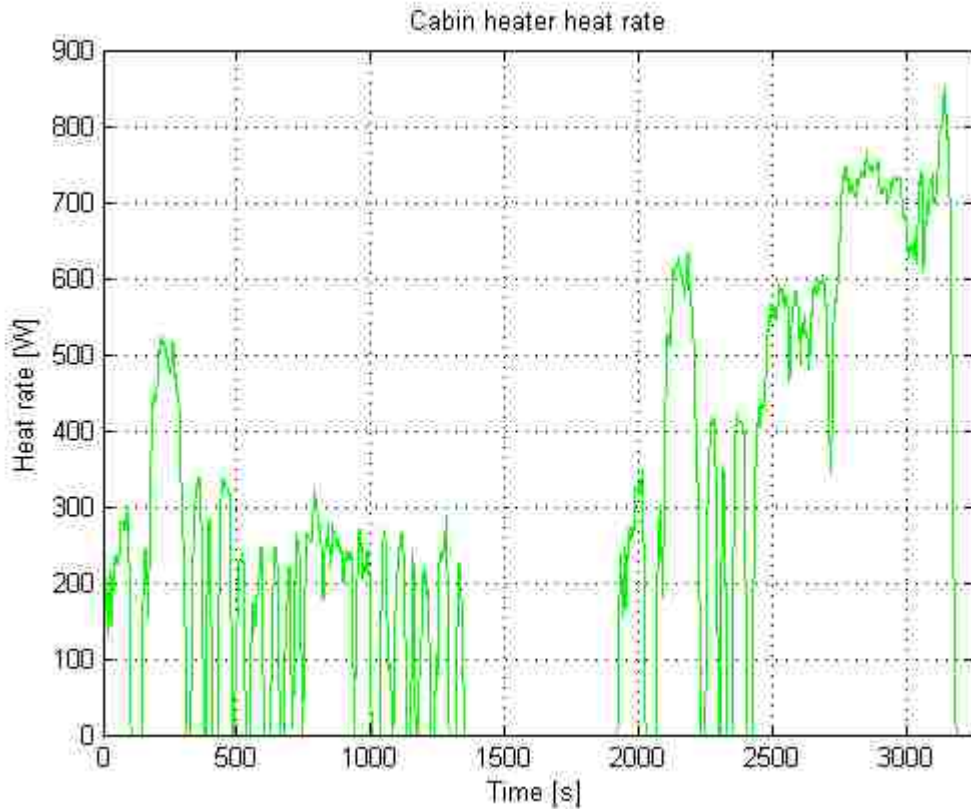


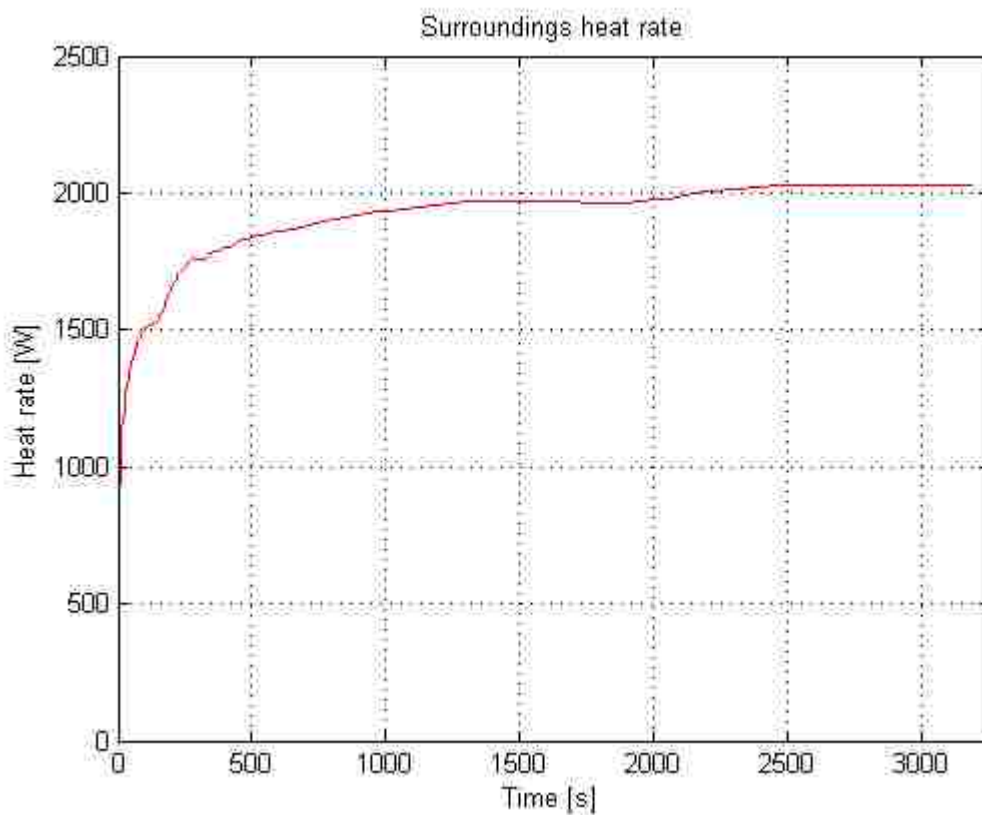
Figure 4.11 - Cabin heater heat rate time trend

#### 4.2.2.6 Analysis of the surroundings heat rate

Since the temperature of the engine during the driving cycle is obviously higher than the one of the surrounding ambient, a spontaneous heat loss takes place for convection from the engine's walls to the air; moreover, considering that the heat going to the surroundings leaving the walls has before to pass from the engine coolant through the thickness of the ICE block, it is necessary to consider an overall heat transfer coefficient (accounting for both the conductive and convective phenomena) and the temperature gradient existing during time between the cooling medium and the external air. Knowing

the thermophysical properties of the 3.6-L Pentastar engine and also its constructive and geometric characteristics, the surroundings heat rate has been determined as a result of the simulation and its time trend is depicted in Figure 4.12.

As can be seen from below Figure 4.12, the magnitude of the surroundings heat rate does not assume considerable values and, moreover, its trend is continuously increasing with time: this is reasonable because the surroundings heat rate is directly linked to the engine coolant temperature that, instant per instant, rises up because of the engine solicitations until the thermostat is opened to control the ICE thermal state.



**Figure 4.12 - Surroundings heat rate time trend**

Finally, comparing the magnitudes of the cabin heater and surroundings heat rates with the other thermal contributions, it is clear that their influence is very low over the final results of the simulation: nevertheless, a careful calculation of these two thermodynamic quantities has to be performed by the model but, in case of future updates

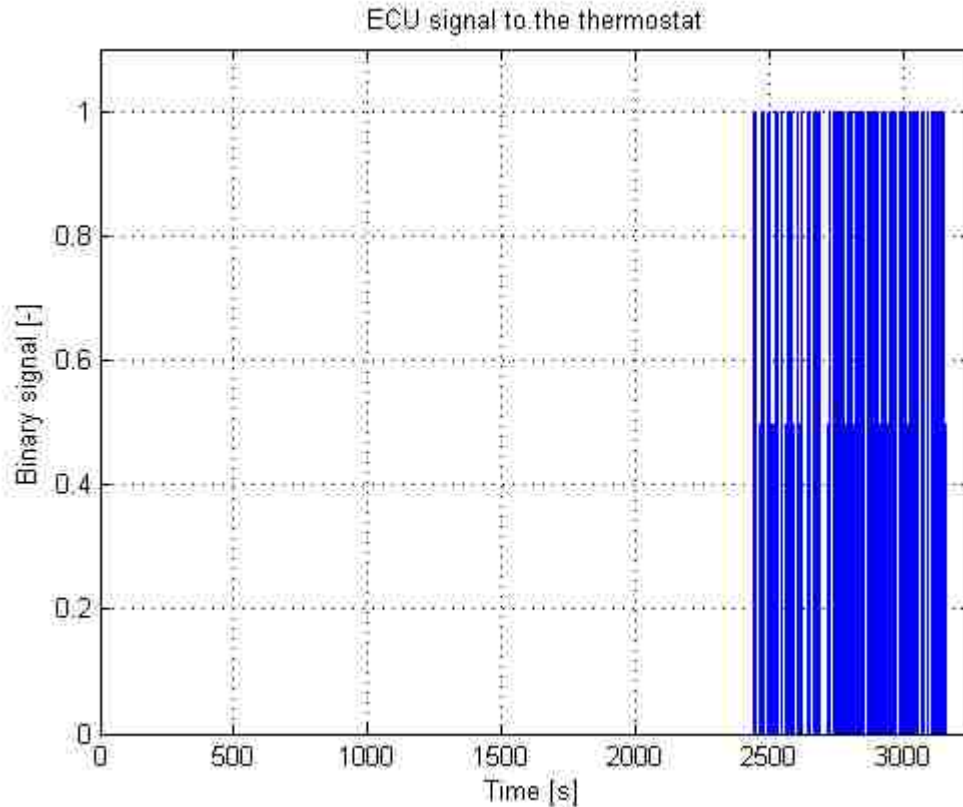
and computational improvements, the attention has to be primarily focused on the logical blocks intended for the determination of the other, most relevant, heat contributions.

#### **4.2.2.7 Analysis of the radiator heat rate**

The last important heat contribution that must be taken into account is the radiator heat rate, probably the most important actor that defines the overall thermal state of the engine cooling medium. The engine radiator has the purpose to dispose the excess of heat from the cooling circuit to the external ambient in order to avoid dangerous ICE overheating; as carefully described in section 4.2.1.2, the amount of coolant that flows through the radiator is defined by the thermostat that, in turn, operates on the basis of the engine working conditions.

In general, given the specifics of the engine model and the characteristics of the driving profile, the thermostat is mapped in order to maintain the temperature of the coolant at a given desired value, optimum for the ICE operations. For the present simulation, in particular, a target value of 85 °C has been imposed through the Matlab® base file in order to regulate the Simulink® model actions: once the simulation has been activated by the user, the software computes during time the investigated temperature of the coolant and, on the basis of its actual value, defines the level of the binary signal that the engine ECU sends to the switch of the thermostat.

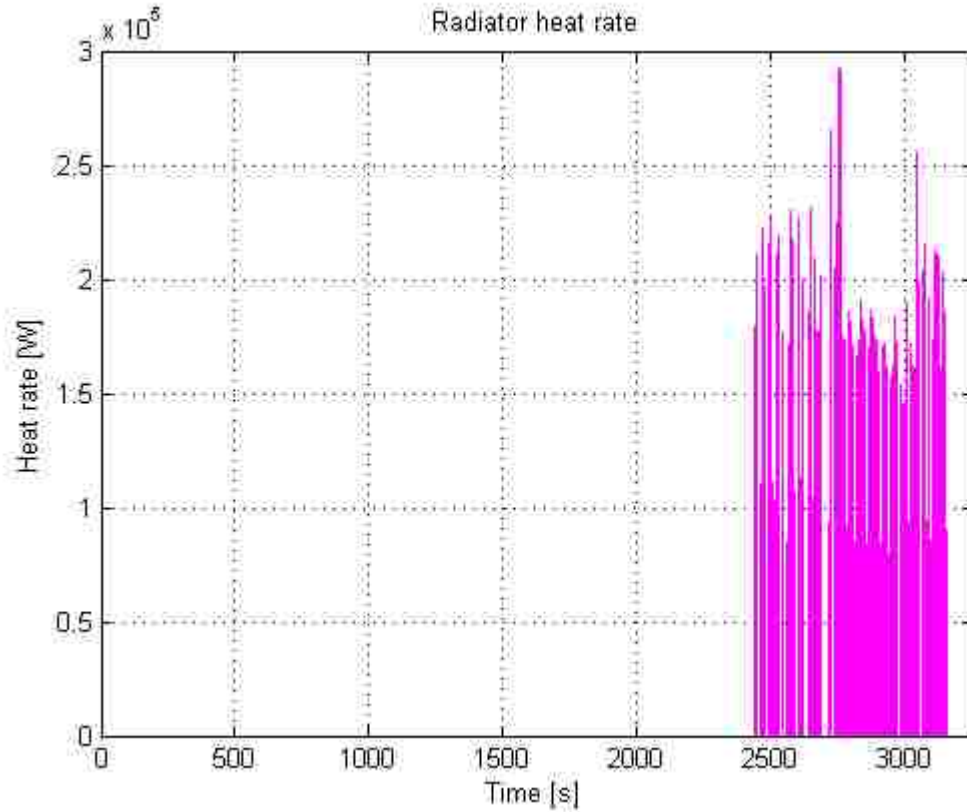
If a 1 value reaches the switch, the Simulink® file build a virtual situation in which the thermostat is opened and lets the coolant flow to the radiator; the coolant temperature has exceeded the limit value imposed by the user and so a certain amount of heat has to be removed from the cooling circuit through the radiator. In Figures 4.13 and 4.14 are depicted the time trends of the ECU switching signal and of the radiator heat rate, given as outputs of the current simulation.



**Figure 4.13 - ECU signal to the thermostat time trend**

From Figure 4.13 it is possible to note that, approximately until second 2420, the ECU signal going to the thermostat is always at a 0 level and this should be caused by an engine coolant temperature that remains lower than the 85 °C limit imposed by the user. Hence, to give validity to the above picture, a comparison with the cooling medium temperature time trend computed by the Simulink® model is necessary: a temperature always lower than 85 °C for the first 2420 seconds of the driving profile is expected while, for the remaining part of the cycle, an almost stable magnitude of 85 °C has to characterize the coolant temperature thanks to the intervention of the radiator. The final result of the simulation, represented by the cooling medium temperature necessary for the comparison, is going to be analyzed in the following sections but, at the moment, it is possible to state that is reasonable that the coolant temperature remains lower in the first section of the cycle because the engine has started from a cold condition and, moreover, because the most severe velocity profile is located at the end of the driving program. In particular, it is precisely around second 2420 that the HWFET cycle begins, imposing to

the vehicle a speed profile of high intensity; this leads to an increased combustion heat rate generated by the engine that strongly warms up the coolant requiring the opening of the thermostat and, finally, the intervention of the radiator.



**Figure 4.14 - Radiator heat rate time trend**

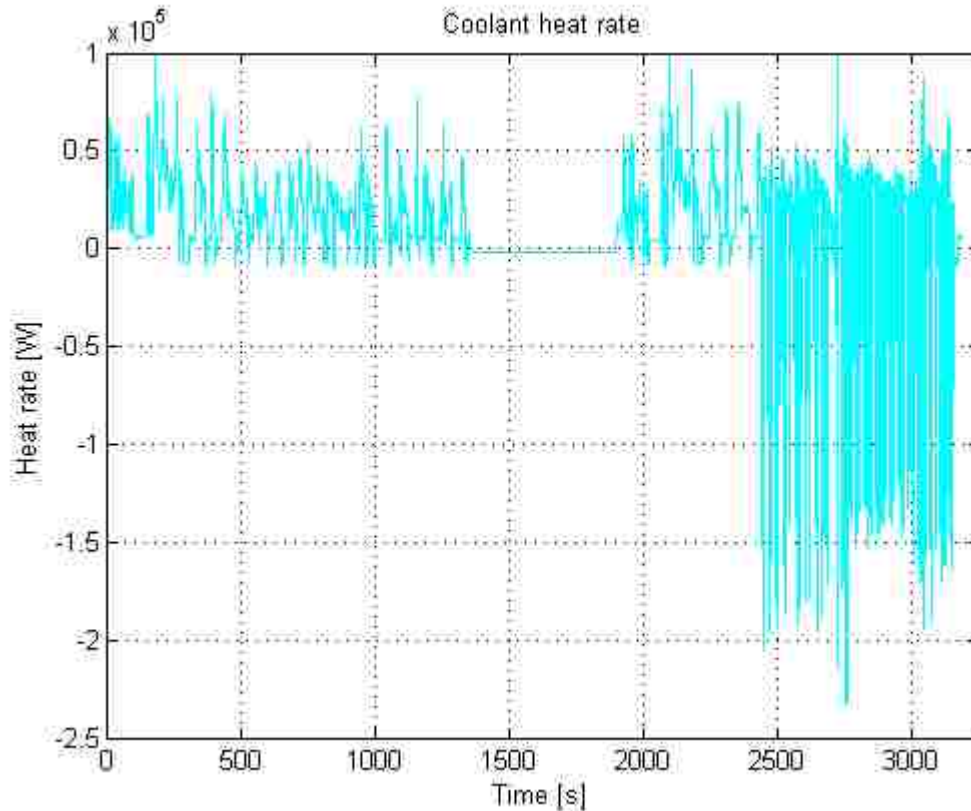
In fact, from the analysis of Figure 4.14, it is possible to point out that, starting from second 2420, the radiator begins to dispose part of the heat of the coolant to the external ambient, trying to maintain the whole cooling circuit at a constant temperature of 85 °C, deemed to be the best for the mechanical operations of the 3.6-L Pentastar engine. The instantaneous magnitude of the radiator heat rate, as can be seen from the picture, is quite high and this is correct since the coolant has acquired a lot of heat during the first 2420 seconds of the cycle and, moreover, because the operations of the radiator are limited to a short period of time, necessary to take the temperature again under the 85 °C limit that the coolant has just exceeded.

As soon as the temperature of the ICE cooling medium comes back to a value lower than the limit imposed by the user, the ECU signal assumes a 0 value and determines the closure of the thermostat: the coolant temperature begins again to rise until the ECU signal switches to a 1 value opening the passage to the radiator, whose final purpose is to remove a considerable amount of heat from the cooling circuit in order to maintain the thermal control of the engine.

#### **4.2.2.8 Analysis of the coolant heat rate**

In order to reach the final target of computing the engine coolant temperature time trend, the Simulink® tool calculates during time the amount of heat instantaneously acquired by the coolant, subtracting all the heat losses contributions to the combustion heat rate values. Figure 4.15 depicts the time trend of the coolant heat rate during the whole driving cycle considered for the simulation and, in this regard, a careful analysis of its fashion is necessary to understand how the thermal phenomena characterize the operations of the engine cooling system. A progressive analysis of the graph below could be useful to better interpret the meaning of the time trend shown by the heat rate going to or leaving the coolant.

- During the “cold start” phase of the FTP-72 program, the coolant begins to acquire a considerable heat amount, since the thermostat is closed and the cooling medium flows through a bypass circuit where it is warmed up rapidly. When the velocity peak of more than 90 km/h is requested by the profile around second 250, the amount of combustion heat rate goes over the value of 120 kW and so the coolant acquires a considerable amount of heat that leads, as it is going to be described in the next section, to a sharp increase of its temperature. The infrequent idle conditions determine a negative coolant heat rate magnitude that, however, lasts for a period that is too short to cause a decrease in the cooling medium temperature. The mean velocity magnitude requested during the “cold start” phase is of 43.585 km/h and it leads to an average heat rate of 23.959 kW going to the coolant.



**Figure 4.15 - Coolant heat rate time trend**

- During the “transient” phase of the FTP-72 cycle, that starts around second 500, the medium speed value settles at 27.494 km/h leading to a lower request of combustion heat rate and, finally, to a lower amount of heat acquired by the coolant. An average heat rate of 15.719 kW is in fact going to the cooling circuit during this phase and, finally, this is reasonable since a combustion heat rate almost always lower than 60 kW is generated by the Pentastar engine from around second 500 to 1300 of the cycle. The frequent idle events, moreover, determine some negative coolant heat rate conditions that cause instantaneous reductions of the coolant temperature, too fast and weak to be detected.
- During the 10 minutes ICE switch off phase, since the speed profile of the driving cycle settles on the abscissa axis, a complete fuel cut-off takes place leading to a null combustion heat rate production. Moreover, the zero engine angular speed and fuel mass flow rate going to the cylinder, cause a null mechanical power, exhaust and cabin heater heat rates; the only heat contribution that remains

different from zero is the one represented by the thermal exchange taking place between the engine's walls and the surroundings through convection. In fact, since the coolant has a relevant thermal inertia and its temperature has already reached considerable values, it tends to remain on high magnitudes that generate a thermal gradient between the engine surface and the ambient air. In particular, during the 10 minutes engine stop phase, a constant surroundings heat rate of about 2 kW characterizes the engine operations, removing heat from the coolant and leading to a decrease of its temperature (that, however, is negligible given the weak intensity of the phenomenon).

- During the final “hot start” phase of the FTP-72 program, that begins and ends around seconds 1900 and 2420, a coolant heat rate time trend similar to the one of the “cold start” phase characterizes the engine cooling circuit because the two speed profiles are identical. The coolant is acquiring again a considerable quantity of heat and, finally, its temperature is increasing approaching the opening limit of the thermostat.
- During the HWFET driving program, finally, the excitation of the engine reaches its maximum since a more intense speed profile is requested with a mean velocity value of 79.248 km/h. The combustion heat rate touches considerably high magnitudes and causes the opening of the thermostat that, to avoid dangerous overheating of the engine, lets the coolant flow to the radiator in such a way it can dispose part of its heat to the external air flowing across the tubes of the U-pattern exchanger. The driving cycle periods characterized by a negative coolant heat rate are very frequent during the highway program because the coolant temperature tends continuously to exceed the 85 °C limit and, because of this, the thermostat and radiator intervene to maintain the thermal control of the engine. As it can be seen from Figure 4.15, the radiator is able to remove up to about 200 kW of heat from the coolant determining a sharp instantaneous decrease of its temperature that has not to exceed the maximum limit imposed by the user depending on the investigated engine model. Obviously, once the coolant temperature has become again lower than 85 °C, the thermostat returns closed and the coolant stops losing heat while acquires energy from the combustion; an average heat rate of 420.362

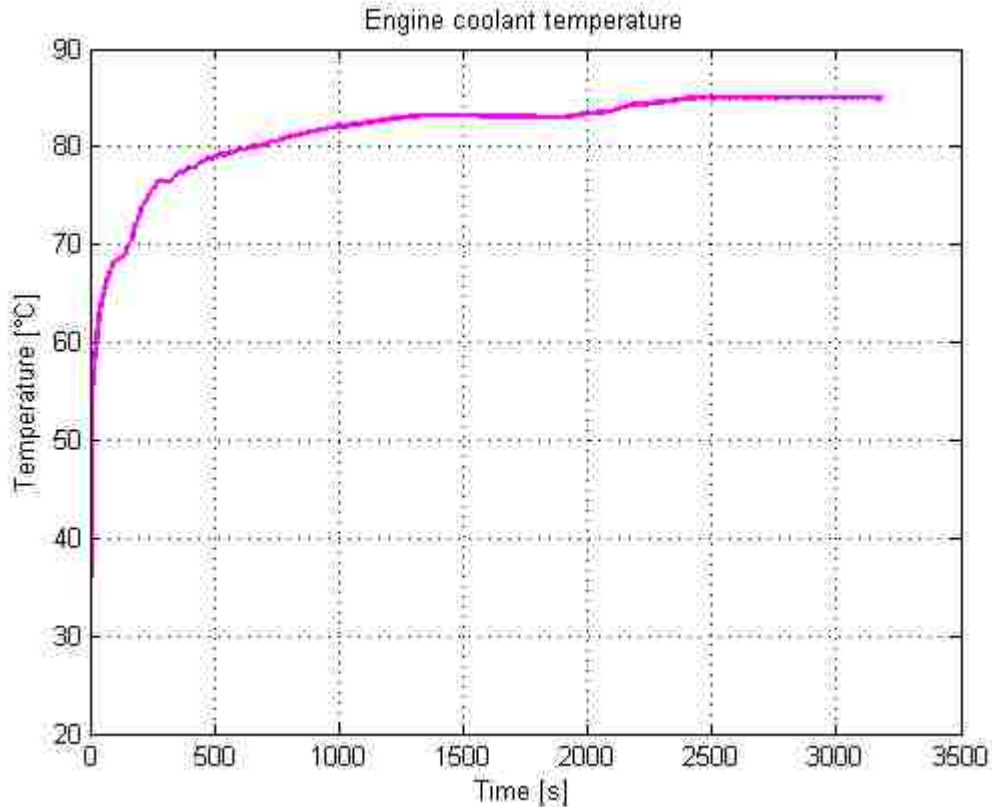


W is finally going to the coolant during the HWFET cycle, representing a condition of thermal equilibrium necessary to maintain the coolant at the constant temperature of 85 °C.

#### **4.2.2.9 Analysis of the coolant temperature time trend**

Now that the coolant heat rate has been determined by the tool, the computation of the engine coolant temperature is possible and is performed by the Simulink® model through the logical loop described in section 3.3.3.7. Figure 4.16 depicts the engine coolant temperature time trend and, hence, represents the final result of the simulation that, moreover, is going to represent the new input of the overall Chrysler prediction software, necessary to better describe the operations of the internal combustion engine of the investigated hybrid electric vehicle model. A careful analysis of the picture below is necessary to understand if the result reflects the time trend of the different heat contributions presented in the previous sections and, finally, if the output of the engine thermal model is characterized by a reasonable trend and accuracy level. As a starting point, it has to be underlined that a boundary condition has been imposed to fix the initial temperature of the coolant and of the whole engine device at the ambient level of 20 °C.

Until second 500, during the “cold start” phase of the city driving program, the temperature of the coolant computed by the engine thermal model experiences a sharp increase from 20 °C up to about 80°C; this is due to a considerable average heat rate of 23.959 kW acquired by the coolant from the heat of combustion that, finally, determines such a high temperature increase inside the ICE cooling circuit. The coolant, in this phase, is flowing through the engine bypass channel because the thermostat is obviously closed and, in this way, the whole ICE block is rapidly led to the high-temperature state necessary to decrease the mechanical friction existing between its moving parts and components. Moreover, such a rapid temperature increase, is due to the fact that the coolant is at 20 °C at the beginning of the driving cycle and so it has a low thermal inertia that makes it capable of rapid and intense temperature changes.

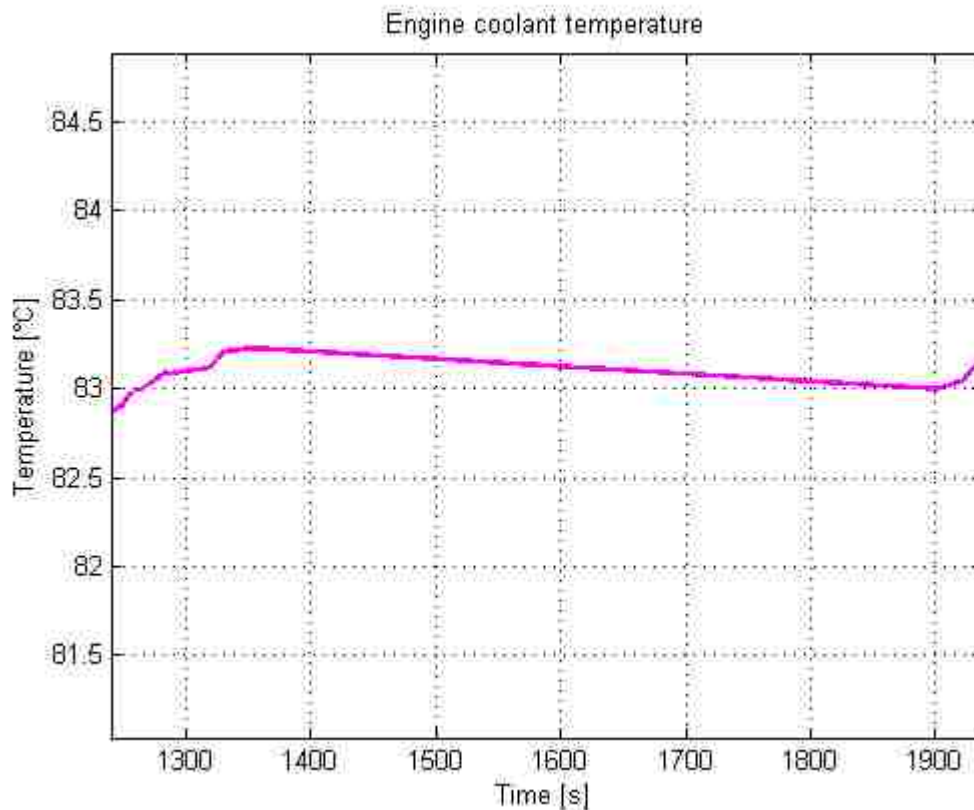


**Figure 4.16 - Engine coolant temperature time trend**

Then, during the “transient” phase of the FTP-72 cycle, that takes place approximately between seconds 500 and 1300, the temperature increase experienced by the coolant is lower than before and due to a less sustained speed profile requested to the vehicle by the driving cycle. The medium speed value settles in fact at 27.494 km/h and the related average combustion heat rate at 23.459 kW, both considerably lower than the medium speed and combustion heat rate values of 43.585 km/h and 35.169 kW that characterize the “cold start” phase of the cycle. Moreover, since at the end of the first phase of the profile the coolant has already reached a high temperature magnitude of about 80 °C, its thermal inertia is increased making difficult to witness further intense temperature rises.

During the 10 minutes ICE stop phase, instead, a slight decrease of the engine coolant temperature can be highlighted and this descending trend is presented in Figure 4.17. The switch off phase begins around second 1300 and lasts until second 1900, when the speed profile presents again non zero values; during this idle phase, the engine is not

burning fuel and so the combustion heat rate assumes null values as it happens to the mechanical power, exhaust, cabin heater and radiator heat rates. The only heat contribution that assumes non zero values during this phase of the driving cycle is the surroundings heat rate: the thermal losses of the engine's walls, in fact, continue to take place for convection with the external air and determine a decrease of the coolant temperature that can be analyzed in the picture below.



**Figure 4.17 - Engine coolant temperature detail (seconds 1300/1900)**

Since the surroundings heat rate magnitudes during the 10 minutes ICE stop phase is only about 2 kW, the temperature decrease of the coolant is almost negligible (less than 0.5 °C); nevertheless, its presence is very important because it gives validity to the results obtained at the end of the simulation. During a fuel cut-off event, in fact, the only thermal phenomenon that characterizes the engine behaviour is represented by a heat loss to the surroundings that, obviously, must determine a decrease of the cooling circuit temperature that has not to be so high given the low intensity of such a thermal exchange.

Starting from second 1900, a new temperature increase of the cooling medium is computed by the software; it approximately ends around second 2420 and is due to the new intense combustion heat rate production taking place during the “hot start” phase of the cycle. As a difference from the starting instant of the simulation, when the coolant has a temperature of 20 °C, at second 1900 its thermal inertia is very high and the consequent temperature gradient caused by the “hot start” profile has a considerably low magnitude, even if the thermal solicitation is the same of the “cold start” phase. Then, around second 2420, the temperature of the cooling medium is finally going to reach the opening limit of the thermostat, fixed by the user before running the simulation at 85 °C, on the basis of the thermal characteristics of the 3.6-L Pentastar engine.

The last part of the investigated driving cycle is represented by the HWFET highway program that, starting around second 2420 and characterized by an intense speed pattern having a 77.580 km/h medium value, finally determines the overcoming of the thermostat opening temperature limit of 85 °C. The average combustion heat rate generated during the HWFET cycle is of 45.126 kW and it leads, precisely, to the opening of the thermostat that, in this way, lets the coolant flow inside the radiator: the amount of heat acquired by the coolant without the intervention of the radiator would be in fact too high and would determine an uncontrolled thermal state of the engine. As soon as the temperature of the cooling medium exceeds the 85 °C limit, around second 2420, the ECU switching signal sent to thermostat assumes a 1 value and, at the same time, the Simulink® model starts to take into account the radiator heat rate for the calculation of the heat amount leaving the engine coolant; instead, as soon as the temperature of the cooling medium becomes again lower than the opening limit of the thermostat, the ECU signal switches to a 0 value, the radiator heat rate is fixed as null by the software and, in this way, the coolant temperature starts again to rise.

Thinking about the concepts described right now it is clear that, thanks to the opening/closing behaviour of the thermostat that allows to control the coolant flow to the radiator, the temperature inside the engine cooling circuit is continuously changing once the 85 °C limit has been reached during the HWFET profile; in particular, the coolant temperature time trend assumes a sawtooth waveform that oscillates around the 85 °C limit itself, as depicted in Figure 4.18.

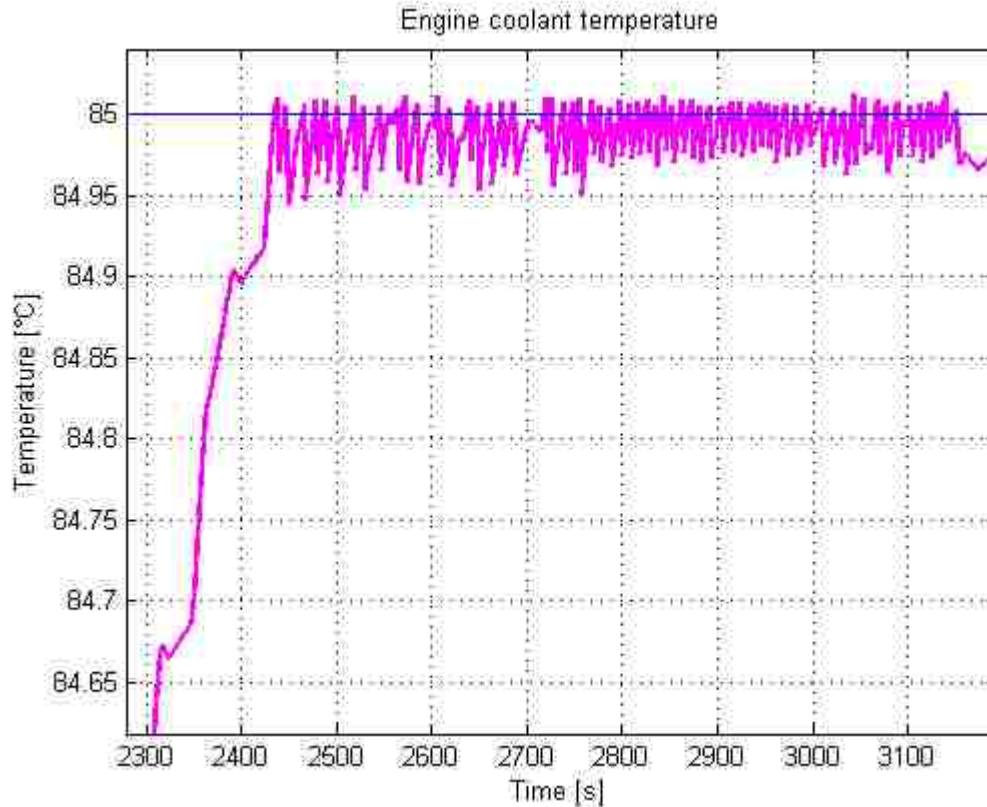


Figure 4.18 - Engine coolant temperature detail (seconds 2300/3200)

In the picture above, the magenta curve and the blue horizontal line represent the engine coolant and thermostat opening temperatures respectively; from a rapid analysis of the graph it is possible to note that, as soon as the coolant temperature exceeds the thermal limit imposed by the user, it immediately decreases thanks to the radiator intervention and becomes again lower than 85 °C. At this point, the thermostat deflects the coolant flow to the bypass circuit where the heat rate generated by the combustion of the fresh charge leads to a further temperature increase that, once the 85 °C limit is exceeded again, determines the new opening of the thermostat.

The coolant temperature time trend depicted in Figure 4.18 demonstrates that the ICE thermal model well represents the behaviour of a typical engine cooling system: the operations of the thermostat are actively determined by the instantaneous values of the coolant temperature that, detected within the logical structure of the Simulink® model, defines if the thermostat is closed or open and, consequently, if the coolant flows through the radiator or the bypass warm up circuit. Moreover, the order of magnitude of all the

heat rate contributions perfectly fits the real dynamic of the phenomenon and leads to an overall coolant temperature time trend that, as carefully explained in the previous paragraphs, correctly follows the physical excitations determined by the investigated driving cycle. To conclude, a thorough analysis of the cooling medium temperature order of magnitude demonstrates that the engine thermal model correctly combines all the input variables defined by the Matlab® base file and, finally, realizes a reliable logical and computational path that makes the software universally usable to simulate the thermal behaviour of internal combustion engine devices.

#### **4.2.3 Internal combustion engine cooling system model validation phase**

It has been highlighted that the results generated by the engine thermal model are characterized by reasonable and reliable time trends and magnitudes, well reflecting the dynamic excitations typical of the driving cycle considered for the simulation. In particular, starting from Figure 4.5, it has been conducted a thorough analysis of all the output graphs created by the software in order to understand if their tendencies respect the input velocity profile of the cycle. The analysis has been performed for all the heat rate contributions and, finally, for the engine coolant temperature that represents the main investigated variable that the tool has to compute: all the evaluations made at the end of the study have been positive and satisfying, giving validity to the whole logical and computational structure of the model.

However, in order to objectively prove the validity of the engine thermal tool, an experimental validation activity is necessary and recommended; it must be done through a comparison between a certain simulated result and its correspondent experimental data set, acquired using the suitable sensors during a physical test procedure on the investigated component. For this case of study, it would be perfect to compare the ICE coolant temperature time trend simulated by the model with experimental temperature data detected, through thermocouples, during tests conducted in the Thermal and NVH department labs at Chrysler. Obviously, the experimental test has to be done on the same engine device and for the same driving cycle that have been considered for the simulation: for the present work, a 3.6-L Pentastar V6 engine has to be tested on a dynamometer while running a “modified” FTP-75 driving profile. Some thermal sensors

have to be suitably placed inside the engine cooling circuit in order to detect the coolant temperature magnitude during every instant of the cycle; then, the experimental temperature curve obtained in this way has to be plotted together with the one simulated by the Simulink® software. If the tendencies and magnitudes of the two curves are similar, it can be stated that the model has been experimentally validated and can work as desired for every type of ICE and driving program that the user wants to investigate. Following Figure 4.19 represents the result of the validation activity conducted for the current case of study and purpose of the thesis project.

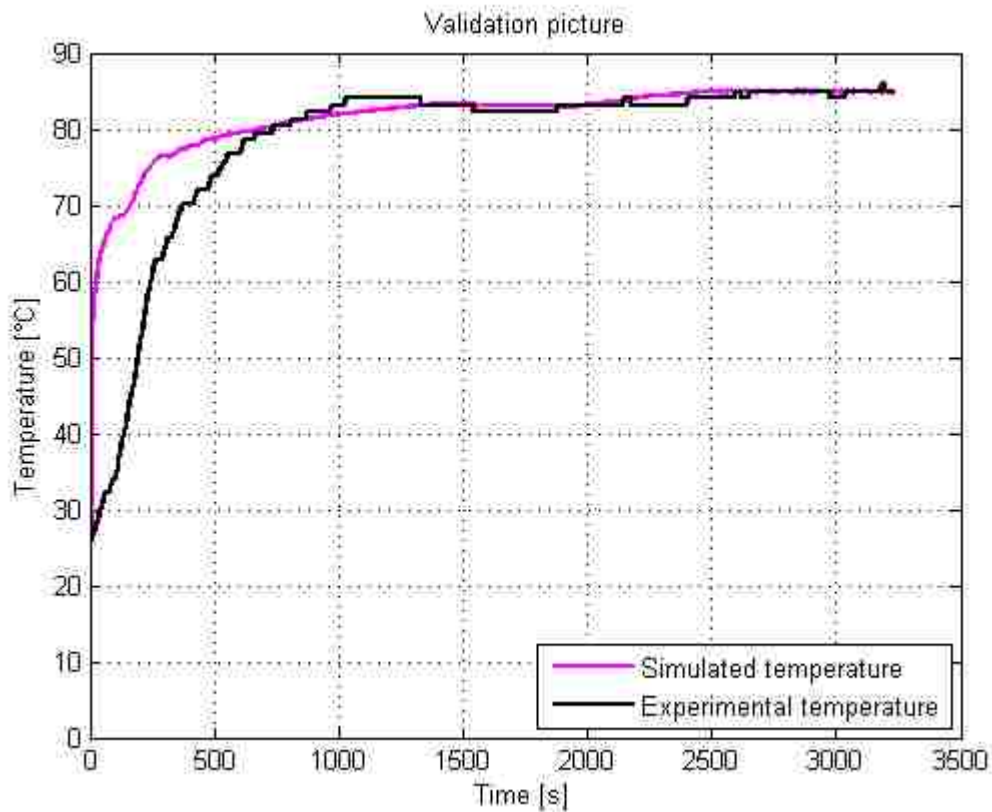


Figure 4.19 - Engine cooling model validation picture

The magenta curve in Figure 4.19 represents the engine coolant temperature simulated by the ICE thermal model while the black one should represent the time trend of the same temperature, experimentally detected during physical tests at the Chrysler labs; however, all the tests set up by the Thermal and NVH teams while working on the 3.6-L Pentastar engine model do not provide with experimental data related to such a

coolant temperature. The final product of the dynamometer test procedures is represented by an Excel® file containing all the data detected through suitable sensors to characterize the evolution of the thermodynamic variables determining the engine behaviour; these quantities are expressed with respect to the driving cycle time vector and can be managed through the Matlab® base file in order to perform validation activities.

Unfortunately, the experimental tests realized on the Pentastar ICE model while running the investigated “modified” FTP-75 cycle have not been prepared placing thermocouples within the engine cooling circuit but, on the contrary, inside the oil circuit that is composed by channels and lines necessary to allow the correct lubrication of the moving engine parts. The oil, thanks to the intervention of a pump activated by the engine crankshaft through a belt and pulley mechanism, is taken from the sump and supplied to the main lubricating circuit that is provided with specific channels passing through holes drilled inside the shaft and main bearings to allow their lubrication, necessary to ensure the correct operations of the whole engine. The oil is warmed up during the driving cycle similarly to what happens to the engine coolant and, when the whole system reaches the optimum thermal operating condition, the temperature level of the oil and the coolant must be the same. Hence, since experimental data related to the engine coolant temperature are not available for this case of study, the validation can be performed using the oil temperature data that are represented by the black curve in Figure 4.19.

It can be seen that, starting around second 750, the simulated temperature of the engine coolant and the experimental temperature of the engine oil assume similar values and present similar trends, slightly increasing until second 2420, when the thermostat opens determining the intervention of the radiator. For the first 750 seconds of the driving profile, instead, the two temperature trends differ one from the other and a thorough explanation is necessary to understand the meaning of the discrepancy. Figure 4.20 gives important indications related to the time trend characterizing the two temperature curves at the beginning of the simulation and it is evident that, approximately between the 60 °C and 75 °C temperature levels, the tendency of the magenta and black curves is the same but shifted of about 200 seconds; this because, as highlighted in the teal circle on the left of Figure 4.21, the simulated temperature rise of the engine coolant is more rapid than the one of the oil and takes 200 seconds less to reach the 60 °C level.



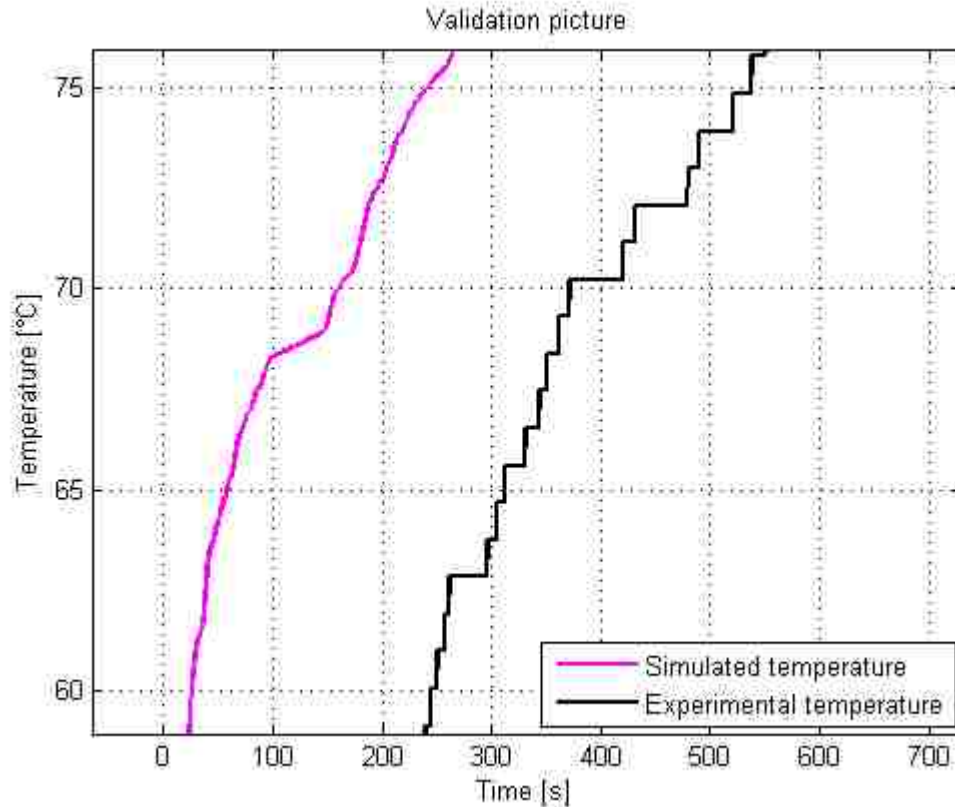


Figure 4.20 - Engine cooling model validation picture detail (seconds 0/700)

After that, the two temperature paths are similar and develop one parallel to the other until both of them converge on the 80 °C level, around second 750 of the cycle, as highlighted in the teal circle on the right of Figure 4.21. The specific simulated engine coolant and experimental oil temperatures evolution, related to the first part of the investigated driving cycle, can be justified considering that the specific heat of the oil is considerably higher than the one of the coolant: in fact, the coolant specific heat is of 3740 J/(kg·K) [53] while the one of a typical engine oil is about 20300 J/(kg·K) [62]. Since the engine coolant specific heat is approximately five times lower than the one of the oil, given a certain quantity of heat acquired by the two fluids, the temperature rise of the coolant is certainly higher and takes place in a shorter period of time leading the cooling medium at the optimum thermal state after a few seconds from the beginning of the cycle. Then, when the temperature of both the coolant and the oil has reached a magnitude higher than 80 °C, their thermal inertia becomes very high making them less likely to change their actual thermal condition; in fact, after second 750, the further

temperature increases are not very high and the time trends of both the curves develop similarly until the opening of the thermostat.

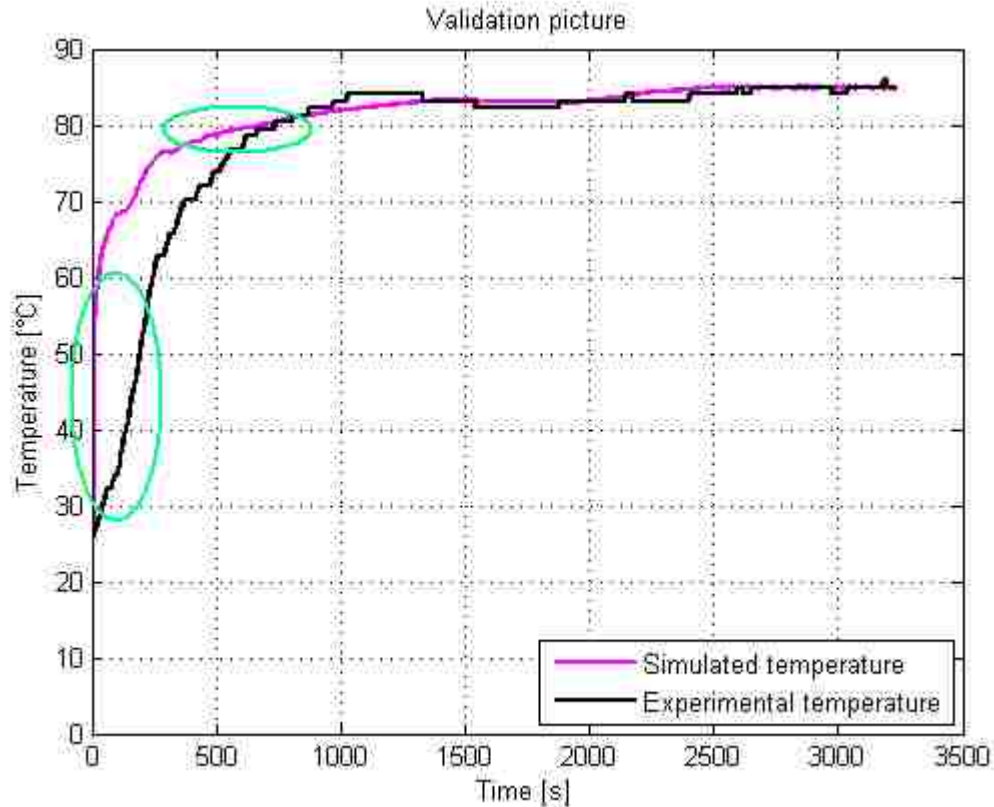


Figure 4.21 - Engine cooling model validation picture with two highlighted sections

Finally, considering the section of the driving profile starting around second 750, it is possible to point out that the simulated coolant temperature and the experimental oil temperature assume approximately the same values and time trends, allowing to validate the operation of the engine thermal model. During the first 750 seconds of the cycle, instead, a considerable discrepancy characterizes the two curves that is caused by the different thermal properties of the fluids: hence, the different initial temperature evolution seems to be reasonable and allows to validate the overall result of the simulation even during the transitory phase of the profile. A complete validation would be possible with experimental data coming from the engine cooling circuit that would allow to realize a precise comparison between the simulated and experimental ICE coolant temperature time trends.

Anyway, the engine thermal model validation described right now can be considered successful, in particular if analyzed together with the discussion of the results presented in section 4.2.2.6; all the outputs computed by the software are reasonable and sufficiently reliable to be used in the overall Chrysler HEV prediction tool to better simulate the thermal behaviour of the investigated engine. At this point, it is possible to integrate the ICE Simulink® model in the Chrysler software and to finally obtain overall HEV fuel economy and performance predictions characterized by a higher level of accuracy: hence, from a company perspective, the design of the new engine thermal tool can be considered successful and of high technical content. Moreover, the software can also be used autonomously to analyze the thermal behaviour of any types of engine model excited by any types of driving profile and to obtain useful indications related to the dynamics of the heat transfer phenomena taking place between the ICE and the whole HEV system. Hence, it is clear that the model is characterized by a notable flexibility level that, considered together with the overall novelties introduced by the software described in section 3.3.5, make it well designed also from an academic point of view.

#### **4.3 Battery cooling system model simulation and validation phase**

A preliminary analysis of the main performance and features offered by the battery cooling system model has been described in the previous chapter, running simulations related to an air cooled solution and using input data received from the battery experts of the Electrified Powertrain department at Chrysler. These simulations have been necessary to evaluate the correctness of the software computations and logical actions and, in particular, have been realized only for preliminary validation purposes. Now, after some meetings and investigations, accurate input data necessary to run thorough simulations have been collected and the actual objective is to conduct an overall analysis intended for the investigation of the best battery thermal scenario, performing also a basic sensitivity study. Considering a battery current profile related to an EPA FTP-72 city driving program, constituted by a “cold start” and a “transient” phase, and a parallel configuration of the battery modules, carefully described in section 3.4.2, a block of simulations has been run to study the HVB temperature time trend and, in particular, to study its dependence on the input variables requested by the model. As it is going to be described

in the following sections, each simulation has been realized storing in an Excel® file the magnitudes of the input data and saving the output graphs generated by the model at the end of the data elaboration; in particular, the simulations have been realized “in blocks”, changing for each block the value of a single input datum and plotting together the final battery temperature curves calculated by the software. In this way, it is possible to understand the influence that this specific input datum has on the thermal behaviour of the HEV battery pack and to obtain indications about its optimum magnitude necessary to reduce the thermal solicitation of the HVB. The possibility to conduct such a thorough study on a specific battery pack equipping a hybrid vehicle running a certain driving cycle, it is offered by the flexibility of the model that can work as an autonomous simulation tool and not only as an integral part of the overall Chrysler HEV prediction software. The results of the simulations that are going to be described in the following sections are characterized by a notable level of accuracy, because the input data obtained from the Electrified Powertrain teams are highly accurate and reliable and allow to conduct a meaningful basic sensitivity study.

#### **4.3.1 Battery pack and driving cycle characteristics and input data**

As explained before, the specific target of the current analysis is to run various simulations using different input data magnitudes and, in particular, studying different battery pack geometries and cooling solutions. Hence, for each simulation block, the input data stored in the Matlab® “Workspace” and entering the Simulink® model are different and are going to be specifically described before running the simulation and analyzing its related results. In order to obtain an orderly and organic work, the overall organization of the following sections is going to be characterized by the presence of a input data table and of the final battery temperature trend graph obtained at the end of the simulation, that is going to be investigated in details. All the input variables of the battery thermal software have been listed and described in the previous chapter but another analysis could be useful to better prepare the study of the results.

- Battery current profile: the thermal behaviour of the battery pack modules is primarily defined by the profile of the current that flows inside the cells, determining the heat dissipation for Joule effect. The profile considered for all the

simulations relates to an EPA FTP-72 city driving program, in a charge sustaining or depleting mode, plotted in below Figure 4.22; it has to be remembered that the charge depleting mode takes place when the battery gives energy to the electric motor to realize a pure electric or hybrid motion while the sustaining mode consists in the recharge action of the HVB.

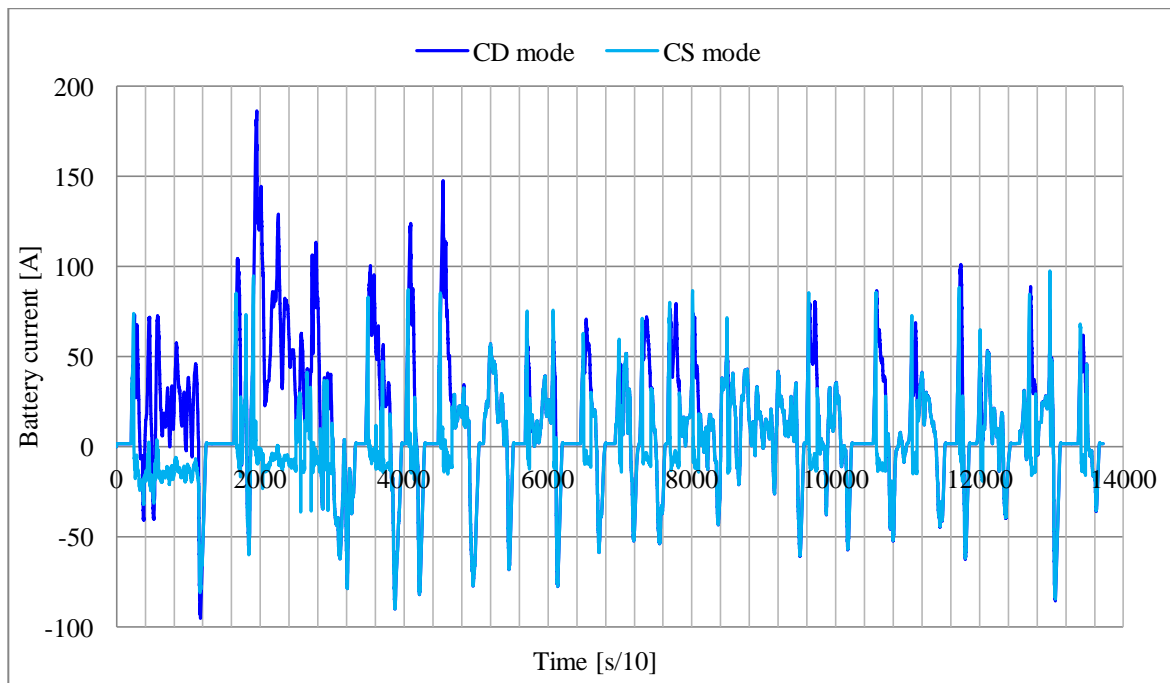


Figure 4.22 - Battery current profile (FTP-72 driving cycle, charge depleting and sustaining modes)

- Battery internal resistance: the internal resistance of the battery is determined by the electrochemistry solution and defines the magnitude of heat dissipation taking place during the investigated driving cycle; typical values used for the simulations range from 1 to 5 m $\Omega$ .
- Cells geometry: the dimensions of the modules and their location inside the battery pack have a considerable influence on the heat exchange phenomena taking place during the HEV operations. Hence, it is important to thoroughly define the height ( $h$ ), width ( $w$ ) and length ( $l$ ) of the cells, together with the distance existing between two adjacent modules ( $d$ ).
- Anode and cathode current collector thicknesses: a copper anode and aluminum cathode current collectors have been considered to model the internal layered

structure of the cells and, in particular, their thickness has been taken into account as varying on the basis of the adopted internal constructive solution. Since the copper and aluminum have been always chosen as the material constituting the anode and cathode collectors, their thermal characteristics have been defined as constant for every simulation. At the same time, also the thickness of the polymer separator has been taken as a constant input for all the cases of study.

- Number of cells: a very important quantity to be defined at the beginning of a simulation is represented by the number of modules constituting the battery pack that covers a decisive role in the definition of the thermal behaviour of the HVB device. In modern HEV NiMH or PHEV/BEV Li-Ion batteries applications, the number of cells is always a multiple of twelve since the logical circuits that constitute the battery management system control unit are organized in channels of twelve parallel transmission lines; the number of these lines determines the computational speed of the control unit and, at the same time, the processing power requested by the hardware and, in this regard, the twelve-BUS technology is the best compromise between the two fighting needs.
- Coolant mass flow rate: the amount of coolant entering instantaneously in the battery pack and flowing between its modules is defined at the beginning of every simulation and it has a considerable influence on the temperature time trend of the whole HVB device. The specific input of the model is represented by the coolant volume flow rate and so it is necessary to know the density of the cooling medium to define its mass flow rate; the unit of measure considered for the input data is the cfm (cubic feet per minute), suitably converted in  $\text{m}^3/\text{s}$  and then in  $\text{kg}/\text{s}$  by the Matlab® base file code.
- Coolant type: the type of coolant used for the simulation has a strong influence on the heat exchange phenomena taking place inside the battery pack because, depending on the considered type of fluid, it is necessary to use the suitable density, specific heat and convective heat transfer coefficient magnitudes that determine the cooling performance of the HVB device. Since the battery pack modeling phase has been realized considering a typical parallel configuration used for hybrid electric vehicles, the specific technology that must be taken into

account is the NiMH one thermally managed with a forced air cooling solution and so the coolant type to be considered is the air. Moreover, also a 50-50 water-glycol solution has been investigated to compare gaseous and liquid cooling systems, even if for the current work it would not be reasonable to consider such a type of coolant because the modules have been considered as completely submerged in the cooling medium (a dielectric liquid solution should be used instead of a water-glycol mixture).

- Ambient temperature: the temperature level of the surrounding ambient must be fixed for each simulation and it has been taken always equal to 29.85 °C (303 K). It defines the initial thermal state of the battery cells and of the cooling medium at the inlet and outlet sections of the battery pack.

#### **4.3.1.1 Definition of the main simulation cases of study**

In the following sections, the various simulations conducted using the newly designed battery thermal model are going to be presented and described in details; in particular, for each simulation, a table of the input and the final battery pack temperature time trend graph are going to be analyzed to study the thermal operations of the investigated HVB device. In order to conduct a basic sensitivity study, the magnitudes of all the input variables listed in the previous sections have been changed step by step and a lot of input matrixes have been created: the purpose is to conduct many simulations related to different electric, geometric and thermodynamic configurations of the battery pack, investigating all the possible combinations of the various input quantities requested by the model.

To simplify the analysis of the simulation results, some main cases of study have been isolated fixing some quantities of the input matrixes that are going to be stored in the Matlab® “Workspace” and changing, for each of these matrixes, other specific variables whose influence on the battery temperature represents the main object of study. For example, fixing the modules geometry, their internal resistance and the type of cooling medium, the number of cells and the coolant volume flow rate are respectively changed to investigate their influence on the thermal behaviour of the HVB device. Some basic configurations of the input matrixes are going to be presented in the following, setting the

geometry of the modules, the thickness of the anode and cathode current collectors and, finally, the type of coolant used to maintain the thermal control of the battery. The internal resistance of the cells, their overall number and the cooling medium volume flow rate represent, instead, the input quantities varying for each simulation and defining the specific temperature curves plotted by the model at the end of the computations. Moreover, also the input current profile can be changed, considering a charge depleting or a charge sustaining mode of operation of the high voltage battery that equips the investigated hybrid electric vehicle model.

#### 4.3.1.2 List of the main simulation cases of study

Given all the quantities presented in section 4.3.1, they have been suitably combined to generate on Excel® some input matrixes from where the Matlab® base file of the battery thermal model picks up the specific values to be associated to the correspondent input variables. Figure 4.23 gives an idea of the upload procedure managed by the Matlab® code that, given the Excel® file “Input matrixes”, takes from the cells C50, B50 and D50, the width, height and length values of the modules and associates them to the suitable variables elaborated on the Simulink® platform.

```
w = xlsread('Input matrixes.xlsx','Foglio5','C50'); %[m] Cell width.  
h = xlsread('Input matrixes.xlsx','Foglio5','B50'); %[m] Cell height.  
l = xlsread('Input matrixes.xlsx','Foglio5','D50'); %[m] Cell length.
```

Figure 4.23 - Upload procedure Matlab® code

These values can be fixed for all the simulations while other ones can be continuously changed to investigate their influence on the thermal behaviour of the battery; in the following sub-sections, in particular, are listed the main simulation cases of study with their related input matrixes, containing the constant variables fixed by the user for the investigated simulation.



#### 4.3.1.2.1 Case of study A

In Table 4.3 are listed the cell dimensions values, the anode and cathode current collectors thickness magnitudes and, finally, the type of coolant considered for all the A-type simulations. The air density is  $1.225 \text{ kg/m}^3$  [52], its specific heat is equal to  $1006.1 \text{ J/(kg}\cdot\text{K)}$  [51] and its convective heat transfer coefficient is  $100 \text{ W/(m}^2\cdot\text{K)}$  [55]. For the simulation results that are going to be presented in the next sections, when speaking about an A-type case of study, the modules geometry, coolant type and current collectors thickness are going to be defined with respect to the values contained in Table 4.3.

Table 4.3 - Main input values considered for the A-type simulations

Cell height	Cell width	Cell length	Coolant type	Anode th.	Cathode th.
80.5 mm	12.5 mm	120.0 mm	Air	12 $\mu\text{m}$	20 $\mu\text{m}$

#### 4.3.1.2.2 Case of study B

In Table 4.4 are listed the cell dimensions values, the anode and cathode current collectors thickness magnitudes and, finally, the type of coolant considered for all the B-type simulations. The 50-50 water-glycol mixture density is  $1083 \text{ kg/m}^3$  [63], its specific heat is equal to  $3740 \text{ J/(kg}\cdot\text{K)}$  [53] and its convective heat transfer coefficient is  $897 \text{ W/(m}^2\cdot\text{K)}$  [64]. For the simulation results that are going to be presented in the next sections, when speaking about a B-type case of study, the modules geometry, coolant type and current collectors thickness are going to be defined with respect to the values contained in Table 4.4.

Table 4.4 - Main input values considered for the B-type simulations

Cell height	Cell width	Cell length	Coolant type	Anode th.	Cathode th.
80.5 mm	12.5 mm	120.0 mm	50-50 W-G	12 $\mu\text{m}$	20 $\mu\text{m}$

#### 4.3.1.2.3 Case of study C

In Table 4.5 are listed the cell dimensions values, the anode and cathode current collectors thickness magnitudes and, finally, the type of coolant considered for all the C-type simulations. The air density is  $1.225 \text{ kg/m}^3$ , its specific heat is equal to  $1006.1$

J/(kg·K) and its convective heat transfer coefficient is 100 W/(m<sup>2</sup>·K). For the simulation results that are going to be presented in the next sections, when speaking about a C-type case of study, the modules geometry, coolant type and current collectors thickness are going to be defined with respect to the values contained in Table 4.5.

**Table 4.5 - Main input values considered for the C-type simulations**

Cell height	Cell width	Cell length	Coolant type	Anode th.	Cathode th.
91.0 mm	26.5 mm	148.0 mm	Air	12 μm	20 μm

#### 4.3.1.2.4 Case of study D

In Table 4.6 are listed the cell dimensions values, the anode and cathode current collectors thickness magnitudes and, finally, the type of coolant considered for all the D-type simulations. The 50-50 water-glycol mixture density is 1083 kg/m<sup>3</sup>, its specific heat is equal to 3740 J/(kg·K) and its convective heat transfer coefficient is 897 W/(m<sup>2</sup>·K). For the simulation results that are going to be presented in the next sections, when speaking about a D-type case of study, the modules geometry, coolant type and current collectors thickness are going to be defined with respect to the values contained in Table 4.6.

**Table 4.6 - Main input values considered for the D-type simulations**

Cell height	Cell width	Cell length	Coolant type	Anode th.	Cathode th.
91.0 mm	26.5 mm	148.0 mm	50-50 W-G	12 μm	20 μm

#### 4.3.1.2.5 Case of study E

In Table 4.7 are listed the cell dimensions values, the anode and cathode current collectors thickness magnitudes and, finally, the type of coolant considered for all the E-type simulations. The air density is 1.225 kg/m<sup>3</sup>, its specific heat is equal to 1006.1 J/(kg·K) and its convective heat transfer coefficient is 100 W/(m<sup>2</sup>·K). For the simulation results that are going to be presented in the next sections, when speaking about an E-type case of study, the modules geometry, coolant type and current collectors thickness are going to be defined with respect to the values contained in Table 4.7.

**Table 4.7 - Main input values considered for the E-type simulations**

Cell height	Cell width	Cell length	Coolant type	Anode th.	Cathode th.
125.0 mm	45.0 mm	173.0 mm	Air	12 $\mu\text{m}$	20 $\mu\text{m}$

#### **4.3.1.2.6 Case of study F**

In Table 4.8 are listed the cell dimensions values, the anode and cathode current collectors thickness magnitudes and, finally, the type of coolant considered for all the F-type simulations. The 50-50 water-glycol mixture density is  $1083 \text{ kg/m}^3$ , its specific heat is equal to  $3740 \text{ J/(kg}\cdot\text{K)}$  and its convective heat transfer coefficient is  $897 \text{ W/(m}^2\cdot\text{K)}$ . For the simulation results that are going to be presented in the next sections, when speaking about a F-type case of study, the modules geometry, coolant type and current collectors thickness are going to be defined with respect to the values contained in Table 4.8.

**Table 4.8 - Main input values considered for the F-type simulations**

Cell height	Cell width	Cell length	Coolant type	Anode th.	Cathode th.
125.0 mm	45.0 mm	173.0 mm	50-50 W-G	12 $\mu\text{m}$	20 $\mu\text{m}$

#### **4.3.2 Battery cooling system model simulation phase**

Once all the variables defined for the considered case of study have been stored in the Matlab® “Workspace”, the other battery and coolant characteristics have to be determined by the user and uploaded in the model in order to be able to run the overall simulation necessary to analyze the thermal behaviour of the battery pack excited by the investigated driving profile. In particular, for each simulation, it must be defined the main case of study type (A, B, C, D, E or F) and the specific magnitude of the battery internal resistance and coolant volume flow rate, the number of modules contained in the pack and, finally, the mode of operation of the electric energy storage device (charge depleting or sustaining). Once all these input quantities have been defined and uploaded in the virtual computational platform, the simulation can be activated and the Simulink® model finally computes the battery temperature time trend that can be plotted as desired by the user, with respect to the driving profile time vector and together with the coolant temperature calculated at the outlet section of the HVB pack. As underlined in the

previous chapter, moreover, the battery thermal tool can be specifically used to run simulations related to every type of battery pack configuration and geometry and to every type of current profile, thanks to its considerable level of flexibility that makes it perfect to perform specific thermal analysis regarding different types of HVB device and driving cycle.

In particular, the battery cooling system model can be used as an autonomous prediction tool that, not integrated in the overall Chrysler model, can run simulation on its own to analyze the thermal behaviour of the investigated battery, not considered as part of a whole hybrid electric vehicle system but intended as an independent device. Moreover, a basic sensitivity study can be realized through the model by changing one at a time, for each main type of case of study, the magnitude of the variable input quantities not included in the above basic matrixes uploaded by the tool. Considering, for example, three different values of modules internal resistance, the influence of this quantity on the thermal behaviour of the battery pack can be thoroughly investigated, keeping constant all the other input variables requested by the model. At the end of three consecutive linked simulations, a final graph presenting three different battery temperature curves is going to be generated by the software, with each one of the curves representing the temperature time trend of a battery characterized by a specific value of internal resistance.

#### **4.3.2.1 Introduction to the simulations**

In the following sections some simulations are going to be carefully studied, focusing the attention on the specific input matrixes uploaded by the tool and on the final output graphs describing the battery temperature time trend. In particular, in order to develop a well organized analysis of the results, each simulation is introduced by a specific table containing information about:

- the basic case of study (simulation type), defined by a capital letter and containing, in turn, the input data related to the cell geometry, coolant type and thickness of the current collectors;
- the operating mode of the battery, that could be a charge depleting or sustaining mode and defines the electric current profile, as shown in Figure 4.22;

- the internal resistance of the battery, that depends on the specific adopted electrochemistry solution and whose magnitude has been determined in the testing labs of the Electrified Powertrain department;
- the number of modules that constitute the battery pack, always considered as multiples of 12 because of the specific logical connection channels configuration;
- the coolant volume flow rate, defined in cfm and converted in a mass flow rate by the Matlab® base file code using the density of the coolant specified by the considered simulation type.

Each of the following tables, moreover, is characterized by a column composed by more than one cell in relation to the input quantity that is varying for the investigated simulation, in order to perform a study of its influence over the whole battery temperature time trend. In some cases, if the purpose of the study is to compare the thermal behaviour of an air cooled and a liquid cooled battery, the simulation is run two consecutive times using two different basic case of study configurations characterized only by a different coolant type. Finally, at the end of each section, the output graph generated by the battery thermal model at the end of the simulation is represented and accompanied by a detailed analysis of its main characteristics.

#### 4.3.2.2 Simulation - 1

Table 4.9 contains all the specifications that define the input variables background of investigated simulation number 1, aimed at analyze the influence of the modules internal resistance on the battery thermal behaviour. The HVB temperature time trends obtained at the end of the simulation are depicted in Figure 4.24, thoroughly analyzed in the following paragraph.

**Table 4.9 - Input variables background of simulation number 1**

Simulation type	Operating mode	Resistance	Cells number	Coolant rate
A	Charge sustaining	2.0 mΩ	72	100 cfm
		2.8 mΩ		
		5.0 mΩ		

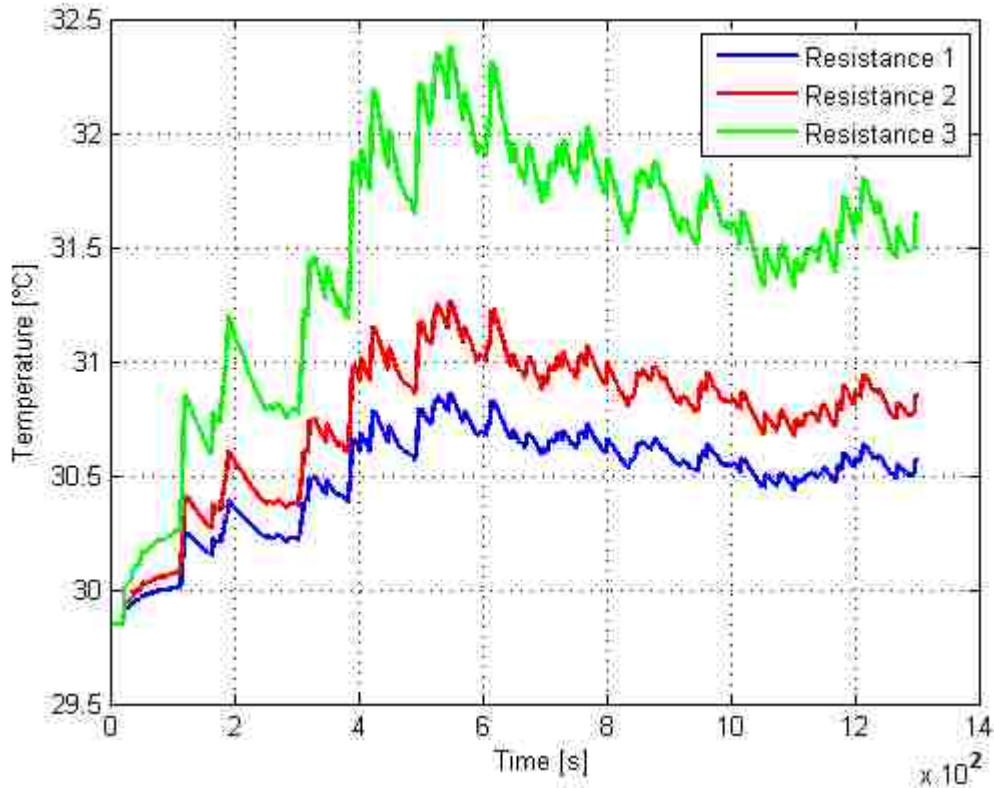


Figure 4.24 - Output graph generated by the simulation number 1

From the analysis of Figure 4.24, it is possible to state that the higher is the internal resistance of the cells and the higher is the temperature increase of the battery during the driving cycle: hence, a direct proportionality exists between resistance and temperature values. Given a certain current profile, in fact, the power dissipation for Joule effect, that causes the temperature increment of the HVB pack, is directly linked to the internal resistance value. The three curves are similar only for the initial 20/30 seconds, after that they assume completely different values satisfying the expectations of a steeper temperature increase in case of a higher battery internal resistance.

Looking at the magnitude of the temperature increase shown in each of the three cases, it is possible to underline that it is not very high but, in general, lower than 3 °C even if considering the highest internal resistance of 5.0 mΩ. This is caused by the fact that a charge sustaining mode is considered for the simulation, that involves a not highly intensive electric current profile characterized by values always lower than 100 A, as can be seen from Figure 4.22. In the following, simulations run using a charge depleting

mode are going to be described and it will be possible to note the presence of a sharper temperature increase, caused by a stronger electric current profile requested to the battery during the driving cycle.

#### 4.3.2.3 Simulation - 2

Table 4.10 contains all the specifications that define the input variables background of investigated simulation number 2, aimed at analyze the influence of the cells number on the battery thermal behaviour. The HVB temperature time trends obtained at the end of the simulation are depicted in Figure 4.25, thoroughly analyzed in the following paragraph.

Table 4.10 - Input variables background of simulation number 2

Simulation type	Operating mode	Resistance	Cells number	Coolant rate
A	Charge sustaining	2.8 mΩ	60	100 cfm
			72	
			84	
			96	

Studying the curves plotted in Figure 4.25, it is possible to underline that the temperature increase of the battery during the driving cycle is directly proportional to the number of modules that constitute the HVB. This is not due by a higher amount of power dissipated inside the pack linked to the higher number of cells because, given the current intensity requested to the battery by the driving profile, this value does not depend on the number of modules contained in the HVB pack. On the contrary, given a fixed amount of coolant mass flow rate, if the number of cells increases then the coolant quantity flowing around a single module shows a certain decrease that, inevitably, leads to an overall worsening of the cooling performance and operations.

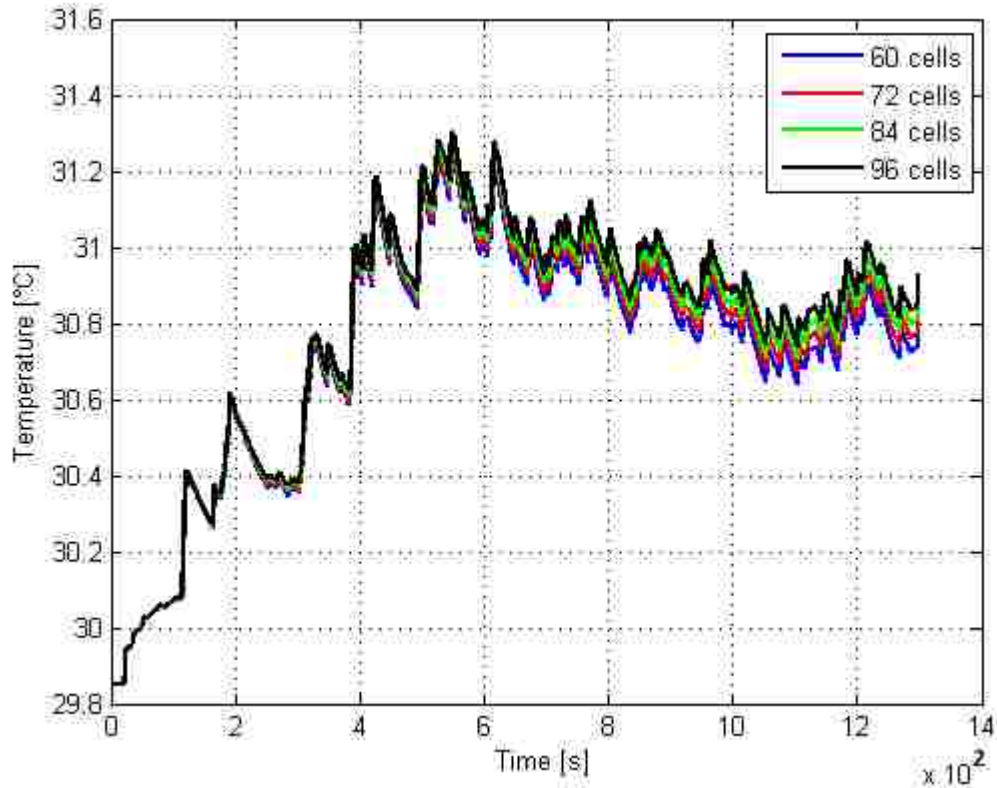


Figure 4.25 - Output graph generated by the simulation number 2

#### 4.3.2.4 Simulation - 3

Table 4.11 contains all the specifications that define the input variables background of investigated simulation number 3, aimed at analyze the influence of the coolant mass flow rate on the battery thermal behaviour. The HVB temperature time trends obtained at the end of the simulation are depicted in Figure 4.26, thoroughly analyzed in the following paragraph.

Table 4.11 - Input variables background of simulation number 3

Simulation type	Operating mode	Resistance	Cells number	Coolant rate
A	Charge sustaining	2.8 mΩ	72	10 cfm
				50 cfm
				100 cfm



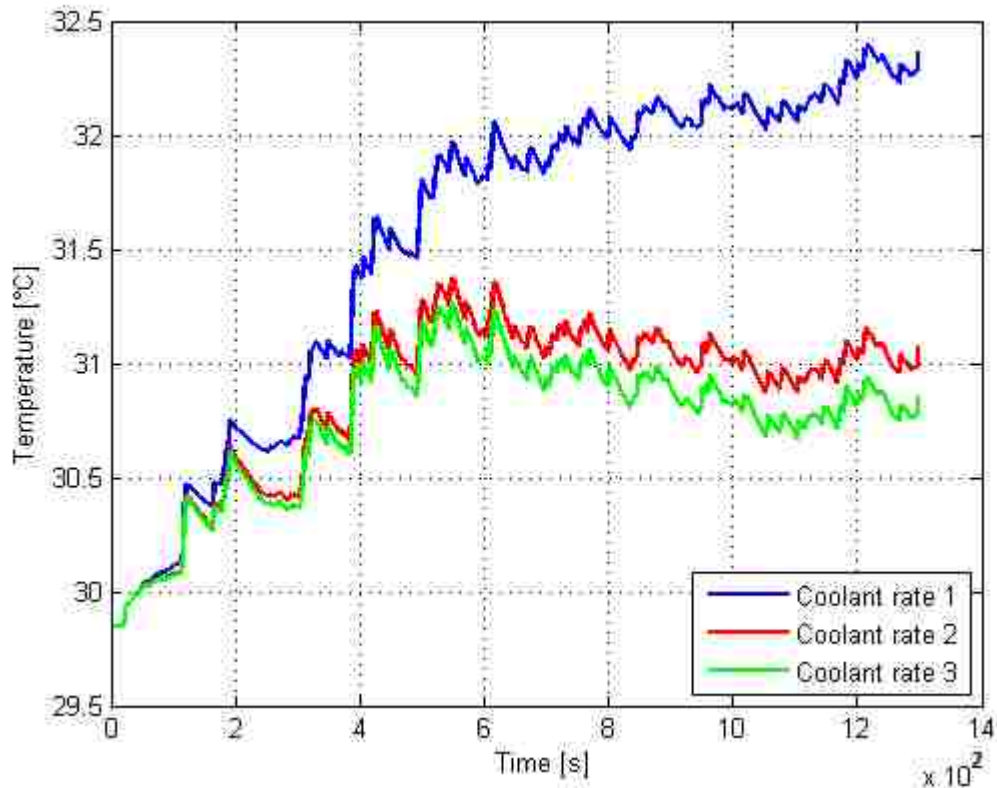


Figure 4.26 - Output graph generated by the simulation number 3

Looking at Figure 4.26, it is possible understand how a higher coolant volume (and mass) flow rate leads to a lower temperature increase inside the battery pack; this is a logical consequence of the higher amount of cooling medium that, instant per instant, touches the external surfaces of the modules allowing a more intensive thermal exchange and so a more effective heat dissipation from the cells. Hence, in case the current profile requested by the investigated HEV to its HVB device is characterized by high magnitudes, it is possible to increase the amount of coolant flowing inside the pack to ensure its thermal control even if its excitation state is highly sustained. In particular, considering the red and green curves, it can be seen that after the first 500 seconds of the cycle, characterized by the more intense current profile, the battery temperature begins to decrease thanks to a sufficiently high quantity of coolant that flows between the modules of the pack and that is able to ensure the desired thermal control of the HVB device at steady state. In case of a lower coolant volume flow rate, represented by the blue curve of Figure 4.26, the battery temperature continues to rise at steady state, not allowing to limit

the maximum temperature reached by the pack even if the current profile has become less sustained: in general, it is clear the necessity to use a sufficiently high quantity of coolant to guarantee that the heat dissipation for Joule effect can be controlled, in particular regarding the maximum temperature reached by the battery that, for operating and safety reasons, must remain under strictly specified values. To conclude, it is important to underline that, increasing the amount of air flowing inside the battery pack to maintain its controlled thermal state, the amount of power necessary to activate the air fans rises, leading to an overall increase of energy consumption determined by the forced air cooling system of the HEV battery.

#### 4.3.2.5 Simulation - 4

Table 4.12 contains all the specifications that define the input variables background of investigated simulation number 4, aimed at analyze the influence of the coolant type on the battery thermal behaviour. The HVB temperature time trends obtained at the end of the simulation are depicted in Figure 4.27, thoroughly analyzed in the following paragraph.

**Table 4.12 - Input variables background of simulation number 4**

<b>Simulation type</b>	<b>Operating mode</b>	<b>Resistance</b>	<b>Cells number</b>	<b>Coolant rate</b>
<b>A</b>	Charge sustaining	2.8 mΩ	72	100 cfm
<b>B</b>				

In Figure 4.27, the blue curve represents the case of an air cooled battery pack while the magenta one refers to a HVB cooled by a 50-50 water-glycol solution; it is necessary to underline that, in both the cases, the coolant volume flow rate entering the pack is the same and equal to 100 cfm.

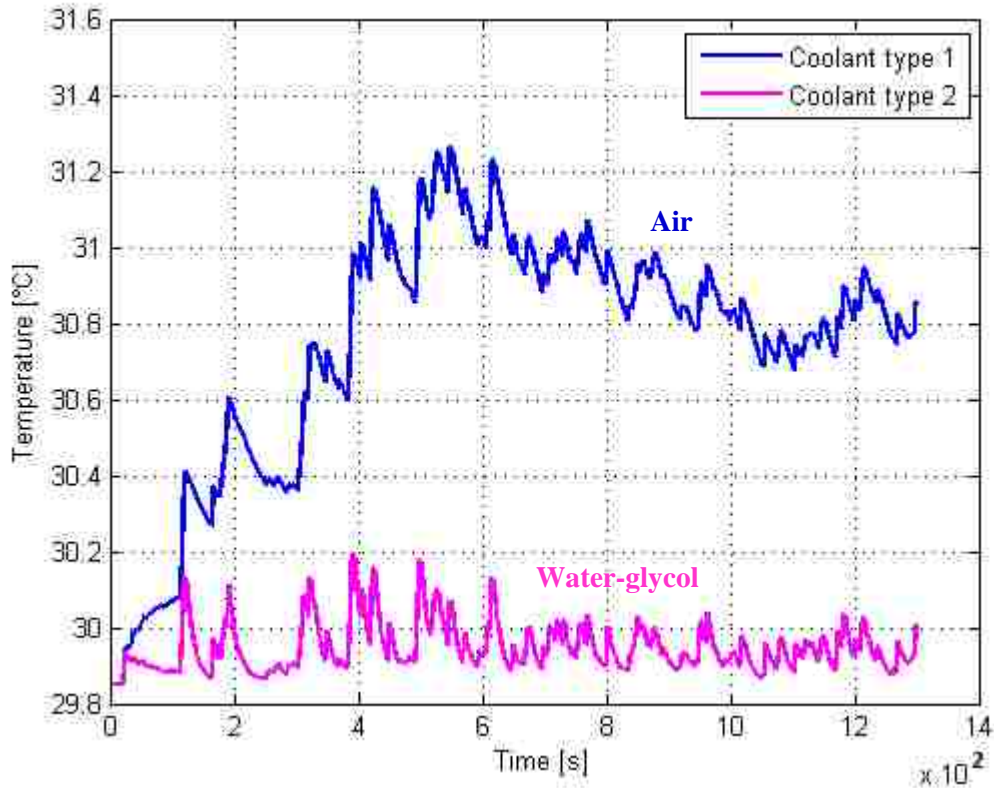


Figure 4.27 - Output graph generated by the simulation number 4

Considering the thermodynamic properties of the air and of the water-glycol mixture, it is possible to state that the latter one has a higher density (almost a thousand times higher than the air one) and a higher specific heat (almost four times higher than the one of the air) and, finally, from the analysis of the basic following Equation 4.3, a straightforward conclusion can be done.

$$\dot{Q} = \dot{m} \cdot c_p \cdot (T_2 - T_1) \quad (4.3)$$

Given a certain temperature gradient experienced by the coolant, whose initial and final temperatures are respectively  $T_1$  and  $T_2$ , the heat rate amount removed from a module of the investigated battery pack is directly proportional to the mass flow rate and specific heat of the coolant itself. Moreover, since the cooling medium mass flow rate is given by the product between the volume flow rate and the density of the fluid, the 50-50 water-glycol mixture has a higher  $\dot{m}$  value with respect to the air. Hence, the higher  $\dot{m}$

and  $c_p$  values of the liquid coolant determine a higher heat rate removal from the battery, whose temperature tends to remain at very low levels, comparable with the initial thermal condition of 29.85 °C. At this point, it is clear that a liquid cooled solution is more effective than an air cooled solution: in fact, for high-energy Li-Ion battery applications typical of PHEV and BEV configurations, in which the current profiles requested to the battery are very strong and dissipates a lot of power during time, the liquid cooled solution is necessary to guarantee the thermal control of the HVB device. Hence, the thermal advantage offered by a water-glycol mixture cooling system are evident but, at the same time, using such a type of cooling solution requires the introduction of suitable battery cells housings necessary to avoid the direct contact of the modules with the coolant that could cause dangerous short circuit. The coatings introduction determines a higher expense to build the battery pack and the same happens also using a dielectric liquid coolant, that can flow in direct contact with the cells but requires notable expenses to be synthesized.

#### 4.3.2.6 Simulation - 5

Table 4.13 contains all the specifications that define the input variables background of investigated simulation number 5, aimed at analyze the influence of the modules internal resistance on the battery thermal behaviour. The HVB temperature time trends obtained at the end of the simulation are depicted in Figure 4.28, thoroughly analyzed in the following paragraph.

Table 4.13 - Input variables background of simulation number 5

Simulation type	Operating mode	Resistance	Cells number	Coolant rate
C	Charge sustaining	1.0 mΩ	72	100 cfm
		2.0 mΩ		
		4.0 mΩ		

Figure 4.28 refers to a simulation intended to investigate the influence that different internal resistance values have on the thermal behaviour of the battery pack; simulation

number 5, in particular, can be compared with simulation number 1 considering a different cells geometry and different resistance values.

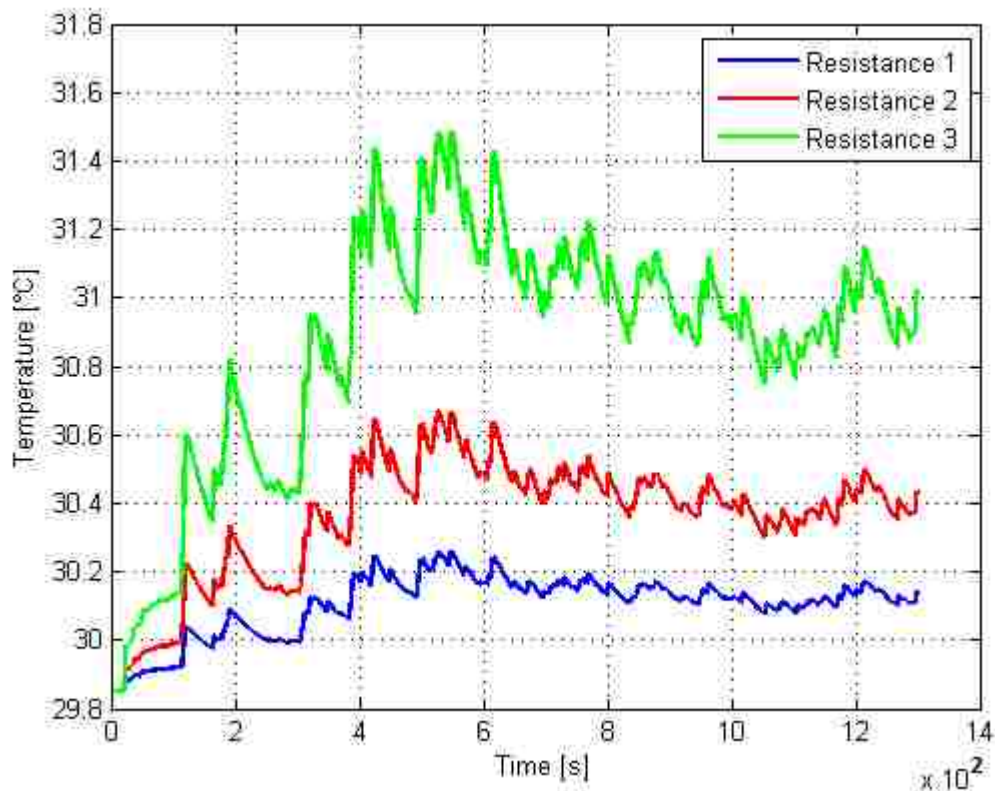


Figure 4.28 - Output graph generated by the simulation number 5

However, taking into account the blue curve of Figure 4.24 and the red one of Figure 4.28, a complete comparison between them can be done since the internal resistance values are the same and the only different input variable is represented by the geometry of the modules, more bulky for the C-type simulation. The maximum temperature value computed during the cycle for the blue curve of Figure 4.24 is of 30.8614 °C while the one computed for the red curve of Figure 4.28 is of 30.6684 °C: the smaller cells of case of study A are characterized by higher overall temperature values because their smaller external surfaces can dispose less heat to the coolant with respect to the bigger cells of case of study C.

### 4.3.2.7 Simulation - 6

Table 4.14 contains all the specifications that define the input variables background of investigated simulation number 6, aimed at analyze the influence of the modules internal resistance on the battery thermal behaviour. The HVB temperature time trends obtained at the end of the simulation are depicted in Figure 4.29, thoroughly analyzed in the following paragraph.

Table 4.14 - Input variables background of simulation number 6

Simulation type	Operating mode	Resistance	Cells number	Coolant rate
D	Charge sustaining	1.0 mΩ	72	100 cfm
		2.0 mΩ		
		4.0 mΩ		

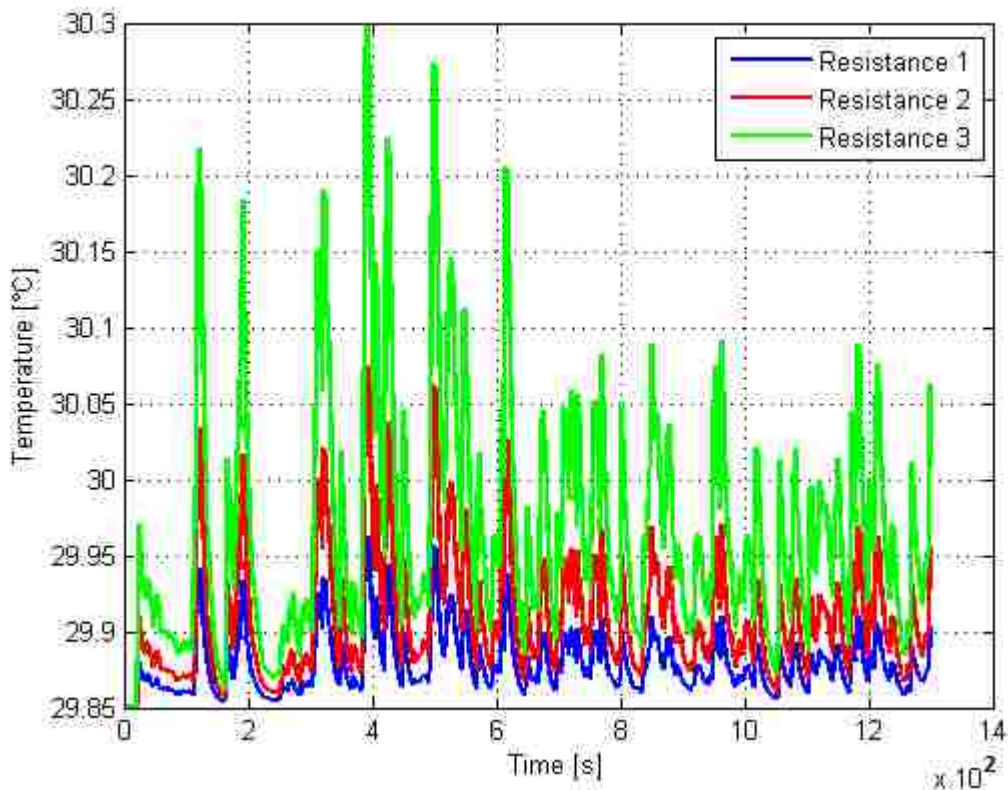


Figure 4.29 - Output graph generated by the simulation number 6

Figure 4.29 has been obtained at the end of simulation number 6, characterized by the same input data of simulation number 5 (that has generated Figure 4.28) but related to

a 50-50 water-glycol cooling medium and no more to a forced air cooled solution. Comparing Figures 4.28 and 4.29, it is clear that, in case of a liquid battery cooling system, not only the general temperature increase experienced by the HVB is lower but, moreover, also the influence on the temperature time trend of the internal resistance values highly decreases: this makes possible to understand that a liquid cooling medium allows to better maintain the thermal control of the device also in case of an unexpected sudden rise of the battery internal resistance that, for example, can happen when the HEV is operating in cold climates.

#### 4.3.2.8 Simulation - 7

Table 4.15 contains all the specifications that define the input variables background of investigated simulation number 7, aimed at analyze the influence of the coolant mass flow rate on the battery thermal behaviour. The HVB temperature time trends obtained at the end of the simulation are depicted in Figure 4.30, thoroughly analyzed in the following paragraph.

**Table 4.15 - Input variables background of simulation number 7**

Simulation type	Operating mode	Resistance	Cells number	Coolant rate
D	Charge depleting	2.0 mΩ	72	0.1 cfm
				1 cfm
				10 cfm

Figure 4.30 refers to a D-type simulation, related to a liquid cooled battery device and to a charge depleting mode of operation that involves higher current magnitudes, leading to a more intensive thermal excitation of the HVB pack. It is interesting to note that, only considering a 0.1 cfm volume flow rate, a stable temperature increase of at least 0.4 °C takes place at steady state while, considering indistinctly a 1 cfm or 10 cfm flow rates, the thermal status of the battery remains approximately at the starting conditions and does not shows a notable dependence on the coolant amount flowing between the battery modules.

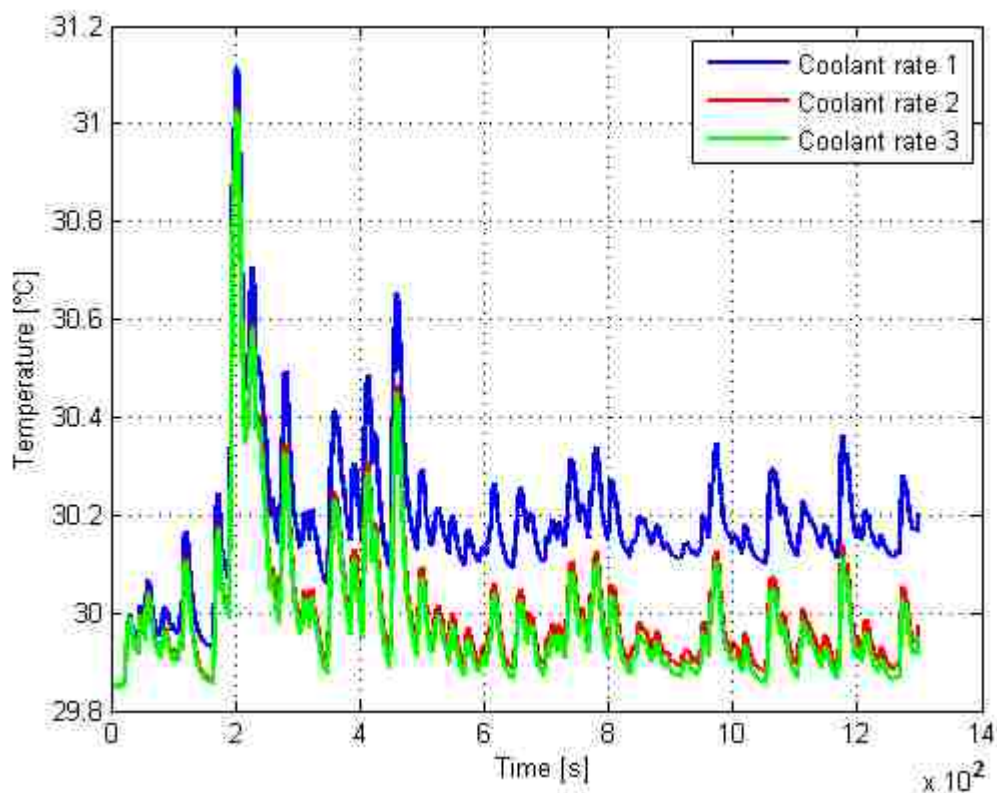


Figure 4.30 - Output graph generated by the simulation number 7

This is due to the high cooling efficiency of the 50-50 water-glycol mixture that can be used in considerably lower amounts with respect to the air to obtain excellent results in the thermal control of the HEV battery: as can be seen from above Figure 4.30, there are not high differences in the HVB temperature time trend if a 1 cfm or 10 cfm coolant volume flow rates are used and so, in order to maintain at steady state a temperature approximately lower than 30.1 °C, it is sufficient to use a 1 cfm coolant rate requesting a lower pump power.

As underlined right now, the presence of a pump capable of generating the coolant flow inside the battery pack is necessary to allow the cooling of the modules and, probably, it requires an energy contribution higher than the one requested by the fans that activate the forced air cooled battery solution typical of mild HEV applications. Moreover, the instantaneous power necessary to activate the battery coolant pump is taken from the ICE crankshaft through a belt and pulley mechanism and, as expected, it is directly proportional to the amount of coolant that is flowing inside the HVB pack.



### 4.3.2.9 Simulation - 8

Table 4.16 contains all the specifications that define the input variables background of investigated simulation number 8, aimed at analyze the influence of the cells number on the battery thermal behaviour. The HVB temperature time trends obtained at the end of the simulation are depicted in Figure 4.31, thoroughly analyzed in the following paragraph.

Table 4.16 - Input variables background of simulation number 8

Simulation type	Operating mode	Resistance	Cells number	Coolant rate
C	Charge depleting	2.0 mΩ	60	100 cfm
			72	
			84	
			96	

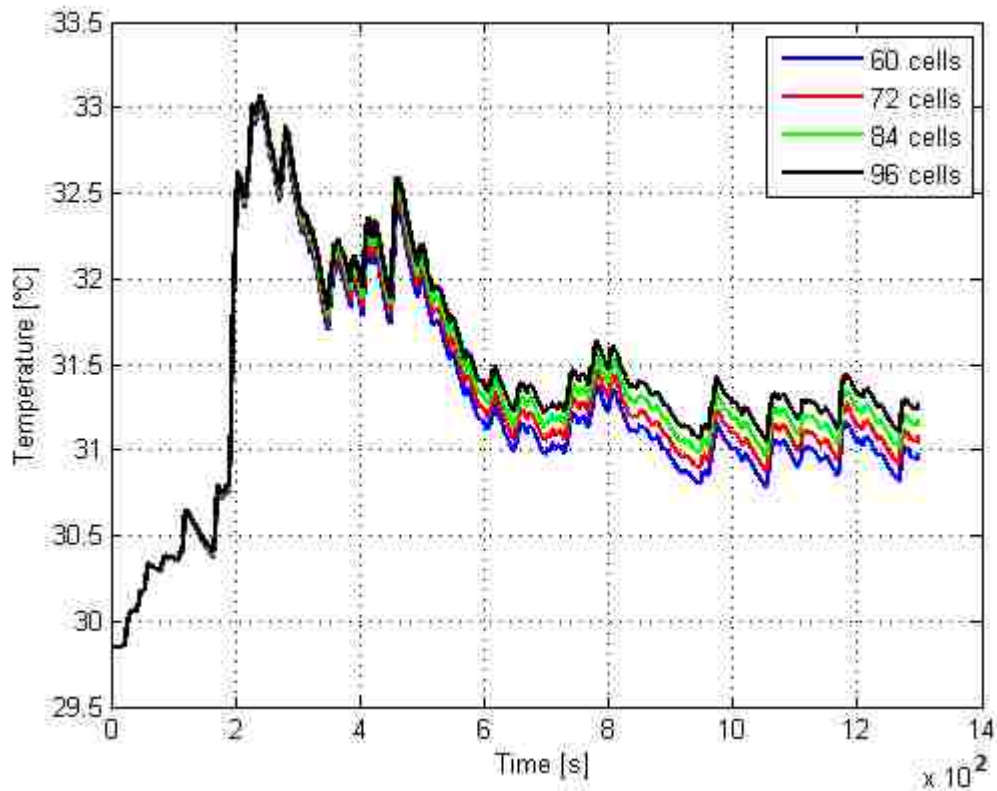


Figure 4.31 - Output graph generated by the simulation number 8

It is very interesting to compare Figure 4.31 with Figure 4.25, obtained at the end of simulation number 2, to better understand the influence of the different input variables on the overall thermal behaviour of the HVB device; their input conditions are the same, excluding the dimensions of the modules and their internal resistance, higher for simulation number 8, and the different battery operating modes, charge sustaining and depleting for simulations number 2 and 8 respectively.

Considering that, for Figure 4.31, the cells are bigger and their internal resistance is lower, the temperature increase shown by the HVB pack should be less intense than the one of Figure 4.25: the higher is the external surface of the modules and the more effective is their cooling mechanism and, moreover, the lower is their internal resistance and the lower is the heat amount produced by the battery.

But, despite of this, the temperature rise experienced during simulation number 8 is definitely higher than the one computed during simulation number 2: this is caused by the charge depleting current profile considered in the last case that, involving more intense current values, that must be raised at the second power to determine the heat dissipated for Joule effect, have a stronger influence on the thermal behaviour of the battery with respect to its geometric and electrochemistry characteristics. Hence, to conclude, it can be underlined that the battery mode of operation has a higher influence on the heat exchange phenomena if compared with the one covered by the modules geometry and internal resistance value.

#### **4.3.2.10 Simulation - 9**

Table 4.17 contains all the specifications that define the input variables background of investigated simulation number 9, aimed at analyze the influence of the cells number on the battery thermal behaviour. The HVB temperature time trends obtained at the end of the simulation are depicted in Figure 4.32, thoroughly analyzed in the following paragraph.

Table 4.17 - Input variables background of simulation number 9

Simulation type	Operating mode	Resistance	Cells number	Coolant rate
D	Charge depleting	2.0 mΩ	60	1 cfm
			72	
			84	
			96	

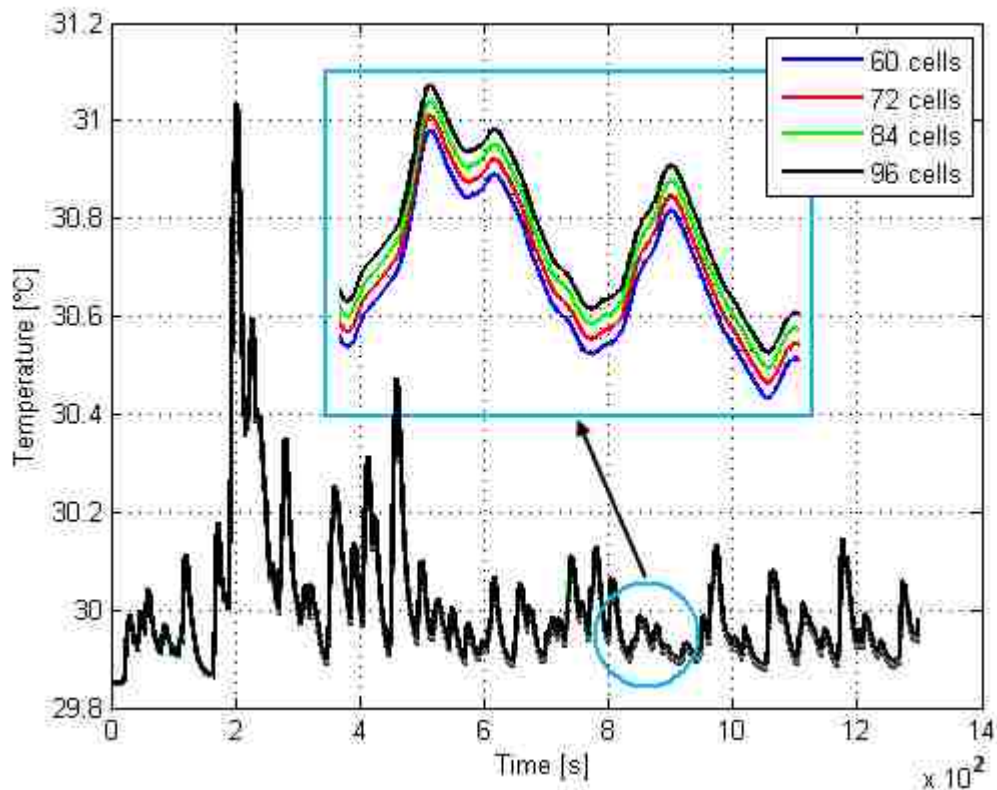


Figure 4.32 - Output graph generated by the simulation number 9

Figure 4.32 has been obtained with the same input conditions of simulation number 8 but considering, instead of an air cooled configuration of 100 cfm, just 1 cfm of 50-50 water-glycol mixture; in terms of coolant mass flow rate, 100 cfm of air correspond to a mass rate 0.0578 kg/s while 1 cfm of liquid coolant corresponds to a mass rate of 0.5111 kg/s. Hence, considering that the water-glycol solution mass flow rate has one order of magnitude more than the air and that, moreover, its specific heat is almost a thousand times higher than the air one, it is clear that the temperature rise shown in Figure 4.32 (3.3 °C) must be more intense than the one of Figure 4.31 (1.2 °C). Moreover, from a careful

analysis of the picture above, it can be seen that the number of cells contained in the pack does not have a notable influence on the thermal behaviour of the battery and, in fact, only zooming the curves it is possible to note the differences existing between their trends. This because, as a difference from simulation number 8 in which the modules number has a notable influence on the temperature time trend of the battery, a 0.5111 kg/s mass flow rate of liquid coolant is high enough to efficiently cool down the HVB cells both in case they are 60 or 96: the mass rate of the coolant, together with its highly effective heat absorption properties, allows to obtain an efficient HVB cooling independent, in practice, from the number of modules that constitute the HEV battery pack.

#### 4.3.2.11 Simulation - 10

Table 4.18 contains all the specifications that define the input variables background of investigated simulation number 10, aimed at analyze the influence of the cells number on the battery thermal behaviour. The HVB temperature time trends obtained at the end of the simulation are depicted in Figure 4.33, thoroughly analyzed in the following paragraph.

**Table 4.18 - Input variables background of simulation number 10**

Simulation type	Operating mode	Resistance	Cells number	Coolant rate
E	Charge depleting	2.0 mΩ	60	100 cfm
			72	
			84	
			96	

Figure 4.33 can be compared with Figure 4.31 to underline again that, given all the same input conditions, the higher are the height, width and length of the modules and the lower is the temperature increase experienced by the whole HEV battery; this because the higher dimensions of the cells allow to obtain a more efficient thermal exchange between them and the coolant that is flowing inside the pack.

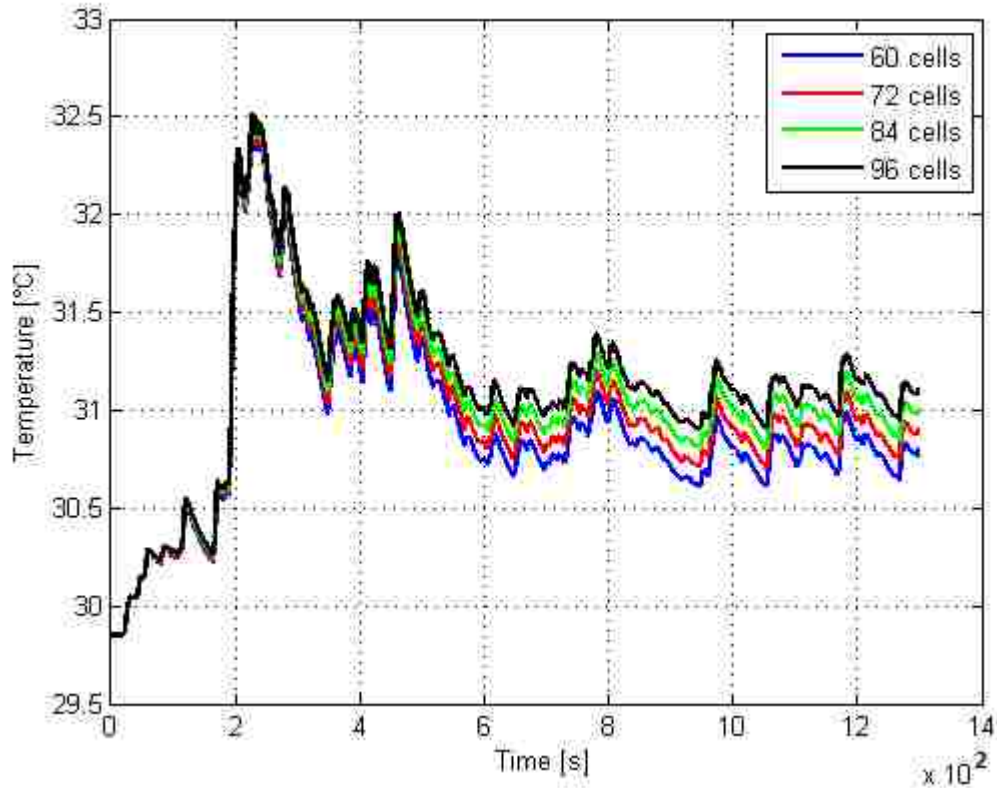


Figure 4.33 - Output graph generated by the simulation number 10

#### 4.3.2.12 Simulation - 11

Table 4.19 contains all the specifications that define the input variables background of investigated simulation number 11, aimed at analyze the influence of the cells number on the battery thermal behaviour. The HVB temperature time trends obtained at the end of the simulation are depicted in Figure 4.34, thoroughly analyzed in the following paragraph.

Table 4.19 - Input variables background of simulation number 11

Simulation type	Operating mode	Resistance	Cells number	Coolant rate
F	Charge depleting	2.0 mΩ	60	0.1 cfm
			72	
			84	
			96	

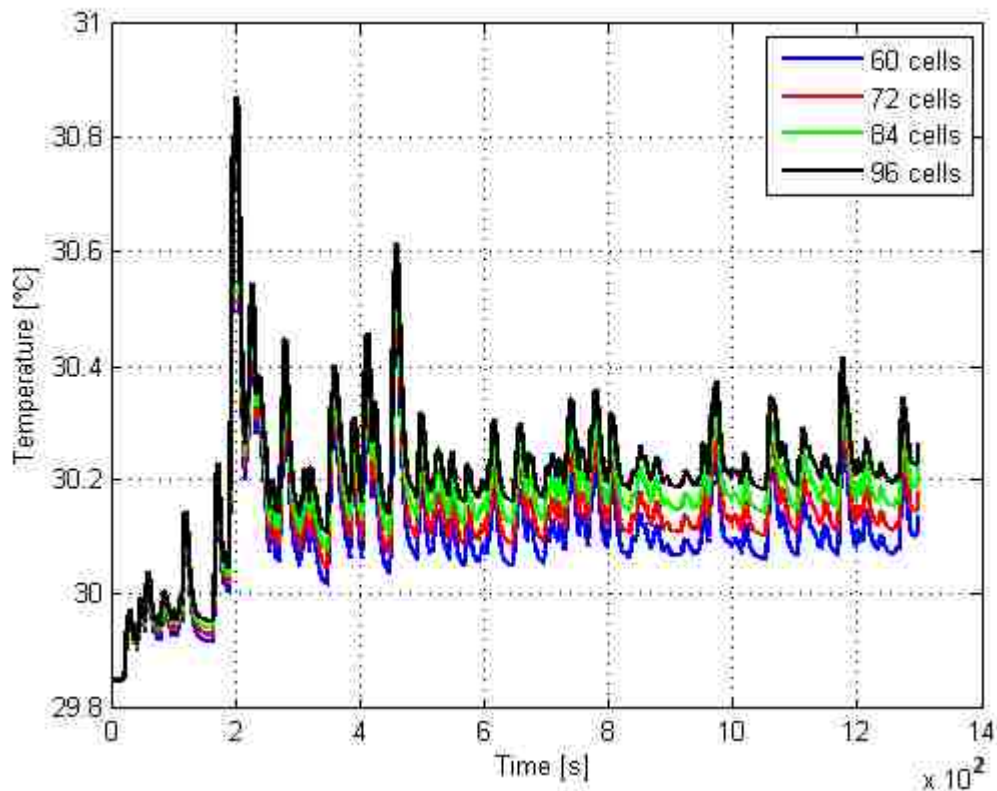


Figure 4.34 - Output graph generated by the simulation number 11

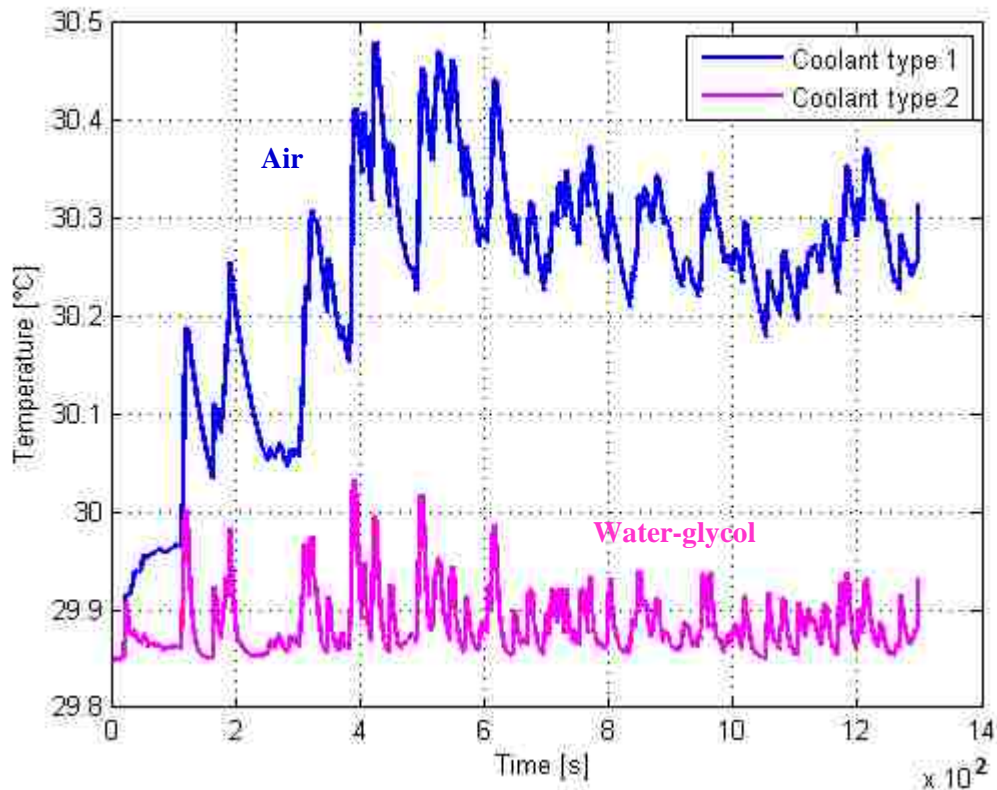
Simulation number 11 directly follows simulation number 10, simply considering a different type and volume rate of coolant, as it happened for simulations 9 and 8; but now, a 0.1 cfm of liquid rate has been taken into account instead of the 1 cfm used for simulation number 9. Again, the liquid cooling solution reduces the temperature increase of the battery during time, whose maximum gradient is in fact of about 1 °C instead of the 2.7 °C experienced in Figure 4.33, but the most important aspect that must be underlined is that the number of cells has now a higher influence on the thermal behaviour of the battery pack. The four curves of the picture above, in fact, appear immediately to be different without zooming on their values and this is caused by the lower amount of coolant considered for the simulation (0.0511 kg/s of water-glycol mixture) that, depending on the modules number, is distributed between the cells in higher or lower quantities that determine a more or less effective cooling phenomenon.

### 4.3.2.13 Simulation - 12

Table 4.20 contains all the specifications that define the input variables background of investigated simulation number 12, aimed at analyze the influence of the coolant type on the battery thermal behaviour. The HVB temperature time trends obtained at the end of the simulation are depicted in Figure 4.35, thoroughly analyzed in the following paragraph.

**Table 4.20 - Input variables background of simulation number 12**

Simulation type	Operating mode	Resistance	Cells number	Coolant rate
<b>E</b>	Charge sustaining	2.0 mΩ	72	100 cfm
<b>F</b>				



**Figure 4.35 - Output graph generated by the simulation number 12**

The lower internal resistance and more bulky modules geometry, lead to temperature values substantially lower than the ones shown in Figure 4.27, obtained

through simulation number 4. In this case, the temperature increase is lowly notable both for the air and liquid cooling solutions and, in general, it could lead to a lower quantity of coolant requested to maintain the thermal control of the battery and, consequently, to a lower energy content necessary to activate the fans or the pump of the battery cooling system. In case of a charge depleting mode of operation, however, the HVB temperature time trends would have touched higher magnitudes for both the coolant type solutions.

#### 4.3.2.14 Simulation - 13

Table 4.21 contains all the specifications that define the input variables background of investigated simulation number 13, aimed at analyze the influence of the battery operating mode on its overall thermal behaviour. The HVB temperature time trends obtained at the end of the simulation are depicted in Figure 4.36, thoroughly analyzed in the following paragraph.

**Table 4.21 - Input variables background of simulation number 13**

Simulation type	Operating mode	Resistance	Cells number	Coolant rate
E	Charge sustaining	2.0 mΩ	96	100 cfm
	Charge depleting			

As expected, from the analysis of Figure 4.36, it is clear that the charge depleting mode of operation, during which the battery delivers the electric current amount requested by the electric motor to propel the vehicle in a hybrid or pure electric mode, is harder than the charge sustaining one, during which the electric current flows to the battery to increase its state of charge.

The higher amount of electric energy involved by the depleting mode leads, obviously, to a more intense thermal solicitation of the battery pack that, to be maintained within safety limits, requests a higher amount of coolant mass that has to flow between the modules of the HVB.



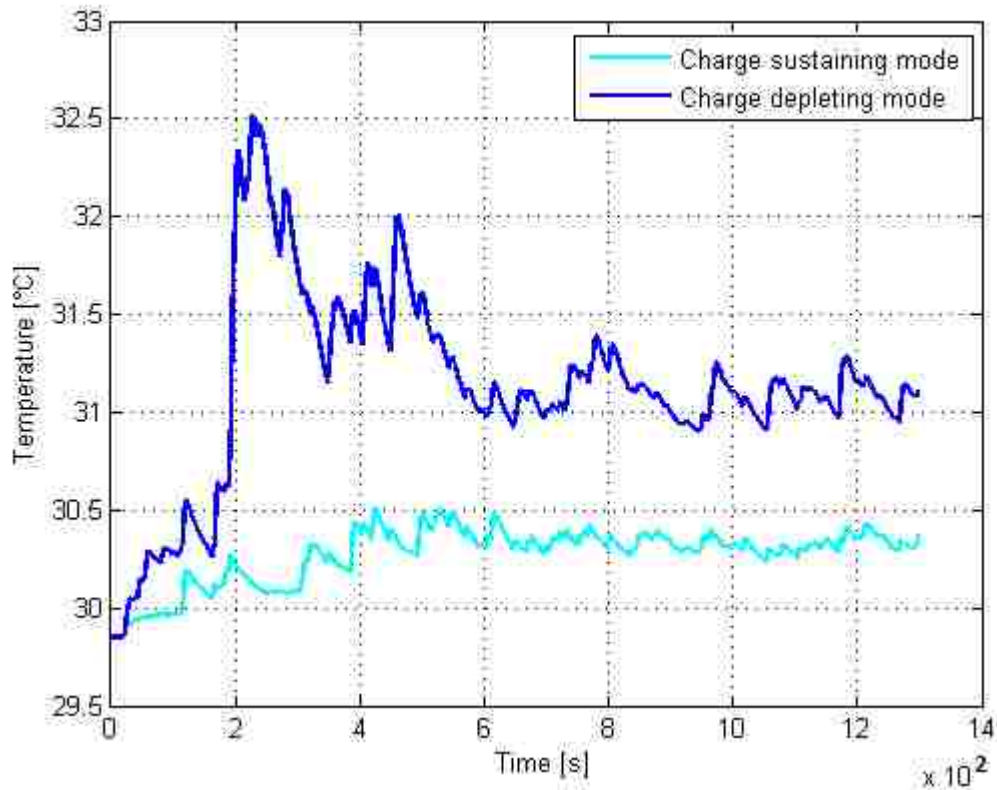


Figure 4.36 - Output graph generated by the simulation number 13

In case of coated cells or dielectric coolant, the liquid cooling solution could be taken into account to better manage the thermal state of the battery pack and to avoid to reach uncontrolled situations that can finally lead to considerable damage to the electric energy storage device and to the whole “electric side” of the HEV.

#### 4.3.2.15 Simulation - 14

Table 4.22 contains all the specifications that define the input variables background of investigated simulation number 14, aimed at analyze the influence of the battery operating mode on its overall thermal behaviour. The HVB temperature time trends obtained at the end of the simulation are depicted in Figure 4.37, thoroughly analyzed in the following paragraph.

Table 4.22 - Input variables background of simulation number 14

Simulation type	Operating mode	Resistance	Cells number	Coolant rate
A	Charge sustaining	2.8 mΩ	96	100 cfm
	Charge depleting			

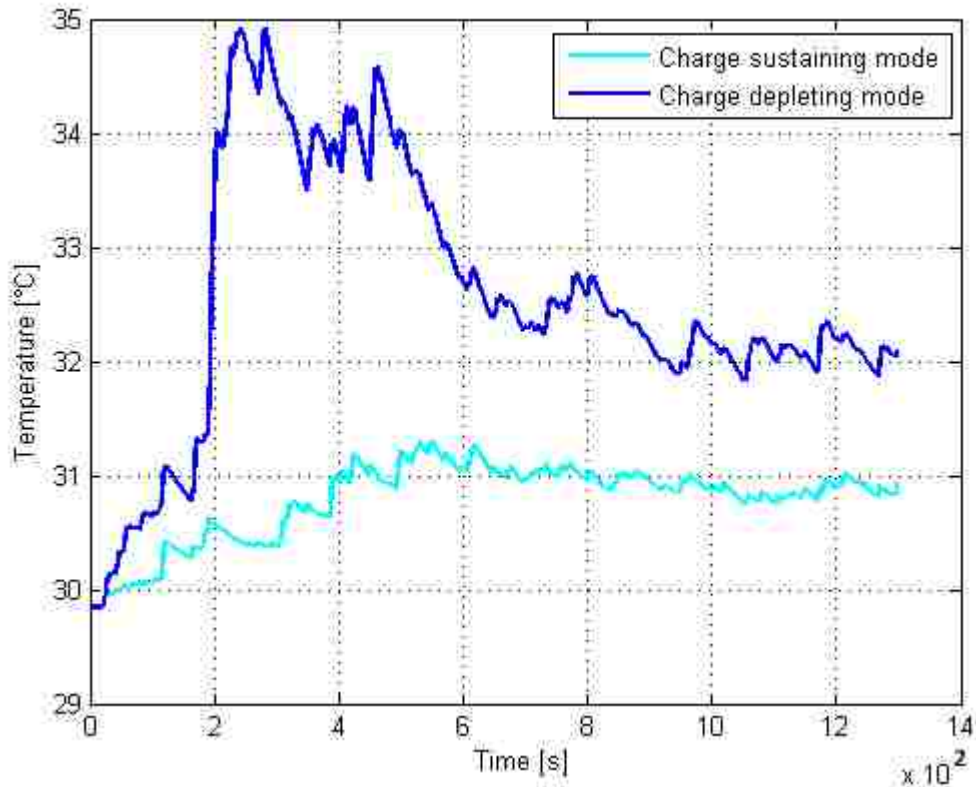


Figure 4.37 - Output graph generated by the simulation number 14

Dealing now with bigger cells characterized by a 40% higher internal resistance, the temperature increases are higher for both the battery operating modes if compared with the results of simulation number 13. The cyan curve stays for a considerable time at a 31 °C level, hence involving a temperature increase of 1.2 °C, while the blue curve remains over the 34 °C limit for about 300 s, determining a considerably sustained thermal excitation of the battery pack. The high number of cells (96), moreover, introduces further complications in control the heat dissipation phenomena taking place during the driving cycle inside the HVB pack device.

#### 4.3.2.16 Simulation - 15

Tables 4.23 and 4.24 contain all the specifications that define the input variables background of investigated simulation number 15, aimed at analyze the influence of the anode current collector thickness on the battery thermal behaviour. The HVB temperature time trends obtained at the end of the simulation are depicted in Figure 4.38, thoroughly analyzed in the following paragraph.

**Table 4.23 - Input variables background of simulation number 15**

Simulation type	Operating mode	Resistance	Cells number	Coolant rate
A	Charge sustaining	2.8 mΩ	72	100 cfm

**Table 4.24 - Input variables background of simulation number 15 (anode collector thickness values)**

Anode collector thickness
1 μm
12 μm
30 μm

Figure 4.38 has been obtained at the end of an A-type simulation, in which the thickness of the anode current collector has been varied using the values contained in Table 4.24 in order to understand what is the influence of this quantity on the thermal behaviour of the battery pack. After a rapid analysis of the picture above, it is possible to state that the influence of the anode collector thickness on the heat exchange phenomena taking place between the HVB modules and the coolant is very low, in fact the three curves assume approximately the same values during the whole driving cycle.

Zooming the image, it can be seen that the curve having the highest temperature profile is the blue one, that refers to the lowest thickness value: in fact, since the anode and also the cathode current collectors are made of high-conductive materials, copper and aluminum respectively, the higher is their thickness and the more effective is the heat disposal from the battery to the coolant. At the same time, calculating the temperature difference existing between the curves at a certain instant of the profile, it results equal to the 0.013% of the temperature magnitude and this demonstrates that the current collectors thickness does not have a relevant influence on the thermal behaviour of the battery: this

because, since the conductivity of the polymeric separator is very low if compared with the other layers of the battery internal structure, an increase of their thickness is not able to overcome the poor thermal contribution involved by the separator itself.

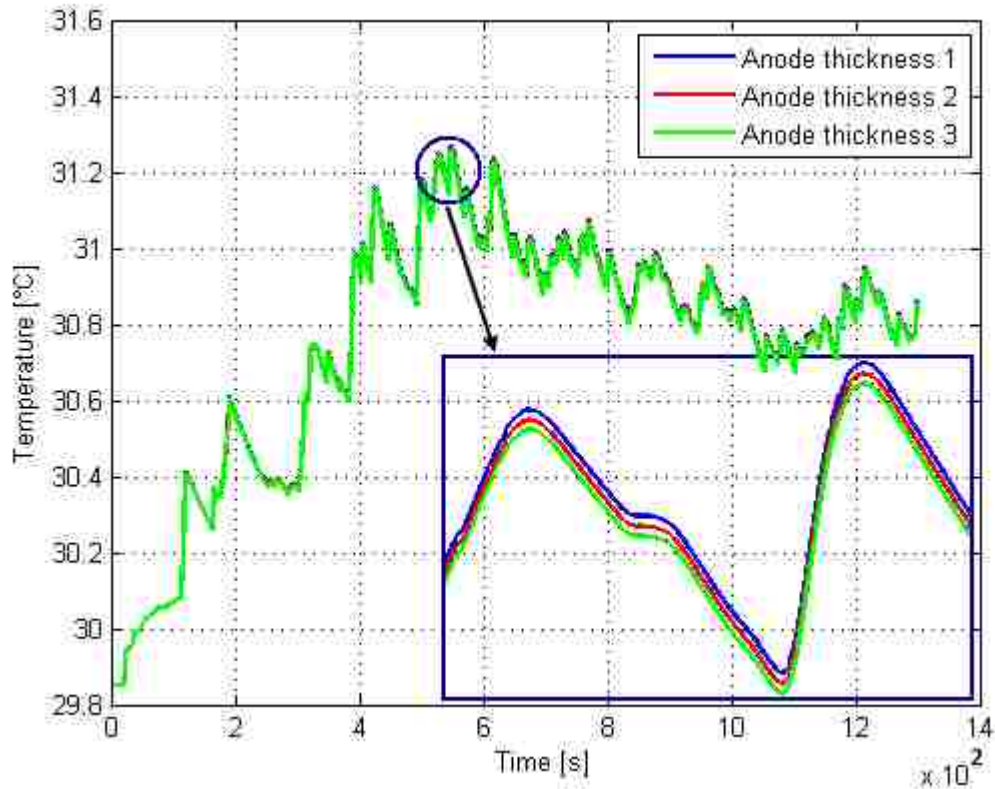


Figure 4.38 - Output graph generated by the simulation number 15

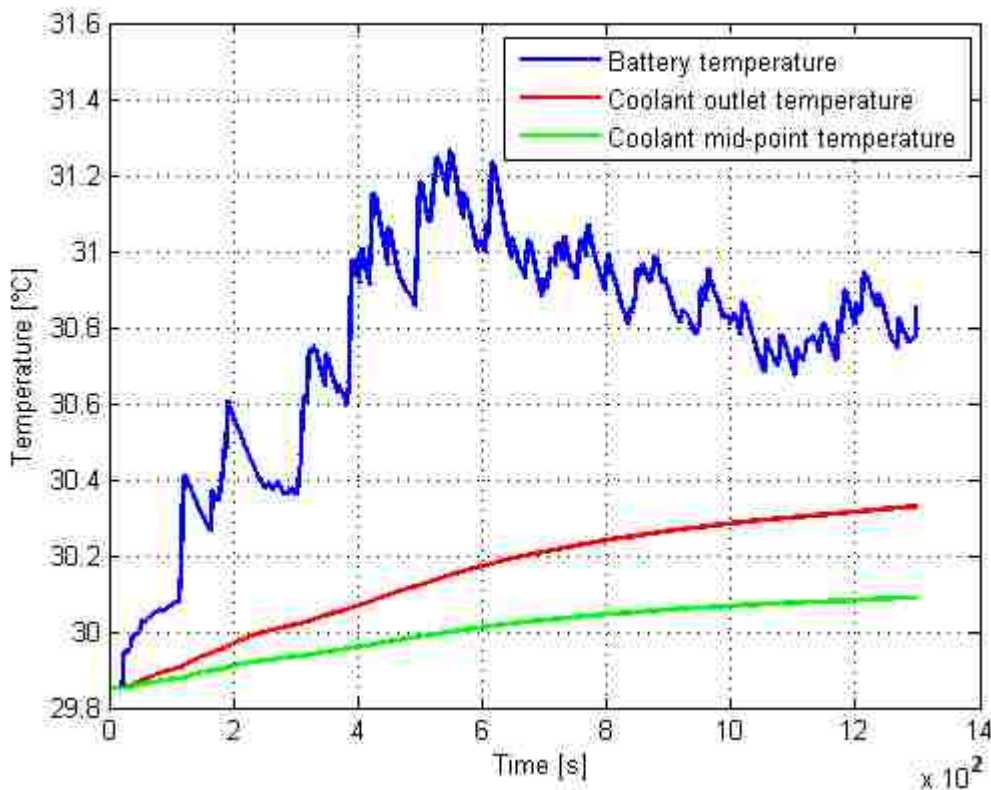
#### 4.3.2.17 Simulation - 16

Table 4.25 contains all the specifications that define the input variables background of investigated simulation number 16, aimed at analyze the battery temperature time trend together with the coolant temperature at the outlet section of the battery pack and at the medium point along the length of the cells. The HVB and coolant temperature time trends obtained at the end of the simulation are depicted in Figure 4.39, thoroughly analyzed in the following paragraph.

**Table 4.25 - Input variables background of simulation number 16**

Simulation type	Operating mode	Resistance	Cells number	Coolant rate
A	Charge sustaining	2.8 mΩ	72	100 cfm

Below Figure 4.39 is useful to study the time evolution of the temperature, during the investigated driving cycle, of both the battery and of the cooling medium at two different sections of the battery pack. The battery temperature curve is exactly the same of Figure 4.27, related to an A-type simulation and to an air cooled solution of a 72 cells HVB with an internal resistance of 2.8 mΩ; in the picture below, this temperature trend is accompanied by the red and green curves that represent the temperature evolution of the air inside the pack at its outlet section and at the mean point along the length of the modules, respectively.



**Figure 4.39 - Output graph generated by the simulation number 16**

Obviously, the temperature of the battery is always higher than the one of the coolant to which it is delivering the heat generated for Joule effect during vehicle

operations and, moreover, the air temperature at the outlet manifold is continuously higher than the temperature at the middle point of the pack along its longitudinal direction (look at Figure 3.36). The tendency of the three curves is comparable since their trend shows a general sharp increase for about the first 600 seconds of the driving cycle while, in the remaining 800 seconds, the temperature of the cells start to partially decrease thanks to the continuative intervention of the coolant, whose temperature continues to rise even if with a less steep trend. At steady state, between the outlet temperature of the coolant and the temperature of the battery modules, a stable temperature gradient of 0.5 °C is established that guarantee a controlled thermal equilibrium of the whole HVB device.

#### 4.3.2.18 Simulation - 17

Table 4.26 contains all the specifications that define the input variables background of investigated simulation number 17, aimed at analyze the battery temperature time trend together with the coolant temperature at the outlet section of the battery pack and at the medium point along the length of the cells. The HVB and coolant temperature time trends obtained at the end of the simulation are depicted in Figure 4.40, thoroughly analyzed in the following paragraph.

**Table 4.26 - Input variables background of simulation number 17**

<b>Simulation type</b>	<b>Operating mode</b>	<b>Resistance</b>	<b>Cells number</b>	<b>Coolant rate</b>
A	Charge depleting	2.8 mΩ	72	100 cfm

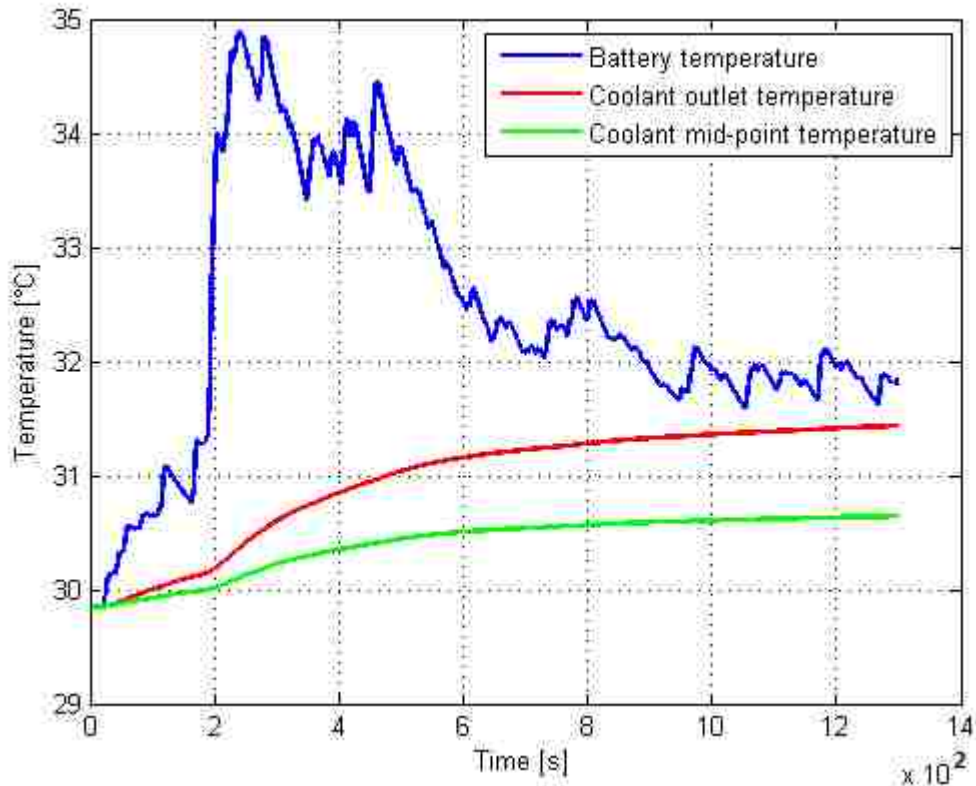


Figure 4.40 - Output graph generated by the simulation number 17

Simulation number 17 has been realized in the same way of simulation number 16 but taking into account a battery charge sustaining mode of operation, during which the current magnitudes are certainly higher than the ones registered during a battery charge depleting mode. The temperature of the battery almost touches the 35 °C and remains higher than 34 °C between seconds 200 and 500 of the driving cycle, determining a sharp increase in the temperature of the cooling medium that, after second 500, roughly assumes a flat trend. Obviously, the heat quantity exchanged by the battery modules and the coolant is considerably higher with respect to simulation number 16 but, at steady state, the condition of thermal equilibrium is reached again with a 0.5 °C gradient existing between the battery and coolant outlet temperatures. Moreover, from both Figures 4.39 and 4.40, it can be seen that the coolant temperature time trend is not characterized by the frequent oscillations typical of the battery temperature blue curve, directly linked with the current profile: this happens because, considering the whole coolant quantity flowing instantaneously inside the pack as a unique entity, its thermal inertia results substantially

higher than the one of the modules and this leads to its tendency to gradually change its thermal state without sudden steep temperature variations.

To conclude, it could be interesting to plot the time trend of the heat rate that characterize for the current simulation the battery thermal state; it is determined by the heat amount generated for Joule effect and by the heat removed from the cells by the coolant to maintain their temperature within controlled limits and, in particular, it is divided for the thermal mass of the HVB and integrated by the software to finally compute the temperature of the device.

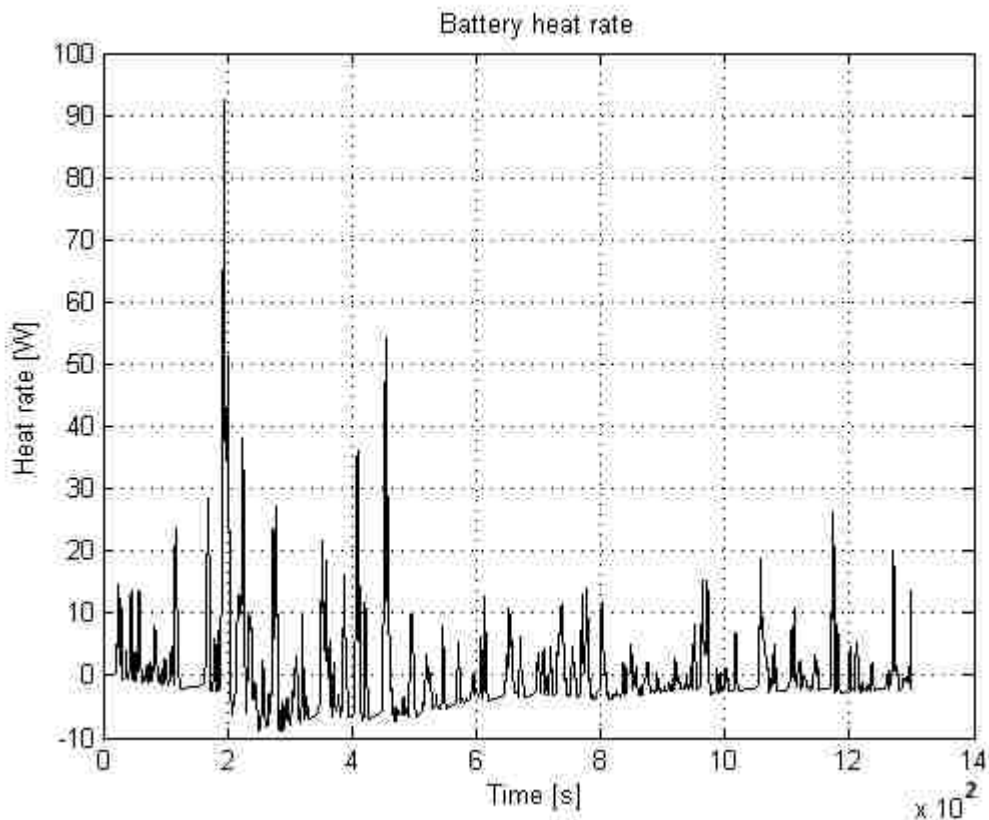


Figure 4.41 - Battery heat rate time trend computed during simulation number 17

Figure 4.41 makes possible to understand that notable heat quantities characterize the battery operations and that the HVB pack cooling system has been thoroughly modeled during the battery thermal software design: the battery heat rate, in fact, is negative for most of the driving cycle time because the coolant is removing heat from the modules to avoid dangerous overheating and, at the same time, the periods during which a



positive heat rate can be found relate to intense current magnitudes and last for short times thanks to the effective intervention of the coolant. Such a type of picture can be plotted by the tool for each of the simulations described in the previous sections to give further validity to the final temperature results and, moreover, to understand what is the order of magnitude typical of the power amount dissipated by the battery during vehicle operations.

#### **4.3.3 Overall analysis of the simulation results and basic sensitivity study**

The Matlab®/Simulink® battery thermal model has been used to run a lot of simulations related to the thermal behaviour of a typical HEV NiMH battery, constituted by a parallel disposition of the modules thoroughly described in the previous chapter. In particular, 17 simulations have been presented right now, each of them introduced by a table, containing all the input conditions fixed by the user, and accompanied by a careful description of the battery temperature time trends computed by the model and related to different values of the variable input quantity whose influence on the thermal behaviour of the battery is investigated through the specific simulation. The possibility to conduct such a thorough study on a specific HEV battery pack operating over a certain driving cycle, it is offered by the flexibility of the model that can work as an autonomous simulation tool and not only as an integral part of the overall Chrysler HEV prediction software. The accuracy of the obtained results is considerably high and satisfactory because the input data received by the experts of the Electrified Powertrain department at Chrysler are reliable and characterized by high level of precision; the general trend of the resultant graphs, moreover, is always reasonable and explainable through straightforward thermodynamic considerations that can be done considering how the battery thermal model has been designed and how it combines and elaborates the various input quantities.

Finally, now that a lot of study cases have been presented, a basic sensitivity analysis can be conducted to highlight which are the most important factors and input variables affecting the temperature trend of the battery during the driving cycle. A careful comparison of all the simulation results described in the previous sections is necessary and it has to be done considering the specific meaning of each one of the input quantities uploaded and managed by the Matlab® base file and by the Simulink® tool. In the

following list are described all the input variables that determine the final battery temperature time trend, sorted on the basis of a decreasing level of importance and influence that they have on the final results.

- Battery electric current profile: the operating mode of the HEV battery, that can be charge sustaining or depleting, determines the profile of the current that is delivered by the battery. This profile, in turn, has a primary influence on the temperature time trend of the HVB pack since it defines the amount of heat dissipated during time for Joule effect. The higher is the current magnitude and the higher are the thermal losses of the device that involve lower overall performance and, moreover, the necessity to use a more effective, and energy requesting, cooling system. In particular, the use of high voltage batteries is precisely linked to the tentative of decreasing the quantity of current flowing through the modules, given a certain amount of electric power requested by the “electric side” of the hybrid vehicle. To conclude, it has to be underlined again that the squared power of the current determines the amount of heat generated by the cells for Joule effect and that, consequently, it has the highest impact on the values that the battery temperature assumes during time.
- Coolant type: the choice to use a specific type of coolant during the HEV battery operations is determined by the thermal excitation of the pack and by the maximum temperature limit that the electric energy storage device is allowed to reach for safety reasons. In fact, the thermal control of the battery takes place in completely different ways depending on the type of fluid used to cool down the modules. The air cooled solution, as demonstrated in the previous sections, is less effective than the liquid one and requires higher volumes of coolant to maintain the desired thermal status of the HVB; instead, if a liquid cooling medium is adopted, the thermal control of the device is certainly easier but a pumping circuit must be introduced to allow the coolant flow between the cells. In general, given the same volume flow rate, the adoption of a liquid coolant such a water-glycol mixture determines a better control of the battery temperatures that are going to be considerably lower than in the case of an air cooling solution. This is not only due to the fact that a liquid cooling fluid has higher values of specific heat but

because, moreover, it has also a considerably higher density with respect to the air and so, given a certain quantity of coolant volume flow rate, the related mass amount is going to be certainly higher.

- **Battery internal resistance:** the internal resistance of the cells has a relevant role in the thermal behaviour of the HVB since, together with the current magnitude, it determines the amount of heat dissipated during time for Joule effect. From simulations number 1, 5 and 6 it is possible to note that its influence on the battery thermal status is highly notable and that it represents one of the main factors to be studied to understand what could be the best cooling solution to be adopted. The modules internal resistance, in fact, is determined by the electrochemistry of the battery that, in turn, mainly depends on the type of vehicle application that it is going to equip; hence, depending on the battery type used for the investigated vehicle model, a specific value of resistance has to be taken into account and then, finally, it is going to determine the best cooling solution to be adopted to maintain the thermal control of the device avoiding dangerous overheating.
- **Modules dimensions:** the geometry of the prismatic cells considered to virtually model the HEV battery pack, is described by the height, width and length measures that finally determine the extension of the external surfaces of the modules. The wider are the surfaces and the higher is the heat quantity exchanged by the cells with the coolant that, finally, leads to a more intense temperature decrease experienced by the HVB pack. Since the thermal conductivity of the modules is definitely higher along the transverse direction, a length and height increase involves more effective thermal modifications than the ones caused by a height and width increase; in the first case, in fact, is the extension of the surfaces perpendicular to the transverse direction that shows an increase, while in the second one the increase affects the surfaces perpendicular to the longitudinal direction, whose thermal conductivity has a very low value due to the series disposition of the battery layers.
- **Coolant volume flow rate:** the total volume of coolant entering the battery pack, through the knowledge of the coolant density, determines the mass of fluid flowing inside the device and between the various modules. The quantity of

cooling medium that, instant per instant, touches the external surfaces of the cells, directly defines the heat amount that can be disposed by the battery to the coolant to maintain an optimum thermal state and avoid overheating. Increasing the coolant amount flowing in the system, the performance of the battery cooling operations increase and, in this way, the temperature of the modules can be finally maintained under more strictly limits requested for safety reasons. Figure 4.42 makes possible to understand that the influence of the modules resistance on the battery thermal behaviour is higher than the one covered by the coolant flow rate. The blue curve, in fact, refers to a 2.8 mΩ resistance and to a 100 cfm air volume flow rate while the magenta one refers to the same air quantity but to a double resistance that, finally, leads to a double temperature increase of the HVB device (because it doubles the amount of heat instantaneously dissipated for Joule effect). The green curve, instead, refers to a 2.8 mΩ resistance and to a 50 cfm air volume flow rate that causes a greater temperature rise, but certainly with a lower influence with respect to the one shown by the internal resistance values.

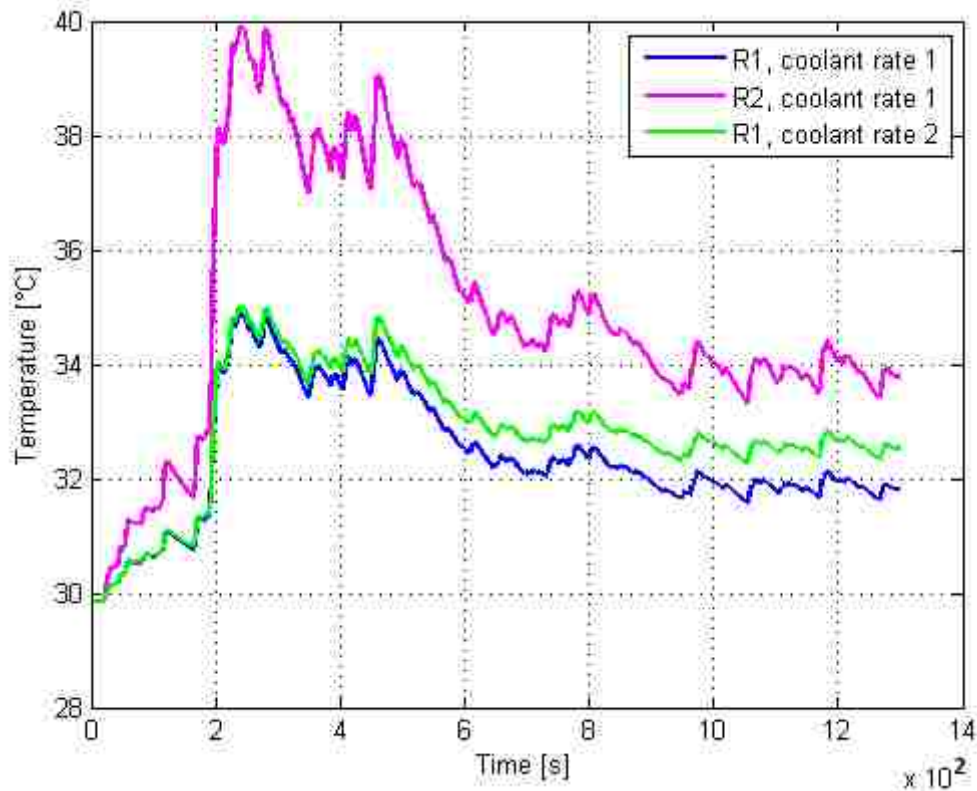


Figure 4.42 - Internal resistance and coolant volume flow rate contribution

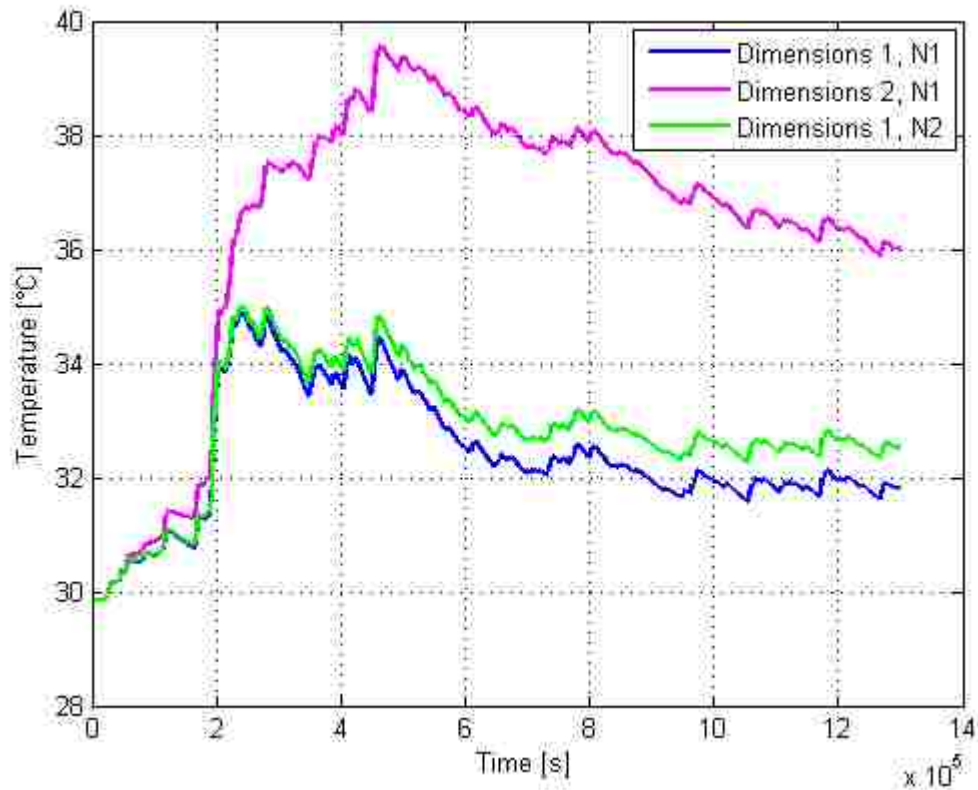


Figure 4.43 - Cells dimensions and number contribution

- Number of cells: the number of modules that constitute the battery pack has a direct influence on the thermal behaviour of the HVB device because, given the overall quantity of coolant instantaneously entering the pack, it defines the specific amount of fluid that flows around a single cell. The higher is the number of modules and the smaller is the coolant mass flow rate that cools down a specific prismatic body and, finally, this determines a worse cooling of the whole battery pack and a consequent higher temperature increase during the driving cycle. Figure 4.43 represents the results of three different simulations, realized with a varying cells geometry and number that are separately or contemporarily halved and doubled to understand their influence on the thermal behaviour of the pack. The blue curve refers to a basic geometry of 60 cells, the magenta one refers to the same modules number but to halved dimensions of the prismatic bodies and, finally, the green one refers to the basic geometry considered for the blue curve but to 120 cells constituting the battery pack. After a rapid analysis of the picture,

it is clear that the number of modules has a notably lower influence on the temperature trend of the HVB with respect to the geometry of the cells that, if halved in all its dimensions, leads to an approximately doubled temperature increase during the driving cycle. Its effect is similar to the one of the internal resistance, that can be studied in Figure 4.42, while the influence of the cells number increase is exactly the same of the coolant flow rate decrease because, doubling the number of modules constituting the battery pack, the final effect is to halve the coolant quantity flowing around all the cells, considered as autonomous entities.

- Current collectors thickness: as demonstrated by simulation number 15, the influence of the anode and cathode current collectors thickness on the thermal behaviour of the HEV battery is very low and can be neglected in case of small modifications in their values. This because of the presence of the polymeric separators interposed between the copper and aluminum layers that, from a thermal point of view, lowers the contribution of the metallic materials in determining the longitudinal and transverse conductivity values. Hence, even in case of highly notable collectors thickness modifications, the overall temperature time trend shown by the battery is going to assume approximately the same values.

#### **4.3.4 Battery cooling system model validation phase**

The final step related to the analysis of the results obtained through the battery thermal model, consists in its validation that should be conducted using experimental data coming from physical tests performed on the investigated HEV battery device. Before going through the validation phase description, it is important to remember another time how the battery model works and what are the main features that it offers. First of all, it must be underlined that the software operations are managed by a Matlab® base file that uploads, from specific matrixes created in Excel® by the user, all the input data necessary to perform the simulations. These input variables refer to different aspects of the investigated case of study, for example to the geometry of the battery cells, to the type

and quantity of coolant used to control the thermal status of the device and to the electric current profile defined by the driving cycle considered for the analysis.

The software can be integrated in the overall Chrysler HEV prediction tool, in order to send the battery temperature values, that it computes during time, to the main logical loop of the Chrysler model, determining an improvement in the accuracy level of the fuel economy and performance predictions: these results, in fact, strongly depend on the thermal state of the battery that, at the moment, is not simulated by the Chrysler tool; however, after the integration of the newly designed battery software, the HVB thermal behaviour is going to be carefully described to better calculate all the temperature-dependent battery variables. At the same time, the new model can also be used alone to run simulations related to the thermal phenomena affecting the operations of the HEV battery pack, considered alone and not as part of a vehicle system; this feature makes possible to conduct thorough sensitivity studies, aimed at determine what are the most important input factors and variables affecting the thermal performance of the investigated HVB device.

The final output of the model is represented by a graph depicting the time trend of the battery temperature, plotted together with the coolant temperature at the outlet of the battery pack, determined instant per instant during the investigated driving cycle; the driving program, in particular, determines the current profile that excites the battery and indicates the amount of electric charge that, instantaneously, is leaving the battery to propel the electric motor or is going to the battery to restore its state of charge. All the simulation results presented in the previous sections are characterized by reasonable and accurate trends, well fitting the current profile characteristics involved by the considered driving program (a city driving cycle FTP-72 has been taken into account for all the analysis).

To specifically prove the validity of the results, a validation procedure should be performed working on the temperature trends obtained at the end of the simulations: a comparison between the simulated battery temperature values and some experimental data sets, obtained through empirical tests physically done on the HVB device, is necessary to understand if both the temperature profiles assume the same magnitudes during the entire driving cycle. Hence, in addition to the simulations realized using the

newly designed thermal software, the same battery pack considered for the virtual analysis must be really tested using the same current profile uploaded on Simulink®; the number of cells, type and quantity of coolant, modules geometry, internal resistance, current collectors thickness and operating mode considered in the real test must be the exactly equal to the ones considered for the virtual simulation. The main problem is that, since the battery thermal tool has been designed as a purely predictive software to be used during the early design stages of new HEV models, the research and development teams at Chrysler do not have the possibility to realize physical tests in the battery testing labs using the same input configuration uploaded on Matlab® and Simulink®.

The software models the whole battery pack considering a simplified case of perfect prismatic cells, distributed in parallel over the entire length of the pack, and this configuration is perfect for a predictive tool that deals with typical HEV applications but does not fit with real cases of study that have been already analyzed in the testing labs, considering a single battery module or an entire pack not connected to the main battery cooling system. However, it is possible to set up new tests referred to a parallel disposition of pouch cells, enclosed in an external battery pack shell inside which the air is flowing to cool down the modules; unfortunately, the organization of the experimental tests requires time and money and, during the internship at Chrysler, there was not the chance to set up the desired experimental analysis necessary to perform the battery cooling system model validation.

Anyway, to give validity to the 17 simulations presented in this chapter, it is mandatory to realize a comparison between a simulated and an experimental battery temperature curve: given the impossibility to set up a test on a battery pack physically representing the configuration of the device modeled in the software, an investigation has been conducted in order to individuate at least one experimental analysis performed in the past that can be virtually implemented, in the best possible way, using the newly designed battery model. In other words, it is not possible to realize a physical test with the same boundary conditions used to run a simulation through the software but, given a test already done on a battery pack, the actual purpose is to run a simulation in the same conditions constituting the test. Hence, several thermal studies have been analyzed in order to find an experimental battery temperature curve to be compared with the results of



a simulation. In particular, a thermal study conducted on a Li-Ion pouch cell, developed at FIAT in 2011, has been taken into account: it describes an experimental thermal analysis conducted on a single Dow Kokam SLPB 100216216H HEV battery module [65], tested in a climatic chamber with a specific current profile and provided with thermocouples on its surface, able to detecting the cell temperature evolution during time. The pouch module investigated for this study is depicted in Figure 4.44 while, in Figure 4.45, the excitation current profile is plotted with respect to time.

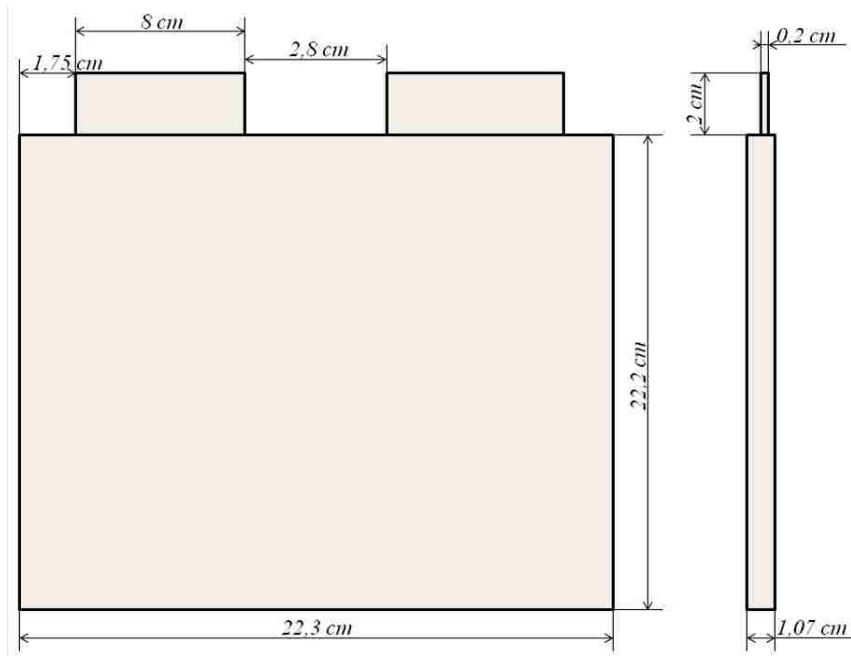


Figure 4.44 - Dow Kokam SLPB 100216216H pouch cell geometry [65]

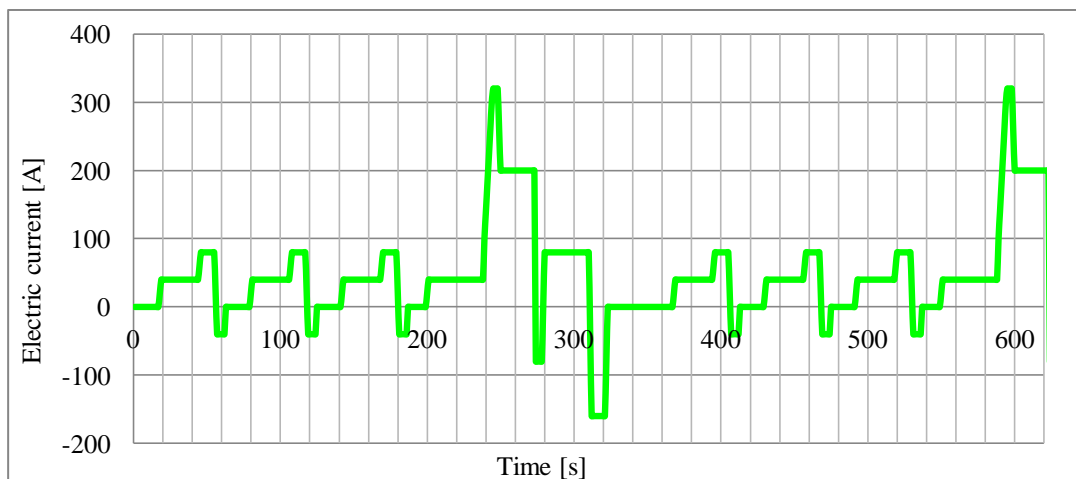
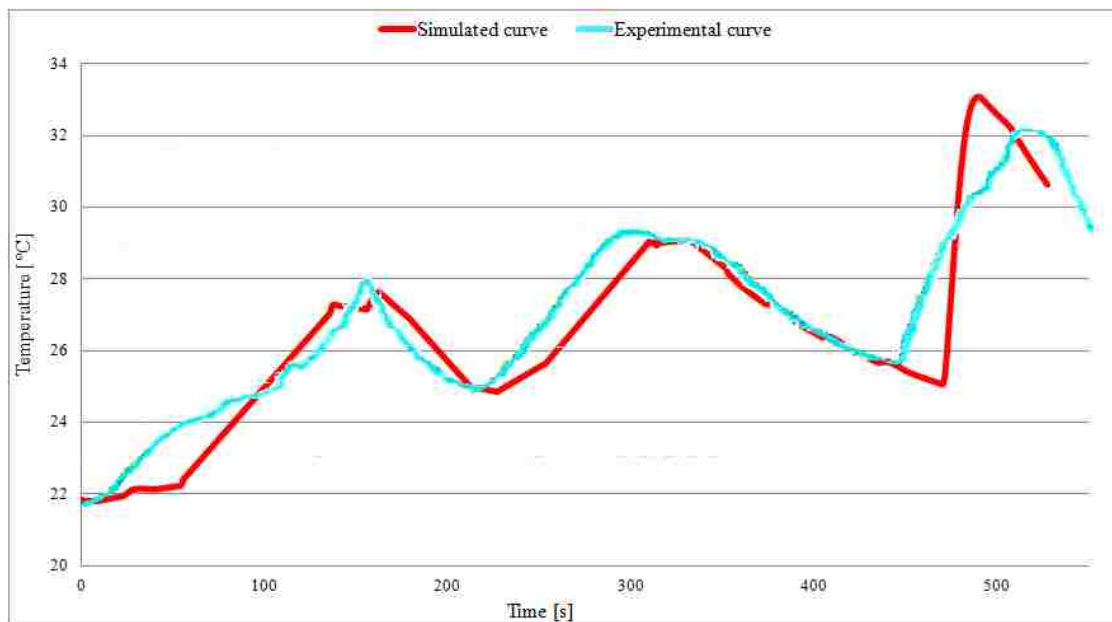


Figure 4.45 - Excitation current profile [65]

Uploading in the Matlab® and Simulink® files all the specific inputs that define this experimental analysis (cell characteristics, electric current profile, cooling conditions), a simulation has been activated in order to obtain a virtual temperature curve to be compared with the experimental one, determined during the test thanks to the thermocouples placed on the cell. In particular, in Figure 4.46, the red line represents the temperature time trend of the module simulated by the software, while the cyan line represents the experimental temperature trend detected by the thermal sensors located on the surface of the device.



**Figure 4.46 - Battery thermal model validation picture**

Even if the two curves are not identical, their time trend and order of magnitude are roughly equal, in particular during the intermediate portion of the cycle. Unfortunately, the data set related to cyan curve of Figure 4.46 is not available and, hence, the magnitude difference existing between the experimental and simulated results cannot be computed; anyway, from a graphical analysis, it can be stated that the validation activity is satisfactory and reinforces the technical contents of the battery cooling system model that has been designed. In fact, while the HVB thermal software considers a battery pack in which the air flows between the modules inside rectangular channels, the experimental study developed in FIAT has been realized placing the pouch cell alone in a climatic

chamber where the air motion was not forced and controlled. Hence, the virtual and experimental tests take place considering the same device but different cooling mechanisms and physical locations of the module and so, considering these boundary conditions, the comparison depicted in Figure 4.46 can be considered a good result.

Finally, the opinions and suggestions of the thermal experts working in the Electrified Powertrain department at Chrysler have been very useful to prove the general correctness of the simulated results: carefully analyzing all the simulations, considering the specific geometry of the cells and the related adopted cooling solutions (type and quantity of coolant), the values of the temperature gradient computed instant per instant by the software have been evaluated as reasonable and satisfying from a prediction point of view. Hence, the results generated by the battery thermal model can be seen as substantially optimal to describe the thermal behaviour of a certain HEV battery pack, excited during an investigated driving profile, and to improve the accuracy level of the fuel economy and performance predictions realized by the Chrysler HEV software.

## CHAPTER 5

### CONCLUSIONS AND RECOMMENDATIONS

In recent years, vehicle hybridization has become an important phenomenon that is actually changing the characteristics and facets of the worldwide automotive scenario. The addition of a new electrified drivetrain, constituted by a powerful battery pack and electric motor, leads to the downsizing of the internal combustion engine, to the braking energy recovery and, finally, to an overall reduction of the fuel consumption and emission level. This thesis investigates the HEV technology and focuses on the design of two simulation software tools, capable of predicting the thermal behaviour of the ICE and HVB that equip a new vehicle model tested in its early design stages. The possibility to simulate the transient and steady state behaviour of the engine and battery pack, in terms of heat exchange phenomena and cooling system performance, has in fact a decisive role in the determination of the most important electrical and mechanical quantities that affect the behaviour of the two devices.

Hence, the first phase of the project relates to the design activity of the two thermal models, realized using Matlab® and Simulink®. The tools are built to simulate the thermal phenomena taking place at the ICE and HVB level, during a virtual test of the investigated HEV while running a driving cycle; the final output results are represented by the engine coolant and battery temperature time trends. In this regard, the design process requires the knowledge of several thermophysical theories and studies, through which it is possible to create computational structures that take into account every operating aspect of the engine and battery devices. The second phase of the thesis involves instead the validation of the models, realized through a comparison between the simulated and experimental temperatures and through a careful analysis of the trends of the results with respect to the time variations of the input variables. Then, the HVB tool is used to run simulations of different batteries and to study the influence of the geometry and electrochemistry of the cells and of the type of coolant on the thermal behaviour of the pack. The last step is finally related to the integration of the two new software in the

overall Chrysler HEV prediction tool, now able to determine with a higher degree of accuracy the results of the simulation activity.

## 5.1 Conclusions

Analyzing the internal combustion engine cooling system model that has been created, its main features and the most important obtained results are listed below.

- It manages a lot of input quantities that, suitably combined and elaborated, allow prediction of the coolant temperature time trend characterizing the investigated engine during a simulation activated for a given driving cycle. In particular, it takes into account several heat rate and power sources, precisely computing the heat quantity instantaneously acquired by the coolant.
- It is flexible because it can be used, in the same way, dealing with any type of engine and input vehicle speed profile. Simply defining the magnitude of the investigated input variables, the model is able to study and predict the thermal behaviour of different engines, tested over different driving cycles.
- It can be integrated in the overall Chrysler HEV prediction software, allowing to better determine, among other quantities, the mechanical efficiency of the ICE that strongly depends on the thermal state of the coolant and of the lubricating oil.
- It can be used as an autonomous tool to analyze the performance of an engine, obtaining preliminary indications about its transient and steady state thermal behaviour given an input speed profile requested by the vehicle.
- It shows that the temperature gradients experienced by the engine coolant are generally intense and, hence, they must be taken into account to characterize the actual performance of the whole vehicle system.
- It is useful to highlight that the intervention of the engine radiator, through a suitable design of the thermostat, is decisive to limit the thermal excitation of the ICE structure.

Analyzing, on the other hand, the features introduced by the battery thermal software and the main results obtained at the end of the simulation phase, the following concepts can be pointed out.

- It determines the cells and coolant temperature time trends for a given input current profile, defined on the basis of the operations requested to the battery by the vehicle.
- It models the internal structure of the cells, with respect to the investigated electrochemistry solution, and it models also the internal structure of the pack, with respect to the geometry and location of the modules.
- It allows to define the type and mass flow rate of coolant used to control the thermal state of the battery, specifying all the thermophysical properties of the fluid that strongly affect the heat exchange phenomena taking place during time inside the battery pack.
- It can be integrated in the overall Chrysler HEV prediction software, allowing to better determine, among the others, the state of charge and open circuit voltage of the battery that strongly depend on the thermal state of the modules.
- It can be used as an autonomous tool to analyze the performance of the HVB, obtaining preliminary indications about its transient and steady state thermal behaviour given the input current profile, the type and quantity of cooling medium and the constructive characteristics of the pack.
- It is activated to analyze different battery configurations and to perform a sensitivity study. Varying the input quantities one at a time, and investigating all the possible combinations, it is possible to understand that the strongest influences on the HVB thermal behaviour are linked to the type of current profile, to the cooling medium flowing inside the pack, to the internal resistance of the modules, to the cells dimension and to the coolant flow rate.
- It allows to determine which are the best battery cooling solutions necessary to maintain the modules temperature under prescribed limits and to satisfy the safety and operating requirements requested by the specific battery pack.

## **5.2 Recommendations**

Further improvements and updates can be realized for both the engine and battery thermal models and, in this regard, some recommendations are provided below.

- All the input quantities could be managed indicating their specific tolerance intervals, in order to obtain information about the accuracy of the final results and about their levels of precision.
- The combustion efficiency considered in the structure of the engine thermal model is treated as constant but it depends on several operating conditions of the device. Hence it could be determined instantaneously realizing a dedicated calculation loop.
- The ICE cooling model validation should be realized considering experimental data related to the engine coolant temperature and not to the temperature of the lubricating oil. The two fluids in fact, despite living about the same thermal phenomena, are characterized by completely different thermal properties and this does not make possible to realize a thorough and complete validation.
- The battery thermal model could be updated taking into account the coating layer that covers all the modules contained in the battery pack. In this way a more precise characterization of the cell structure could be finally obtained.
- The temperature of the coolant along the transverse direction considered on the inlet side of the pack is treated as constant. It should be treated as variable, instead, because of the heat exchange phenomena taking place along the longitudinal direction of the modules and, in this regard, it should be computed over the whole transverse length of the pack with a suitable logical loop.
- The validation activity of the HVB thermal model should be realized setting experimental studies in the battery testing labs at Chrysler. Considering specific battery devices, physically tested in laboratory sessions with a given input current profile and cooling system configuration, the modules temperature should be detected through thermocouples during time. The trend obtained in this way has finally to be compared to the simulated temperature, in order to realize an accurate validation of the model and to better understand the level of precision of its results.
- The Chrysler HEV prediction model could be finally activated to predict the performance and fuel economy of an investigated hybrid model, before and after the integration of the newly designed ICE and HVB thermal software. In this way,

it would be possible to individuate and quantify the improvements introduced by the new tools in terms of final prediction results.



## REFERENCES

- [1] C. Gomes, “Global Auto Report,” Scotiabank Economics, Toronto, Ontario, Canada, 2013.
- [2] “Do Your Bit to Control Global Warming,” Green Leap Delhi, OMLogic Consulting, 2012. Available at: <http://www.greenleapdelhi.org.in/do-your-bit-to-control-global-warming/>.
- [3] S. Davis, S. Diegel, R. Boundy, “Transportation Energy Data Book: Edition 31,” Oak Ridge National Laboratory, Oak Ridge, Tennessee, United States of America, 2012.
- [4] A. Emadi, “Handbook of Automotive Power Electronics and Motor Drives,” Taylor & Francis Group LLC, 2005.
- [5] R. Spotnitz, “State of Battery Performance and Projected Automotive Needs,” American Lithium Energy Corporation, Battery Technology Symposium, Conference Paper, 2008.
- [6] M. Beliveau, J. Rehberger, J. Rowell, A. Xarras, “A Study on Hybrid Cars: Environmental Effects and Consumer Habits,” Worcester Polytechnic Institute, Worcester, Massachusetts, United States of America, Bachelor’s Thesis, 2010.
- [7] “Technology Roadmap: Electric and plug-in hybrid electric vehicles,” International Energy Agency, Paris, France, 2011.
- [8] “United States Environmental Protection Agency,” Wikipedia, Wikimedia Foundation, 2013. Available at: <https://en.wikipedia.org/wiki/United-States-Environmental-Protection-Agency>.

- [9] “Hybrid vehicle,” Wikipedia, Wikimedia Foundation, 2013. Available at: [https://en.wikipedia.org/wiki/Hybrid\\_vehicle](https://en.wikipedia.org/wiki/Hybrid_vehicle).
- [10] “Hybrid vehicle drivetrain,” Wikipedia, Wikimedia Foundation, 2013. Available at: [https://en.wikipedia.org/wiki/Hybrid\\_vehicle\\_drivetrain](https://en.wikipedia.org/wiki/Hybrid_vehicle_drivetrain).
- [11] S. Baldizzone, “Performance and Fuel Economy Analysis of a Mild Hybrid Vehicle Equipped with Belt Starter Generator,” University of Windsor, Windsor, Ontario, Canada, Master’s Thesis, 2012.
- [12] I. Viorel<sup>1</sup>, L. Szabó<sup>1</sup>, C. Ştet<sup>1</sup>, L. Löwenstein<sup>2</sup>, “Integrated Starter-Generators for Automotive Applications,” Technical University of Cluj<sup>1</sup>, Cluj, Romania and Siemens Transportation Systems<sup>2</sup>, Erlangen, Germany, Acta Electrotehnica, Volume 45, 2004.
- [13] “Case study: Toyota Hybrid Synergy Drive,” Toyota Motor Corporation, Toyota, Aichi, Japan, Technical Report, 2003.
- [14] “Toyota Hybrid System: THS II,” Toyota Motor Corporation, Toyota, Aichi, Japan, Technical Report, 2003.
- [15] R. Spotnitz, “Challenges for Electrochemical Energy Storage,” Battery Design LLC, 2012.
- [16] “Lexus Hybrid Drive,” Lexus, Toyota Motor Sales, United States of America, 2013. Available at: <http://www.lexus.eu/hybrid/#/GoodBetterBest>.
- [17] D. Yifan<sup>1</sup>, L. Yugong<sup>1</sup>, L. Keqiang<sup>1</sup>, R. Yong<sup>2</sup>, Z. Anjian<sup>2</sup>, D. Zhihui<sup>2</sup>, Y. Qinshan<sup>2</sup>, “Hierarchical Control for a Full Hybrid Vehicle with Single Motor and Double Clutches,” Tsinghua University<sup>1</sup>, Beijing, China and Chongqing

- Changan New Energy Vehicle<sup>2</sup>, Chongqing, China, IEEE Technical Paper, 2011.
- [18] M. Duvall, "Battery Evaluation for Plug-In Hybrid Electric Vehicles," Electric Power Research Institute, Palo Alto, California, United States of America, IEEE Technical Paper, 2005.
- [19] I. Husain, "Electric and Hybrid Vehicles: Design Fundamentals," CRC Press LLC, 2005.
- [20] V. Barkhordarian, "Power MOSFET Basics," International Rectifier, El Segundo, California, United States of America, 2012.
- [21] "IGBT Applications Handbook," ON Semiconductor, Phoenix, Arizona, United States of America, Technical Report, 2012.
- [22] "Science: Electrolysis," GCSE Bitesize, BBC, London, United Kingdom, 2013. Available at: <http://www.bbc.co.uk/schools/gcsebitesize/science/add-gateway-pre-2011/periodictable/electrolysisrev1.shtml>.
- [23] S. Nallabolu, "System Level Modeling and Simulation for Hybrid Electric Vehicle Propulsion," Ingolstadt University of Applied Science, Ingolstadt, Germany, Master's Thesis, 2010.
- [24] G. Brusaglino, G. Pede, E. Vitale, "Sistemi di Propulsione Elettrica ed Ibrida: dalla Sorgente a Bordo all'Attuazione Meccanica," ENEA, ATA, CIVES, 2009.
- [25] K. Young<sup>1</sup>, C. Wang<sup>2</sup>, L. Wang<sup>2</sup>, "Electric Vehicle Battery Technologies," Ovonic Battery Company<sup>1</sup>, Rochester Hills, Michigan, United States of America and Wayne State University<sup>2</sup>, Detroit, Michigan, United States of America, 2013.

- [26] D. Linden, T. Reddy, "Handbook of Batteries: Third Edition," McGraw-Hill, 2002.
- [27] F. Nemry, G. Leduc, A. Muñoz, "Plug-in Hybrid and Battery-Electric Vehicles: State of the research and development and comparative analysis of energy and cost efficiency," European Commission, Brussels, Belgium, JRC Technical Notes, 2009.
- [28] Y. Xing, E. Ma, K. Tsui, M. Pecht, "Battery Management Systems in Electric and Hybrid Vehicles," City University of Hong Kong, Hong Kong, China, Energies, Volume 4, 2011.
- [29] P. Crovetto, "Electric and Electronic Systems for Vehicles: Electric Systems in Vehicles," Politecnico di Torino, Torino, Italy, 2012.
- [30] M. Kromer, J. Heywood, "Electric Powertrains: Opportunities and Challenges in the U.S. Light-Duty Vehicle Fleet," Massachusetts Institute of Technology, Cambridge, Massachusetts, United States of America, 2007.
- [31] "Advanced Thin Film Sodium Sulfur Battery," Trans Ionics Corporation, The Woodlands, Texas, United States of America, Technical Report, 2005.
- [32] A. Pesaran, G. Kim, M. Keyser, "Integration Issues of Cells into Battery Packs for Plug-In and Hybrid Electric Vehicles," International Battery and Hybrid Electric Vehicle Symposium, Conference Paper, 2009.
- [33] A. Pesaran, A. Vlahinos, T. Stuart, "Cooling and Preheating of Batteries in Hybrid Electric Vehicles," The 6<sup>th</sup> ASME-JSME Thermal Engineering Joint Conference, Conference Paper, 2003.

- [34] A. Pesaran, "Battery Thermal Management in EVs and HEVs: Issues and Solutions," Advanced Automotive Battery Conference, Conference Paper, 2001.
- [35] G. Kim, A. Pesaran, "Battery Thermal Management System Design Modeling," International Battery and Hybrid Electric Vehicle Conference and Exhibition, Conference Paper, 2006.
- [36] A. Pesaran, A. Vlahinos, S. Burch, "Thermal Performance of EV and HEV: Battery Modules and Packs," National Renewable Energy Laboratory, Golden, Colorado, United States of America, 2000.
- [37] A. Pesaran, S. Burch, M. Keyser, "An Approach for Designing Thermal Management Systems for Electric and Hybrid Vehicle Battery Packs," Fourth Vehicle Thermal Management Systems Conference and Exhibition, Conference Paper, 1999.
- [38] T. Yuksel, J. Michalek, "Evaluation of the Effects of Thermal Management on Battery Life in Plug-in Hybrid Electric Vehicles," Carnegie Mellon University, Pittsburgh, Pennsylvania, United States of America, 2012.
- [39] "Driving cycle," Wikipedia, Wikimedia Foundation, 2013. Available at: [http://en.wikipedia.org/wiki/Driving\\_cycle](http://en.wikipedia.org/wiki/Driving_cycle).
- [40] "New European Driving Cycle," Wikipedia, Wikimedia Foundation, 2013. Available at: [http://en.wikipedia.org/wiki/New\\_European\\_Driving\\_Cycle](http://en.wikipedia.org/wiki/New_European_Driving_Cycle).
- [41] "FTP-75," Wikipedia, Wikimedia Foundation, 2013. Available at: <http://en.wikipedia.org/wiki/FTP-75>.

- [42] P. van Bree, A. Veltman, W. Hendrix, "Prediction of Battery Behavior Subject to High-Rate Partial State of Charge," IEEE Transactions on Vehicular Technology, Volume 58, IEEE Technical Paper, 2009.
- [43] Y. Chiang, "How does temperature affect the life of a battery?," Massachusetts Institute of Technology, Boston, Massachusetts, United States of America, 2008.
- [44] "Simulink," Wikipedia, Wikimedia Foundation, 2013. Available at: <http://en.wikipedia.org/wiki/Simulink>.
- [45] "Internal combustion engine," Wikipedia, Wikimedia Foundation, 2013. Available at: [http://en.wikipedia.org/wiki/Internal\\_combustion\\_engine](http://en.wikipedia.org/wiki/Internal_combustion_engine).
- [46] "Lower and Higher Heating Values of Gas, Liquid and Solid Fuels," Oak Ridge National Laboratory, Oak Ridge, Tennessee, United States of America, Biomass Energy Data Book, Appendix A, 2011.
- [47] M. Moghaddam, A. Moghaddam, N. Zanjani, E. Salimipour, "Improvement fuel properties and emission reduction by use of Diglyme-Diesel fuel blend on a heavy-duty diesel engine," 2<sup>nd</sup> International Conference on Environmental Engineering and Applications, Conference Paper, 2011.
- [48] A. Haury, J. Volkering, "Modelisation of the engine coolant warming-up behavior," Chalmers University of Technology, Göteborg, Sweden, Master's Thesis, 2011.
- [49] F. Millo, "Macchine: Richiami di Termodinamica, Proprietà dei Combustibili," Politecnico di Torino, Torino, Italy, 2011.

- [50] M. Bahrami, "Advanced Conduction Heat Transfer," Simon Fraser University, Burnaby, British Columbia, Canada, 2010.
- [51] "Air – Specific Heat at Constant Temperature and Various Pressures," The Engineering ToolBox, 2013. Available at: <http://www.engineeringtoolbox.com/air-specific-heat-various-pressures.html>.
- [52] "Density of air," Wikipedia, Wikimedia Foundation, 2013. Available at: [http://en.wikipedia.org/wiki/Density\\_of\\_air](http://en.wikipedia.org/wiki/Density_of_air).
- [53] S. D'Ambrosio, "Combustion Engines and their Application to Vehicle: Engine Cooling System," Politecnico di Torino, Torino, Italy, 2012.
- [54] "Thermal Conductivity of Metals," The Engineering ToolBox, 2013. Available at: <http://www.engineeringtoolbox.com/thermal-conductivity-metals.html>.
- [55] "Convective Heat Transfer," The Engineering ToolBox, 2013. Available at: [http://www.engineeringtoolbox.com/convective-heat-transfer-d\\_430.html](http://www.engineeringtoolbox.com/convective-heat-transfer-d_430.html).
- [56] R. Shah, D. Sekulić, "Fundamentals of Heat Exchanger Design," John Wiley & Sons, 2003.
- [57] V. Ravello, "Vehicle effective integration of e-components," Centro Ricerche FIAT, Orbassano, Italy, 2012.
- [58] O. Gross, C. Brown, "Design and Integration of the Fiat 500e High Voltage Battery System," Advanced Automotive Battery Conference, Conference Paper, 2013.

- [59] K. Yeow, H. Teng, M. Thelliez, E. Tan, “3D Thermal Analysis of Li-ion Battery Cells with Various Geometries and Cooling Conditions Using Abaqus,” SIMULIA Community Conference, Conference Paper, 2012.
- [60] “Exhaust gas recirculation,” Wikipedia, Wikimedia Foundation, 2013. Available at: [http://en.wikipedia.org/wiki/Exhaust\\_gas\\_recirculation](http://en.wikipedia.org/wiki/Exhaust_gas_recirculation).
- [61] “Chrysler Begins Production of All-New Pentastar 3.6-liter V-6 Engine,” Car and Driver, Hearst Communications, 2012. Available at: <http://blog.caranddriver.com/chrysler-begins-production-of-all-new-pentastar-3-6-liter-v-6-engine/>.
- [62] N. George, V. Obianwu, A. Akpan, I. Obot, “Lubricating and cooling capacities of different SAE 20W – 50 engine oil samples using specific heat capacity and cooling rate,” Archives of Physics Research, Volume 1, 2010.
- [63] “Ethylene Glycol Heat-Transfer Fluid,” The Engineering ToolBox, 2013. Available at: [http://www.engineeringtoolbox.com/ethylene-glycol-d\\_146.html](http://www.engineeringtoolbox.com/ethylene-glycol-d_146.html).
- [64] “Red Line WaterWetter: Cooling System Requirements,” Red Line Synthetic Oil Corporation, Benicia, California, United States of America, Technical Report, 2012.
- [65] P. Carattoli, “Studio termico di una batteria al litio,” Politecnico di Torino, Torino, Italy, Master’s Thesis, 2011.



## VITA AUCTORIS

NAME: Gabriele Catacchio

PLACE OF BIRTH: Milano, Italy

YEAR OF BIRTH: 1989

EDUCATION: Liceo Scientifico G. Peano, High School Scientific Diploma, Cuneo, Italy, 2003-2008.

Politecnico di Torino, BSc in Automotive Engineering, Torino, Italy, 2008-2011.

Politecnico di Torino, MSc in Automotive Engineering, Torino, Italy, 2011-2012.

University of Windsor, MSc in Mechanical Engineering, Windsor, Ontario, Canada, 2012-2013.

PUBLICATIONS: “Development of a Predictive Model for Regenerative Braking System”, IEEE Transportation Electrification Conference and Expo, Detroit, Michigan, United States of America, Conference Paper, 2013. Authors: Andrea Caratti, Gabriele Catacchio, Carlo Gambino, Narayan Kar.